UAB

Universitat Autònoma de Barcelona

UAB

Universitat Autònoma de Barcelona

Departamento de Microelectrónica y Sistemas Electrónicos

Integrated sensors for overcoming Organ-On-a-Chip monitoring challenges

Autor: Ana Moya Lara

Directores: Dr. Gemma Gabriel Buguña
Dr. Eloi Ramon Garcia

Tutor: Dr. Jordi Aguiló Llobet

Memoria de Tesis
presentada para optar al título de

Doctor en Ingeniería Electrónica y de Telecomunicación

Septiembre 2017

Universitat Autònoma de Barcelona

INSTITUT DE MICROELECTRÒNICA DE BARCELONA · **CSIC**

Dr. Gemma Gabriel Buguña, Investigadora del Consejo Superior de Investigaciones Científicas, Dr. Eloi Ramon Garcia, Investigador del Consejo Superior de Investigaciones Científicas y Profesor Asociado del Departamento de Electrónica de la Universidad Autónoma de Barcelona, y Dr. Jordi Aguiló Llobet, Catedrático del Departamento de Microelectrónica y Sistemas Electrónicos de la Universidad Autónoma de Barcelona,

Certifican

que la Memoria de Tesis *Integrated sensors for overcoming Organ-On-a-Chip monitoring challenges* presentada por Ana Moya Lara para optar al título de Doctor en Ingeniería Electrónica y de Telecomunicación se ha realizado bajo su dirección en el Instituto de Microelectrónica de Barcelona perteneciente al Centro Nacional de Microelectrónica del Consejo Superior de Investigaciones Científicas y ha sido tutoritzada en el Departamento de Microelectrónica y Sistemas Electrónicos de la Universidad Autónoma de Barcelona.

Directores	Dr. Gemma Gabriel Buguña	. . . .
	Dr. Eloi Ramon Garcia	. . . .
Tutor	Dr. Jordi Aguiló Llobet	. . . .

Bellaterra (Cerdanyola dels Vallès), 26 de Septiembre de 2017

A mi familia.

Learn from yesterday, live for today, hope for tomorrow.

The important thing is not to stop questioning.

Albert Einstein

Resumen

Los dispositivos **'Organ-On-a-Chip'** han revolucionado la forma de conocer la biología que hasta el momento se ha venido realizando con los cultivos celulares. Estos sistemas, que contemplan el co-cultivo en tres dimensiones y tecnología microfluídica, tienen como propósito mimetizar la fisiología humana con sistemas de cultivo *in-vitro*. Su finalidad es la de incrementar el conocimiento de los procesos biológicos, así como también de disponer de una herramienta de diagnóstico efectiva para el análisis de diferentes fármacos. A medida que aumenta la complejidad biológica de los sistemas de cultivo, la necesidad de analizar y monitorizar su respuesta también aumenta.

En la actualidad, el análisis de los sistemas 'Organ-On-a-Chip' se basa principalmente en métodos analíticos convencionales que en la mayoría de casos implica la muerte del cultivo celular, la alteración del sistema microfluídico para la recolección de muestras, la imposibilidad de hacer análisis en tiempo real e incluso el aumento del coste y la complejidad del sistema en su conjunto.

Es en este contexto en el que esta tesis intenta desarrollar herramientas para la monitorización de parámetros celulares en tiempo real en sistemas 'Organ-On-a-Chip', ya que se han convertido en una valiosa estrategia para la comprensión de los procesos biológicos complejos que ocurren. Se proponen dos estrategias que no comprometen el funcionamiento del sistema 'Organ-On-a-Chip' como tal. Una de ellas tiene por objetivo monitorizar parámetros físicos de forma externa al sistema de cultivo, usando plataformas modulares que incorporan varios sensores y que pueden ser conectadas en línea con el sistema microfluídico sin intervenir en su funcionamiento. En concreto, se han integrado sensores electroquímicos miniaturizados en un sustrato plástico usando técnicas convencionales de microfabricación y prototipaje rápido, para la medición simultánea de los parámetros de oxígeno disuelto e iones de Na^+, K^+ y pH. La otra estrategia desarrollada en esta tesis va un paso más allá, dado que integra los sensores dentro del mismo sistema 'Organ-On-a-Chip', embebiéndolos en la propia membrana donde se realiza el cultivo celular. El reto consiste en integrar sensores de bajo coste de manera más eficiente, en una membrana flexible, muy porosa y delgada. Esto es posible gracias al uso de la tecnología de impresión por inyección de tinta como alternativa a las costosas tecnologías de microfabricación convencionales. Específicamente, se han incorporado y validado sensores electroquímicos de oxígeno disuelto en un sistema real de 'Liver-On-a-Chip' que permite monitorizar el consumo de oxígeno de un cultivo de células epiteliales renales en tiempo real.

Ambos son planteamientos válidos, y la elección de uno de ellos dependerá del interés biológico que puede tener realizar mediciones externas o internas al sistema de cultivo, y del grado de complejidad tecnológico que ello implique.

x

Abstract

Organ-On-a-Chip devices have changed the way to know the biology being indispensable in the evolution and understanding of the cell culture systems. Organ-On-a-Chip systems are based in three-dimensional microfluidic co-culture models and their purpose is to reproduce a real microenvironment in order to mimic human pathophysiology using *in-vitro* multicellular models. Their finality is to increase the understanding of the biological processes as well as to develop improved diagnostics and more effective tools for drug screening analysis. As the biological complexity of the cell cultures under investigation increases, the need to analyze and monitor cell culture response also increases.

Currently, analysis of Organ-On-a-Chip cell cultures still mainly relies on conventional analytical methods which in most cases involve the death of the cell culture, the disturbance of the microfluidic system for sample collection, the impossibility to observe real-time events, or even the increase of the cost and the complexity of the whole systems.

In this context, this thesis work is focused on the development of monitoring tools to allow the analysis of Organ-On-a-Chip parameters in real-time, becoming a valuable strategy for understanding complex biological processes. Two proposed strategies have been addressed for the real-time monitoring without compromising the operation of the system. The first deals with the monitoring of physical parameters externally to an Organ-On-a-Chip systems, using modular sensing platforms connected in-line with the microfluidic system without disturbing it. For this purpose, miniaturized electrochemical sensors have been integrated in a plastic substrate using conventional microfabrication and rapid-prototyping techniques, for the simultaneous measurement of dissolved oxygen, Na^+, K^+ and pH parameters. The other strategy developed in this thesis goes one step further, with the integration of the sensors inside the Organ-On-a-Chip, embedded in the cell culture membrane. The challenge is to integrate efficiently and cost-effectively the sensors in a high porous and very thin and flexible membrane without damaging it. This is possible because inkjet printing technology is selected as an alternative to the conventional microfabrication technologies due to their digital material deposition without any direct contact with the membrane. Specifically, an array of electrochemical dissolved oxygen sensors have been implemented and validated in a real Liver-on-a-chip system using rat and human epithelial cells.

Both proposed strategies are valid approaches, and the choice of one of them is depending on the biological interest, their interest in measuring parameters externally or inside the cell culture system, and the degree of technological complexity involved.

Contents

List of Figures

List of Tables

List of Acronyms

Dissertation Summary

This Chapter describes the dissertation overview of this thesis, where the most relevant aspects are briefly introduced.

1.1   Motivation of the work

The way to develop and understand the cell culture systems has notably evolved since the first artificial tissue culture in 1907 [18]. Over the next century, multidisciplinary efforts in cell biology and bioengineering have led to highly functional *in-vitro* culture platforms enabling the controlled presentation of microenvironmental signals [19]. The purpose of the developed platforms is to reproduce, as true-to-life as possible, the real environment in order to mimic human pathophysiology. Therefore, cell biology systems are moving from the conventional two-dimensional (2D) *in-vitro* models [20] to more complex three-dimensional (3D) systems in order to solve the discrepancies to capture the real features of the cellular microenvironments [21]. Based on this context, the concept of Organ-On-a-Chip (OOC) platforms emerges [22, 3]. Microengineering strategies provide a number of unique advantages and benefits in studying organ biology [23]. An OOC system implies a microfluidic cell culture device that contains continuously perfused chambers inhabited by living cells and arranged to simulate tissue- and organ-level physiology [24, 25]. These miniaturized organ models have several advantages over conventional models, such as more accurate prediction of the human responses, since they are able to capture the structural, mechanical, chemical, and communicative complexity of *in-vivo* systems [26]. Continuous improvement of these models led to a widespread use in diverse application areas, mainly trying to replace animal test due to their time consumption, high costs,ethical concerns and also they often fails to predict human patophysiology [27, 28]. This goal is complex due to the difficulty to mimic living tissues and organs, maintaining physicochemical microenvironments like in *in-vivo* conditions. Nowadays the OOC systems field still lack of development and research for a real future applicability.

Besides the development of microphysiological environments of human tissue or organ recapitulating *in-vivo* structure and function, the capability to analyze and monitor its real-time response to drugs or other stimulation is of utmost importance. For this reason, the incorporation of monitoring tools in the OOC systems is essential to allow the continuous improvements of these models. However, as the biological complexity of the cell cultures under investigation increases, the difficulty to integrate monitoring tools with these system is a challenge. Currently, analysis of OOC cell culture is still mainly based on optical measurement techniques using time-lapse brightfield and fluorescence microscopy [29]. This conventional analytical methods require manual sample collection from the microfluidic systems, large working volumes, and frequent system disturbance, and thus are not suitable for miniaturized OOC platforms. Consequently, over the past few decades, tremendous progress has been initiated towards the development of sensors for cell culture applications. Great efforts are made each year for the development of miniaturized sensors thus improving their benefits. Currently, a broad variety of online measurement tools has been integrated to measure crucial parameters such as oxygen [30, 31], pH [32], glucose and lactate [33]. However, most of these systems can not be widely applied in microfluidics system mostly due to the complex fabrication processes along with more cost-intensive and bulky experimental setups thus increasing the overall chance of failure.

Recently, different published review articles about cell monitoring and OOC systems claim for the necessity

of integrating functional and real-time monitoring tools [34–37]. For this purpose, it must be necessary to pave the way to interface existing biomimetic OOC models to achieve *in-situ* monitoring of physicochemical parameters. Due to the different metabolic processes that cell cultures have, this monitorization can be inside or outside the cell culture area by using measurement systems that can be connected with the OOC microfluidic devices without interfering with its function as shown in 1.1. In both cases, the difficulty to overcome is to avoid adding more complexity to the current OOC systems achieving a cost-effective sensing platform. It is in this sense that the motivation of this thesis appears for the accomplishment of this ambitious goal.

(a) External sensing platform **(b) Embedded sensors in OOC**
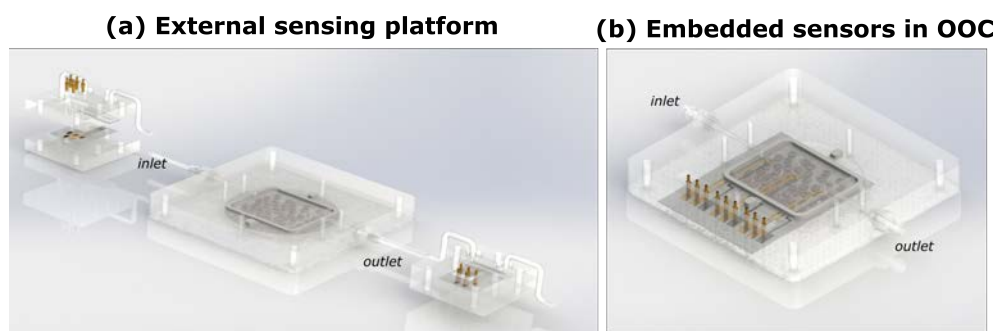
Figure 1.1 | Two strategies proposed in this thesis for the monitoring of physicochemical parameters in an Organ-On-a-Chip using, (a) two multi-sensing platforms connected externally to the inlet and outlet of the cell culture system, and (b) embedded sensors in the cell culture membrane of the Organ-On-a-Chip system.

1.2 Main Contribution of this thesis

In the *in-vitro* study of organs and tissues, the ability to analyze and monitor in real-time the cell culture response is of paramount importance. For this reason, this thesis is focused on the development of functional monitoring tools compatible with microfluidic technology for OOC systems. In a first stage, it has been developed a sensing device using conventional microfabrication technology to measure physical parameters **externally** in OOC systems (Figure 1.1(a)) and, in a second stage, it has been tackled the challenge to incorporate sensors **embedded** in the OOC systems (Figure 1.1(b)). To achieve this, moving from conventional microtechnology to printing technology was of vital importance in order to integrate, in a cost-effective way, the sensors embedded in the OOC system without disturbing it.

Following are described the main and the specific objectives of this thesis to obtain the final goal. After this, it is presented the list of publications that comprise this work in which Ana Moya is the first author of all of them, and are published in first-quartile journals. The section finishes with the outline of this dissertation presenting a brief summary of each chapter.

1.2.1 Objectives of the thesis

The ambition of this thesis deals with the development of low-cost electrochemical sensors for OOC systems monitoring. In general terms, the goal is to develop functional, reliable and low-cost systems to solve a necessity in real analysis. The developed sensors need to be designed allowing their integration with microfluidic systems. Different fabrication techniques have been employed during this work, depending on the requirements of each application. For this reason, the two main objectives are:

- **To develop a functional and modular monitoring tool to control cell culture parameters externally to the OOC system by using conventional microfabrication technologies**. To achieve this objective some specific sub-objectives are proposed:

  - To develop and characterize a dissolved oxygen (DO) microsensor array on Pyrex® substrate.

  - To validate the sensor performance measuring the oxygen profile inside a biofilm grown in a flat-plate bioreactor.

  - To develop and characterize an array of four integrated sensors in a single platform using flexible polymeric substrate for the measurement of DO, pH and sodium and potassium ions.

  - To validate the multisensing platform with physiological samples, concretely, with artificial and real urine samples, simulating the output of a renal tubular OOC system.

- **To monitor cell culture parameters with sensors embedded in the OOC system by using inkjet printing technology**. To achieve this objective, the following objectives have been addressed:

  - To characterize different conductive and insulator inks used to develop inkjet-printed sensors in order to assess their printability, morphology and electrical properties that have not been reported before.

  - To develop a complete electrochemical DO sensor platform by inkjet printing on polymeric substrate and to study their functionality and electrochemical response.

  - To integrated DO sensors embedded in the cell culture membrane of a liver OOC system, overcoming the technological difficulties to fabricate sensors on a delicate, ultraflexible and porous substrate.

  - To validate the sensor in a Liver-On-a-Chip system using primary human and rat cultured hepatocytes.

1.2.2 List of publications

The publications included in this list shall be considered for the evaluation of this thesis dissertation. A reproduction of each publication can be found on the indicated chapter summarized below.

Paper I. A. Moya, X. Guimerà, F.J. del Campo, E. Prats-Alfonso, A.D. Dorado, M. Baeza, R. Villa, D. Gabriel, X. Gamisans and G. Gabriel. Profiling of oxygen in biofilms using individually addressable disk microelectrodes on a microfabricated needle, Microchim. Acta. 182 (2014) 985–993. doi:10.1007/s00604-014-1405-4. (Q1, IF:4.58).

* The author's contribution: planning and performing the design of the sensor, its characterization, calibration and experimentation, and writing the main parts the manuscript.

Paper II. A. Moya, X. Illa, I. Gimenez, Y. Lazo, R. Villa, A. Errachid and G. Gabriel. Miniaturized multiparametric flexible platform for the simultaneous monitoring of ionic compounds: Application in real urine. Accepted (uncorrected proof) in Sens. Act. B, September 2017. (Q1, IF:5.4).
* The author's contribution: planning and performing the design of the sensors, their encapsulation and characterization, calibration and experimentation, and writing the main parts of the manuscript.

Paper III. A. Moya, G. Gabriel, R. Villa and F. Javier del Campo. Inkjet-printed electrochemical sensors, April 2017, Curr. Opin. Electrochem. doi:10.1016/j.coelec.2017.05.003.
* The author's contribution: finding and reading the state-of-art of publications related to electrochemical sensors and inkjet printing published in the last two years and writing parts of the manuscript.

Paper IV. A. Moya, E. Sowade, F.J. del Campo, K.Y. Mitra, E. Ramon, R. Villa, R.R. Baumann and G. Gabriel. All-inkjet-printed dissolved oxygen sensors on flexible plastic substrates, Org. Electron. 39 (2016) 168–176. doi:10.1016/j.orgel.2016.10.002. (Q1, IF:3.39).
* The author's contribution: planning and performing the characterization of the used inks, the inkjet printing of the sensors, the characterization and calibration of the sensors and writing the main parts of the manuscript.

Paper V. A. Moya, M. Ortega-Ribera, E. Sowade, M. Zea, X. Illa, E. Ramon, R. Villa, G. Gabriel. Real-time oxygen monitoring inside an organ-on-a-chip device using integrated inkjet-printed sensors. The article has been SUBMITTED to Lab-on-chip journal in September 2017. (Q1, IF:6.05).
* The author's contribution: planning and performing the design of the sensors, their fabrication using inkjet printing technology, their characterization and calibration, the experimental measurement and writing the main parts of the manuscript.

1.2.3 Thesis outline

With regards to the objectives that steered the course of this thesis and the articles pointed out in the previous section, the dissertation is organized in five well-defined chapters which are summarized below.

Chapter 1 entitled *'Dissertation summary'* presents the dissertation overview, where the most relevant aspects of this thesis are briefly introduced.

Chapter 2 entitled *'Introduction to monitoring in Organ-On-a-Chip systems'* describes the background of the OOC models, with an overview of the evolution of the cell culture systems and the monitoring tools for the analysis of OOC systems.

Chapter 3 entitled *'Microfabricated electrochemical sensors for measuring externally to an Organ-On-a-Chip'* is focused on the first main objective of the thesis; the development of a monitoring tool to analyze parameters externally to the OOC systems using microfabrication techniques. This chapter has a short

introduction to the conventional microfabrication technology and an overview of the electrochemical sensors used in this work. Next, two developed monitoring devices are described and validated in two published papers. The first work **(Paper I)** describes the complete characterization of an array of eight electrochemical oxygen sensors fabricated in a rigid substrate validated in a biofilm grown in a microfluidic flat-plat bioreactor. The second work **(Paper II)** evolved with the fabrication of a single low-cost microfluidic multisensing platform that can be connected at the inlet and outlet ports of a microfluidic OOC system for the simultaneous measurement of DO, Na^+, K^+ and pH compounds, for the specific case of monitoring a renal tubular tissue. This second work describes the fabrication and characterization of each sensor and is applied to urine samples obtained, in order to simulate the output of a renal tubular OOC system.

Chapter 4 entitled *'Inkjet-printed electrochemical sensors embedded in an Organ-On-a-Chip'* is dedicated to the second main objective of the thesis; the development of sensors to be integrated inside theOOC system by using inkjet-printing technology. This chapter has a short introduction about printed electronics and inkjet printing technology including a review about the use of Inkjet printing (IJP) for the development of electrochemical sensors **(Paper III)**. Next, it is demonstrated the potential of inkjet printing technology as an alternative to standard microfabrication techniques in the area of micro-sensors by the fabrication of DO sensors on a flexible and polymeric substrate **(Paper IV)**. In a second stage, it is developed the integration of the DO sensors fabricated by inkjet-printing embedded in the OOC systems, directly fabricated on the delicate, ultraflexible and porous cell culture membrane and validated with an hepatocyte cell culture for Liver-On-a-Chip system **(Paper V)**.

Chapter 5 entitled *'Conclusions and future work'* summarizes the main conclusions of this thesis, as well as conclusions that are drawn from the research.

1.3   Thesis framework

The main part of this thesis has been carried out in the facilities of the Instituto de Microelectrónica de Barcelona (IMB-CNM) del Consejo Superior de Investigacions científicas (CSIC).

Ana Moya has received a FPI pre-doctoral scholarship granted by the Ministry of Economy, Industry and Competitiveness (MICINN), Spain. This scholarship has given her the opportunity to make two international stays during the thesis period. Ana Moya spent 4 months (April-July 2014) in the Université de Lyon, Institut des Sciences Analytiques, under the supervision of prof. A. Errachid. Ana Moya spent another 4 months (April-July 2015) in the Technische Universität Chemnitz, in the Digital Printing and Imaging Technology group, leaded by prof. R. R. Baumann. Three articles of the five presented articles that compose this thesis and several contributions to scientific conferences have been carried out with the collaboration of both groups.

The work presented in this thesis dissertation has been developed in the framework of two projects funded by the Spanish government DPI2011-28262-C04 and CTM2012-37927-C03 (MINECO/FEDER, EU). Both projects have currently their continuity to DPI2015-65401-C3-3-R and CTQ2015-69802-C2-1-R (MINECO/FEDER, EU).

Introduction to monitoring in Organ-On-a-Chip systems

How science of cell culture systems has evolved into Organ-On-a-Chip (OOC) systems?

What has happened with the evolution of the monitoring tools to analyze these cell culture systems?

The purpose of this chapter is to answer both questions. Here, it is presented a review of the advances in cell culture systems since a broad spectrum of diverse *in-vitro* models of cell culture exists, which differ in their biological complexity, from the simplest two-dimensional (2D) monolayer to the more complex three-dimensional (3D) OOC models. At the same time, it is described the change on the monitoring tools to achieve their integration with these cell culture systems. Microtechnology tools, together with advances in bioengineering, have been fundamental contributions to this progress.

2.1   Cell culture systems

2.1.1   Evolution of cell culture systems

Cell culture is the process by which cells are grown under controlled conditions, generally outside of their natural environment. Environment regulates the physicochemical properties (pH, oxygen, temperature and osmotic pressure) and a suitable medium is required to supply the essential nutrients (amino acids, carbohydrates, vitamins, minerals), growth factors, hormones and gases (CO_2, O_2). These elements provide to the environment a distinct physiological character, and a set of extracellular cues that work in concert to regulate cell structure, function, and behavior [1]. The combination of these biochemical, physical, and physicochemical factors constitutes the cell microenvironment as shown in Figure 2.1.

The composition of essential components was discovered by the physiologist Sydney Ringer more than one century ago and is still used today as the main source for some basal media [38]. He studied different salt solutions containing the chlorides of sodium, potassium, calcium and magnesium suitable for maintaining the beating of an isolated animal heart outside of the body [39].

Cell culture allows the researcher to isolate specific factors for experimentation outside the complex *in-vivo* microenvironment. By doing this, scientists can make logical hypotheses of the effects of those factors, and through controlled experimentation elucidate the mechanisms that regulate cell function. The goal in cell culture is two-fold: to recapitulate as closely as possible the cellular microenvironment while maintaining enough simplicity to achieve statistically significant results in a reasonable amount of time. Often, there is a trade off between these two aspects, and model accuracy is sacrificed for higher throughput, or viceversa.
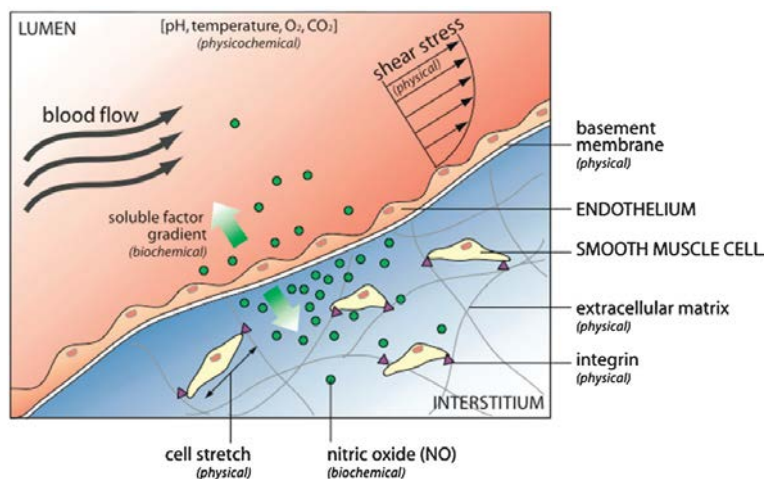
Figure 2.1 | Diagram of a cell microenvironment formed by physical, biochemical and physicochemical factors. Source: [1].

Cell culturing has notably evolved since 1885 when Wilhelm Roux removed a portion of the medulla plate of an embryonic chicken, maintaining it in warm saline for several days on a flat glass plate and establishing the principle of tissue culture [40]. In 1897 Leo Loeb placed skin fragments of guinea pig embryo in agar and coagulated serum, then inoculated into an adult animal and obtained reproduction of mitotic epithelial cells. However, this graft tissues and fluids conducted in a living animal, was not strictly considered as a

cell or tissue culture. The first work with artificial tissue culture is credited to the biologist and anatomist Ross Granville Harrison. In 1907 he deposited fragments of frog embryo in hanging drops of coagulated frog lymph and observed the formation of nerve fibers from protoplasmic extensions [18, 41]. Harrison overcomes challenges of basic culture and developed a reproducible technique using plastic dishes. These dishes are commonly known as the Petri dish and Julius Richard Petri is generally credited with this invention in 1877 [42]. Although our understanding of molecular and cell biology has increased tremendously over the time, the methods used today are surprisingly similar to those employed by Harrison in 1907. We still rely on undefined biological material in plastic dishes for **2D cell culture**.

With the advance of biochemistry, molecular biology, cell biology and other areas of biological knowledge, it has been possible to introduce new techniques to produce new cell culture models. Currently, a broad spectrum of diverse *in-vitro* models of cell culture exists, which differ in their biological complexity. *In-vitro* cell culture systems have evolved from simple 2D monolayer cell cultures of one cell type and **monotypic 3D culture** up to more sophisticated models integrating different cell types in a more physiological relevant cell culture environment. These cell culture systems have been used in different research areas of application. They have been indispensable to study virology and have helped to decrease the use of experimental animals. Otherwise, cell culture has been used in pharmacology and toxicity studies, testing the effect of different drugs, interactions of drug-receptor type, resistance phenomena and cytotoxicity among others. One field of application rather studied in recent years has been tissue engineering. Basically, some studies have been done related to the production of tissue *in-vitro* as skin or cartilage for treatment of burns, auto-grafting, differentiation and induced differentiation [43, 44].

Figure 2.2 shows a diagram of the evolution of the different cell culture systems. This evolution starts from the simplest static two-dimensional monolayers models to the more sophisticated and dynamic three-dimensional co-cultures models. In next sections is described each type of cell culture systems dividing them in two groups: before the introduction of the microfluidics in cell culture systems **(static systems)** and with the use of microfluidics **(dynamic systems)**.

2.1.1.1 Static cell culture systems

Two-dimensional monolayer models

In the traditional 2D monolayer cell culture systems, a single type of cells is adhered and grown on a plastic or glass flat surface as micro-well plates, flaks and Petri dishes. Such monolayer setting allows all the cells to receive a homogeneous amount of nutrients and growth factors from the medium during the growth. The monolayer is mainly composed of proliferating cells, since necrotic cells are usually detached from the surfaces and easily removed during medium change. Although, cell culture conditions can vary for each cell type, and while most of them require flat surface plates others can be grown free floating in culture medium. Most cells in the body are non-circulating, and therefore depend on attachment to the surrounding extracellular matrix (ECM) for survival. Cells are anchored to the ECM via cell-surface integrity that are responsible not only for the physical attachment of cells to the matrix, but also for sens-
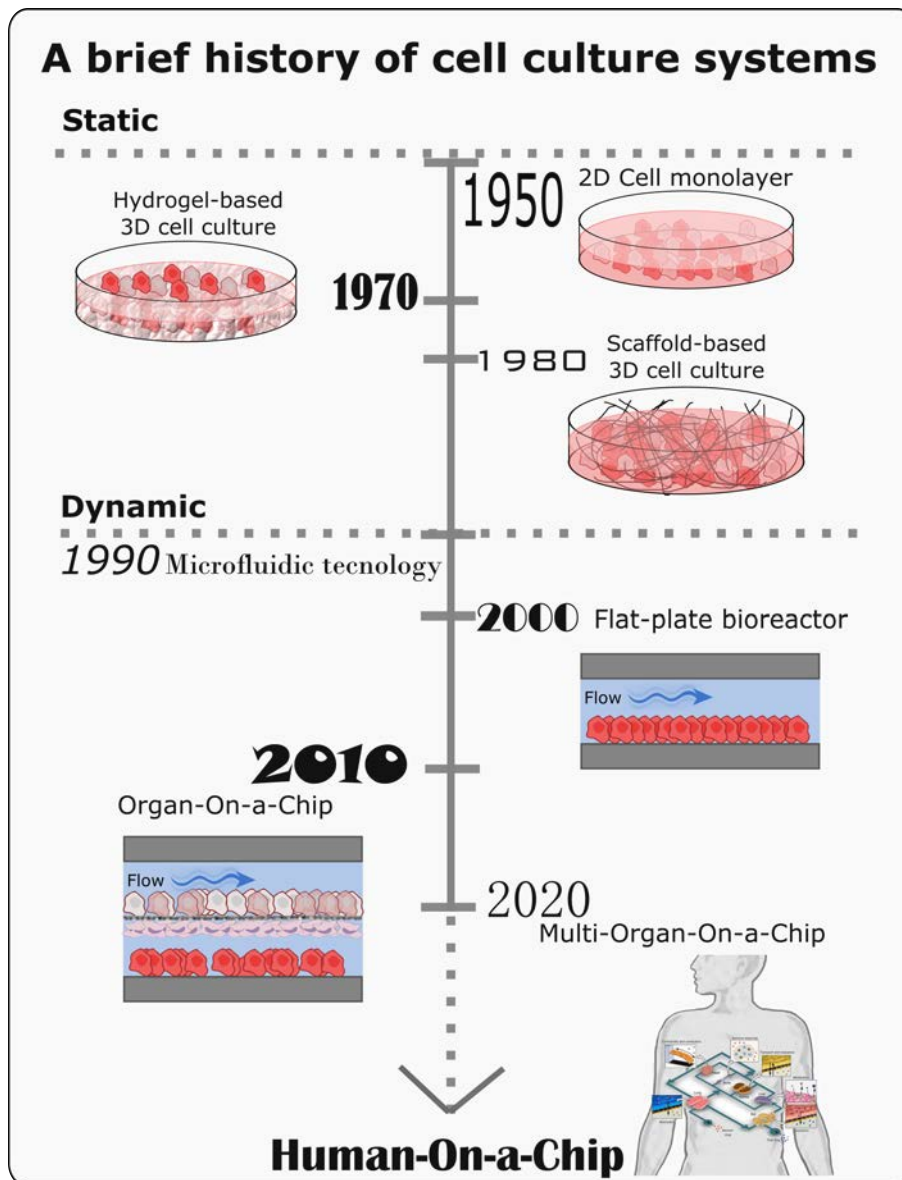
Figure 2.2 | Schematic of the evolution over time of the cell culture systems from the simples 2D models to the complex Organ-On-a-Chip (OOC) models.

ing and transducing mechanical signals from focal adhesion sites to the cytoskeletal machinery within the cell [45]. These signals are known to drive various cellular processes that include migration, proliferation, differentiation, and apoptosis.

During the last century, the majority of cell culture studies have been performed on 2D surfaces because of easy, convenience and high cell viability of these models. These conventional 2D cell culture systems have notably improved the understanding of basic cell biology, but despite their demonstrated value in biomedical research, they cannot support many studies, like, the tissue-specific, differentiated functions of many cell types or accurate predict of *in-vivo* tissue functions and drug activities. Some reasons of this failure are that cells grown in 2D culture are usually more flat and stretch than they would be *in-vivo*.

The abnormal cell morphology in 2D culture influences many cellular processes including cell proliferation, differentiation, apoptosis, and protein expression [46]. In basic cases and applications, the simplicity of 2D cell culture systems is not always an inherent drawback, but, unfortunately, in complex studies where cellular output and communication is important, this simplicity does not accurately represent the entire system of interest and fail to reconstitute the *in-vivo* cellular microenvironments.

Three-dimensional hydrogels and scaffolds models

In conventional 2D cell culture, the structure of the cells changes as they grow, inducing cells distort and flatten, forming a simple monolayer and therefore eliminating the cell-to-cell interactions. Efforts to address the limitations in 2D cell cultures led to the development of 3D cell culture matrices. Maintaining the 3D structure of a cell is a key challenge in cell culture. Various influences determine the phenotype of cells *in-vivo*, including interactions with neighboring cells, interactions with the ECM, and systemic factors [46]. The first 3D cell culture models were developed over 50 years ago [47] based on hydrogels composed of either natural ECM molecules and synthetic polymers. **Hydrogels** are composed of interconnected pores with high water retention, which enables efficient transport of substances such as nutrients and gases. Several different types of hydrogels from natural and synthetic materials are available for 3D cell culture, including animal ECM extract hydrogels, protein hydrogels, peptide hydrogels, polymer hydrogels, and wood-based nanocellulose hydrogel [48].

In the body, nearly all cells reside in an ECM consisting of a complex 3D fibrous meshwork with a wide distribution of fibers and gaps that provide complex biochemical and physical signals. These 3D cell culture matrices, also known as **scaffolds**, were introduced in the 80s to support the formation of 3D matrices [49, 50]. Architectural and material diversity is much greater on 3D matrices than on 2D substrates. These matrices, or scaffolds, are porous substrates that can support cell growth, organization, and differentiation on or within their structure, which induce cells to polarize and to interact with neighboring cells [51]. They can take many forms, including cells randomly interspersed in ECM or clustered in self-assembling cellular microstructures known as organoids [52]. The ability to create scaffolds depends highly on the capabilities of the manufacturing process used [53]. Eric Simon in 1988, showed that electrospinning could be used to produced nano- and submicron-scale polystyrene and polycarbonate fibrous scaffolds specifically intended for use as *in-vitro* cell substrates. During the pass of the time, a number of other techniques were used to create 3D microtopographies that represents a biological structure [54]. In addition, while biomaterial scaffolds have been a mainstay in the field for years, the strategic importance of enhanced biomaterial functionality depends quite heavily on what we learn about cells and tissues.

These 3D models have been very useful for studying the molecular basis cell function. For instance, these models have demonstrated that the matrix stiffness and topography contribute to the nature of adhesion, morphogenesis, differentiation, and viability [55, 56]. Nonetheless, they also have limitations. Organoids are highly variable in size and shape, and it is difficult to maintain cell in consistent positions in these structures for extended analysis. Another drawback of these 3D models is that functional analysis of entrapped cells is often hampered by the difficulty of sampling luminal contents, and it is difficult to

harvest cellular components for biochemical and genetic analysis. Furthermore, cells are usually not exposed to normal mechanical cues, including fluid shear stress, tension and compression, with influence the cell culture function. The absence of fluid flow also precludes the study of how cultured cells interact with circulating blood and immune cells. For this reason, with the evolution in microengineering strategies, the introduction of microfluidics systems have introduced new complex systems to realize the cell culture nearest to reproduce *in-vivo* conditions [57].

2.1.1.2 Dynamic cell culture systems

Nearly three decades ago, microfluidic technology started to be applied to biological assay in order to solve the limitations that cell culture systems based on static models had. Microfluidics technology was through to overcome the main static difficulties to mimic *in-vivo* cells function [58]. Microfluidics provide control over many system parameters that are not easily controlled with the 3D static cultures (scaffolds or hydrogels), overcoming their limitations and facilitating the study of a broad array of physiological phenomena [58].

Microfluidic technology was found in the early 1990s and dramatically grew in the field of chemistry, physics, biology and special in cell research. Research in microfluidic was initially dominated by studies in chemistry and physics at the microscale [59]. Once knowledge was made available on how to exploit the chemical and physical aspects of microfluidics, it was used to benefit in biology field. Microfluidic systems represent a new kind of cell culture vessel that expands the ability to control the local cellular microenvironment [60]. The strengths of microfluidic cell culture mainly come from changes of some physical properties when the scale of culture systems is reduced [30]. The physical design of microfluidic devices affects the cell microenvironment of cultured cells [61]. Design considerations for useful application of microfluidic devices in cell biology were described by Walker et al. [62], who introduced the concept of effective cell culture volume as an indicator of cellular control over the microenvironment in the cell culture device.

A wide variety of microfluidic cell culture models have been developed to mimic and control the cellular microenvironment [1]. The first dynamics systems were based on the simple 2D cell cultures. These **2D perfused systems**, in contrast to static cell culture models, have been shown to better sustain liver cell functions [63]. The perfused culture system are designed to precisely control the *in-vitro* cell culture environments by regulating the exchange of nutrients as well as the presentation of both chemical (e.g. soluble stimuli) and physical (e.g. mechanical, electrical) signals [19]. However, these 2D systems, although they better mimic a real microenviroment than static systems, provide misleading information and more realistic models with the used of co-cultures emerged as **flat-plate culture systems**. In these systems, the cells are able to adhere to the plates in order to create an homogeneous microenvironment, as well as the culture medium can adequately come into contact with seeded cells, which allows sufficient mass transfer. In addition, such a system can easily be scaled up and allow high-throughput screening or studying of zonation-dependent phenomena involving drug metabolism and toxicity [64]. One major disadvantage of flat-plate culture systems is that the cells are exposed to high-shear stress. Consequently, they may detach

from their scaffold and quickly lose their viability and function because they are anchor-dependent cells. One of the first complete studies of adherent cell culture in a flat-plate system was performed by Tilles et al. [65]. They constructed a microchannel microfluidic system from polycarbonate and glass, and primary rat hepatocytes were seeded in co-culture with fibroblasts. The authors found that increasing flow rate led to diminished viability and function. At low flow rates, hepatocyte function remained stable for 10 days.

So far, progress in the area of biology-related microfluidic systems has been mostly in proof-of-principle demonstrations, with large research efforts toward testing the behavior of various cell types in different geometries and on different platforms [26]. However, general progress has been somewhat hindered by the lack of a complete understanding of why living cells behave differently when moved from macroscale culture to confined microscale geometries [66].

During the last decades, thanks to the continued progress in microfabrication and microfluidics, there has been tremendous effort in the development of systems to mimic the natural phenotype of the cells in 3D environments [67]. The final goal of these systems is the development of *in-vitro* models of human organs, and they have been named **Organ-On-a-Chip (OOC)** systems [58].
OOC systems are microfluidic devices for culturing living cells in continuously perfused chambers in order to model physiological functions of tissues and organs [25]. It offers great capabilities to create miniaturized *in-vivo* physiological models that mimic cell interactions and simulate the body metabolism in both the healthy and diseased states. The simplest construction of these OOC systems is based in a single, perfused, microfluidic chamber containing one kind of cultured cell that exhibits functions of one tissue or organ type. In more complex designs, two or more microchannels are connected by porous membranes, lined on opposite sides by different cell types, to recreate interfaces between different cells. These systems can incorporate physical forces, including physiological levels of fluid shear stress, cyclic strain and mechanical compression [68].

More recently, the integration of an increasing number of functional organs on one platform holds great promise to build a **Human-On-a-Chip** systems [69]. This concept is also commonly called Multi-Organ-On-a-Chip when two or more organs are developed in connected microfuidics systems. First attempts to combine multiple organs have already been made [69–72]. Shuler et al. [73] is one of the first published works and their platform features a lung, liver and other tissues compartment and revealed the enormous potential of multi-organ integration. This goal is not an easy task due to many challenges such a maintaining variety of cell types on one device, use of a re-circulating common medium, replicating inter-organ interactions, and transport of nutrients and soluble factors at a physiologically relevant level. This technology is still in its infancy. However, despite their difficulties, the future direction relies on the development of multi-organ-chips with the ultimate goal to build a Human-On-a-Chip system as a promising bright future in industrial and medical applications.

2.1.2   Main applications of an Organ-On-a-Chip system

In-vitro models of human cell culture have the potential to assist in understanding the physiological events that characterize the human immune response [74]. For this reason, OOC systems have become a powerful tool to avoid drug testing in animals. For many years, animals have been often used as models to study human response [75] and have been successfully used to enhance the understanding of the human disease and have made significant contributions to the development of powerful therapies [76]. However, such models inevitably display differences from the human metabolism and the disease state and therefore may correlate poorly with the human conditions [77, 28, 27]. It becomes clear that the significant differences between human and animal metabolism requires the use of human cells. New approaches increasing the biological relevance of cell culture models are of great interest to the life sciences community.

The simplicity of traditional *in-vitro* models, usually consisting of a single cell type, making them robust enough and suitable for high throughput research, but unfortunately providing only little biological relevance to the complex biological function of the human body since their simplicity poorly represent complex pathophysiology behaviour that not closely mimic the *in-vivo* microenvironments [78, 79]. On the contrary, OOC models are biomimetic systems that represent key functional units of living human organs, providing advantages over the 2D culture models. These microenginnering co-culture models recapitulate the complex interactions between different types of cells [80] from a single atom to a multi-organ system in order to mimic a complete body system. These systems could be used as specialized *in-vitro* models that permit simulation, mechanistic investigation and pharmacological modulation of complex biological process [21].

These cell-based assays have been an important pillar of the drug discovery process to provide a simple, fast, and cost-effective tool to avoid large-scale and cost-intensive animal testing. Due to the relative simplicity of these systems, compared to animal models, it becomes possible to investigate cell signaling by monitoring the metabolites transported from one tissue to another in real-time. This allows studying detailed physiological events and in consequence understanding the influence of metabolites on a specific tissue/organ function as well as on the healthy/diseased state modulation.

Following are described some of the most relevant publications related with the cell culture of different type of organs, with the common main goal to study their function or/and their response to some drugs.

Lung-On-a-Chip
Huh et al. [2] described the first biomimetic microsystem that reconstructs the critical functional alveolar-capillarity interface of the human lung (Figure 2.3). Their device reproduce complex integrated organ-level responses to bacteria and inflammatory cytokines introduces in the alveolar space. The microsystem combines microfluidics and controlled vacuum to produce cyclic stretching, enhancing epithelial and endothelial uptake of nanoparticles and stimulating their transport into the microvascular channel.
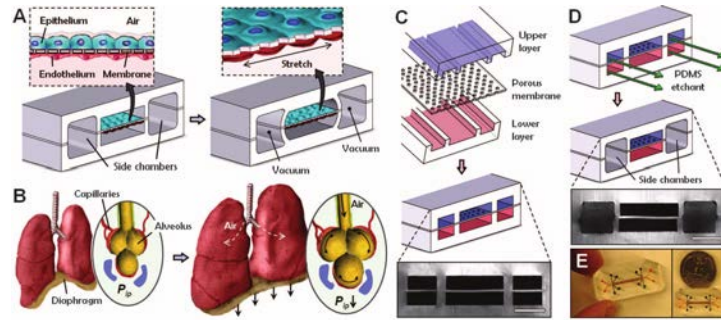
Figure 2.3 | Biologically design of a human breathing Lung-On-a-Chip microdevice. (A) The microfabricated lung mimic device uses compartmentalized PDMS microchannels to form an alveolar-capillary barrier.(B) Inhalation process in the living lung. (C) Microchannels formed with PDMS containing an array of through-holes with an effective diameter of 10 μm. (D) Two large side chambers to which vacuum is applied to cause mechanical stretching. (E) Images of the microfluidic device. Source: [2].

Gut-On-a-Chip

Kim et al. [3] described a biomimetic Gut-On-a-Chip microdevice composed of two microfluidic channels separated by a porous flexible membrane coated with ECM and lined by human intestinal epithelial cells that mimics the complex structure and the physiology of living intestine (Figure 2.4). This microdevice recapitulated multiple dynamic physical and functional features of human intestine that are critical for its function within a controlled microfluidic environment that is amenable for transport, absorption, and toxicity studies, and hence it should have great value for drug testing as well as development of novel intestinal disease models.
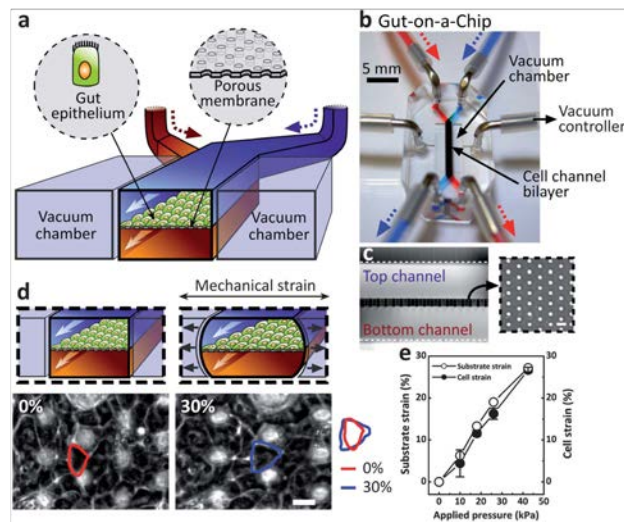
Figure 2.4 | (a) A schematic of the Gut-On-a-Chip device showing the flexible porous membrane, (b) a photographic image of the device composed of clear PDMS elastomer, (c) a cross-sectional view of the top and bottom channels (both 150 μm high), (d)schematics (top) and phase contrast images (bottom) of intestinal monolayers cultured within the Gut-On-a-Chip in the absence (left) or presence (right) of mechanical strain, (e) quantization of the mechanical strain produced in the PDMS membrane (open circles) and in the adherent gut epithelial cells (closed circles) as a function of pressure applied by the vacuum controller. Source: [3].

Liver-On-a-Chip

Bhise et al. [4] reported the development of a Liver-On-a-Chip platform for long-term cell culture of 3D human spheroids for drug toxicity assessment (Figure 2.5). The engineered bioreactor could be interfaced with a bioprinter to fabricate 3D hepatic constructs of spheroids encapsulated within photocrosslinkable gelatin methacryloyl hydrogel. Moreover, the designed bioreactor allowed the *in-situ* monitoring of the culture environment by enabling direct access to the hepatic construct during the experiment without compromising the platform operation.
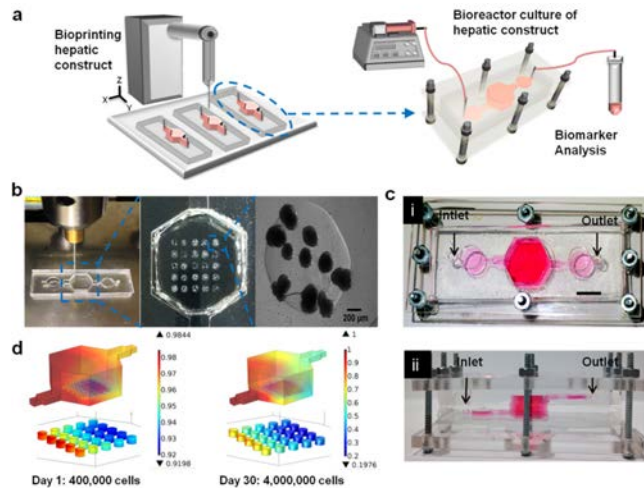
Figure 2.5 | (a) Schematic of the hepatic bioreactor culture platform integrated with a bioprinter and biomarker analysis module, (b) bioprinting photocrosslinkable hydrogel-based hepatic construct within the bioreactor as a dot array, (c)(i) top-view (i) and side-view (ii) of the assembled bioreactor with the inlet and outlet fluidic ports as indicated, and (d) oxygen concentration gradient in the bioreactor. Source: [4].

Kidney-On-a-Chip

One of the first Kidney-On-a-Chip system was developed by Jang et al. [5]. They studied a renal tubular epithelial cell culture exposed to luminal shear stress and a transephitelial osmonic gradient, using a collection Duc-On-a-Chip (Figure 2.6). They demonstrated the effects of changes in the luminal or basolateral microenvironments testing a wide range of parameters with the aim of developing a simple tool for drug screening for study renal physiological and patophysiological parameters.
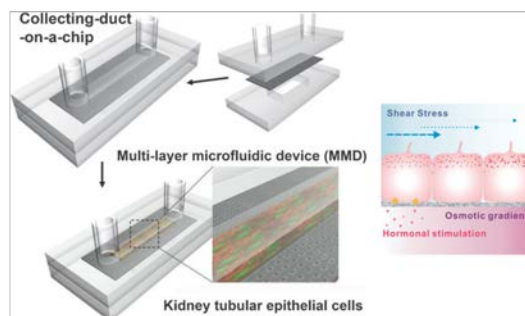
Figure 2.6 | Schematic of the Duct-On-a-Chip with renal cells culture inside the channel used to study the effect of changes environmental parameters. Source [5].

Table 2.1 summarizes the main works related to microphysiological OOC models that have been developed in the last decades to mimic organ and tissue, such as: kidney, lung, intestine, etc. and their applicability. Mainly they were used in drug tests. Still, even though a lot of important factors from the microenvironment that can be artificially engineered *in-vitro* have been identified, a huge challenge remains. Namely, how to design and build *in-vitro* systems that generate these microenvironmental factors in a straightforward, high-throughput and reproducible way. The high complexity of these models becomes more unpredictable and more prone to variations based on slight differences in the starting situation. This unpredictability of the model leads to less robust measurements. For this reason, the most widely used *in-vitro* models are still based in simple conventional assays.

	Cells type	Applications	Ref
Lung-on-a-Chip	Alveolar epithelial and endothelial cells. Airway epithelial cells. Pulmonary microvascular endothelial cells.	Response to bactia and cytokines. Toxicity study of silica nanoparticles.	[2, 70, 81, 82] [83]
Liver-on-a-Chip	Hepatocytes. Vascular enodothelial cells. Stelar cells. Kuppffer cells. Fibroflast.	Maintain phenotypic functions and simulated morphology of lobules. Toxicity testing.	[84–87]. [88][4]
Kidney-on-a-Chip	Renal tubular epithelial cells.	Molecular transport.	[89, 5, 90].
Gut-on-a-Chip	Intestinal ephitelial cells. Enterocytes. Globet cells.	Absorption, distribution, metabolism, elimination and toxicity studies.	[3, 22, 91, 92].
Tumor-on-a-Chip	Tumor spheroids.	HTS screening of single and combinatorial arrays.	[93–95].
Vessel-on-a-Chip	Endothelial and smooth muscle cells.	Growth of microvasculature; studying the effects of chemokines.	[96, 97]
Human-On-a-Chip	Slices of whole organs	Studying effects of drugs on multiple organ systems.	[70, 98, 72, 79].

Table 2.1 | Summary of microengineered Organ-On-a-Chip models and their main applications.

2.2 Monitoring techniques

2.2.1 Advances in monitoring tools for cell culture systems

The ability to monitor live cells *in-vitro* is critical for cell biology research. Direct monitoring of cells in real-time in specific and changing environments has become a valuable strategy for understanding biological processes and is now redefining the ways that we learn and use cells in laboratory. Process in live-cells

monitoring tools are in continuous progress day by day. The recently developed techniques allows to capture valuable parameters, to take decisions from cellular data over time, and at a scale, that was previously impossible.

Monitoring tools cover a broad type of techniques, related with cell imaging and sensors for measuring physico/chemical parameters. In this section, an overview of the evolution of the most relevant monitoring tools to evaluate cell culture systems is described.

2.2.1.1   Monitoring tools for static cell culture systems

Methods used to measure process have largely changed to be adapted depending on their challenge. Though it was invented more than 400 years ago, the **optical microscope** is still the leading visualization tool and one of the gold standards for biological analysis. In 1653, Petrus Borellus wrote the first publication on the use of microscope in medicine [99]. He described 100 observations and applications, including how to remove ingrowing eyelashes that are invisible to the naked eye. However, the first real use of the microscope in biological field is attributed to Antony Van Leeuwenhoek, who in the late 17th century fabricated his own microscope with high quality lenses and he saw bacterias, yeast and blood cells [100]. The microscope has been improved and modified for better observation of cells and microorganisms. As a result, cell theory has been created and modified to be what we know today.

During the past century, several microscopy modalities emerged, finding numerous techniques such as fluorescence microscopy, differential interference contrast microscopy, phase contrast microscopy, dark field microscopy, confocal microscopy, etc. In the last two decades, these methods became even more powerful with the introduction of super-resolution techniques to break the diffraction limit of conventional microscopy systems [101]. The advances in computational tools and automation make the microscope an instrument that can access all scales and it is still imperative in the modern biology studies [102]. The substantially evolution of microscopic techniques over years makes them the conventional method par excellence for monitoring cell culture systems.

The conventional 2D cell culture system developed in Petri dishes described in section 2.1, basically used microscopes [103] and **fluorescent techniques** [104] for their analysis. Advances in microscopy technology and fluorescent intrallecular probes provide researchers unprecedented access to the inner dynamics of living cells. Some of the drawbacks found in these conventional techniques are related with sample manipulation, destabilization of measured signals due to interventions to load a sample since cell assays usually involve rather large sample volumes, coupled to the time-consuming experiments and mostly due to the lack of processes automation. Despite these drawbacks, the majority of studies currently performed still rely on static 2D monolayer culture on Petri dishes with the used of the microscope as a main monitoring tool. To facilitate handling of samples, standard processes of cell observation and characterization rely on cell fixation. However, fixed-cell assays are invasive techniques which only permit observation of cells at endpoints of the experiments, with limited possibilities to extrapolate kinetics or reveal slow, transient or rare cellular events that can only be observed in real-time.

With the evolution of the cell culture system, there was a growing need of time-lapse investigation for better characterization of cell populations, for example, to study cell proliferation, morphology, cytotoxicity, cell variability, cell-cell interaction, cell-substrate interaction, etc. The evolution of the studies in the conventional cell culture systems is highly dependent on the development of sensors technology for monitoring and controlling culture media parameters. An alternative form of measuring cell behavior that replaced the commonly used microscopic observations utilizes electrical sensing. **Chemical sensors** were introduced in the biological field at the beginning of 20th century. Chemical sensors types are defined in Chapter3. Electrochemical sensors, together with optical sensors are most used types of chemical sensors. The history of **electrochemical sensors** starts basically with the development of the glass electrode by Cremer in 1906 [105]. He was the first to report that an electrical potential which develops across a glass membrane is proportional to the pH difference across that membrane. The pH glass electrode application in biology was the pioneering work of F. Haber and Z. Klemensiewicz in 1908 [106]. A next step in the use of the pH glass electrode was taken by Phyllis Margaret Tookey Kerridge, who in 1925 used it for analysis of blood samples [107].

From the invention of the glass electrode, other ion monitoring sensors were further developed using the same basis. Sodium and potassium are important ions to be controlled in a some types of cell culture systems, as they are developed in this work, they will be widely introduced in Chapter 3. First sodium sensor was introduced in 1925 [107], however, it was not until 1957 that George Eisenman [108] develop a working sodium glass electrode. Potassium sensor took longer to become available, and it was not until 1970 when a functional potassium sensor was used [109].

During the following years, more relevant parameters for continuous measurement in biological media were developed based on chemical sensors. Among them, oxygen is an important regulator parameter in cell culture systems and its monitoring is of great importance since oxygen plays a crucial role in the behavior and viability of many types of cells as well as the properties of human organs [110]. The performance and evolution of the oxygen electrochemical sensor is also introduced in Chapter 3. The first oxygen sensor was developed by Leland C. Clark in 1956 [111]. His first version was designed to measure the concentration of oxygen in blood samples. In 1960 emerged the development of a **biosensor**, when Clark also described the first glucose biosensors used in blood samples [112, 113]. Biosensors are defined as specific types of chemical sensors comprising a biological recognition element and a physico-chemical transducer. These sensors have gained increased interest for the study of cell cultures and currently are widely used in the investigation for toxicological screening and for drug testing [114, 115].

As it has been mentioned, together with the electrochemical sensors, other type of chemical sensors widely used in biology are the optical sensors [116]. The invention of lasers in 1960s opened a new window for researchers to study the optical fibers for data communication, sensing and other applications in the next decade. Development of optical sensors started in 1977 even though some isolated demonstrations were made in earlier days like the work of Bergam in 1968 who described one of the first oxygen sensor [117] which was subsequently applied in biology by Lübbers and Optiz, in 1975 [118].

At the same time, these sensors evolved into new types of pysico-chemical measurements experimenting an important change related with their miniaturization. Thanks to the evolution of microtechnology, the macroscopic electrodes started to be reduced in dimensions with the objective to be used within the cell culture systems in a less invasive way and with the possibility to deliver real-time and online information. Most metabolic processes are dynamic and occur on time scales of few minutes or even less. Thus, studying time-resolved responses of cell cultures to environmental changes or upon the application of a defined compound dosage often requires continuous read-out to ensure that occurrences of important events are not missed.

The advent of microfabrication allowed the replacement of traditional electrochemical cells and bulky electrodes with easy-to-use sensing devices and has led to significant advances in the development of miniaturized solid-state electrochemical sensors and sensor arrays. These miniaturized sensors are described in Chapter 3. The same happened with the biosensors [119] and the optical sensors [120].

With the same objective to integrate miniaturized monitoring systems to measure real-time parameters appeared the planar electrodes [121]. In 1972, Thomas et al. [122] published the first paper describing a planar **Multielectrode array (MEA)** for use in recording from cultured cells. The **MEA** poses an alternative to the tradition glass micropipette electrode with a major application in the field of neural stimulation and recording [123]. Micropipette electrodes were invented by Ralph Wlado Gelfan in 1927 [124] and their first application in biology for the specific purpose of electrical stimulation is attributed to Ralph Wlado Gerard [125] in 1930. Therefore, **MEA** have also been successfully used to investigate growth and migration of monolayer cell cultures [126].

The evolution to the 3D cell culture using hydrogels or scaffolds systems increased the way to study the biology, achieving more predicted results. These types of 3D cell cultures are basically analyzed using conventional microscope techniques. With the evolution of the microscopes (scanning electron microscopy and confocal fluorescent microscopy) it has been achieved the morphological studies of the cell attachment on the surfaces of the 3D constructs [127]. The need for a quick and economical method that allows visualization of the 3D distribution of cells still exists while also allowing quantification of distribution and infiltration in the scaffold is required.

Other conventional monitoring techniques

Inmunoassay methods are conventional monitoring techniques routinely applied in all the biological laboratories. An immunoassay is a biochemical test that measures the presence or concentration of a macromolecule or a small molecule in a solution through the use of an antibody or an antigen. Rosalyn Sussman Yalow and Solomon Berson are credited with the development of the first immunoassays in the 1950s [128]. The **enzyme-linked immunosorbent assay (ELISA)** is the most frequently applied type of assay. It is a popular format of "wet-lab" type analytic biochemistry assay that uses a solid-phase enzyme immunoassay (EIA) to detect the presence of a substance, usually an antigen, in a liquid sample or wet sample. ELISA was invented by Eva Engvall and Peter Perlmann, they published the first paper on the ELISA procedure in 1971 as a replacement for radioimmunoassays [129].

Also a routinely used the technique is **cell staining**. Cell staining is a necessary and useful technique for

visualizing cell morphology, structure and cell viability under a microscope. Other important applications of the technique are proliferation studies, to identify the type of cell or the expression of a protein or to observe different cell population.

The main drawback of these conventional methods is that all of them must be done at the end of a growth experiment, which implies the cell death and in an offline way. Also, some of them require long assay time and sometimes involve troublesome liquid-handling procedures and large quantitative of expensive antibody reagent. Despite this high drawback, these technique continue being the most used.

2.2.1.2 Monitoring tools for dynamic cell culture systems

All the monitoring methods described until now has been designed primarily to meet the requirements of static cell culture systems. As previously explained in section 2.1, the necessity to develop more sophisticated models for the mimetic of *in-vivo* microenvironment involves the use of microfluidic systems. With the emergence of the microfluidic technology, a new challenge appear to combine the integration of microfluidics and monitoring tools with cell culturing units without disturbing them [130], which means without interrupting the overall culturing process by sampling of medium, increasing the risk of contamination. **Lab-On-a-Chip (LOC)** system is a more general idea derived from the miniaturized total chemical analysis system (μTAS) concept that was proposed by Manz et al. in 1990 [131]. LOC systems emerged as a powerful fields creating new opportunities for sample preparation and processing on a single chip. A LOC is a miniaturized device that integrates into a single chip one or several analysis, which are usually done in a laboratory. Miniaturization of biochemical operations normally handled in a laboratory has numerous advantages, such as cost efficiency, parallelization, ergonomy, diagnostic speed and sensitivity.

Despite Manz work was presented in 1990, the first real LOC systems was set in 1979, when a miniaturized gas chromatograph was realized on a silicon wafer by Stephen Terry et al. [132]. However, major LOC research began in the late 80s with the development of microfluidics and the adaptation of microfabrication processes for the production of polymeric devices. Microfluidic technology allows the analysis and use of reduced volume of samples, chemicals and reagents minimizing the global fees of applications. In LOC systems many operations can be executed at the same time thanks to their compact size, shortening the time required for experiments. They also offer a substantial parameter control, which allows to automate the process while preserving the performance. They have the capacity to both process and analyze samples with minor sample handling. Although LOC system has multitude of advantages, it still has many limitations. In Table 2.2 main advantages and limitations of LOC are summarized and compared to conventional monitoring tools.

Centering in the sensing task, microsensor technologies have been developed over the past several decades for a variety of applications. Various important tasks had been miniaturized taking advantages of the use of the LOC, including cell culturing [133][23], cell separation and sorting [134][135], cell lysis [136], DNA and RNA amplification [137], fluorescent labeling [138], analytical techniques for micro-arrays [139], and sens-

Lab-On-a-Chip (LOC) system

LOC Advantages	LOC Limitations
Low Cost: Numerous tests performed on the same chip, reducing the cost of each individual analysis.	**Industrialization:** Most LOC technologies are not yet ready for industrialization. Currently, fabrication technologies are not standard.
High parallelization: Their capacity for integrating microchannels, LOC allows that several analysis can be performed simultaneously.	**Signal/noise ratio:** When miniaturization increases the signal/noise ratio also increases. LOC provides poorer results than conventional techniques.
Ease of use and compactness: Diagnostics using LOC requires a lot less handling and complex operations.	**Ethics and human behaviour:** Without regulations, real-time processing may generate some fears of the untrained public diagnosing potential infections at home.
Reduction of human error: Since it strongly reduces human handling, automatic diagnoses reduce the risk of human error compared with classical analytical processes.	**Needs an external system to work:** Even if LOC devices can be small and powerful, they require specific machinery such as electronics or flow control systems to be able to work properly. External devices increase the final size and cost of the overall system.
Faster response time and diagnosis: At the micrometric scale, diffusion of chemicals, flow switch and diffusion of heat is faster.	
Low volume samples: Because LOC systems only require a small amount of sample for each analysis, decreasing the cost of analysis by reducing the use of expensive chemicals.	
Real-time process control and monitoring: One can control in real-time the environment of a chemical reaction in the LOC, leading to more controlled results.	
Expendable: Due to their low price, automation and low energy consumption, LOC devices be able to be used in outdoor environments without the need for human intervention.	
Sharing the health with everybody: LOC will reduce diagnostic costs, the training of medical staff and the cost of infrastructure. As a result, LOC technology will make modern medicine more accessible to developing countries at reasonable costs.	

Table 2.2 | Advantages and limitations of a Lab-On-a-Chip system compared with conventional tools.

ing [140]. Their miniaturized size and versatile features as well as their high sensitivity and low-detection limits enable monitoring of various analytes in cell culture systems at high temporal and spatial resolution. Microsensors systems have to be low-cost and compatible with microfluidic system with the capability to measure in real-time and continuous mode without sampling, against other techniques that involves manual

sampling and sometimes with a previous sample preparation before measurement at discrete time points. This makes LOC applications suitable for clinical diagnostics and 'near-patient' or Point-of-Care (POC) testing. In many ways, the features of LOC devices fulfil the requirements for a POC diagnostic device: low consumption of reagents and samples, miniaturization of devices and fast turn-around time for analysis.

Although such microfluidic and micro electromechanical systems have achieved high levels of integration and are capable of performing various important tasks on the same chip such as cell culturing, sorting and staining, imaging of these LOC platforms still rely on conventional microscope systems [141] [142]. This might partially limits their potential impact, especially for POC applications. In this context, novel approaches are emerging using microfluidic technologies coupled with high-resolution live-cell imaging provide the possibility to study cells at both single and multicellular levels while controlling cell growth and environmental stimuli [143].

2.2.2 Overview of monitoring techniques for Organ-On-a-Chip systems

During the last two decades, with the emergence of OOC systems, the design principles of LOC devices have been extended to platforms of tissue and organ engineering. In the *in-vitro* studies, control of cell culture conditions is of paramount importance in order to achieve results that are as predictive of the *in-vivo* situation as possible. However, as the biological complexity of the cell cultures under investigation increases, the difficulty to integrate monitoring tools with these systems also increases. In consequence, the demand of monitoring tools integrated with OOC systems increase quickly and it is currently a challenge. Conventional analytical methods require manual sample collection from the microfluidic system, large working volumes, and frequent system disturbance, and thus are not suitable for miniaturized OOC platforms. By integrating and automating standard laboratory routines, microfluidics technology allows to overcome these limitations, saving time, resources and improving the quality and reproducibility of the results.

Despite the great promise, creating an OOC system is not a simple process, with a number of obstacles to overcome. The most important of these obstacles are faced when trying to characterize the behaviour of the OOC platforms, especially when real-time, repeated measurements are needed. Due to its great impact in research improvement and efficiency, the overcoming of this challenge is trying to be solved by several research groups, by increasing the degree of complexity of the assays but also yielding more reliable and reproducible results.

2.2.2.1 Currently monitoring techniques

In section 2.1.2 some of the most popular OOC systems have been described. Following is explained the way that these works used for the analysis of some parameters.

The Lung-On-a-Chip microsystem described by Huh et al. [2] simulated a pulmonary inflammation by introducing a medium containing a potent proinflamatory mediator into the alveolar microchannel. They monitored the expression of the intercellular adhesion molecule–1 in real-time using a high resolution, flu-

orescent microscopy.

The work reported by Bhise et al. [4] for the development of a Liver-On-a-Chip platform was designed to allow the *in-situ* monitoring of the culture environment. In their developed system a reservoir tube was connected at the outlet port to collect culture media during the experiment for biomarker analysis without compromising the platform operation.

Jang et al. [5] who developed a Kidney-On-a-Chip system for the study of a renal tubular epithelial cell culture used fluorescent microscopic techniques. To perform the inmmunocytochemistry analysis, they removed the cell culture membrane substrate at the end of the experiment.

The Gut-On-a-Chip described by Kim et al. [3] recapitulated multiple dynamic physical and functional features of human intestine. The evaluation of the tight junction of cell monolayer was done using confocal immunofluorescence microscopy and by measuring trans-epithelial electrical resistance (TEER) using an Ag/AgCl electrode wire and a commercial multimeter which was introduced in both microchannels.

As can be seen above, most of the works presented until now uses conventional monitoring techniques to analyze cell cultures, such as different types of microscopes that can be adapted to the devices to measure in real-time, or collecting samples from the microfluidic channel and making a post-analysis. Other works introduce commercial available sensors increasing the complexity and cost of the whole system.

It is of paramount importance the development of new strategies to control physical and chemical parameters in real-time, and in a cost-effective way. First attempts emerged during this year trying to solve the challenge to integrate monitoring tools with OOC systems. These systems are following described.

2.2.2.2   First attempts to integrate sensing devices

Recently published works, all of them dated in 2017, show different approaches to integrate sensors with OOC systems to perform automated, *in-situ*, real-time and continuous measurement of a variety of parameters that would otherwise be impossible to monitor with conventional monitoring systems.

Zhang et al. [6] build a multi-sensing platform with optical (mini-microscopy), physical (pH, oxygen, temperature), and biochemical (soluble biomarkers) sensors to monitor long term responses of OOC models of disease and drug effects (Figure 2.7). The main drawback of the Zhang system is that sensors are placed externally to the cell culture system and some parameters can only be monitored with the sensors in contact with the cells. To give an example, this could happen for rapid success mechanisms that need to be monitored in real-time, for small concentration changes or because the type of measurement require the integration of the sensor in the cell culture area.
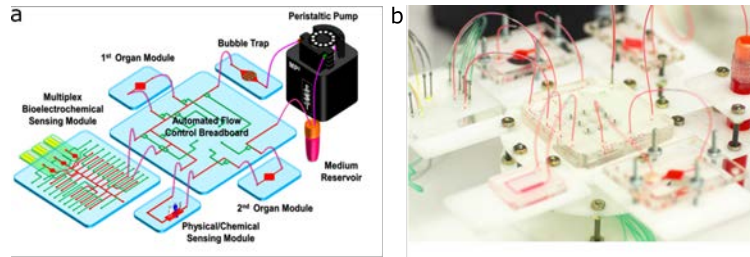
Figure 2.7 (a) Schematic of the integrated microfluidic device consisting of modular components including microbioreactors, breadboard, reservoir, bubble trap, physical sensors, and electrochemical biosensors, (b) Photograph of an integrated platform. Source: [6].

One of the parameters that only can be monitored inside the cell culture system is TEER. OOC with embedded electrodes that enable accurate and continuous monitoring of TEER (Figure 2.8), a broadly used for measuring the tissue health and differentiation, and real-time assessment of electrical activity of living cells. Recently, Henry et al. [7] reported for the first time embedded electrodes for TEER measurements, patterned onto the polycarbonate substrate forming the top and bottom covers of the OOC system.
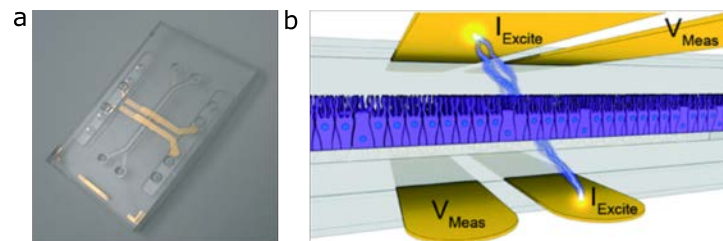
Figure 2.8 (a) Photograph of the assembled TEER-chip, dimensions are 25 x 40 mm, and (b) schematic view of the TEER-chip and 4-point impedance measurement chosen to measure TEER and capacitance. Source: [7].

Another work which integrates sensors embedded in the OOC system is Lind et al. [8]. They introduced a new approach to integrate sensors inside a cell incubator environment fully based on 3D printing techniques for continuous electronic readout of contractile stress of cardiac micro-tissues (Figure 2.9). They used OOC without the use of a microfluidic system, and for this reason, it was easier the integration of the sensing elements.
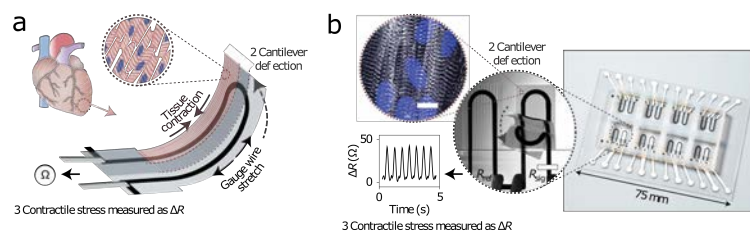
Figure 2.9 (a)Sketch of the device principle. Contraction of an anisotropic engineered cardiac tissue (1) deflects a cantilever substrate (2), thereby stretching a soft strain gauge embedded in the cantilever, and (b) the fully printed final device. Insert 1: Confocal microscopy image of cardiac tissue on the cantilever surface. Insert 2: Images of a cantilever deflecting upon tissue contraction. Insert 3: Resistance signal. Source: [8].

As a last example, Curto et al. [9] presented for the first time the coupling of organic electrochemical transistors with microfluidics to achieve multi-parametric monitoring of living cells (Figure 2.10). Measurement of changes in the cell layer capacitance and resistance during flow over an extended period of time. The sensing elements were placed at the glass bottom cover of the system using conventional microtechnology techniques and the system was also located on a microscope stage.
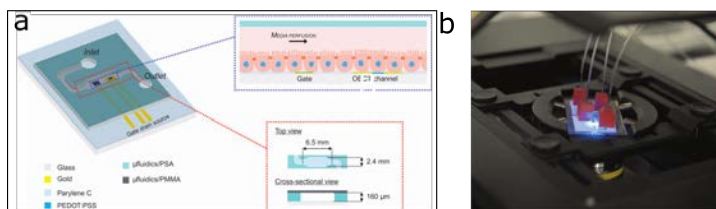
Figure 2.10 (a) Graphical representation of the developed platform integrating the sensing elements with microfluidics, and (b) a picture of a fully assembled microfluidic platform located on a microscope stage. Source: [9].

As can be noticed, there are very few works related with the integration of sensors with an OOC system. Regrettable, it is not only required the integration and automation of analytical tools, there is also a strong need of cost effective and easy-to-use systems over this novel and fruitful technology. The fabrication methods for the different components need to be compatible, and all target features and functions must be preserved over the duration of an experiment; the cell cultures must remain viable and functional, the microfluidic handling needs to be robust and precise, and the sensors must satisfy the detection specifications, including sensitivity and selectivity. Although, OOC systems have drawn attention, integration of complicated microsystems that can closely mimic the *in-vivo* environments still need further optimization. A perfect combination of monitoring tools and systems biology may help in overcoming these challenges.

2.3 Summary of key point in the evolution of cell culture and monitoring systems

In summary, as has been shown in the above sections, *in-vitro* cell culture systems has notably evolved since 1885, thanks to the advance in the microtechnology and bioengineering fields. As shown in Figure 2.11 the appearance of microfluidics technology has been key points in this evolution. Before that, the first attempts to overcome the shortcoming of *in-vitro* 2D models, were based on 3D hydrogels and scaffolds structures. They increased the way to study the biology, achieving more predicted results than the 2D models. With the emerge of the microfluidics, cell culture systems increased in their biological complexity, allowing the development of 3D OOC systems to provide efficient methods to reproduce organs in *in-vitro* conditions. As can be seen in Figure 2.11 the future direction relies on the development of Multi-Organ-on-Chips with the ultimate goal to build a Human-On-a-Chip system being capable of replacing animal experimentation during pre-clinical testing to accelerate the entry of promising drug candidates into the clinical phase. A summary of the advantages and limitations of the different cell culture systems is presented in Table 2.3.
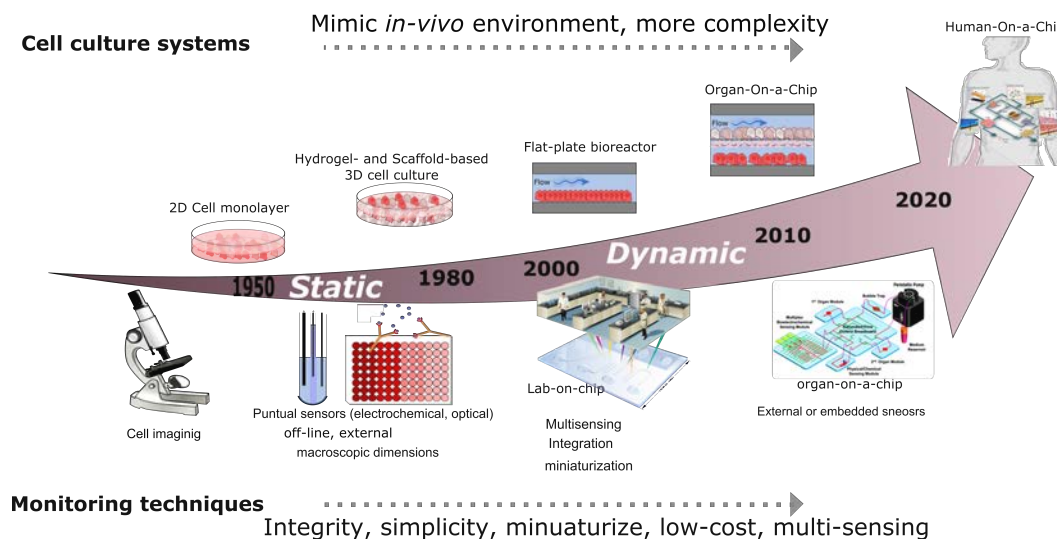
Figure 2.11 | Evolution of the cell culture systems over the time and, in parallel, the
adaption of the monitoring tools to the different cell culture systems.

Related with the monitoring systems, as shown in Figure 2.11, they have also evolved during the years, always trying to meet the requirements of different cell culture systems. The evolution of the studies in the conventional cell culture systems was highly dependent on the development of analysis technology for monitoring and controlling culture media parameters. Advances in microengineering allowed the development of new monitoring tools. More sophisticated techniques has allowed the analysis of a wide range of cell culture parameters. Sensors appeared as an alternative form of measuring cell behavior. During time, chemical sensors have evolved in terms of miniaturization forming part of the LOC systems. The main advantages of a LOC systems are: low contamination risk, easiness of handling and scaling-up to create cost-effective and compact diagnostic tools. The convergence of LOC and cell biology has permitted the study of human physiology in an organ-specific context, introducing a novel model called OOC. However, due to the complexity of the OOC systems, it is not easy to achieve their motorization with integrated LOC tools.

The reality is that as of today, the motorization in OOC systems is mainly based in the same analysis techniques used in the simplest 2D cell culture systems, such as microscopes, ELISA and stains. First attempts to integrate sensors inside the OOC systems have shown the relevance of monitoring in real-time to capture changes in the properties of living cells to obtain complete information about what is happening inside the OOC. However, new ideas and methods must be considered to improve and build a functional OOC with the goal to create a cost-effective and compact diagnostic tool, to allow the study of drugs avoiding the animal experimentation.

	Advantages	**Limitations**	**Motorization**
Monolayer 2D	Simplicity, convenience, cell viability	Not good predication. Non-physiological environment.	Conventional external high-cost systems. Sample collection.
3D hydrogels and scaffolds	Topography and adhesion	Not exposure to normal mechanical cues of body	Difficult to harvest cellular components for analysis. Difficult of sample collection for measuring with conventional systems.
3D microfluidic OOC	Realistic model. Mimic *in-vivo* conditions with mechanical cues of body.	Complexity, proof-of-principle demonstrations	Sampling disturbing microfluidic. High demand of real-time monitoring tools. Not compatible with some conventional monitoring tools.

Table 2.3 Summary of the evolution of cell culture models, defining their advantages and limitations and showing the principal monitoring systems used to analysis the cell culture state and response.

.

Microfabricated electrochemical sensors for measuring externally to an Organ-On-a-Chip

The purpose of this chapter is to develop different sensing tools fabricated using microfabrication techniques in order to measure physicochemical parameters externally to an Organ-On-a-Chip (OOC) system. A brief overview of conventional microfabrication techniques is presented. In addition, since the miniaturized sensors used along this thesis work are based on electrochemical techniques, also, an overview of electrochemical sensors is described.

Concretely, two different approaches are developed. The first one deals with an array of microelectrodes on Pyrex® substrate to perform simultaneous dissolved oxygen (DO) measurements. This device is validated with the DO measurement of a depth biofilm grown in a flat plate bioreactor. The second approach deals with a multi-sensing system fabricated in polymeric substrate. This platform incorporates DO, pH, Na^+ and K^+ sensors addressed to be used in combination with any microfluidic cell culture system. Its applicability is demonstrated with real urine, simulating the output of a renal OOC system.

3.1   Overview of microfabrication technologies

Microfabrication can well be regarded as the major key technology for the creation of most of the devices around us, such as computers, phones, tv, etc. This technology has undergone a sea change in recent years [144]. The role of equipment has been the fuel of this change. New processing steps have been developed and old ones have become cleaner and more sophisticated. Another important reason for the rapid growth of microtechnology is the improved understanding of the physics and chemistry of films, surfaces, interfaces, and microstructures, which has been possible due to the remarkable advances in analytical instrumentation during the past thirty years.

Microfabricated devices, also known as Microelectromechanical system (MEMS), micromachines, microsystems, etc. have several applications attaining commercial or scientific success. Microfabrication techniques have introduced enormous advantages in the fabrication of chemical sensors at the micro scale, such as miniaturization, reduction of sample volumes needed for the measurements, and a decrease in the response time. In particular, miniaturization of sensors has a considerable impact on the most recent developments of monitoring tools for LOC systems.

In a microfabrication process, sensors are fabricated by consecutive deposition and patterning of conductive and insulator materials onto a flat substrate called wafer. Microfabrication involves the combination of a series of lithographic, and additive or subtractive processes to create structures of micrometric and/or nanometric features on a planar substrate [145, 146]. To achieve these goals, the entire microfabrication environment needs to be strictly controlled from the point of view of temperature, humidity, particle concentration and airflow. A cleanroom is a facility with such strict environmental control and is where microfabrication processes take place. An extensive overview of the different techniques involving the microfabrication processes can be found in literature [144–148], while here only a brief summary of the main methods employed in this thesis is described.

Photolitography: Photolitography is at the core of any microfabricated device, as it is the set of operations involved in the transfer of the desired patterns onto a physical substrate. Photolitography involves the use of photosensitive resists that are selectively activated using Ultraviolet (UV) light through a previously designed photomask. Photoresists can be positive or negative depending on the behavior after UV exposure. In the former, the photoresist exposed through the transparent portions of the mask become soluble in a developing solution, while in the latter it becomes insoluble, as shown in Figure 3.1(a). During this process, the wafer and the masks are put into contact during exposure, then they are separated and finally, the exposed photoresist is removed in the developing solution.

Thin-film deposition: Thin-films are deposited for a variety of different purposes in microstructures (masking-materials, structural materials, sacrificial materials, electrical devices, etc.). They are formed by either chemical reaction driven processes or physical processes. In the development of electrochemical devices, the most common deposited materials used are metals and dielectric (insulator) materials. Metals

are used to create electrodes, conducting tracks and contact pads. In this work, metals such as gold and platinum are deposited using sputtering or evaporation methods (Figure 3.1(b)). Evaporation involves the heating of a source material to a high temperature, generating a vapor that condenses on a substrate to form a film [146]. In sputter deposition, a target made of a material to be deposited is physically boarded by a flux of inert-gas ions (usually argon) in a vacuum chamber. Atoms and molecules from the target are ejected and deposited onto the wafer [146]. Noble metals, like gold and platinum, requires the use of an intermediate layer to improve their adhesion to the substrate, i.e. titanium, nickel or chrome. Dielectric materials are often used for electrical isolation of the electrodes. The two most common films are silicon dioxide and silicon nitride. Silicon dioxide could be thermally grown and also deposited via chemical vapor deposition (CVD) while silicon nitride is always deposited using the CVD. In addition, polymeric materials could be also used as passivation layers such as SU-8 and polyimide (PI). In particular, SU-8 is a negative photoresist with optimal dielectric properties and biocompatibility, which are required in biological applications [149].
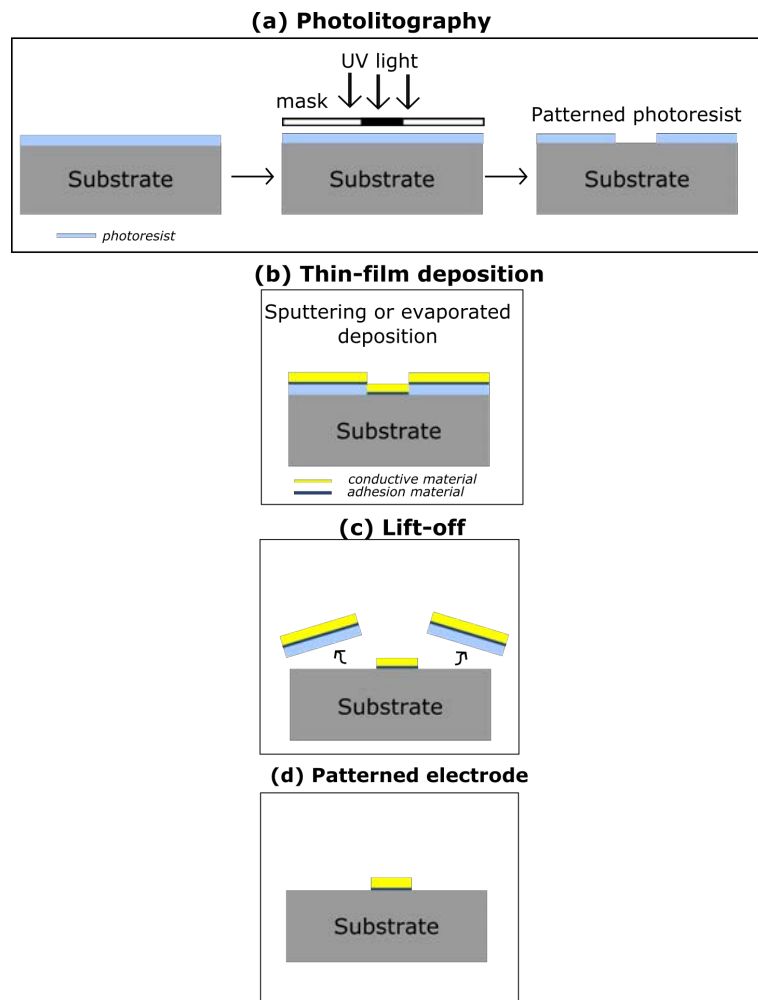
Figure 3.1 Basic microfabrication processes, (a) starting with the photographic step coating of a substrate with a photoresist and exposure through a photomask, (b) deposition of the functional metals, (c) lift-off to transfer the pattern to the substrate and (b) patterned metal on the substrate.

Lift-off: A lift-off process is the combination of a photolithography step where a negative photoresist is structured, a thin-film deposition and the final wash out of the photoresist which remains under the thin-film (Figure 3.1(c)). In particular, the photoresist is removed in a wet bath composed of the appropriate solvent. Acetone is normally used when the mask is a simple photoresist layer, but in some cases strong etchants may be required. Following this strategy, when removing the photoresist the material deposited on top of it is also removed, and only the material that was in the "holes" having direct contact with the underlying substrate stays as it shown in Figure 3.1(d).

3.1.1   Substrate Materials

Due to the importance of microelectronics, silicon is probably the most extensively used substrate in the fabrication of thin-film devices. However, microfabrication has also been demonstrated in glass, some polymers and other substrates like ceramic or compound semiconductors.

Silicon

Silicon is the most common material in microfabrication, owing to its role in the fabrication of integrated circuits. It comes in a single-crystal wafer form, with typical diameters of 75–200 mm and thicknesses of 0.25 – 1.0 mm. In addition to its excellent electrical properties, silicon also possesses outstanding mechanical properties, enabling the design of micromechanical structures [150]. There exists a wide range of ways to micromachine silicon, and the ability to do this in combination with integrated-circuit fabrication leads to the potential to form monolithically integrated microsystems. For biological or medical microsystems, silicon is not usual the material of choice. It is not optically transparent, preventing the use of transmission microscopy, and its cost is expensive for fabricating disposable devices.

Glass

Glass provides some unique features, being the most relevant its optical transparency. Glass wafers are available in many different compositions and sizes. Two important examples are fused silica and borosilicate wafers. Fused silica wafers are pure amorphous silicon dioxide (SiO_2). They can withstand high temperatures ($T_{softening}$ = 1580 °C), are optically transparent down to short wavelengths, and have very low autofluorescence. Borosilicate wafers, of which the most common is Pyrex®, are much less expensive than fused silica (and can be less expensive than silicon). They can be easily bonded to silicon but cannot be exposed to the high temperatures needed for some thin-film depositions and have higher autofluorescence than fused silica. In the first application of this work, which will we described in section 3.3, Pyrex® is the selected substrate for the development of sensors.

Polymers

Polymer is often the least expensive substrate material. The role of polymers as substrate materials is gaining importance in recent years [151][152]. Polymers offer a broad range of parameters as well as material and surface chemical properties which enable micrometric design features that cannot be realized by any other class of materials [153]. They are widely used for disposable devices, which minimize issues of sterilization, clogging and drift. For these reasons, are fabricating polymer microdevices, especially for disposable clinical applications.

Polymers can be divided into three different types depending on their physical properties: thermosets,

thermoplastics and elastomers. The main parameter to be considered in this classification is the glass-transition temperature (Tg), which can be described as the critical temperature at which a non-crystalline material changes its behavior from being 'glassy' to being' rubbery.

- **Thermosets**, or often called resins, are materials that cannot be reshaped once cured. The process of curing changes the resin into an infusible, insoluble polymer network, and is induced by the action of heat or suitable radiation. If heated further, the polymer decomposes or burns instead of melting. Typical examples of thermoset polymers in microfabrication are the epoxy resin are SU-8, PI (Kapton®), polyester (polyethylene naphthalate (PEN), polyethylene terephthalate (PET)), etc. The PI Kapton® was the selected polymer used in this first part of the work as a flexible substrate which is compatible with photolitography techniques.
- **Thermoplastics** are materials that show a distinct softening at Tg, which makes them processable around this temperature. Thermoplastic materials include the technical polymers which can be structured using replication methods like injection molding or hot embossing. The most typical thermoplastic used in microfluidics are poly(methyl methacrylate) (PMMA) and polycarbonate (PC), which were the first materials used for polymer microfabrication [152]. Later, cyclo olefin polymer (COP) has attracted much attention due to their favorable properties [151] and has also been used as a substrate for developing microdevices using photolitographic techniques.
- **Elastomers** or rubbers, are materials which have the ability to undergo deformation under the influence of a force and restore its original shape once the force has been removed. poly(dimethylsiloxane) (PDMS) is the most commonly used elastomer due to its low-cost and easy handling and, despite of its limitations, has become one of the most prevalent materials to manufacture microfluidic devices [154].

However, not all the polymers can be processed with microfabrication techniques. Most of them are incompatible with conventional techniques which involve the use of resins and organic solutions. Thermosetting polymers and some thermoplastic like COP [151] are the only used polymers in microfabrication.

3.1.2 Rapid prototyping techniques

In addition to microfabrication techniques, standard manufacturing techniques may be required for the fabrication of fluidic components and interfaces in order to connect the microsensors with the macro-world [155]. These techniques involve mostly cutting and bonding operations, and extend the range of materials beyond silicon and glass.

Rapid prototyping techniques are used to reduce the cost and time of microfabrication. It is a good practice to design new systems from the outside because ultimately any miniaturized device needs to be interfaced and used in a macro-world [147]. In this work, several cutting techniques are used for the encapsulation of the developed sensors and for the fabrication of the microfluidic cells.

Milling

Milling is among the oldest techniques used in the manufacture of objects, and is very suitable for the

production of electrochemical flow cells [156]. Milling uses rotary cutting tools to carve structures from a block of material (Figure 3.2(a)). The introduction of micrometric sized tools in the 1990s has enabled the fabrication of microfluidic devices [157]. Milling can be used to produce microfluidic channels directly on a suitable substrate such as PMMA, polytetrafluoroethylene (PTFE) or aluminium. However, milling finds its most common application in the fabrication of chip holders and flow cells. Milling is used to produce mm–cm-sized objects with features down to a few hundred microns. Although it is possible to find end-mill tools with diameters down to 35–50 μm, these can only be used by extremely qualified staff running high-end equipment where spindle vibration is strictly controlled.

Blade Cutting

Blade cutting has been around for a long time in the graphic arts industry, where it is routinely used to cut out vinyl and adhesive films. However, it is a relatively new technique in the development of electrochemical devices [158]. This technique is based on a blade mounted on a plotter head, and it can be classified according to how they hold the blade (Figure 3.2(b)). In the most common cases, the blade rotates freely in the head, and the offset between the blade tip and its rotation axis facilitates the orientation of the cutting edge in the cutting direction. These are known as *drag-knife* plotters, and enable the production of structures down to 200 μm. At the other end there are so-called *tangential* plotters where the blade is fixed and the head is rotated and oriented in the cutting direction by a motor. These enable the fabrication of smaller features than *drag-knife* plotters with much higher precision, but they are also significantly more expensive. Blade cutting has been used in the construction of fully functional microfluidic devices made in pressure sensitive adhesive tapes, and also in the development of non complex paper microfluidic devices.

Laser Cutting

Laser cutting works by melting and vaporizing material using a laser beam [159]. An advantage of laser cutting compared to milling or blade cutting is that it is a contactless technique, which means that the material does not suffer mechanical stress during the cutting operation (Figure 3.2(c)). Different laser types are used for manufacturing and prototyping. Desktop and low-power CO_2 lasers (10.6 mm wavelength, in the long-infrared range) are an excellent choice for prototyping purposes, as they enable working on a wide range of materials barring carbon and metals, and some other high-density materials [160]. Laser cutting is faster than milling, but the high local temperatures achieved around the cut line can lead to problems such as the formation of burn in some polymeric materials, or to cracking of brittle materials such as glass and ceramics.

(a) Milling   (b) Blade cutting   (c) Laser cutting
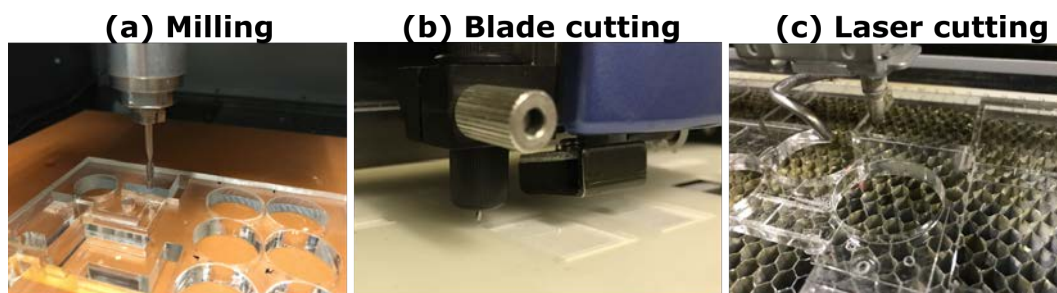
Figure 3.2 | Rapid protyping techniques: (a) milling technique, (b) blade cutting and (c) laser cutting.

3.2 Overview of electrochemical sensors

As it has been described in chapter 2, the development of sensors for cell culture applications has been continually progressing over the past few decades. With the advance of microfabrication technologies, the evolution and miniaturization of sensors has provided useful tools widely used in the monitoring of cell culture systems. In this thesis work, **chemical sensors** have been developed in order to be used in the analysis of cell culture parameters. The International Union of Pure and Applied Chemistry (IUPAC) define a chemical sensor as "a device that transform information, ranging from the concentration of specific sample component to a total composition analysis, into an analytically useful signal. The chemical information may be originated from a chemical reaction of the analyte or from a physical property of the system investigated" [161].

Chemical sensors are commonly classified following two main criteria: the nature of the recognition element or the transduction mechanism. Regarding the nature of the recognition elements, chemical sensors can be divided into chemosensors, when using ionophores or macromoleculars receptors, and biosensors, when using enzymes, antibodies, oligonucleotides or chemical receptors. On the other hand, the transduction mechanism divides the chemical sensors into optical (absorbance, reflectance or luminescence sensors), electrochemical (amperometric, potentiometric or impedimetric sensors), electric (metal-oxide semiconductors sensors, organic semiconductors sensors, electrolytic conductivity sensors or electric permittivity sensors), mass (piezoelectric or acoustic wave devices), magnetic, thermometric and radiometric sensors.

The sensors used along this work are based on an electrochemical transduction. This detection method is ideally suited for their integration in miniaturized systems, as clearly pointed out by Nyholm [162]. An overview of analytical chemistry development demonstrates that **electrochemical sensors** represent the most rapidly growing class of chemical sensors. Approximately 7000 peer-reviewer papers concerning electrochemical sensors were published in 2016 according to Scopus Web Site, showing the considerable research effort underway in this field. The easy miniaturization of the electrodes could involve a decrease in the reagents consumption and in the sensor size, allowing low limits of detection and wide response range. Compared to optical sensors, which are also widely used for monitoring cell culture system, electrochemical sensors are especially attractive because of their remarkable detectability, experimental simplicity, integrity and low-cost. Moreover, electrochemical devices do not need sophisticated instrumentation, since it is relatively simple since it directly converts chemical information into an electrical signal [163]. The interest in electrochemical sensors continues unabated today, stimulated by the wide range of potential applications. They have a leading position among the presently available sensors that have reached the commercial stage.

Table 3.1 shows the electrochemical sensors classification regarding the measurement technique [164]. The common electrochemical sensors transducers and the usual analytes for each type of measurement are also shown.

Measurement type	Transducer	Usual analyte
Amperometric	Metal or carbon electrode.	O_2, sugars, alcohol.
	Chemically modified electrodes (CME).	Sugar, alcohol, phenols, oligonucleotides.
Potentiometric	Liquid junction ion selective electrode.	K^+, Cl^-, Ca^{2+}, F^-.
	Glass electrode.	H^+, Na^+.
	Solid-state ion selective electrode	Redox species.
	Ion-sensitive field-effect transistor (ISFET).	H^+, K^+.
Impedimetric	Interdigitated electrode (IDE). Metal electrode.	Urea, charged species, oligonucleotides.

Table 3.1 | Electrochemical sensors classification regarding the measurement technique including the common transducer type and the usual measured analytes.

In the following section, it is described the working principle of the electrochemical sensors used in this thesis work. The description of the transduction method of the diverse electrochemical sensors is widely described in the bibliography [165][166]. Here, just a brief summary about amperometry and potentiometry techniques is introduced, centering in the evolution and miniaturization of the developed electrochemical sensors: DO, Na^+, K^+ and pH.

3.2.1   Amperometric sensors

Strictly, amperometric is a sub-class of the voltammetry technique. Voltammetry provides an electroanalytical method in where the current is linearly dependent upon the concentration of the electroactive species (analyte) involved in a chemical or biological recognition process at a scanned or fixed potential [167]. Some of the most common techniques of voltammetry with scanned potential are: cyclic voltammetry, square-wave and stripping voltammetry. When the potential is fixed during the time, the technique is called amperometry. In amperometry technique, the continuous measured current results from the oxidation or reduction of an electroactive species in a chemical reaction [168], and this current is related to the concentration of the analyte presented.

The first known amperometric sensor was the oxygen electrode developed by Leland C. Clark in 1956 [111]. His first version was designed to measure the concentration of oxygen in blood and was first tested in dogs. In this device, oxygen entering the system through a gas-permeable membrane is reduced to water in a noble metal electrode when a voltage is applied, obtaining a current proportional to the amount of oxygen reacting. Figure 3.3a shows the first version of Clark-type sensor where two electrodes are in contact with an electrolyte solution and separated to the analyte medium by a permeable membrane. In 1962, Clark also described the first glucose biosensor using his first system to determine the depletion of oxygen by the action of glucose oxidase on glucose [112]. Clark's work and the subsequent transfer of his technology to Yellow Spring Instrument Company led to the successful commercial launch of the first dedicated glucose biosensor in 1975 [169]. This great invention has inspired numerous scientists of later generations to develop other sensors using the Clark oxygen electrode as a basis.

During this thesis work, the DO parameter is monitored along all applications. Oxygen is an important regulator of normal cell behaviour since it is one of the most important indicators of biological activity during cell culture and microbial development. Following, is presented in detail the amperometric DO sensor used in this work.

3.2.1.1 Dissolved oxygen sensor

Monitoring DO is one of the domains of amperometry. The oxygen sensors developed in this work are based on the Clark-type oxygen electrodes that are the simplest form of as amperometric sensor. Many modifications to the original design of this device have been proposed since the publication of the relevant Clark's patent [170], but the essential basis of the sensor remains unchanged. As it has already been described, its working principle is based on the diffusion of the oxygen through a gas-permeable membrane to an oxygen reduced at the electrode (cathode), which typically is a noble metal electrode like platinum or gold, related to a Ag/AgCl reference electrode (anode) at a fixed potential. The measured current is proportional to the concentration of oxygen in the solution. This linear dependence was first discovered by Heinrich L. Danncel in 1897 [171].

The reduction of oxygen at the cathode (called working electrode) is accompanied by the oxidation of the anode material. In the first version of Clark-type sensor, the reference electrode worked as anode as shown in Figure 3.3(a.1). This implies some drawbacks, like the consumption of the anode material and the alteration of the electrolyte composition. To avoid this, in 1966 Ross and Mass [172] proposed the using an
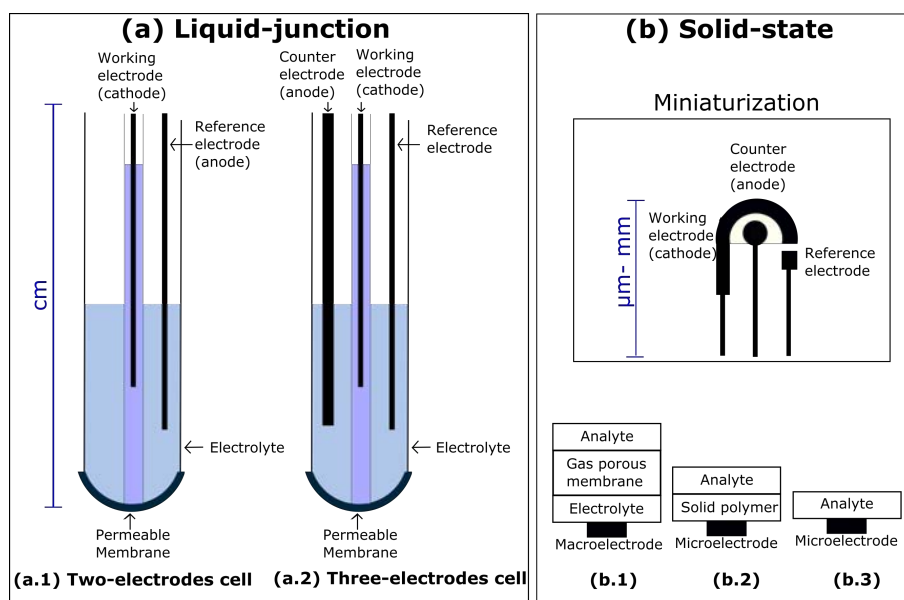
Figure 3.3 | (a)Clark-type amperometric dissolved oxygen sensor in a two-electrodes cell configuration (a.1) and in a three-electrodes cell configuration (a.2), and (b) Solid-state of an amperometric construction in different configurations ways, with the electrolyte and porous membrane (b.1), a solid polymer (b.2) and a membrane-free configuration (b.3).

inert counter electrode as an anode in a three-electrodes configuration. According to this principle, there is a balancing of oxygen consumption at the cathode against oxygen production at the anode. Figure 3.3(b) shown the schematic of the Clark-type oxygen sensor with the three-electrodes configuration.

The oxygen reaction that take places at the cathode (reduction), and the reaction occurring at the anode (oxidation) converts the products from the cathode back into reactants. The balanced redox reaction in acid solution is summarized as 3.1:

$$O_2 + 4H^+ + 4e^- \rightarrow 2H_2O \tag{3.1}$$

And in alkaline solution, the redox reactions is defined as 3.2:

$$O_2 + 4e^- + 2H_2O \rightarrow 4OH^- \tag{3.2}$$

Clark-type sensors measure oxygen partial pressure and not its concentration, for this reason, to know the concentration value, it is necessary to know the temperature and salinity of the analyte when the measurement takes place. Clark-type oxygen sensors have found usage in a wide range of applications such as: sensors in clinical diagnosis [173], water and gas environment monitoring [174] as well other diverse applications. There is a wide need for oxygen sensors and numerous major manufacturers of analytical apparatus (including, Radiometer, Beckmann, Philip Harris, Unisens, etc.) sell modified Clark-type sensors. Despite the commercial popularity and the wide usage of these sensors, several drawbacks and limitations to the Clark sensor are known. Some of these drawbacks are the instability of readings, uniform signal drift, changes in sensor response time, formation of gas bubbles in electrolyte, and so forth. However, their construction simplicity makes them the best candidate to miniaturize in order to extend even more their applicability. The next section addresses the miniaturization of a DO sensor using the principle basis of the Clark-type sensor.

3.2.1.2 Miniaturization of dissolved oxygen sensor

Several amperometric electrochemical sensors have been developed over the past sixty years. Most of the commercially available electrochemical sensors have macro dimensions that do not allow their direct use in media with small volumes. The evolution of the microenginnering has allowed that this type of sensors could be miniaturized [175]. The strategy to achieve the miniaturization of the sensors is based on the replacement of traditional electrochemical cell and bulk electrodes. For their replacement, the use of **solid-state planar electrodes** was introduced with the evolution of suitable material combinations and the microtechnologies (Figure 3.3(b)). Various types of miniaturized Clark-type oxygen sensors have been proposed since 1986 [176–179].

For the development of miniaturized sensors, the most common technique is the microfabrication technology, which has been described in the first section of this chapter. However, with the increase in the demand of low-cost sensors for a single-use and for on-site monitoring [180], other fabrication methods have increased its use in the fabrication of planar electrochemical structures. Screen-printing technology

is widely used since the 1990s for this purpose. Printing technologies offers high-volume production with extremely inexpensive sensors. Other advantages of printing technologies are the variability of used materials, their flexibility, accessibility, non-vacuum and ecological friendly fabrication processes, their good reproducibility and good compatibility with electronic devices and circuits, and their good mechanical and electrical resistivity [181]. The use of printing techniques for the development of electrochemical sensors is introduced and developed in 4.

For the miniaturization of a whole amperometric system, the internal electrolyte solution and the porous membrane can be replaced by solid polymers (From Figure 3.3(b.1) to 3.3(b.2). Initial reports of solid polymer electrolytes being integrated with sensors technology appeared in 1980s [176]. One of the first reports of a polymeric solid-state amperometric oxygen sensors used Nafion$^{®}$ as a membrane [182, 183]. The ionic polymer Nafion$^{®}$ has existed since 1960s when DuPont developed it [184]. Nafion$^{®}$ is one of the most used polymers due to its high proton conductivity [185], high H_2O diffusivity, high gas permeability, its chemical and electrochemical inertless, and its compatibility with process used for electrode fabrication. One of its drawback is that it is necessary to employ a contacting liquid to hydrate the polymer, thereby maintaining ionic conductivity and controlling the dependence of the response on relative humidity [186]. In the simplest construction, it is possible to work without the use of membrane, exposing the active electrodes directly to the analyte sample (Figure 3.3c.3). This 'membrane-free' construction improves the response time and sensitivity of the sensor however, only can be used in few applications since the active electrodes are influenced by interfering compounds [187]. The implementation of the membrane and electrolyte as a polymer makes the system more robust and prolong their lifetime [188, 189].

In many cases the miniaturization is limited because of the necessary functional elements. In summary, in order to construct a successful microsensor, a number of aspects must be taken into account:

1. The design of the sensor in order to reduce the electrochemical crosstalk between different electrodes.
2. The development of a reliable reference electrode with potential stability and a long life time.
3. The replacement of internal electrolyte using different hydrogels or polymers.
4. The bonding strategies and durability of the oxygen-permeable membrane and the substrate.

It deserves special attention to the big efforts that have been done regarding to the second item. The traditional macroscopic reference electrodes cannot be completely miniaturized and a pseudo-reference electrode must be fabricated. The standard material historically used as a reference electrode in cell culture applications is silver-silver chloride (Ag/AgCl). Its use for microprobes has been shown through chlorination of thick electrodeposited silver layers [190]. Despite the well-known behavior of Ag/AgCl, when these electrodes are microfabricated they typically have a very short lifetime due to dissolution of the thin AgCl layer, and when the chloride coating is dissolved, the standard potential radically changes [191]. For this reason, big efforts have been done in the miniaturization of reference electrodes with stable Ag/AgCl potentials using also solid polymers, as is the case of the polyvinyl butyral (PVB) polymer membrane [192]. Currently, the integration of a reliable pseudo-reference electrode represents a key challenge for eletrochemical microsensors [193, 194], and their miniaturization is not easy and not completely solved nowadays.

3.2.2 Potentiometric sensors

In potentiometric technique the analytical information is obtained by converting the recognition process into a potential signal, which is logarithmically proportional to the concentration (activity) of species generated or consumed in the recognition event. The Nernst equation logarithmically related the measured electrode potential, E, to the relative activities of the redox species of interest i:

$$E = E^0 - \frac{RT}{Z_i F} ln \frac{a_0}{a_R} \tag{3.3}$$

where E^0 is the standard half-cell reduction potential and a_0 and a_R are the activities of the oxidized and reduced species, R is the universal gas constant; T is the absolute temperature; F is the Faraday constant; Z_i is the number of moles of electrons exchanged in the electrochemical reaction.

A typical potentiometric sensor has a two-electrode structure, where one electrode is the indicator and the other is the reference. Normally, the transduction and measurement of the potential relies to zero intensity, however, other potentiometric systems called field-effect transistors (FETs) has a different transduction mode.

Potentiometric sensors have found the most widespread practical applicability since the early 1930s, due to their simplicity, familiarity and cost. The key element of the potentiometry technique is the development of the indicator electrode. Depending on the construction of this indicator electrode there are different types of potentiometric devices, such as ion selective electrode (ISE), glass electrode, metal oxide electrodes and FETs.

Potentiometric sensors are simple in their setup as well as in the electronic equipment necessary for operation and data acquisition. The effort for maintenance and calibration is low. Sensor signals are obtained directly *(in-situ)* and provide real time information for process control. In spite of their simplicity, the applications of electrochemical sensors require an improved knowledge about the influences of the measuring conditions such as temperature, pressure and chemical composition on the sensor signal, which determine the limits of application. In addition, the long-term stability of potentiometric sensors is significantly determined by the potential stability of the reference electrode.

The ISEs are the most representative potentiometric sensors. These type of sensors convert the activity of a target ion into an electrical potential as a measurable signal. This potential signal is generated by a charge separation at the interface between the ion-selective membrane and the solution due to selective partitioning of the ionic species between these two phases. The electrical response to an ISE is provided by a reference electrode (usually Ag/AgCl) in contact with the internal solution that contains chloride ions at constant concentration [167]. During the time, potentiometric sensors have also varied in their design, specifically in electrode dimension, electrode material, and choice of membrane to improve performance, lifetime and reliability, while reducing cost and size. The first developed ISE was the glass membrane sensor as a pH sensor that was developed by M. Cremer in 1906 [105]. In these type of systems the ISE is made of a doped glass membrane that is sensitive to a specific ion (Figure 3.4(a.1)). Around 1967, Ross introduced

the concept of liquid membrane electrode selective for calcium [195]. This type of ISE is based on water immiscible liquid substance produced in a polymeric membrane (Figure 3.4(a.2)). Based in this concept, two years later, Wilhelm Simon [196] developed the first neutral carrier–based liquid membrane ISE for potassium. Bloch and co-workers introduced the first ionophore-based solvent polymeric membrane based on polyvinyl chloride (PVC) [197], a matrix still widely used today (Figure 3.4(a.3)). This revolutionized the manufacturing of liquid membrane ISEs and made them much more suitable for miniaturization.

Over the past half century, ISEs have evolved into well-established, routine analytical tools, with sensors for more than 60 analytes. The membranes of the majority of these ISEs contain lipophilic complexing agents that selectively bind to their target ions. Such complexing agents are referred to as ionophores or carriers [198]. The large number of ionophore-based ISEs developed over the last fifty years made possible to use ISEs in various types of routine analyses including clinical analysis [199], environmental analysis [200] or cell culture systems [201].

All these conventional systems described above are based on the junction-liquid set-up, where the back side of ISE membranes is in contact with an electrolyte in order to obtain stable potentials. Although ISEs with an internal solid contact, which allows a much simpler fabrication, are already known for more than 30 years [202], until recently they have not shown sufficient potential stability. Currently, intensive research is taking place in this area. An internal contact with conducting polymers [203] seems to be especially promising.

The potentiometric sensors developed in this thesis work are based in planar **solid-state** construction approach. A brief summary of the evolution of developed Na^+, K^+ and pH sensors are described in the following section.
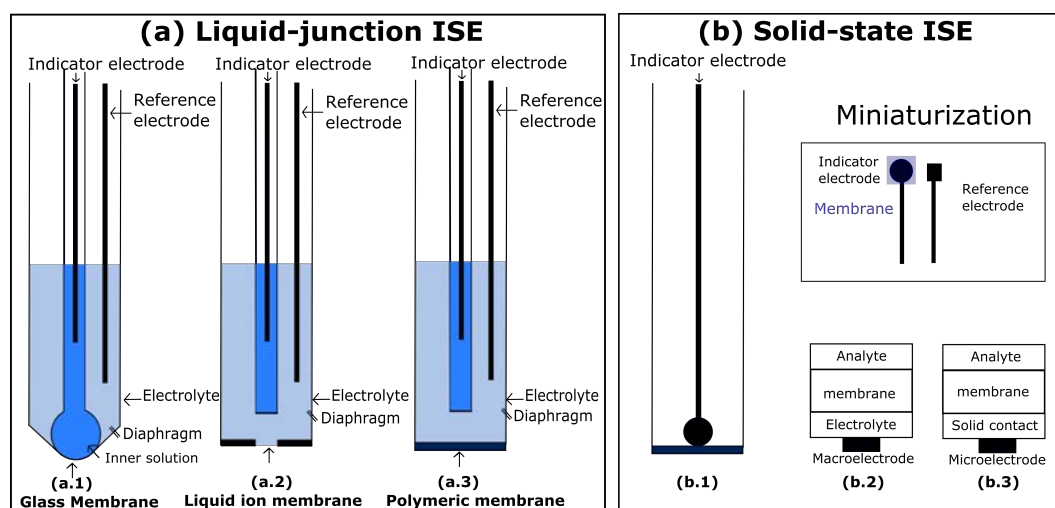
Figure 3.4   (a) Liquid-junction potentiometric ISE in a combination with the reference electrode with (a.1) glass membrane, (a.2) liquid ion membrane, and (a.3) polymeric membrane, (b) Solid-state potentiometric ISE, (b.1) in a macroelectrode construction, (b.2) Scheme of liquid-junction construction and (b.3) Scheme of miniaturize system replacing the electrolyte with a solid contact membrane.

3.2.2.1   Potentiometric Na$^+$ and K$^+$ ion selective electrodes sensors

Monitoring of extracellular ion activities can be of interest in applications involving the study of tissue and organs. As an example, this has an special interest in cells whose function is sensitive to extracellular ion concentrations or depends on the establishment and maintenance of ion concentrations gradients through epithelial barriers [204].

Currently, one the most used techniques for measuring ions is flame photometry [205]. This technique provides a good method for measuring Na$^+$ and K$^+$ ions in samples. However, there has been a great interest in replacing it owing to its low throughput, manual operation with a time consuming procedure. The Na$^+$ and K$^+$ ISEs fulfilled this need and offered other additional benefits [206].

The potentiometric Na$^+$ and K$^+$ ISEs have been evolved during years. Glass membranes were the first used type of ISE. The response of the glass membranes to Na$^+$ ion has been observed as early as 1925 [107]. However, until 1957 that George Eisenman [108] could not develop a working Na$^+$ glass electrode. However, the glass K$^+$ electrode developed by Eisenman lacked of sufficient selectivity over other ions commonly existing in blood samples, especially Na$^+$. Since Na$^+$ and K$^+$ need to measured together in a clinical application, it no was until the early 1970s when they were used since more selective liquid K$^+$ membrane electrodes became available [109]. Nowadays glass electrodes are fabricated in a great variety of shapes and sizes depending on the demands.

3.2.2.2   Miniaturization of potentiometric ion selective electrodes

Over the past three decades, the interest in the development of simple and portable analytical devices has continued to grow due to the high demand for point-of-care and in-field testing applications. Conventional ISEs have several limitations that need to be overcame in order to meet the demand for portable analytical devices with small sample volumes, easy maintenance simple operation, and low-cost. ISE's miniaturization is achieved by the development of solid-state sensors in which the liquid contact is replaced by solid elements. In solid-state ISEs a solid contact is formed between the sensing membrane and an electron-conducting substrate to replace the liquid contact, serving as an ion-to-electron transfer. Solid contact potentiometric ISEs have nowadays similar performance characteristics to conventional inner-solution ISEs.

Among the electroactive materials available today, conducting polymers have emerged as a promising ion-to-electron transducers for solid contact ISEs [207]. In this type of solid-state ISE, the conducting polymer is coated with a conventional ion-selective membrane, and the ion-selectivity is determined mainly by the ion-selective membrane. Some examples of solid-state ISE constructions are: carbon cloth coated with a conventional plasticized PVC-based K$^+$ selective membrane [208], carbon nanotubes (CNTs) drop-coated with a K$^+$-selective polyacrylic membrane [209], PVC-based molecularly imprinted polymers [210] or graphene coated with an ionophore-doped polymeric membrane [211].

In potentiometric measurements the reference electrode plays an important role in the measurement. It provides a stable and reproducible sample-independent electrical potential. Similar to solid-state ISEs, solid-state reference electrodes do not rely on a liquid contact to an internal reference element and instead rely on a solid contact layer sandwiched in between a hydrophobic reference membrane and an underlying

electronconducting substrate. Although huge efforts have been done, the major challenges of miniaturized reference electrodes still remain [212].

3.2.2.3 Potentiometric pH sensor

As previously described in Section 3.2.2, the first developed potentiometric sensor was the pH sensor based on the glass electrode developed by M. Cremer in 1906 [105]. The first application of the pH sensor in biology was the pioneering work of F. Haber and Z. Klemensiewicz in 1908 [106]. Different approaches were lately introduced [213]. In the next several decades, the rapid development of the ISE came with the introduction of non-glass membranes. Although different types of pH sensors emerged, even today, the most commonly used pH sensors are still the glass membrane based electrochemical electrodes.

The pH of an aqueous solution is defined as the negative common logarithm of the molar concentration of hydronium ions (H_3O^+), given by pH = -log[H_3O^+]. The usual range of pH is 0 to 14, where pH = 7 is the neutral value. Two possible mechanisms for pH sensing can be found: redox reactions and ion-selective permeation.

Redox reaction: The material over the sensing electrode can be reduced or oxidized with H_3O^+ and a potential difference is generated by the free energy change a reversible chemical reaction approaching their equilibrium conditions.

ISE permeation: The sensing material acts as an ion-selective membrane and the concentration gradient of [H_3O^+] ions at both sides of the membrane also generates a potential difference.

In this thesis work, a metal oxide pH sensor has been developed, specifically iridium oxide (IrOx) material. In this type of sensors different conductive and semi-conductive materials can act as indicator element of a pH. IrOx is an outstanding material for pH measurements over wide ranges, with fast response, and high durability, stability and biocompatibility [214]. Several approaches for the preparation of the IrOx sensor fabrication can be used: iridium thermal oxidation, electroplating, anodization, sputtering and sol-gel processing. The IrOx films produced by these techniques near-Nerstian response because the amount of transferred electrons equals to the amount of reacted H_3O^+. However, IrOx prepared by electrochemical deposition showed super-Nerstian response (sensitivities greater than 59 mV/pH) with a sensitivity of around 70 mV/pH. This can be explained because electrochemically deposited IrOx is an hydrated material in an aqueous environment and contains iridium ions with different valences (+3 and +4) [215].

The general iridium reaction is described in 3.4 as:

$$Ir^{IV} oxide + xH^+ + ne^- \leftrightarrow Ir^{III} oxide + yH_2O \tag{3.4}$$
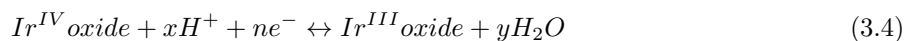
If IrOx is fully hydrated, the redox reaction is:

$$2Ir(OH)_2O^- + H_2O \leftrightarrow Ir_2O(OH)_3O_3^{3-} + 3H^+ + 2e^- \tag{3.5}$$
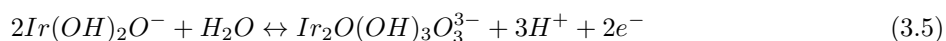
Other metal oxides that have also been studied, but their pH sensitivities are not as high as IrOx, are nano-copper oxide, cobalt oxide and tungsten oxide among others.

In addition to metal oxides, many conductive polymers are also used as potentiometric sensors. Their pH sensitivity is attributed to their functional groups, which can be protonated and deprotonated at different pH levels. Two widely studied conductive polymers are polyaniline (PANI) [216] and polypyrrole (PPY) [217]. Considering other organic materials such as parylene, although normally it is used as an insulating material, also displayed a pH sensitivity of 16.3 mV per pH between pH of 4 and 10 [218]. Although the sensitivity of parylene is low, its process compatibility with existing microelectronics fabrication technologies makes it suitable for low-cost applications [219]. CNTs are also evaluated as a pH sensitive material with a Nernst response [220].

3.2.2.4 Miniaturization of potentiometric metal oxide pH sensor

Conventional glass electrodes that are commonly used for pH measurements are bulky, fragile and expensive, which hinders their application in miniaturized systems and encouraged searching for alternatives. Metal oxide electrodes are mechanically robust devices that can be easily miniaturized using different technologies depending which characteristic its necessary to achieve. Miniaturized systems make possible the study of pH changes in small sample volumes and so be useful for clinical or biological applications.

The degree of miniaturization is determined by the desired sensor size and by the technological process. For several applications, favorably planar sensor geometry can be achieved. If necessary, the concept of disposable sensors can be pursued for economical reasons. This could be the case when long-term stability of the sensor signals is not necessary or when sterilization processes can degrade sensor functional elements. Guth et al. [10] reported a review about the development in electrochemical sensors with an overview about the miniaturization of a pH sensor as shown in Figure 3.5.

Figure 3.5 | Miniaturization of potentiometric pH sensors. On the left-hand side a commercial pH sensor with diameter 12 mm (commercial standard) is shown; the next three sensors are made by conventional techniques; the three sensors on the right-hand side are fabricated by printing techniques. Source: [10].

3.3 Application of microfabricated electrochemical sensors

This section shown the developed monitoring tools using microfabrication technology addressed to monitor physical parameters externally to microfluidic systems. This section is divided in two subsections, where each one corresponds to a published work in a relevant scientific journal. The first one is focused in the development and complete characterization of a miniaturized array of DO sensors on a rigid substrate and its validation in a flat-plate bioreactor. The second one goes one step further and integrates four sensors for the simultaneous measurement of DO, pH, Na^+ and K^+. This multi-sensing platform uses plastic as a substrate and their validation is done in real urine samples.

3.3.1 Paper I: Profiling of oxygen in biofilms using individually addressable disk microelectrodes on a microfabricated needle

The first paper presented in this Chapter, **Paper I**, is a published article about the development of an array of electrochemical DO sensors using microfabrication technologies, which allows the development of microelectrodes with dimensions smaller than 50 μm. Microsensors are integrated in a Pyrex® needle, in a line of eight electrodes situated to make real-time measurements. Sensors are carefully designed taking into account the application where the needle is addressed. In the publication, it is shown the complete description of the sensors design, their fabrication, the electrochemical calibration and their validation measuring the DO concentration profile within a biofilm grown in a flat-plate biorector, by simultaneously measuring the oxygen consumption at different depths inside it.

This article has been reproduced from Microchmica Acta journal, with permission from Springer [*]:
A. Moya, X. Guimerà, F.J. del Campo, E. Prats-Alfonso, A.D. Dorado, M. Baeza, R. Villa, D. Gabriel, X. Gamisans, G. Gabriel, **Profiling of oxygen in biofilms using individually addressable disk microelectrodes on a microfabricated needle**, Microchim. Acta. 182 (Nov-2014) 985–993. doi:10.1007/s00604-014-1405-4.

This work has been also presented in different conferences with their corresponding Proceedings:

- Conference **Biotechniques for Air Pollution Control & Bioenergy 2013**: Guimerà X., Moya A., Prats-Alfonso E., Dorado A.D., Villa R., Gamisans X., Gabriel D., Gabriel G. Development of a novel microsensor for the study of oxygen profiles in biofilms. Biotechniques for Air Pollution Control & Bioenergy. Presses des Mines, 275-285, 2013.

- Conference **EUROSENSORS, 2014**:A. Moya, X. Guimerà, F.J. del Campo, E. Prats-Alfonso, A.D. Dorado, M. Baeza, R. Villa, D. Gabriel, X. Gamisans, G. Gabriel, Biofilm Oxygen Profiling using an Array of Microelectrodes on a Microfabricated Needle, Procedia Engineering. 87 (2014) 256–259. doi:10.1016/j.proeng.2014.11.654.

- Conference **Biotechniques for Air Pollution Control & Bioenergy 2015**: X.Guimerà, <u>Ana Moya</u>, D. Gabriel, R. Villa, A.D. Dorado, G. Gabriel, X. Gamisans, Simultaneous oxygen and pH profiling within biofilms using a minimally invasive multi electrode array sensor, Biotechniques Ghent 2015: The 6th international conference on biotechniques for air pollution control: Ghent, Blegium: 2-4 September 2015.

- Conference **International Conference on Biofilm Reactors 2017**: Xavier Guimerà Villalba, <u>A Moya</u>, D Gabriel, R Villa, Antonio David Dorado Castaño, G Gabriel, Javier Gamisans Noguera. A novel MEMS-based sensor for simultaneous pH and dissolved oxygen profiling in biofilms. 10th International Conference on Biofilm Reactors, 2017.

- Conference **Biotechniques for Air Pollution Control and Bioenergy**: Xavier Guimerà Villalba, <u>A Moya</u>, D Rodríguez, D Gabriel, R Villa, Antonio David Dorado Castaño, G Gabriel, Javier Gamisans Noguera. Simultaneous dissolved oxygen and pH continuous monitoring through biofilms using a minimally invasive microsensor. 7th International Conference on Biotechniques for Air Pollution Control and Bioenergy. A Coruña. Spain, July 19-21, 2017.

The development of this work has led to their applicability and has been published in important scientific journals:

- X. Guimerà, <u>A. Moya</u>, A.D. Dorado, R. Villa, D. Gabriel, G. Gabriel, X. Gamisans, Biofilm dynamics characterization using a novel DO-MEA sensor: mass transport and biokinetics, Applied Microbiology and Biotechnology. 99 (2015) 55–66. doi:10.1007/s00253-014-5821-5.

- O. Estrada-Leypon, <u>A. Moya</u>, A. Guimera, G. Gabriel, M. Agut, B. Sanchez, S. Borros, Simultaneous monitoring of Staphylococcus aureus growth in a multi-parametric microfluidic platform using microscopy and impedance spectroscopy, Bioelectrochemistry. 105 (2015) 56–64. doi:10.1016/j.bioelechem.2015.05.006.

---

* Note that sections, equations and references numbering in the reproduced research article follow the ones of the published version.

ORIGINAL PAPER

Profiling of oxygen in biofilms using individually addressable disk microelectrodes on a microfabricated needle

Ana Moya · Xavier Guimerà · Francisco Javier del Campo · Elisabet Prats-Alfonso ·
Antonio David Dorado · Mireia Baeza · Rosa Villa · David Gabriel · Xavier Gamisans ·
Gemma Gabriel

Abstract A novel microelectrode array sensor was fabricated using MEMS technology on a needle, and then applied to real-time measurement of dissolved oxygen (DO) inside biofilms. The sensor consists of eleven gold disk microelectrodes, a rectangular auxiliary electrode along them, and an external and internal reference electrode. Three kinds of sensors were designed and their responses were characterized and evaluated under various conditions. The arrays exhibit a linear response to DO in the 0–8 mg·L^{-1} concentration range in water, high sensitivity, repeatability, and low limits of detection (<0.11 mg·L^{-1} of DO) and quantification (0.38 mg·L^{-1} DO). The sensors were validated against a commercial Clark-type microelectrode and applied to profiling of DO in a heterotrophic biofilm cultivated in a flat-plate bioreactor. It is shown that the sensor array can provide a multipoint, simultaneous snapshot profile of DO inside a biofilm with high spatial resolution due to its micrometric dimensions. We conclude that this new sensor array represents a powerful tool for sensing of DO biofilms and in numerous bioprocesses.

Ana Moya and Xavier Guimerà authors contributed equally to this study.

A. Moya · F. J. del Campo · E. Prats-Alfonso · R. Villa · G. Gabriel
Instituto de Microelectrónica de Barcelona, IMB-CNM (CSIC),
Esfera UAB, Campus Universitat Autònoma de Barcelona,
08193 Bellaterra, Barcelona, Spain

X. Guimerà · A. D. Dorado · X. Gamisans
Department of Mining Engineering and Natural Resources,
Universitat Politècnica de Catalunya, Avinguda de les Bases de
Manresa 61-73, 08240 Manresa, Spain

M. Baeza
Department of Chemistry, Facultat de Ciències, Edifici C-Nord,
Universitat Autònoma de Barcelona, 08193 Bellaterra, Barcelona,
Spain

D. Gabriel
Department of Chemical Engineering, Universitat Autònoma de
Barcelona, EdificiQ, 08193 Bellaterra, Barcelona, Spain

A. Moya · E. Prats-Alfonso · R. Villa · G. Gabriel (✉)
Biomedical Research Networking Center in Bioengineering,
Biomaterials and Nanomedicine (CIBER-BBN), Zaragoza, Spain
e-mail: gemma.gabriel@imb-cnm.csic.es

Introduction

Biofilm formation affects most waste-water and waste-gaseous treatment processes. Both treatment bioreactors use biofilms to remove pollutants [1, 2], it is therefore critical in bio-reactor design to understand the phenomena and mechanisms governing biofilm growth dynamics.

Among the many chemical species that can be found and monitored inside biofilms, oxygen is perhaps the most important, as it is the primary electron acceptor in most aerobic biological processes. The local concentration of oxygen inside a biofilm reveals the existence of different zones [3], either aerobic or anaerobic, which can explain the biodegradation processes linked to characteristic oxygen profiles. In addition, knowledge of oxygen concentration gradients allows the description of mass transfer [4] and biokinetics [5] processes, allowing the development of more rigorous models.

When characterizing biofilms [6], microsensors are suitable powerful tools for the determination of chemical parameters with a high spatial resolution. In the measurement of dissolved oxygen, the most widely used analytical methods are based on fiber-optic [7] and electrochemical [8] microsensors. Both techniques are implemented in several

applications, including waste-water oxygen analysis [3] because of their ability to make real time and continuous measurements in small volumes. Features of optical sensors include chemical inertness, internal reference, stability, high sensitivity to small oxygen concentration changes and flow-rate independence [7]. The amperometric method, on the other hand, affords simplicity of operation, high sensitivity and high design flexibility.

Clark-type microsensors [8] are the most electrochemical commonly used probes and at the present considered the gold standard [9] in biofilm oxygen sensing. Such DO sensors consist of an electrochemical three-electrode system with a reference electrode (RE), an auxiliary/counter electrode (CE) and a working electrode (WE) in an aqueous solution. Such three-electrode system is isolated from the medium by a selective gas-permeable membrane across which oxygen diffuses towards the cathode (WE), at a rate proportional to its partial pressure. Thus the reduction current generated at the cathode is directly proportional to the oxygen concentration in the test solution. The working electrode potential is typically set around -800 mV (vs Ag/AgCl) so that the overall reaction (Eq. 3) can take place following two consecutive two-electron reduction steps [10]:

$$O_2 + 2e^- + H_2O \rightarrow HO_2^- + OH^- \tag{1}$$

$$\underline{HO_2^- + 2e^- + H_2O \rightarrow 3OH^-} \tag{2}$$

$$O_2 + 4e^- + 2H_2O \rightarrow 4OH^- \tag{3}$$

Clark-type microsensors have been widely used to monitor biofilms and sediments [11, 12]. However, their manufacture presents important limitations [13]. Most of these sensors are hand crafted from pulled glass capillaries, and so their main limitations are the fragility and high unit cost of the devices, the tip-size variability between different probes, and the difficulty to bundle several microelectrodes in arrays of controlled geometry.

Another limitation shared by Clark-type microsensors and optical sensors lays on the fact that they are restricted to single point measurements performed one at a time, which makes the acquisition of DO profiles inside biofilms extremely tedious and inaccurate. Important efforts have been made in the past to measure DO profiles in biofilms [14–16], some of them based on microfabricated microneedles [17]. The reported profiles are obtained by mounting the microelectrode on a micromanipulator and driving it into the biofilm in a series of recording and penetration steps.

Microfabrication techniques represent a much more versatile approach to microelectrode design, enabling the fabrication of electrodes of wide ranging sizes, geometries and arrangements. Thus, it is possible to create nano- and

microelectrodes and their arrays [18–21], including disks [20, 22], bands [23, 24] and 3D structures [25–27], and wire them either in parallel or individually [18, 20]. On top of that, microfabrication techniques allow the cost-effective mass-production of microsensors that can be deployed in a vast number of applications.

The device presented in this work enables the determination of the oxygen concentration profile within a biofilm by simultaneously measuring the oxygen consumption at different depths inside it. This novel DO-MEA sensor to measure DO profiles overcomes the limitations presented both by optical and Clark-type microsensors by producing multipoint, instant DO measurements in biofilms in-situ. Amperometric techniques enable these simultaneous measurements in a simple way.

Materials and methods

Reagents and instrumentation

All solutions used in the sensor development were prepared with deionized water (conductivity less than 1 μS·cm^{-1}). Chemicals used (K$_3$[Fe(CN)$_6$], K$_4$[Fe(CN)$_6$], KNO$_3$, KOH, H$_2$O$_2$ and Na$_2$SO$_3$) were of analytical grade and used as received from (Sigma-Aldrich, www.sigmaaldrich.com), without further purification.

Microelectrode characterization and sensor calibration were carried out with an 8-channel potentiostat 1030A Electrochemical Analyzer (CH-Instruments, USA; http://chinstruments.com). Control experiments were performed using a commercial Ag/AgCl (3 M KCl) electrode as RE and a platinum ring electrode as CE both from (Metrohm, Germany; www.metrohm.com). However, the RE and the CE incorporated in the microsensor needle were also used in the profiling experiments. The microfabricated sensors were calibrated in controlled dissolved oxygen solutions against an OXI 325 (WTW, Germany; http://www.wtw.de) oxygen probe.

A Clark-type commercial microelectrode (OX-25, Unisense, Denmark, www.unisense.com) with a tip diameter of 25 μm, connected to a 4-channel amplifier Microsensor Multimeter (Unisense, Denmark) was used for biofilm profiling in control experiments. Profiles were obtained with the aid of a micromanipulator MM33-2 (Unisense, Denmark).

Calibration of DO-MEA sensor

Microelectrodes (microfabrication process description is detailed in the Electronic Supporting Information, Fig. S1) required activation before use. Several known gold-cleaning methods were investigated [28]. Adequate electrode activation was indicated by Ip and ΔE_p values consistent with

reversible electrode kinetics [29] (electrode preparation is detailed in the Electronic Supporting Information).

Sensors were calibrated in the oxygen concentration range between 0 and 8 mg·L^{-1} DO range according to [30]. Oxygen was measured amperometrically using a set-up Fig. S2 (Electronic Supporting Information). The sensor was polarized at −850 mV vs Ag/AgCl (3 M KCl). The DO concentration was adjusted bubbling different nitrogen (O$_2$ free) - air (21 % O$_2$) mixtures through a 0.1 M KNO$_3$ solution, and a magnetic stirrer was used to ensure better mixing of the solution.

Figure 1 shows linear sweep voltammograms from 0 to −1 V at a scan rate of 25 mV·s^{-1} in a 8 mg·L^{-1} DO oxygen solution using the commercial Ag/AgCl (3 M KCl) RE and Pt CE, and with both integrated in the needle Au microelectrode array. The figure shows that the two signals are shifted about 250 mV due to the use of different reference electrodes. The difference in the limiting currents values of the second step was because different needles were used, with small differences depending on their state of activation.

These voltammograms allowed us to select the −850 mV vs Ag/AgCl, operating with the external reference system, and −600 mV vs Au for the integrated three-electrode system, as the optimal potential value for the determination of the dissolved oxygen concentration (Fig. 1). This is because that potential involves the complete four electron reduction of oxygen, and therefore a higher sensitivity. Note that at this potential the hydrogen evolution reaction does not take place at a significant rate and therefore does not interfere with the main process under study.

The concentration of DO in the cell was measured with a commercial DO probe and correlated with the measured polarization currents of each gold microelectrode in order to build the calibration curves.

Growth of an aerobic biofilm

The suitability of the DO-MEA sensor for biofilm profiling of an aerobic biofilm was checked comparing the response of the microfabricated sensor with that of a commercial DO Clark-type microsensor. A flat plate bioreactor (FPB) was designed and constructed as in Fig. S3 (Electronic Supporting Information) to grow a well-defined biofilm. The FPB was designed according to [31], and was manufactured in PMMA. The reactor consisted of an open channel of 20 cm length and 3.5 cm width. Inoculation was performed by filling the channel with 35 mL of sludge of 2 g SSV·L^1 from a pilot plant bioreactor treating synthetic waste-water.

A mineral medium solution (prepared according to [32]) was supplied to the reactor using glucose as carbon source. The hydraulic residence time ranged from 4 to 8 h throughout the FPB operation. The FPB included an internal recycle flow within the reactor corresponding to a linear velocity between 0.1 and 10 m·h^{-1}. Two peristaltic pumps (MCP Standard, Ismatec, Germany) fed and purged the reactor, while a Miniplus 3 peristaltic pump (Gilson, France) was used for internal recirculation.

DO profiles were recorded directly on the biofilm growing in the reactor using both microsensors. DO-MEA sensor profiles were obtained immersing the sensor, the RE and the CE into the biofilm and keeping it still during amperometric recording. The recording time was 15 s for an 8-points profile. Clark-type microsensor profile registration was carried in a similar manner. Probe position was controlled by a micromanipulator, but a multimeter was used instead of a potentiostat to monitor its response. The measurement time depends on the depth of the profile; each step on the profile requires 15 s of acquisition plus the time required for changing position within the biofilm.

Results and discussion

Amperometric DO determination

The oxygen reduction amperometric signal is affected by medium composition (particularly pH) and also by the electrocatalytic properties of the microelectrodes, which can be improved thorough the activation procedures described above. In a first stage, the response was characterized using external reference and auxiliary electrodes. Following this, the measurements were repeated using the auxiliary and pseudo-reference electrodes integrated in the needle. The measurement system had not much noise and the use of a Faraday cage was not necessary, making easier the biofilm profiling monitoring in the FPB.

Fig. 1 Linear sweep voltammetry results. Average of measured currents and their standard deviation plotted against the potential applied on eight WE against the external (●) and the integrated three-electrode reference system (▼). Linear sweeps were made in an oxygen saturated saline solution (8 mg·L^{-1} DO). First (*1*) and second (*2*) reduction peaks can be observed in linear sweep voltammograms both with an external reference and with an integrated reference

DO-MEA sensor activation and electrochemical characterization

Electrodes were activated as described in the section Electrode Preparation (Electronic Supporting Information). After activation, the DO-MEA sensor was characterized using cyclic voltammetry in a ferro/ferri cyanide solutions from 500 to −200 mV, at a scan rate of 100 mV·s^{-1}. The stability and durability of the electrodes after activation was evaluated by the continuous monitoring of the voltammogram Ip over a period of 35 days. The objective of this test was to study the reproducibility and stability of the DO-MEA sensor response of two sets: a) electrodes activated only the first day and b) electrodes reactivated on a daily basis.

Figure 2 shows the evolution of the ferro/ferri cyanide reduction peak current of two different needles. The electrodes of the daily reactivated needle recovered their optimum response (Ip within ±1.8 %) with the maximum sensitivity evaluated later with the calibration curve. On the other hand, the needle that was not reactivated throughout the testing period lost sensitivity over time, and after 5 weeks their Ip decreased down to 40 % of the initial, optimum state. In addition, the standard deviation between electrodes of the Ip value of these electrodes response increased as time passed. This activity loss was due to electrode fouling caused by the biofilms tested. However, despite sensitivity losses, the sensor continued responding to changes in DO concentration. Because the application presented in this work does not required continuous measurements, it was possible to activate the electrodes before each day of experiments to ensure maximum sensor performance for each profile acquired.

DO-MEA sensor calibration

The linearity and sensitivity of the electrochemical response of the three different DO-MEA sensors designs were verified in the calibration medium 0.1 M KNO$_3$ by bubbling a series of
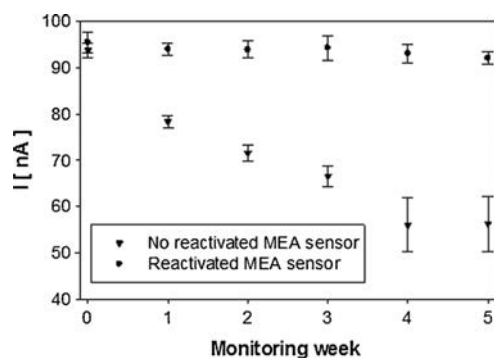
Fig. 2 Evaluation of the activation stability for a reactivated needle (●) and other no reactivated (▼). The oxidation current peak of the voltammogram corresponds to the average and the standard deviation of 8 electrodes of the same DO-MEA sensor

nitrogen/air gas mixtures as detailed in section of biofilm DO profile study. Figure 4 summarizes the reduction currents measured at microelectrodes of different size under different DO concentrations. The points represent the average from the eight different microelectrodes on each needle, and the error bars represent standard deviation arising from the eight microelectrodes. These results were measured simultaneously using the 8-channel multipotentiostat with the external reference electrode.

The sensors displayed excellent linearity between 0 and 8 mg·L^{-1} DO range with correlation factors (r^2) greater than 0.99 for all three microelectrodes sizes, demonstrating that the sensors are suitable for the determination of DO.

In addition to the calibration curves, the DO concentrations can be estimated experimentally from the microelectrode calibration response, or theoretically from the equation corresponding to a diffusion controlled limiting current (I$_{lim}$) (defined in Electronic Supporting Information).

The experimental results in 0.1 M KNO$_3$ were in good agreement with current values obtained from eq. (S2), considering a passivation recess height of 1.9 μm. The experimental obtained sensitivities were: for the electrode diameter of 50 μm, 2.41±0.08 nA·L·mg^{-1} DO; for the electrode diameter of 25 μm, 1.10±0.08 nA·mg^{-1}·L DO and for the smallest diameter of 10 μm, 0.35±0.02 nA·mg^{-1}·L DO. In terms of current density (j), the obtained values were: j$_{50μm}$=1.23, j$_{25μm}$=2.24 and j$_{10μm}$=4.46 A·m^{-2}, where smaller electrodes sizes display higher current densities thanks to the greater contribution of hemispherical diffusion to their edges. Approximately thirty DO-MEA sensors (twenty for the design with bigger electrodes, and five of other types each) were calibrated and all showed good reproducibility with a standard deviation between microelectrodes less than 0.08 nA·mg^{-1} DO. This analysis was completed studying the repeatability of the measurement resulting in a good behavior. Besides the effect of the overlapping neighboring electrodes diffusion layers in the array [18, 20, 33] was also considered, and the separation between electrodes was decided in order to minimize this effect. This effect was higher for smaller DO-MEA design, where inter-electrodes distance was 35 μm, and was minimized for the bigger design with an inter-electrode distance of 100 μm.

Although the intercepts shown in Fig. 3 are very close to zero, sensors response showed a residual current in absence of oxygen which could be caused either by the presence of residual DO due the limited efficiency of the deoxygenation procedure, or by a current due to the onset of the hydrogen reduction on the electrodes surface, since the working potential selected is limiting at the reaction as was illustrated in section of biofilm DO profile study. This offset was approximately 1 nA for the 50 μm design, 0.65 nA for the 25 μm electrode and 0.48 nA for the 10 μm design.

Profiling of oxygen in biofilms using microelectrodes
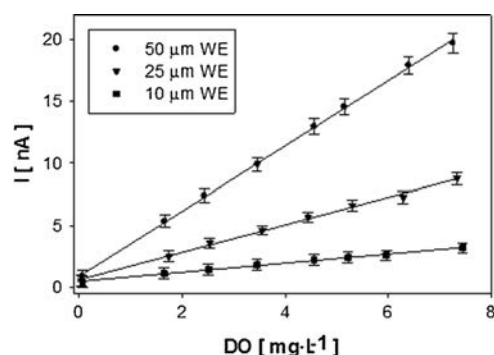
Fig. 3 Calibration curves obtained for the reduction of oxygen for the three different designs. Currents were measured at – 850 mV vs. Ag/AgCl RE and Pt CE. The points correspond to the average current and the standard deviation for eight different electrodes of the same DO-MEA sensor

Other important parameters worth taking into account are the limits of detection and quantification defined by IUPAC (defined in Electronic Supporting Information).

Table 1 shows the L_D and L_Q values according eq. S3 and eq. S4 obtained experimentally for the three different designs. Overall, calibration tests revealed a high sensitivity and repeatability and low detection and quantification limits of the developed sensors.

Three-point calibration curves of the DO-MEA were made in the mineral medium used for biofilm growth (data not shown) with respect to a Ag/AgCl external reference electrode before and after each experimental biofilm profile monitoring. The sensor performed linearly as in KNO_3 and exhibited a sensitivity of 2.36±0.09 nA·L·mg^{-1} DO. This 2 % lower sensitivity confirms the good performance of the device for this application. Furthermore, its applicability without covering the electrode with an oxygen-permeable membrane, as is usually done in the Clark-type sensors, provides advantages over the protected ones as higher sensitivity and faster response.

Effect of the mineral medium in the DO-MEA microsensor response

In order to determine the working range of the sensors, their response in media of different composition was also studied. The effects of mineral medium composition and of pH on the

Table 1 Limit of detection and Limit of quantification for the three different designs

Microelectrode diameter (μm)	O_2 L_D (mg L^{-1})	O_2 L_Q (mg L^{-1})
50	0.04±0.01	0.15±0.03
25	0.07±0.02	0.22±0.08
10	0.11±0.03	0.38±0.01

DO-MEA sensor performance are detailed in the Electronic Supporting Information. Results in Fig. S4 (Electronic Supporting Information) indicate that changing the salt anion of the supporting electrolyte has no effect on the sensor sensitivity, however, changes in ionic strength significantly affected the sensor response. In addition, the oxygen signal was nearly unaffected by pH changes in the 6<pH<8 range (Table S1 in the Electronic Supporting Information).

Needle integrated three-electrode system

Since biofilm thickness may range from several microns to a few millimeters and biofilms are often grown in small reactors in order to study them, it is necessary to integrate the RE and the CE in the needle avoiding external electrodes and, thus, reducing the experimental system dimensions. At this stage, one of the integrated microdisk electrodes in the DO-MEA was used as pseudo-reference electrode while the rectangular macroelectrode was used as CE. The main difference introduced with the integrated three-electrode system configuration was that the reduction potential shifts ±250 mV. The different studies, described in the previous section for the external reference system, were carried out with the integrated three-electrode system, obtaining the same sensor behavior. In order to improve the stability of the pseudo-reference, the electrode surface was previously oxidized, subjected it to a continuous anodization, so that it would keep a more stable potential over time [34]. The oxidized pseudo-reference electrode was evaluated with a continuous measurement of its potential versus a commercial Ag/AgCl (3 M KCl) electrode in KNO_3 0.1 M for 18 h. The drift rate of the integrated reference was 0.68 mV·h^{-1}, which was considered acceptable for short-term measurements such as those conducted in the present study. However, long-term measurements require a reference with a lower drift, which will be achieved in future work, using an integrated Ag/AgCl reference. The calibration of the integrated three-electrode system microsensor was made using the same procedure used with the external commercial RE and CE. With the new selected potential of −600 mV, the calibration curve for the integrated configuration presented a satisfactory response of 2.07±0.07 nA·L·mg^{-1} DO with a R^2 of 0.99. Detection and quantification limits were also estimated, resulting in 0.05±0.01 DO and 0.17±0.06 mg·L^{-1} DO respectively. These results shows a good response with the use of the integrated system, with a small loss of sensitivity and L_D and L_Q respect the external reference system, due the reduction potential selected and a different needle was used.

In Table 2 the main characteristics of the microneedle here described have been compared with the common commercial available dissolved oxygen microsensors, both optical and electrochemical microsensors

Table 2 Figures of merit of comparable methods for profiling of dissolved oxygen with commercial products based on microsensors

Method/Materials used	Analytical ranges	O_2 L_D (mg L^{-1})	Spatial resolution (μm)	Response time (s)	Comments	References
Electrochemical, gold electrode	0–8 ppm	0.04±0.01	10–50	5–10	- 8 Simultaneous mesurements - Compatible with other μISE	*This work*
Optical sensor	0–45 ppm	0.015±0.005	50	10	- Measurements in liquid and gas phase - No consumption of oxygen - Single measurement - pH range 1–14	Presens (www.presens.de)
	0–22.5	0.02	< 50 Tapered tip 140 μm Flat-broken tip	1 30	- Fragile - Display photobleaching - More photostable than tapered sensor tips - Long-term stable - More robust	Loligo Systems (www.loligosystems.com)
	0–200 mmHg	–	250	20–30	- Flexible - Manual temperature compensation	Oxford Optronix (www.oxford-optronix.com)
Electrochemical Clark type, gold electrodes	0–8 ppm	0.01	10–500	1–3	- Single measurement - pH range 1–14	Unisense (www.unisense.com)
	0–20 ppm	–	2000	12	- Probe can be plugged directly into any standard pH meter	Lazar Research Laboratories (www.lazarlab.com)

Profiling of oxygen in biofilms using microelectrodes

Biofilm DO profile study

The suitability of the developed DO-MEA microsensor for biofilm monitoring was evaluated in a heterotrophic aerobic biofilm grown in a FPB. DO profiles were obtained using DO-MEA microsensors with both the external and the integrated RE/CE configuration, and compared to the commercial Clark-type microsensor, widely applied and validate for biofilm monitoring. The thickness of heterotrophic biofilms, typically around 1 mm, allowed using any of the three different DO-MEA designs. The largest MEA sensor design was selected for biofilm monitoring because the 50 μm electrodes due to their higher sensitivity in terms of total current and the lower detection and quantification limits. During the detection process, DO is consumed, however this value has been estimated to be as low as 2.5×10^{-9} mg of DO due to the micro-sized dimensions of the electrodes. Since convection inside biofilms can be neglected, the volume of biofilm affected by the measurement can be obtained using Einstein's relation $\delta = \sqrt{(2Dt)}$ (where D [m$^2 \cdot$s^{-1}] is the DO diffusion coefficient and t=15 s) is 7.1×10^{-11} m^3. The alteration produced by this consumption is extremely local and the biofilm is able to quickly recover its initial conditions, and so this perturbation in the oxygen concentration around the electrodes can be considered negligible.

Both sensors were tested maintaining the same position within the biofilm, for this reason a 3D micromanipulator was used. DO profiles (Fig. 4, right) were obtained by three consecutive 8-point measurements for both DO-MEA microsensor configurations (Fig. 4, left) to cover a total of 24 measurements per microsensor (Fig. 4 left). For the Clark-type microsensor, each measurement was made every 50 μm using the micromanipulator.

The DO profiles with the different microsensors are showed in Fig. 4. The first thing to note when comparing different types of sensor is the different DO concentration measured in the liquid-biofilm interface, being 6.4 DO and

6.8 mg·L^{-1} DO for the DO-MEA sensor with the external and the integrated reference system respectively, and 6.1 mg·L^{-1} DO for the Clark microsensor. These small differences in the concentration measured were maintained throughout all the profile within the biofilm, and became clear again from 1800 μm depth, where according to Clark sensor oxygen was totally depleted, while both DO-MEA sensor profiles indicated that DO was not depleted after 2400 μm. Despite these slight differences in the measured concentrations, all sensors showed the same behavior, being able to observe the same slopes along the three measured DO profiles. Therefore results showed that, considering the response of Clark microsensor as a standard, DO-MEA sensor, with both configurations, detected a slightly higher DO. This fact could be explained by changes in bacteria activity at the recording time of the profiles, because these were not carried out simultaneously. However the most probable cause was the bigger dimensions of the needle width, 500 μm, than that of the Clark microsensor, which altered the biofilm structure, facilitating the entrance of some of the bulk liquid to the biofilm and causing a misleading sensor reading. In order to reduce the disturbance during biofilm profiling, the DO-MEA sensor will be made of a flexible polymer, with a maximum thickness of 50 μm.

Overall, both sensors responses exhibited the same trend, thus confirming the suitability of the developed DO-MEA sensor for biofilm monitoring. The DO-MEA sensor also allowed obtaining the profile more easily, in three 8-points consecutives measurements, reducing the profile variations caused by the dynamics of the biofilm.

Furthermore, in the near future, the use of such microfabricated device will enable the integration of ion selective membranes, which may be deposited selectively in specific microelectrodes in a single needle. The combination of several different modified microelectrodes will enable the acquisition of a specific biofilm profile for a previously defined analytes such as for example oxygen, sodium, potassium

Fig. 4 *Left*: Schematic representation of the three consecutive DO-MEA measurements. *Right*: Microprofiles of DO within an aerobic heterotrophic biofilm using the MEA microsensor with external (♦) and three internal configurations (■), and the commercial Clark-type microsensor (▼)
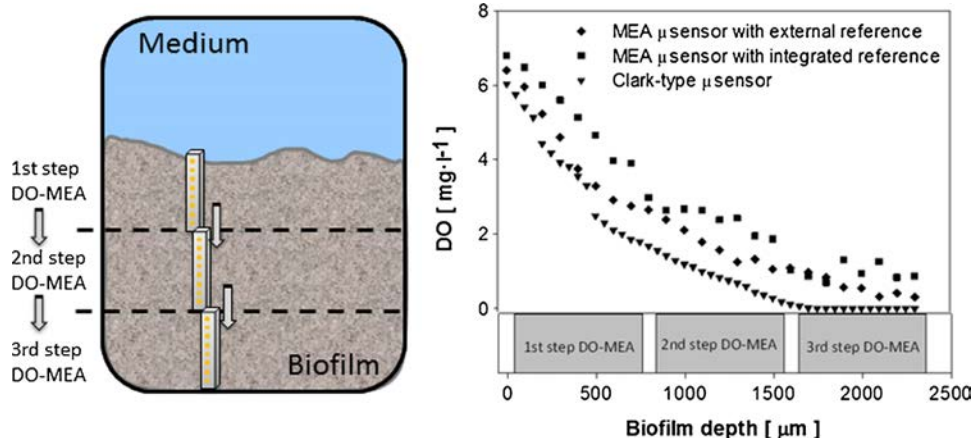
or sulphides. These will provide to this novel platform of high versatility for obtaining desired and specific profiles for deeper studies of biofilms.

Conclusions

The technological improvement and the versatility of the standard microfabrication techniques open the possibility to multiple studies of biofilms with different thickness, even in micro scaled biofilm reactors, at a low cost per sensor and high robustness. The DO-MEA sensor showed a good performance, providing reliable instantaneous information of the activity inside biofilms. DO-MEA sensor exhibited an excellent linear response in the range 0–8 mg·L^{-1} DO for the three different tested designs, with diameters of 50, 25 and 10 μm. The detection and quantification limits of the three designs have been determined, showing low values in all cases.

From the DO-MEA sensor characterization in different conditions and mediums, it can be concluded that the sensor may be suitable under a wide range of conditions (pH, and mineral medium composition and concentration), widening the variety of bioapplications where it can be used.

The developed DO-MEA sensor overcomes most of the commercial Clark-type microsensors drawbacks, such as the high cost per sensor and fragility. In addition, it enables the performance of simultaneously measuring at multiple points. This novel sensor represents an essential tool to record a biofilm profile in a single measurement, reducing significantly the acquisition time of a complete profile. This sensor becomes an extremely important tool that will enable advances in biofilm characterization, obtaining mass transfer and biokinetics phenomena related information. Understanding of these processes will be a key issue to progress in the optimization of applied biotechnologies.

This microfabricated needle has been the proof of concept for DO sensing in this application. However, further technological improvements of these sensors are ongoing for on the one hand reduce the thickness of the needle and thus minimize the damage of the biofilm structure, and on the other hand to cover the electrode area with oxygen-permeable membranes for opening its applicability to extreme biofilm growth conditions.

References

1. Cohen Y (2001) Biofiltration - the treatment of fluids by microorganisms immobilized into the filter bedding material: a review. Bioresour Technol 77:257–274. doi:10.1016/S0960-8524(00)00074-2

2. Gavrilescu M, Macoveanu M (2000) Attached-growth process engineering in wastewater treatment. Bioprocess Eng 23:95–106

3. Okabe S, Itoh T, Satoh H, Watanabe Y (1999) Analyses of spatial distributions of sulfate-reducing bacteria and their activity in aerobic wastewater biofilms. Appl Environ Microbiol 65:5107–5116

4. Ning Y-F, Chen Y-P, Li S et al (2012) Development of an in situ dissolved oxygen measurement system and calculation of its effective diffusion coefficient in a biofilm. Anal Methods 4:2242. doi:10.1039/c2ay25132a

5. Zhou X-H, Liu J, Song H-M et al (2012) Estimation of heterotrophic biokinetic parameters in wastewater biofilms from oxygen concentration profiles by microelectrode. Environ Eng Sci 29:466–471. doi:10.1089/ees.2010.0456

6. Denkhaus E, Meisen S, Telgheder U, Wingender J (2007) Chemical and physical methods for characterisation of biofilms. Microchim Acta 158:1–27. doi:10.1007/s00604-006-0688-5

7. Wang X, Wolfbeis OS (2014) Optical methods for sensing and imaging oxygen: materials, spectroscopies and applications. Chem Soc Rev 43:3666–3761

8. Clark LC, Wolf R, Granger D, Taylor Z (1953) Continuous recording of blood oxygen tensions by polarography. J Appl Physiol 6:189–193

9. Revsbech NP, Jørgensen BB (1986) Microelectrodes: their use in microbial ecology. In: Marshall KC (ed) Adv Microb Ecol. Springer US, pp 293–352

10. Paliteiro C (1994) (100)-Type behaviour of polycrystalline gold towards O2 reduction. Electrochim Acta 39:1633–1639. doi:10.1016/0013-4686(94)85147-6

11. Jeroschewski P, Steuckart C, Eickert G, Kuhl M (1998) A H2S microsensor for profiling biofilms and sediments: application in an acidic lake sediment. Aquat Microb Ecol 15:201. doi:10.3354/ame015201

12. Hang Gao FS (2011) Aerobic denitrification in permeable Wadden Sea sediments. ISME J 5:776. doi:10.1038/ismej.2010.166

13. Wu C-C, Yasukawa T, Shiku H, Matsue T (2005) Fabrication of miniature Clark oxygen sensor integrated with microstructure. Sens Actuators B Chem 110:342–349. doi:10.1016/j.snb.2005.02.014

14. Carlos de la Rosa TY (2006) Development of an automation system to evaluate the three-dimensional oxygen distribution in wastewater biofilms using microsensors. Sens Actuators B-Chem 113:47–54. doi:10.1016/j.snb.2005.02.025

15. Zhou X-H, Qiu Y-Q, Shi H-C et al (2009) A new approach to quantify spatial distribution of biofilm kinetic parameters by in situ determination of oxygen uptake rate (OUR). Environ Sci Technol 43:757–763. doi:10.1021/es802373q

16. Kumar A, Hille-Reichel A, Horn H et al (2012) Oxygen transport within the biofilm matrix of a membrane biofilm reactor treating gaseous toluene. J Chem Technol Biotechnol 87:751–757. doi:10.1002/jctb.3800

17. Lee J-H, Lim T-S, Seo Y et al (2007) Needle-type dissolved oxygen microelectrode array sensors for in situ measurements. Sens Actuators B Chem 128:179–185. doi:10.1016/j.snb.2007.06.008

18. Davies TJ, Ward-Jones S, Banks CE et al (2005) The cyclic and linear sweep voltammetry of regular arrays of microdisc electrodes: fitting of experimental data. J Electroanal Chem 585:51–62. doi:10.1016/j.jelechem.2005.07.021

19. Menshykau D, O'Mahony AM, del Campo FJ et al (2009) Microarrays of ring-recessed disk electrodes in transient generator-collector mode: theory and experiment. Anal Chem 81:9372–9382. doi:10.1021/ac9017633

20. Godino N, Borrisé X, Muñoz FX et al (2009) Mass transport to nanoelectrode arrays and limitations of the diffusion domain approach: theory and experiment. J Phys Chem C 113:11119–11125. doi:10.1021/jp9031354

21. Menshykau D, Cortina-Puig M, del Campo FJ et al (2010) Plane-recessed disk electrodes and their arrays in transient generator–collector mode: the measurement of the rate of the chemical reaction of electrochemically generated species. J Electroanal Chem 648:28–35. doi:10.1016/j.jelechem.2010.07.003

22. Ordeig O, del Campo J, Muñoz FX et al (2007) Electroanalysis utilizing amperometric microdisk electrode arrays. Electroanalysis 19:1973–1986. doi:10.1002/elan.200703914

23. Lanyon YH, Arrigan DWM (2007) Recessed nanoband electrodes fabricated by focused ion beam milling. Sens Actuators B Chem 121: 341–347. doi:10.1016/j.snb.2006.11.029

24. Del Campo FJ, Abad L, Illa X et al (2014) Determination of heterogeneous electron transfer rate constants at interdigitated nanoband electrodes fabricated by an optical mix-and-match process. Sens Actuators B Chem 194:86–95. doi:10.1016/j.snb.2013.12.016

25. Laczka O, del Campo FJ, Muñoz-Pascual FX, Baldrich E (2011) Electrochemical detection of testosterone by use of three-dimensional disc-ring microelectrode sensing platforms: application to doping monitoring. Anal Chem 83:4037–4044. doi:10.1021/ac1031594

26. Sánchez-Molas D, Esquivel JP, Sabaté N et al (2012) High aspect-ratio, fully conducting gold micropillar array electrodes: silicon micromachining and electrochemical characterization. J Phys Chem C 116:18831–18846. doi:10.1021/jp305339k

27. Prehn R, Abad L, Sánchez-Molas D et al (2011) Microfabrication and characterization of cylinder micropillar array electrodes. J Electroanal Chem 662:361–370. doi:10.1016/j.jelechem.2011.09.002

28. Fischer LM, Tenje M, Heiskanen AR et al (2009) Gold cleaning methods for electrochemical detection applications. Microelectron Eng 86:1282–1285. doi:10.1016/j.mee.2008.11.045

29. Bard AJ, Faulkner LR (2001) Electrochemical methods: fundamentals and applications. Wiley, New York

30. Wolff CM, Mottola HA (1978) Enzymic substrate determination in closed flow-through systems by sample injection and amperometric monitoring of dissolved oxygen levels. Anal Chem 50:94–98. doi:10.1021/ac50023a026

31. Lewandowski Z, Beyenal H (2013) Fundamentals of biofilm research, Second Edition. CRC Press

32. Dorado AD, Baeza JA, Lafuente J et al (2012) Biomass accumulation in a biofilter treating toluene at high loads – part 1: experimental performance from inoculation to clogging. Chem Eng J 209:661–669. doi:10.1016/j.cej.2012.08.018

33. Del Campo FJ, Ordeig O, Vigués N et al (2007) Continuous measurement of acute toxicity in water using a solid state microrespirometer. Sens Actuators B Chem 126:515–521. doi:10.1016/j.snb.2007.03.038

34. Murphy VG, Barr RE, Hahn AW (1976) Control of electrode aging by a periodic anodization technique. In: Grote J, Reneau D, Thews G (eds) Oxyg Transp Tissue — II. Springer US, pp 69–75

Electronic Supplementary Material

Profiling of oxygen in biofilms using individually addressable disk microelectrodes on a microfabricated needle

Ana Moya[a,e,†], Xavier Guimerà[b,†], Francisco Javier del Campo[a],
Elisabet Prats-Alfonso[a,e], Antonio David Dorado[b], Mireia Baeza[c], Rosa Villa[a,e],
David Gabriel[d], Xavier Gamisans[b], Gemma Gabriel[a,e,*]

[a]*Instituto de Microelectrónica de Barcelona, IMB-CNM(CSIC), Esfera UAB, Campus Universitat Autònoma de Barcelona, 08193Bellaterra, Barcelona, Spain*

[b]*Department of Mining Engineering and Natural Resources, Universitat Politècnica de Catalunya, Avinguda de les Bases de Manresa 61-73, 08240 Manresa, Spain*

[c]*Department of Chemistry, Facultat de Ciències, Edifici C-Nord, Univeritat Autònoma de Barcelona, 08193 Bellaterra, Barcelona, Spain*

[d]*Department of Chemical Engineering, Universitat Autònoma de Barcelona, EdificiQ, 08193 Bellaterra, Barcelona, Spain*

[e]*Biomedical Research Networking Center in Bioengineering, Biomaterials and Nanomedicine (CIBER-BBN),Zaragoza, Spain*

Microfabrication of DO-MEA sensor

The DO-MEA sensor consisted of an array of eleven gold disk microelectrodes fabricated on a 500µm thick Pyrex wafer (Fig. S1). Because the multipotentiostat used in this work has eight channels, only eight out of eleven WE could be operated simultaneously, and one of the other three as a pseudo-reference electrode. A rectangular CE (2.500 mm x 0.115 mm) was also fabricated running along the needle axis along the microdisk array, which was configured as a single row as shown in Fig. S1. Due to the wide range of biofilm thicknesses, three different DO-MEA sensor designs were manufactured and characterized. Microelectrodes with 50 µm, 25 µm and 10 µm diameter and separations between electrodes of 50 µm, 50 µm and 25 µm, respectively, were used in this study.

Microsensors were fabricated in the clean room facilities at the Barcelona Microelectronics Institute (Spain), through standard photolithography techniques as it is well reported in the literature [1–3]. In summary, three metal layers were deposited by sputtering over a Pyrex wafer (Fig. S1a-b). A thin titanium layer (15 nm) was deposited first to improve the adhesion of subsequent metals, a second nickel layer (15 nm) was deposited provide a diffusional barrier and prevent the formation of intermetallic Ti-Au compounds, and a final gold layer (150 nm) was deposited. Subsequently, electrodes and metal tracks were patterned using selective wet etching baths following a standard lithographic process (Fig. S1c). Finally, in this work, SU-8 negative photoresist was chosen as the passivation material due to its optimal dielectric properties and ease of implementation [4]. In particular, a 1.9 µm SU-8 layer was spin-coated and the electrode active area and the connection pads were defined (Fig. S1d).

* Corresponding author. Tel.: +34 93 594 77 00x2506 fax: +34 93 580 02 67. *E-mail address:*
gemma.gabriel@imb-cnm.csic.es
† These authors contributed equally to this study.

After the clean room process, a disk saw was used to dice the wafer into individual needle-shaped chips (>300) of dimensions 10.85 mm x 1.25 mm per probe. Next, each of these probes was fixed on a printed circuit board (PCB) and wire bonding was used for electrical connections. To protect the wire bond connection, the packaging process ended with the complete coverage of the PCB with a thermocurable resin (H77, Epotek, USA).
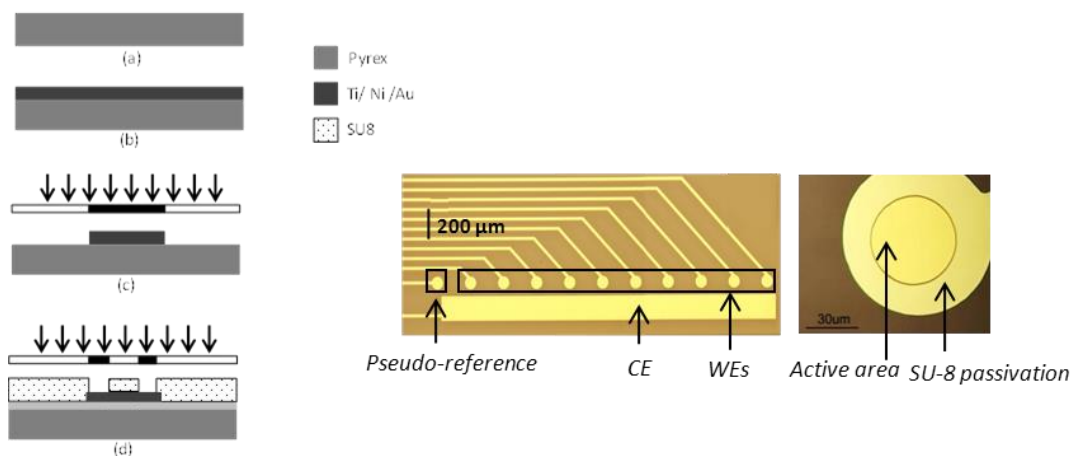
Fig. S1. Left: The process of fabricating the microelectrode arrays using standard photolithographic techniques. Right: DO-MEA design of 11 gold disk microelectrode array and a rectangular macroelectrode on a 500 μm thick Pyrex substrate and featuring SU-8 passivation.

Electrode preparation

For the sensor surface cleaning Hellmanex III, (Hellma Analytics, Germany), isopropanol (LC/MS grade) and acetone (HPLC grade) (both from Fisher Scientific, UK).

Microelectrodes required activation before use. Several known gold-cleaning methods were investigated. Immersion of the sensor for 1hour in a solution of 75% v/v 50mM KOH and 25% v/v of H_2O_2 was the selected method to clean the DO-MEA sensors. This method is the mildest we found for the removal of the SU-8 traces from the surface of the microfabricated electrodes.It was found that immersion must be repeated three times to obtain an optimal response of the sensor. Other cleaning methods such as: applying a potential sweep in a potassium hydroxide solution (KOH Sweep), cycling the electrode potential in a weak sulfuric acid solution (H_2SO_4), or applying a suitable potential waveform in KNO_3 solution were also tested, also resulting in a good activation response. However, repeated electrode activation was necessary, and the least aggressive method was treatment by KOH + H_2O_2. The conditions used in each method can be found elsewhere [5].

Before activation in KOH+H_2O_2, the electrodes were cleaned with standard washing proceduresin ausing a 2% v/v Hellmanexsolution in deionized water, acetone and isopropanol followed by deionized water to remove grease and organic deposits.

Before and after the cleanning procedure, each electrode was subjected to a cyclic volammetry from 500 mV to -200 mV, at a scan rate of 100 mV·s^{-1} in 0.01M ferro/ferri cyanide and 0.1M KNO_3 solution to determine its state of activation. Resulting voltammograms, display the electrochemical characteristics in terms of absolute potential between the reduction and

oxidation peak (ΔE_p) and the current reduction/oxidation peak (I_p). Adequate electrode activation was indicated by Ip and ΔE_p values consistent with reversible electrode kinetics.

Detailed schematic of the calibration set-up.

The DO-MEA sensor was calibrated in the 3-electrode calibration cell (1), with a commercial RE (2) and CE (3), and the WEs (4). A potentiostat (5) was used to apply the voltages and to measure the currents during sensor calibration. The DO concentration inside the calibration cell was adjusted by bubbling a gas mixture (6) and measured by a commercial DO sensor (7).

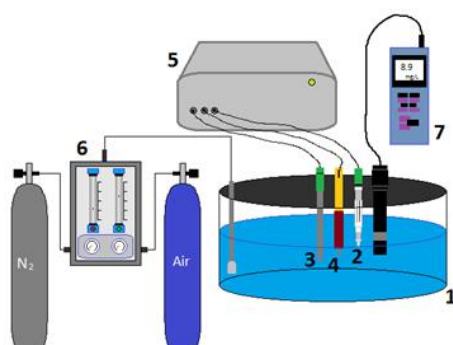Fig. S2. Schematic of the calibration set-up.

Schematic of the FPB and the devices used to measure DO concentrations profiles
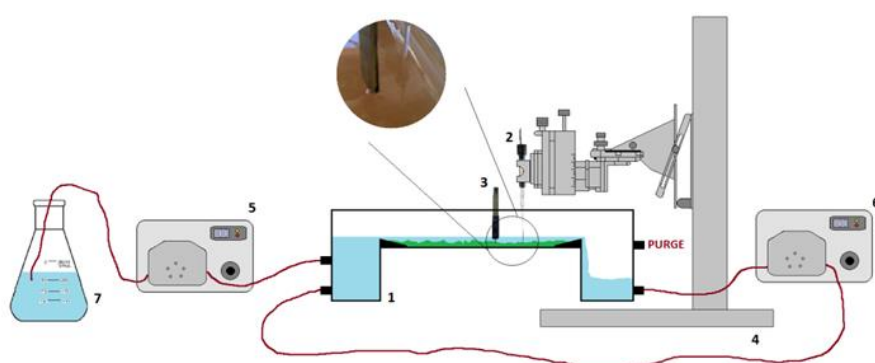
Fig. S3. Schematic of the FPB and genereal setup.

Flat Plate Bioreactor (1), DO Clark-type microsensor (2), DO MEA sensor (3) and micromanipulator (4). Instrumentation for the reactor operation: feeding (5) and recirculation (6) pumps, mineral medium stock solution (7).

Theoretically equations corresponding to a diffusion controlled limiting current

For an inlaid microdisc electrode, the steady-state current is described by eq. S1. However, most microfabricated microelectrodes, including the ones in the needle presented in this work, are recessed, which negatively affects mass transport. Bond et al. [6] derived the following equation (eq. S2) that describes the current response of recessed microelectrodes [7–9].

$$I \lim_{inlaid} = 4 \cdot n \cdot F \cdot D \cdot c \cdot r \qquad (S1)$$

$$I \lim_{recessed} = \frac{4 \cdot n \cdot F \cdot D \cdot c \cdot r}{\left(\frac{4 \cdot L}{\pi \cdot r} + 1 \right)} \qquad (S2)$$

Where n is the number of electrons transferred during oxygen reduction reaction, F [C·mol^{-1}] is the Faraday constant, D [m^2·s^{-1}] is the DO diffusion coefficient, r [m] is the microelectrode radius, c [mol·m^{-3}] is the DO concentration and L [m] is the height of the passivation layer producing the recess. Another way to describe the behavior of microelectrodes of any geometry is by means of numerical simulations [8], although eq. S2 sufficed for the purposes of the present work.

Detection and quantification limits determination

Sensor calibration was completed by determining the detection and quantification limits (L_D and L_Q respectively), which were calculated according to IUPAC standards [10], using eq. S3 and S4 respectively.

$$L_{D,DO} = \frac{3 \cdot S_B}{S} \qquad (S3)$$

$$L_{Q,DO} = \frac{10 \cdot S_B}{S} \qquad (S4)$$

where S_B is the standard deviation of ten measurements in blank conditions (0% O$_2$), and S the slope of the calibration curve (sensitivity). These equations consider a linear calibration curve, normal distribution data and constant variance in each measurement. The 0% O$_2$ concentration condition was reached by adding a saturated Na$_2$SO$_3$ solution to remove the dissolved oxygen in the 0.1M KNO$_3$ solution.

Effect of the mineral medium in the DO-MEA microsensor response

In order to determine the working range of the sensors, their response in media of different composition was also studied. Since the most important variables in the study of biological systems are the nature of the medium, the effects of mineral medium composition (Fig. S4) and of pH (Table S1), the effect of these parameters on the DO-MEA sensor performance was studied separately.
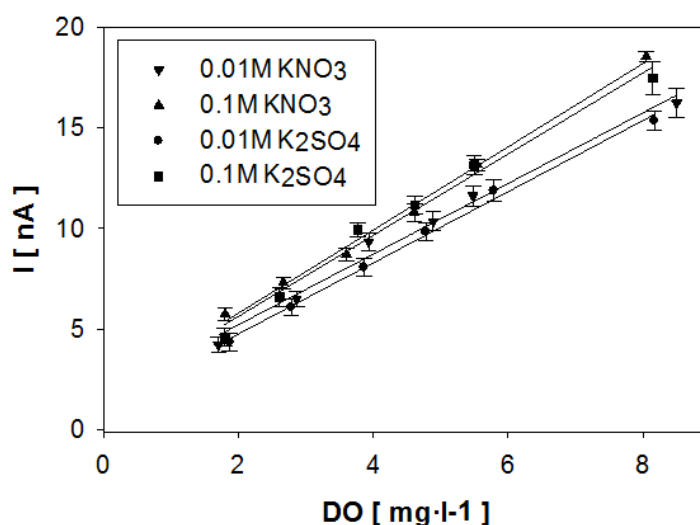
Fig. S4 Mineral medium composition effect on DO-MEA sensor response. The points correspond to the average current and the standard deviations for eight different electrodes of the same DO-MEA sensor in four different solutions (0.01 M KNO_3, 0.1 M KNO_3, 0.01 M K_2SO_4 and 0.1 M K_2SO_4).

Results indicate that changing the salt anion of the supporting electrolyte has no effect on the sensor sensitivity as can be observed comparing the KNO_3 and K_2SO_4 calibration curve slopes (sensitivities), where differences of less than 1 % were found. However, changes in ionic strength significantly affected the sensor response. The figure shows that a ten-fold dilution of the supporting electrolyte resulted in a 13 % sensitivity decrease.

In addition, the effect of the medium pH on the DO-MEA microsensor behaviour was also tested. Table 2 summarizes the results obtained from eight microelectrodes in a KNO_3 solution at six different pH between 2 and 10. It is important to note that the polarized potential, where the measurements were done, change depending of the pH value. A linear sweep was done before each pH experimental in order to detect the limiting current value of the second reduction step.

Table S1. Summary of electrode responses of different medium pH. Sensitivity increases with pH.

pH	Sensitivity ($nA \cdot mg^{-1} \cdot L$ DO)	Sensitivity deviation ($nA \cdot mg^{-1} \cdot L$ DO)	Offset (nA)	R^2
10	2.79	0.02	1.10	0.999
8	2.52	0.09	1.04	0.998
6	2.41	0.08	0.98	0.994
4	1.70	0.09	2.80	0.995
3	1.7	0.2	5.91	0.996

2	1.3	0.2	6.22	0.990

Results show that the oxygen signal was nearly unaffected by pH changes in the 6<pH<8 range, as reported in [11]. Out of this range, pH has a strong effect on the sensor sensitivity. This effect appears because the oxygen reduction potential increases with pH, reducing the interferences caused by the formation of hydrogen and resulting in more sensitive oxygen detection at alkaline pH. The deviation in the sensor sensitivity was affected in the same way by pH because at lower pH the contribution to the current from the hydrogen evolution reaction increases relative to that from the oxygen reduction. This behaviour is clearly shown by the offset displayed by the different calibration curves, and which increases in acid conditions. Despite the variable response of the sensor response at different pH, satisfactory correlation coefficients were obtained (Table 1), indicating that the sensor operation is adequate over the pH range tested.

References

1. Gabriel G, Erill I, Caro J, et al. (2007) Manufacturing and full characterization of silicon carbide-based multi-sensor micro-probes for biomedical applications. Microelectron J 38:406–415. doi: 10.1016/j.mejo.2006.11.008

2. Guimera A, Gabriel G, Plata-Cordero M, et al. (2012) A non-invasive method for an in vivo assessment of corneal epithelium permeability through tetrapolar impedance measurements. Biosens Bioelectron 31:55–61. doi: 10.1016/j.bios.2011.09.039

3. Bonilla D, Mallén M, de la Rica R, et al. (2011) Electrical Readout of Protein Microarrays on Regular Glass Slides. Anal Chem 83:1726–1731. doi: 10.1021/ac102938z

4. Del Campo FJ, Abad L, Illa X, et al. (2014) Determination of heterogeneous electron transfer rate constants at interdigitated nanoband electrodes fabricated by an optical mix-and-match process. Sens Actuators B Chem 194:86–95. doi: 10.1016/j.snb.2013.12.016

5. Fischer LM, Tenje M, Heiskanen AR, et al. (2009) Gold cleaning methods for electrochemical detection applications. Microelectron Eng 86:1282–1285. doi: 10.1016/j.mee.2008.11.045

6. Bond AM, Luscombe D, Oldham KB, Zoski CG (1988) A comparison of the chronoamperometric response at inlaid and recessed disc microelectrodes. J Electroanal Chem Interfacial Electrochem 249:1–14. doi: 10.1016/0022-0728(88)80345-0

7. Menshykau D, O'Mahony AM, del Campo FJ, et al. (2009) Microarrays of Ring-Recessed Disk Electrodes in Transient Generator-Collector Mode: Theory and Experiment. Anal Chem 81:9372–9382. doi: 10.1021/ac9017633

8. Godino N, Borrisé X, Muñoz FX, et al. (2009) Mass Transport to Nanoelectrode Arrays and Limitations of the Diffusion Domain Approach: Theory and Experiment. J Phys Chem C 113:11119–11125. doi: 10.1021/jp9031354

9. Menshykau D, Cortina-Puig M, del Campo FJ, et al. (2010) Plane-recessed disk electrodes and their arrays in transient generator–collector mode: The measurement of the rate of the chemical reaction of electrochemically generated species. J Electroanal Chem 648:28–35. doi: 10.1016/j.jelechem.2010.07.003

10. Currie LA (1968) Limits for qualitative detection and quantitative determination. Application to radiochemistry. Anal Chem 40:586–593. doi: 10.1021/ac60259a007

11. Campo FJD, Ordeig O, Muñoz FJ (2005) Improved free chlorine amperometric sensor chip for drinking water applications. Anal Chim Acta 554:98–104. doi: 10.1016/j.aca.2005.08.035

3.3.2 Paper II: Miniaturized multiparametric flexible platform for the simultaneous monitoring of ionic compounds in microfluidic cell culture systems: Application in real urine

The second paper presented in this Chapter, **Paper II**, is a published article focused in the development of a single low-cost microfluidic multisensing platform that can be connected at the inlet and outlet ports of a microfluidic OOC system, for the simultaneous measurement of dissolved oxygen, Na^+, K^+ and pH compounds. This platform is fabricated in Kapton® substrate using microfabrication technologies and rapid prototyping techniques. Their applicability is addressed to any type of microfluidic system, and here it is validated for the specific case of monitoring a renal tubular tissue, with the use of urine samples.

This article is In Press 'Accepted Manuscript' in Sensors and Actuators: B journal *:
Ana Moya, Xavi Illa, Ignacio Gimenez, Yoskaly Lazo-Fernandez, Rosa Villa, Abdelhamid Errachid, Gemma Gabriel. **Miniaturized multiparametric flexible platform for the simultaneous monitoring of ionic compounds: Application in real urine**. In Press 'Accepted Manuscript'.

This work has been also presented in different conferences with their corresponding Proceeding:

- Conference **SENSORS, 2014 IEEE**: A. Moya, X. Illa, E. Prats-Alfonso, N. Zine, G. Gabriel, A. Errachid, R. Villa, Flexible microfluidic bio-lab-on-a-chip multi-sensor platform for electrochemical measurements, in: IEEE SENSORS 2014 Proceedings, 2014: pp. 1018–1021. doi:10.1109/ICSENS.2014.6985176.

- Conference **EUROSENSORS 2014**: A. Moya, N. Zine, X. Illa, E. Prats-Alfonso, G. Gabriel, A. Errachid, R. Villa, Flexible Polyimide Platform based on the Integration of Potentiometric Multi-sensor for Biomedical Applications, Procedia Engineering. 87 (2014) 276–279. doi:10.1016/j.proeng.2014.11.661.

Note that sections, equations and references numbering in the reproduced research article follow the ones of the published version.

Miniaturized multiparametric flexible platform for the simultaneous monitoring of ionic: Application in real urine

Ana Moya[a, d, e], Xavi Illa[a, d], Ignacio Gimenez[b], Yoskaly Lazo-Fernandez[b], Rosa Villa[a, d], Abdelhamid Errachid[c], Gemma Gabriel[a, d, *]

[a] *Instituto de Microelectrónica de Barcelona, IMB-CNM (CSIC), Esfera UAB, Campus Universitat Autònoma de Barcelona, 08193 Bellaterra, Barcelona, Spain*
[b] *Instituto Aragonés de Ciencias de la Salud (IACS), IIS Aragón, Universidad de Zaragoza, Spain*
[c] *Université de Lyon, Institut des Sciences Analytiques, UMR 5280, CNRS, Université Lyon 1, ENS Lyon, 5 rue de la Doua, F-69100 Villeurbanne, France*
[d] *Biomedical Research Networking Center in Bioengineering, Biomaterials and Nanomedicine (CIBER-BBN), Spain*
[e] *Universitat Autònoma de Barcelona (UAB), Spain*

ABSTRACT

Biomonitoring is a research topic that has largely relied on cell culture systems. Recently, the development of "Organ-on-a-Chip" (OC) platforms and the need for a continuous monitoring of these systems has increased its interest. However, the biomonitorization in these systems is still at its infancy due to the difficulty to adapt the sensors to microfluidic OC systems. In this work we have fabricated a modular, versatile, scalable, multi-analyte sensing platform, which integrates dissolved oxygen (DO), Na^+, K^+ and pH sensors for monitoring their concentrations in small volume of biological fluids. The platform is fabricated by means of rapid prototyping techniques using polymeric substrates, and incorporates all the necessary elements to measure the four analytes. It was designed with four gold sensing electrodes, and integrates a gold counter electrode and an Ag/AgCl pseudo-reference electrode for the electrochemical measurements in small volumes (0.83 µL) of samples. The sensors featured good sensitivities of 3.60 ± 0.2 nA (mg L^{-1}) for DO and 69 ± 1 mV decade^{-1} for pH. Na^+ and K^+ µISE exhibited sensitivities of 57 ± 1 mV decade^{-1} and 52 ± 2 mV decade^{-1}, and low limits of detection 5×10^{-6} M and 0.5×10^{-5} M respectively. This platform allows the dynamic measurement of the biological fluids parameters simultaneously, in real time and with a rapid response. The versatility of the platform allows its adaptation in any microfluidic cells culture systems. The novel multi-sensor platform has been validated in controlled buffers and with artificial urine (AU). A proof-of-concept using real mice urine (RU) has been carried out, demonstrating the good behaviour of the multi-sensing platform.

© 2017.

1. Introduction

The growth of a cell culture is a complex biological process that requires monitoring of various biological parameters in real time. Conventional two-dimensional (2D) cell culture systems are being largely used, but often the results obtained from these systems do not readily translate to *in-vivo* scenarios due to the fundamental difference of these reductive models compared with native tissues and organs [1]. It is in this context where microfluidic cell culture systems [2–5] and more advanced "Organ-on-a-Chip" systems (OC) have emerged to recreate a more physiological microenvironment [6–10].

In the field of biomonitoring, the interest in integrating sensors for in situ monitoring of cell growth has increased in the last decade [11–13]. Up to now, most of the systems which present miniaturized devices with integrated electrochemical sensors are still based on static cell cultures systems [14,15]. However, multiparameter electrolyte monitoring in microfluidic cell cultures is barely used and poses challenges. Conventional analytical methods require manual sample collection from the microfluidic system, large working volumes, and frequent system disturbance, and thus are not suitable for miniaturized platforms.

The analysis of real samples implies the determination of several ions. Analytes of interest are related to acidification, respiration and some ions, such as sodium and potassium among the most general ones [16,17]. Oxygen consumption [18] and acidification [19] are both indicative of cell metabolism. They are among the most relevant biological parameters, well suited for the sensitive detection of cellu-

lar response to drugs or toxic compounds or just to monitor of cell life activity [20]. Monitoring of extracellular ion activities can be of interest in applications involving the study of tissue/organs whose function is sensitive to extracellular ion concentrations (excitable cells like neurons or muscle) or depends on the establishment and maintenance of ion concentrations gradients through epithelial barriers [11].

In order to obtain biologically relevant information, it is necessary to use a system capable to measure multiple ions from small volumes in a greatly short and real time. To achieve this, the miniaturization and the simultaneous measurement of ions are important issues for the application; however, it is also necessary to achieve a cost-effective system. The use of polymeric substrates for developing microfluidic systems for electrochemical applications has increased during the last years [21–23]. Specifically, several studies have presented platforms for potentiometric measurements made with flexible polyimide Kapton® [24,25] overcoming the cost limitations that suppose the use of silicon substrates. The use of Kapton® as a substrate has many attractive properties in contrast to other low-cost materials such as thermal and mechanical stability, high chemical resistance, and low dielectric constants.

In this contribution we present a single low-cost platform based on Kapton® and encapsulated on a microfluidic device using laminated polymers by means of rapid prototyping techniques [26,27]. It incorporates four electrochemical sensors for the non-invasive measurement of: dissolved oxygen (DO), Na^+, K^+ and pH. The electrode array is formed by 4 gold electrodes, one working electrode (WE) for the amperometric measurement, and three other electrodes for each potentiometric measurement, a common integrated Ag/AgCl pseudo reference electrode (pRE), and a gold counter electrode (CE). For Na^+ and K^+ measurements, microsensors are based in the most common construction of micro ion-selective electrodes (µISE) which consist on an ion-selective polymeric membrane containing the specific ionophore [28,29]. The polymeric membrane is deposited on top of a conducting polymer material based on electropolymerized pyrrole (PPy) layer since is one of the most stable contact layer known [30,31]. The pH sensor is obtained with the electrochemical coating iridium oxide (IrOx) layer of its sensing electrode [32,33].

Special care has been taken with the combination and integration of all the different sensors, because the fabrication methods need to be compatible. Another goal was to find conditions for sensor storage preserving adequate sensitivity and selectivity for the detection of several analytes.

As a proof of concept, the platform was validated measuring the Na^+, K^+ ions and pH using artificial urine samples (AU) with different ion concentration levels and also with real mouse urine (RU) samples obtained from mice fed with gel food formulated to contain varying amounts of sodium and potassium. DO in urine is not a relevant physiological parameter and has to be measured under very stringent conditions that cannot be met with the use of stored samples. However, oxygen control is essential for cell cultures systems since is vital in the energy metabolism of cells and, moreover it is an important regulatory parameter, influencing cell differentiation and tissue zonation [34,35]. We are currently using this platform for DO measurements successfully, in projects involving monitoring of metabolic activity in human cell cultures.

Our efforts have been focused on developing a more realistic device that combines low volume microfluidics with multi-analyte sensing, allowing the detection in biological fluids (including cell culture media) of different ions simultaneously. Special attention has been done in fabricating a versatile, modular, scalable platform that can be placed in series with different microfluidic cell culture systems, to

monitor chemical species in real time. Simplicity in the design and miniaturization of multisensing platform will facilitate adapting the platform to sense other analytes in cell culture monitoring.

2. Material and methods

2.1. Reagents

All solutions used in the sensors development were prepared with deionized water (conductivity less than $1 \, \mu \, cm^{-1}$). Although specified, all the reagents were bought at Sigma-Aldrich, and used as received. For the electrode surface cleaning, activation and characterization were used ethanol (LC/MS grade), sodium nitrate (KNO_3), potassium hexacyanoferrate(III) $K_3[Fe(CN)_6]$ and potassium hexacyanoferrate(II) $K_4[Fe(CN)_6]$. For the integration of the pRE were used a commercial silver solution (silvrex-s) from Enthone-Omi; ammonia, nitric acid (HNO_3), hydrochloric acid (HCl), polyvinyl butyral (PVB), methanol and sodium chloride (NaCl). For the development of the pH sensor were used iridium trichloride trihydrate ($IrCl_3 \cdot 3H_2O$), oxalic acid ($H_2C_2O_4 \cdot 2H_2O$) and potassium carbonate (K_2CO_3). For pH sensor calibration was used HCl and sodium hydroxide (NaOH). For the preparation of the µISE were used 2-nitrophenyl octyl ether (o-NPOE), dioctyl sebacate (DOS), dibutyl phosphate (DBP), potassium tetrakis(4-chlorophenyl)borate (KTpClPB), polyvinylchloride (PVC), potassium ionophore I, sodium ionophore X, tetrahydrofuran (THF), chloroform, acetonitrile, pyrrole, NaCl and cobaltabis (discarbollide) ions ($Cs[Co(C_2B_9H_{11})_2]$ from KATCHEM spol. The nitrate salts of all cations used for the characterization (Na^+, K^+, Li^+, Ca^{2+}, Mg^{2+}) were of the highest purity available. Phosphate-buffered saline (PBS) was used to storage the sensors. Finally, for the preparation of AU samples were used urea, uric acid, creatinine, $Na_3C_6H_5O_7 \cdot 2H_2O$, NaCl, KCl, NH_4Cl, $CaCl_2 \cdot 2H_2O$, $MgSO_4 \cdot 7H_2O$, $NaHCO_3$, NaC_2O_4, Na_2SO_4, $NaH_2PO_4 \cdot H_2O$ and Na_2HPO_4.

2.2. Equipment

All measurements were carried out at room temperature. The activation and characterization of the gold electrodes, and also the electrodeposition of the IrOx and PPy films, were performed in a single compartment cell with a standard three-electrode system using an 8-channel potentiostat (1030A Electrochemical Analyzer, from CH-Instruments). These experiments were done using a commercial Ag/AgCl double junction reference electrode (from Thermo Orion), and a platinum ring electrode as auxiliary electrode (from Metrohm). The silver of the pRE was electrodeposited vs a platinum film, by an Autolab (PGSTAT 12, from Chemie BV). Scanning Electron Microscopy (SEM, Auriga-40, from Carl Zeiss) was used to study the morphology of the electrodeposited films.

The oxygen sensor was calibrated in controlled dissolved solutions against an oxygen probe (OXI 325, from WTW). Oxygen concentrations were changed by a nitrogen-air distributor. DO sensor calibration and the characterization [35] was done using the 8-channel potentiostat (1030A Electrochemical Analyzer, from CH-Instruments). The pH sensor calibration was done in different pH solutions and a commercial pH-meter was used for the correlation of the obtained potentials (GLP22, from Crison). The calibration of the pH and µISE sensors were done using home-made data acquisition system set-up with four multi-channel microelectrodes to measure open circuit potential, connected and controlled by a personal computer. For all calibrations was used a magnetic stirrer to quickly homogenize their concentrations.

For the experimental validation, the measured Na^+, K^+ ions of different sample of mouse urine were correlated using an atomic spectrometer (929 Solar AA Spectrometer, ATI Unicam, from Prince Technologies B.V).

2.3. Microfluidic platform fabrication

The multi-sensor platform is composed of three different polymeric layers. The bottom one is a 127 μm thick polyimide film (Kapton® 500HN, DuPont) that incorporates an array of six gold microelectrodes: four gold electrodes, a WE for the amperometric measurement, and three for each potentiometric measurement, a pRE and a CE. The middle layer is a structured Polyethylene terephthalate (PET)-two-side adhesive sheet of 175 μm of thickness (AR8939, obtained from Adhesives Research Europe) where the microfluidic channel is defined, and the top layer is a 188 μm cyclo-olefin polymer (COP) film (Zeonex ZF14-188, purchased from Ibidi GmbH) that acts as a cover and where the inlet and outlet of the microfluidic channel are defined.

The platform was fabricated in the clean room facilities of the IMB-CNM (CSIC), at a wafer level (Fig. 1A). In brief, 10/100 nm Ti/Au layers were evaporated on the Kapton® film to fabricate the microelectrodes via lift-off using the AZ5214E image reversal photoresist. The Ti layer was used to improve the adhesion between gold electrodes and polymeric substrate. The active area of the electrodes and the geometry of the microfluidic channel were defined by structuring a PET-two-side adhesive sheet and bonding it to the Kapton® substrate, obtaining a total channel dimension of 9.5 mm x 0.5 mm. The sample volume required to fill the channel is 0.83 μL. This passivation strategy avoids further passivation and reduces fabrication time and costs. A COP sheet was used to close the channel due its optical transparency as it is necessary to observe inside the channel. Both, COP and PET sheets were cut in Roland GX-24 cutter plotter and were manually aligned using a custom made tool [27]. After the fabrication and encapsulation processes, the sensors were individualized by cutting them using the cutter plot obtaining 14 sensors per wafer with total dimensions of 14 mm x 25 mm (Fig. 1B). The connection to the electrode pads was done by using a zero insertion force (ZIF) connector. This strategy reduces the costs and the fabrication time and also allows the reusability of the connectors.

Finally, a custom holder fabricated in polymethymethacrylate (PMMA) was used for easy handling of the chip as shown in Fig. 1C. The holder was designed in order to have both fluidic and electrical access to the electrodes in a reliable and simple manner and with the possibility to place and remove the chip in an easy way.

2.4. Sensors development

Microelectrodes require activation before its use. Among the different gold-cleaning methods investigated [36], we chose the application of a suitable potential waveform to clean the multi-sensor platform. In particular, five pulses alternating between − 2 V and 0 V during 10 s in a KNO_3 electrolyte solution were performed. Adequate electrode activation was indicated by Ip and ΔEp values consistent reversible electrode kinetics [37]. For this, cyclic voltammetry (CV) measurements in ferro/ferricyanide (10^{-2} M) were carried out in static and dynamic way. Before activation, the electrodes were cleaned by sonication in ethanol for 5 min and rinsed in deionized water to remove grease and organic deposits.

2.4.1. pRE development

The integrated pRE was developed by electrodepositing silver onto the gold microelectrode (electrode labelled 1 in Fig. 2A). The active area of the pRE was 0.05 mm^2. The sensor surface was submerged in the silver solution, with a concentration of 32 g/L, and a constant current of 10 μA during 120 s was applied. After that, in order to achieve the purity of the silver layer, the surface was cleaned submerging it in concentrated ammonia during 1 h and after, in HNO_3 (0.1 M) during 2 h [38]. For the chlorination, the electrodes with the silver film were submerged in HCl (0.1 M) and a voltammogram from 0 V to 0.2 V was applied. In order to achieve a stable Ag/AgCl pRE in presence of different ion compounds, a PVB solution in methanol where NaCl was dispersed, was drop-casted onto the pRE. This type of membrane presents an outstanding stability to change in solution concentration, light, pH and redox potential [39]. Stability of the pRE potential was studied for 24 h in a KCl (3 M) solution exhibiting a good stability with a drift rate less than 0.11 mV h^{-1}. Fig. 2A.1 shows the SEM image of a Ag/AgCl pRE integrated in the platform before the deposition of the PVB membrane.

2.4.2. DO sensor development

DO was measured with amperometric method. Clark type microsensors [40] are the most commonly used probes in this type of measurement, where a polarized potential is applied to the WE and the reduction of the current generated at it is directly proportional to the oxygen concentration of the solution. The necessary three electrodes were integrated in our platform; a pRE (electrode labeled 1 in
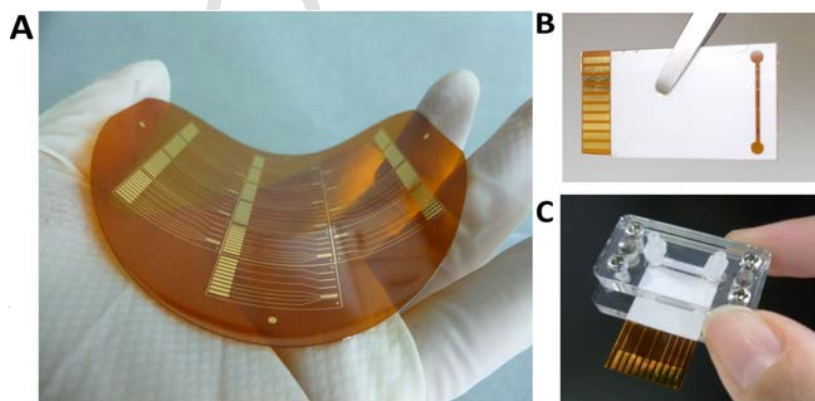
Fig. 1. A) Flexible polyimide multi-sensor platform fabricated on flexible Kapton® substrate at wafer-level; B) Individualized multi-sensor with a total dimensions of 14 × 25 mm, passivated by PET sheet which defines the microfluidic channel of 9.5 × 0.5 mm; C) PMMA custom holder for fluidic and electrical access.
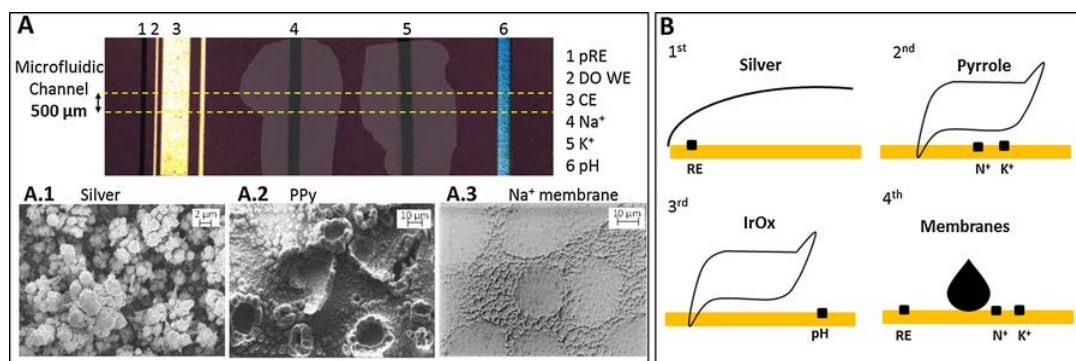
Fig. 2. A) Image of the platform after the development of the microsensors. It incorporates the pRE (Ag/AgCl), the three electrodes for the DO measurement, the Na^+ µISE and the K^+ µISE membranes deposited onto the PPy layer and the coated IrOx for the pH measurement; SEM images of A.1) Ag/AgCl pRE; A.2) gold microelectrode after growing PPy[3,3'-Co(1,2-C2B9H11)2]; and A.3) the deposited cocktail Na^+ membrane, B) Schematic of the required order for the sensors development processes.

Fig. 2A), a WE (electrode labelled 2 in Fig. 2A) and a CE (electrode labelled 3 in Fig. 2A). The active area of the CE was 0.25 mm^2, ten times higher than area of the WE (0.025 mm^2). Sensors were calibrated in the oxygen concentration range between 0 and 8 mg L^{-1} DO as it is well described in our previous work [35]. The sensor was polarized at -850 mV as the optimal potential value for the determination of the DO concentration. The DO concentration was adjusted by bubbling different nitrogen (O$_2$ free) $-$ air (21% O$_2$) mixtures through a KNO$_3$ (0.1 M) solution, and a magnetic stirrer was used to ensure better mixing of the solution. The concentration of DO in the cell was measured with a commercial DO probe and correlated with the measured polarization currents of each microelectrode in order to build the calibration curves. Sensor resolution was evaluated using a definition of limit of quantification (LOQ) and limit of detection (LOD) defined by IUPAC [41]. LOQ is equal to the blank conditions (0% O$_2$) plus ten times their standard deviation. The LOD is obtained with the same blank conditions plus three time their standard deviation.

2.4.3. Na^+ and K^+ sensor development

Na^+ and K^+ were measured with a potentiometric method. The most common construction of the µISE requires an ion-selective membrane of a polymeric type containing the specific ionophore [28]. PVC is conventionally used as a membrane matrix since PVC-membrane enhances the retention of the membrane components and extends the lifetime of the electrode [29]. In addition, a conventional ISE has an inner electrolyte solution that makes more difficult its miniaturization. In order to solve it, many investigations have been dedicated to the replacement of the internal solution for a conducting polymer used as a solid-contact layer [42,43].

In this work, for the development of the µISE, a conductive solid internal contact layer between the gold electrode and the sensing membrane was prepared by electropolymerization of the pyrrole (10^{-1} M) in presence of Cs[Co(C$_2$B$_9$H$_{11}$)$_2$] (3.5 × 10^{-2} M) in acetonitrile over the surface of the gold sensing electrode (electrode labelled 4 and 5 in Fig. 2A), with an area of 0.1 mm^2. The high over oxidation resistance provided by the cobaltabis(discarbollide) represents a significant improvement in the long term stability of such membranes as it is described in [44]. The electrodeposition conditions of the PPy films were carefully studied to ensure the best adhesion and charge transfer between the electrodes and the membranes. The best response was obtained by applying a redox potential from -0.2 V to 1.1 V at a scan rate of 100 mV s^{-1} during 10 cycles. Fig. 2A.2 shows a SEM image of the electrodeposited PPy layer.

Finally, different PVC-membranes compositions were studied. In particular, three different membranes with different plasticizers were prepared and studied, since the solvent used in the composition of the membranes influences the characteristics of microelectrodes, such as the dielectric constant of the membrane and the mobility of the ionophore molecules [45]. They were prepared by mixing 1 wt.% of commercial ionophore, 33 wt.% of PVC matrix, 65.5 wt.% of plasticizer (DOS, o_NPOE or DBP) and 0.5 wt.% of KTpClPB additive; all dissolved in 5 mL of THF with 0.5 mL of chloroform [46–48]. This mixture was deposited manually on top of the PPy layer surface (sodium membrane over the electrode labelled 4 and potassium membrane over the electrode labelled 5 as shown in Fig. 2A), and kept then in air overnight at room temperature in order to evaporate the solvent. They were subsequently hydrated in PBS buffer for at least 24 h before use and always stored in the same solution. Fig. 2A.3 shows the SEM image of electrode labelled 4 covered by the sodium membrane.

Calibration curves were obtained by adding successive aliquots of sodium or potassium nitrate solutions (prepared with a concentration range of 1–10^{-5} M by serial dilution) under magnetic stirring, to increase the concentration of the anion from 10^{-8} M to 10^{-1} M in a calibration buffer of 25 mL. The µISE produce a potential which is related to the activity of a specific ion in the presence of others. Variations in potential were recorded after stabilization and the value was plotted as a function of the logarithm of the each ion activity which was calculated according to the Debye-Hückel approximation [49].

2.4.4. pH sensor development

For the potentiometric pH sensor, we implemented the growth of iridium oxide films method described in [32] on the gold electrode with 0.1 mm^2 area (electrode labelled 6 in Fig. 2A). The platform was immersed in a solution that contained IrCl$_3$·3H$_2$O (0.2 mM), H$_2$C$_2$O$_4$·2H$_2$O (1 mM) and K$_2$CO$_3$ (5 mM) dissolved in distilled water. This solution had been aged at 37 °C for 4 days and stored at 4 °C until used. Anodically electrodeposited iridium oxide films (AEIROF) were obtained by a dynamic potential sweep method consisting of 50 potential sweeps between open circuit potential (near 0.0 V) and 0.6 V at scan rate of 10 mV s^{-1}. The response of the AEIROF pH sensor was studied in terms of open circuit potential evolution over a pH range between 2 and 11. The sensor was calibrated in PBS buffer and also in AU samples. The pH was modified under mechanical stirring, by serial addition of either NaOH or HCl. The pH changes were monitored in parallel using a commercial pH-meter.

2.5. Experimental procedure

The experimental validation of the platform was done in three different samples: in controlled buffer, AU and in RU. AU was prepared according to [50]. Table S1 (Supporting Information) shows the concentration values selected for the used AU.

For the extraction of the RU, 9-week old C57B6 male mice were housed in metabolic cages and fed gel food formulated to contain standard amounts of sodium and potassium (Na^+ 0.3%, K^+ 0.8%, Cl^- 0.37%, Control) [51]. Urine was collected daily under a layer of mineral oil to prevent evaporation in sterile containers. On the third day, mice were divided in four groups: one was kept on Control diet; the others were switched to one of three experimental diets containing high levels of sodium (NaCl 4%, HighNa), potassium (KCl 4%, HighK), or both (NaCl 4%, KCl 4%, HighNaK). Urine was collected for two extra days. All samples were kept frozen until analyzed. Experimental procedures were revised and approved by our local animal research ethics committee (CEAEA, Universidad de Zaragoza, Spain).

For the experimental measurement of the urine ion compounds, the samples were diluted 1:100 in distilled deionized water and inserted by microfluidic channels in the developed multisensory platform. In order to correlate the obtained measurement of the multisensor, the ion concentrations in biological samples were also measured with an Atomic Spectrometer, in this case, urine was diluted 1:5000 in 5 mM CsCl solution. Concentrations of Na^+ and K^+ in the diluted samples were determined by flame photometry against appropriate standards prepared in the same diluent. Linear fit of the standard values was employed to calculate absolute ion concentrations in the biological samples, after correction for dilution. Each individual sample was quantified in duplicate. Results are shown as the average of 2 mice exposed to a particular experimental diet.

3. Results and discussion

In this work the best way to integrate all sensors optimizing the electrode modification step by step was carefully studied in order to reduce interferences between processes. Most of the published multiparametric focus on individual sensor preparation and characterization, without taking into account the presence of the other sensors lacking a prove of validity [52,53]. Three different electrodepositions processes were required for the development of all the sensors, as shown in Fig. 2B. Silver electrodeposition was selected as the first one in order to not affect the other sensors by its immersion in the silver solution, and subsequent cleaning in concentrated ammonia and nitric acid. Then, a PPy layer was electrodeposited, leaving the electrodeposition of IrOx as the last electrodeposition process. IrOx is the most delicate layer and it is necessary to avoid its contact with the other solutions. The last step was the manual deposition of sub-microlitre volumes of the three membranes (Na^+, K^+ and PVB) (Fig. 2B). Furthermore, big efforts were done to find the best working conditions, taking into account their preparation, optimization, calibration and storage, which benefit all the sensors included in the platform. In the following sections, the study of individual optimum working conditions for either sensor, and its relation with the rest of the system is presented. PBS was the selected medium to store the sensors due to its composition rich in NaCl and KCl. These ions are adequate to keep the μISE membranes and the high quantity of chloride (Cl^-) helps the PVB membrane to have a stable Cl^- concentration for maintaining the Ag/AgCl stable reference electrode. Also,

PBS is a good buffer to store the IrOx sensor of K^+ is required to keep their electrodeposited film stable.

3.1. Platform calibration in buffer

In order to check the correct response of the microelectrodes after the cleaning and activation process detailed in section 2.4, CV were carried out in static and dynamic conditions. Fig. S1A (Supporting Information) shows the response of the different microelectrode dimensions in ferro/ferricyanide (10^{-2} M) solution. Fig. S1C (Supporting Information) shows typical CV responses of gold electrodes at different scan rates for static conditions. All the voltammograms show consistent peak current (I_p) values when compared with the state currents predicted by Randles-Sevcik [54] as shown in Fig. S1E (Supporting Information). Also, the gold microelectrodes were tested in dynamic conditions at different flow rates. In this case the voltammograms of Fig. S1 B and D (Supporting Information) presented the expected sigmoidal shape, with a consistent limiting current (I_{lim}) values compared with Levich's equation [55]. There is a lower limit for the flow rate (< 25 μL/min) under which the current deviate from theory. This is because axial diffusion becomes significant [56]. The ΔEp obtained was 59 mV as a reversible electrode kinetics behavior [37].

3.1.1. DO calibration

The amperometric DO response was studied as in our previous work, where it was also stated that activation of the sensor was needed before its calibration [35]. In this work, the sensor was calibrated using external CE and RE and compared with the integrated CE and pRE configuration. The comparison of reduction potentials using both electrodes configurations was studied as shown in Fig. S2A (Supporting Information). The final selected potential was −850 mV for the calibration measurement of the DO concentration. Fig. S2 B (Supporting Information) shows the calibration curve of the polarized current measured for eight different DO concentrations in the range between 0 and 8 mg L^{-1}. The sensor exhibited a good performance, displaying excellent linearity in all the DO concentration range. DO sensor exhibited a sensitivity of 3.60 ± 0.2 nA (mg L^{-1}) and a correlation factor of 0.995 using the integrated three electrodes configuration. LOD and LOQ were also estimated, resulting in 0.11 ± 0.02 mg L^{-1} and 0.38 ± 0.05 mg L^{-1} respectively. These results show a good response in a wide range of concentrations with low limit of detection allowing their use for detection of cellular response to some drug, to monitor cell activity and also to control possible bacterial contamination.

3.1.2. Na^+ and K^+ calibration

The crucial direction in the research over potentiometric sensors has been miniaturization. Sensor miniaturization imposed modification of electrode construction. The simplest arrangement is the use of a conducting polymer material as ion to electron transducer between the sensing electrode and the ion-selective polymeric membrane. The electrodeposition and characterization of the conducting PPy layer is shown in Fig. S3 (Supporting Information). SEM image in Fig. 2A.2 shows the roughness surface of the PPy layer which improves the stability of the overlaying coated membrane.

The response of the μISEs was studied for three different plasticizers (DOS, o_NPOE, DBP). Fig. S4 (Supporting Information) shows the response with the different membranes composition. We selected the plasticizer that provided the best results in terms of sensitivity, linear range and LOD. For the Na^+ sensor, the membrane prepared with DOS as plasticizer gave the best behaviour, resulting a Nerstian response of 57 ± 1 mV decade^{-1}, with linear response to the

activity of sodium ions over the range 1×10^{-5} M to 1×10^{-1} M. The LOD was determined from the intersection of the two extrapolated segments of calibration plots. The use of DOS plasticizer gave a LOD of 5×10^{-6} M, which was about one logarithmic unit better compared with the other two plasticizers. The presence of this additive in the selective membrane increases the sensitivity and LOD of the membrane to Na$^+$ changes compared with the other used plasticizers, by reducing the interference [57]. For the K$^+$ membrane, the best performance was obtained with the use of the DBP membrane. In this case, the resulting sensitivity was 52 ± 2 mV decade^{-1} and presented a linear response range from 8×10^{-5} M to 1×10^{-1} M with a LOD of 0.5×10^{-5} M. That means that the sensors cannot recognize concentration changes lower than the LOD. The obtained LOD were enough to use the developed µISE in our application for detect in real-time concentrations of sodium and potassium in mice urine fed with different diets.

After the selection of the best membrane, both sensors were studied in terms of sensitivity, LOD, measuring range, pH range, selectivity coefficients, response time and life time. Table 1 summarizes the characteristics of the sensors response. These results are comparable with other previously described, as shown in Table S2 (Supporting Information). The response time of the µISEs is presented in Fig. S5 (Supporting Information). The microelectrodes reached the equilibrium response in a very short period of about 5 s, faster than other reported µISE shown in Table 2 (Supporting Information). This improvement in the response time was achieved through the PPy[3,3′-Co(1,2-C$_2$B$_9$H$_{11}$)$_2$] layer due its high ion-transfer and mobility between the adjacent solution and the polymer matrix [31]. The potential response of the microelectrode was not influenced in the pH range between 3 and 12 as shown in Fig. S6 (Supporting Information). Outside this pH range, the ionophore complex in the membrane behaves as an anion-exchanger and what is sensed is the chloride anion or the hydroxide anion [58].

The selectivity is clearly one of the most important characteristics of this type of sensors determining if a reliable measurement in a real sample is possible. An ideally selective ionophore interacts only with the target analyte, avoiding any stabilization of an interfering ion in the membrane [59,60]. The potentiometric selectivity coefficients $\left(K_{ion,M}^{pot} \right)$ of our µISE were evaluated using the matched potential method (MPM) [61]. The log $\left(K_{ion,M}^{pot} \right)$ values for Na$^+$ and K$^+$ membranes are presented in Table 1. Fig. S7 (Supporting Information) presents the experimental plots. These values are comparable to those reported in the literature as shown in Table S2 (Supporting Information).

Finally, Fig. S8 (Supporting Information) shows the evolution of the sensitivity of each type of µISE during three months. During this time, the microelectrodes exhibited a Nerstian response with a reduction of about 15% for both µISE after the third week. The microsensors remained without any further degradation of their response during the next month demonstrating the good behaviour of the PPy layer, which increases the stability of the microelectrodes.

3.1.3. pH calibration

IrOx films were prepared by electrochemical techniques, generating hydrated IrOx layers where the pH sensitivity depends on the oxidation state of the IrOx [62]. In these cases the obtained sensitivities are greater than 59 mV decade^{-1}, meaning the transduction mechanism involves more hydrogen ions than the transferred electrons in the redox reaction. For this reason, just after IrOx film electrodeposition, the sensor was stored in PBS during 24 h for conditioning purposes. The sensor was calibrated with the integrated pRE exhibiting a linear super-Nerstian response between pH ranging from 2 to 11, with an average slope of 69 ± 1 mV decade^{-1} (n = 5). Fig. S9A (Supporting Information) shows the calibration curve. The response time of the sensor was very fast (<5 s). The obtained results were comparable with previously published response time, linear pH range and slope values [63], and were adequate for the determination of pH in the experimental urine. Long term stability was measured on AEIROF sensors stored at room temperature and immersed in PBS at pH 7. Calibration curves recorded every 5 days over a month (Supporting Information Fig. S9B) show sensor sensitivity remained constant after the fifth day with a deviation of ± 2 mV.

3.2. Platform calibration in artificial urine

The platform was first validated in AU samples. AU is a solution of water mixed with different organic and inorganic components like urea, creatinine, uric acid, chlorides, sulfates, phosphates,etc, widely used for studies and developments in scientific research [50]. Main advantages of an artificial solution over real urine is the control over

Table 1
Specification of the µISE sensors using the best plasticizer response; DOS for Na$^+$ membrane and DBP for K$^+$ membrane.

	Na$^+$ µISE (n = 10)	K$^+$ µISE (n = 10)
Sensitivity	57 ± 1 mV decade^{-1}	52 ± 2 mV decade^{-1}
Detection Limit	5×10^{-6} M	0.5×10^{-5} M
Measuring range	1×10^{-5} M–1×10^{-1} M	8×10^{-5} M–1×10^{-1} M
pH range	3–12	3–12
Selectivity coefficient	-2.31 (K$^+$)	-2.11 (Na$^+$)
log $\left(K_{ion,M}^{pot} \right)$	-2.33 (Li$^+$)	-2.45 (Li$^+$)
	-4.41 (Ca^{2+})	-3.69 (Ca^{2+})
	-4.41 (Mg^{2+})	-3.75 (Mg^{2+})
Response time	<5 s	<5 s
Life Time	>3 months	>3 months

Table 2
Measured urine Na$^+$ and K$^+$ concentration (mM) of the µISE compared with flame photometry measurements for the three different mice diets. Measured pH values obtained with the custom AEIROF sensor.

	DAY 1					DAY 4				
	Na$^+$ (mM)		K$^+$ (mM)		pH	Na$^+$ (mM)		K$^+$ (mM)		pH
	Flame Photometry	µISE Platform	Flame Photometry	µISE Platform		Flame Photometry	µISE Platform	Flame Photometry	µISE Platform	
Sodium diet	88.7	90.2 ± 0.3	233.4	235.2 ± 0.4	6.9 ± 0.3	408.2	418.2 ± 0.2	152.6	148.5 ± 0.6	7.2 ± 0.3
Potassium diet	62.3	63.4 ± 0.4	206.4	206.8 ± 0.5	6.8 ± 0.2	41.3	43.3 ± 0.3	341.6	344.8 ± 0.5	7.1 ± 0.3
Mixed diet	50.8	53.2 ± 0.4	212.5	213.4 ± 0.5	6.8 ± 0.2	272.2	275.2 ± 0.3	271.9	279.8 ± 0.4	6.9 ± 0.2

its composition, a longer shelf-life and easier storage. All this facilitates the use of this solution to test our integrated multielectrode platform before its validation in real samples.

The μISE were calibrated in nitrate mediums (as shown in Section 3.1.2) and also in chloride mediums using the integrated pRE in order to validate its functionality. In both mediums they exhibited a good performance as shown in Fig. 3 demonstrating that the sensitivities were not influenced by the change in the medium. Six different AU solutions containing different ion molarity were used for the development of the calibration curves. Obtained sensitivities were in good agreement with the results obtained in the buffer calibration mediums.

The pH electrode was also calibrated in the AU medium, where the pH was modified by additions of HCl or NaOH. Fig. S9A (Supporting Information) shows that the sensor exhibited a linear response in a pH range between 3 and 9, and was not influenced by the matrix components of the urine. In terms of sensibility measures in AU did not alter the values, obtaining a value of 68 mV decade^{-1}.

3.3. Analysis of real urine samples

The determination of ion compounds in biological samples is a challenging task. Beyond the selectivity required, the sensors must be impervious to unspecific interferences, such as biofouling, due to the attachment of components of the matrix onto the sensing membranes, which may result in significant signal drift and even permanent damage [64]. In order to reduce these unspecific interferences [65], each RU was diluted with deionized water 1:100 before being measured.

The samples used for analyzing Na$^+$, K$^+$ and pH were obtained from different mice fed with special diet of sodium, potassium or mixed sodium/potassium. The measurements were done with the urine samples collected the first day, before starting the special diet, and with the ones collected the fourth day [51]. To perform the ion determination, sensors were first calibrated in AU as shown in the previous section. A small volume sample (0.83 μL) was enough to fill the sensing chamber. Open circuit potentials were recorded each second, during 80–90 s for each μISE and pH sensor as shown in Fig. 4. The same measurement was repeated three times. Using the mean value of the recorded potentials, we extracted the ion activity. Deviations in the registered potential were neglected since uncertainty in the activities came mainly from the interpolation. We have calculated the interpolation error using the standard deviation formula of propagation of uncertainty with a calibration curve [66]. From the obtained activities, we calculated the corresponding concentration values using Debye–Hückel limiting law and approximating the ion strength value from the AU compounds.

As can be seen in Fig. 4, each specific diet basically changed the ion concentration between the first and the fourth day. Concretely, in the case of the mouse with a sodium diet, the concentration of Na$^+$ in the urine increased 4.7 times. In this urine, K$^+$ concentration decreased 1.6 times its initial value. When mice were fed a high potassium diet, the opposite behavior just happened. Na$^+$ concentration was reduced 1.5 times from day 1 to day 4, whereas K$^+$ concentration increased 1.6 times. These changes were as expected due to the mechanisms employed by the kidney to regulate final urinary excretion of Na$^+$ and K$^+$.

Potassium secretion in the collecting duct is achieved at the expense of reabsorbing sodium, a process stimulated by hormone aldos-
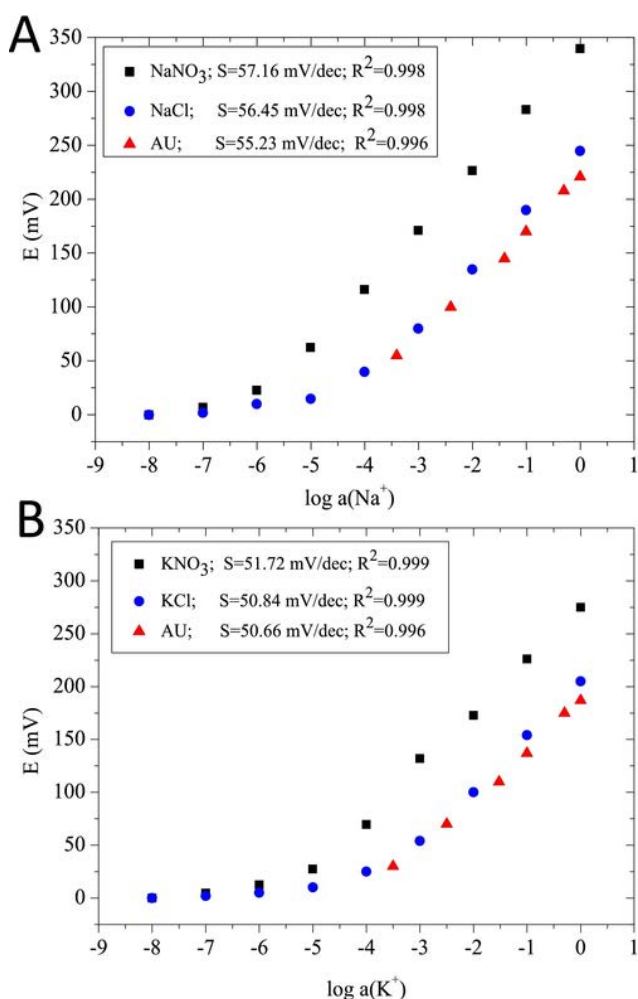
Fig. 3. Potentiometric response of the μISE at different ion concentration in Cl$^-$ and NO$_3$ medium and artificial urine for A) Na$^+$ membrane and B) K$^+$ membrane.
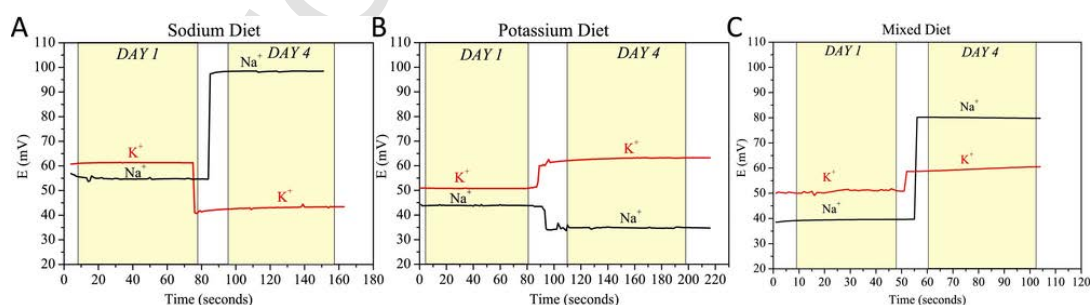
Fig. 4. Potentiometric response of Na$^+$ and K$^+$ μISE of mouse urine with A) a sodium diet, B) a potassium diet and C) a mixed diet.

terone. An excess dietary sodium is excreted by inhibiting aldosterone secretion and reducing collecting duct sodium reabsorption, which in turn reduces potassium secretion. Table 2 shows the measured Na^+ and K^+ concentrations for the three different diets using the integrated µISE multi-sensors are in good agreement with those obtained by flame photometry [51]. Deviations in the concentration values obtained between both techniques can be explained due to the effect of different ions present in the urine, which can interfere with the measurement of the analyte of interest. There is also an indeterminate error due to the approximation of the ionic strength used to determine the concentration values from the obtained activities of the µISE. Thus, our µISE sensors have demonstrated enough sensitivity and specificity to work satisfactorily over a broad range of physiological and pathological values. Although the ion interference is less of a problem with atomic spectroscopy, our work demonstrates that ISE sensors are advantageous for real time monitoring of ion concentrations in complex biological matrixes. µISE sensors are also far more affordable that atomic spectroscopy, which in addition generally requires higher sample volumes that those employed in the current work. Ion concentration monitoring will be instrumental for the realization of 3D organotypic culture of epithelia based organs, such as the kidney, or reproducing excitable tissues.

Finally, Table 2 also details the pH values recorded for each sample using the AEIROF pH sensor. As can be seen, the type of diet did not affect the urine pH, maintaining values between 6.8–7.2 pH, which is a normal urinary pH. The measurement of pH complemented that of oxygen, allowing the investigation of the metabolic state of cells in the system. For instance, proliferative cells, including cancer cells but also most mammal cells in culture, exhibit glycolytic metabolism, while the physiological metabolism in vivo is determined by oxidative phosphorylation in the mitochondria. Determining oxygen consumption and acidification by lactic acid production is a well-established method to estimate the type of predominant energy metabolism.

4. Conclusions

This work describes the fabrication and validation of a multisensing platform embedded in a versatile and low-cost microfluidic device. The platform integrates all the necessary microelectrodes for the electrochemical measurement of DO, Na^+, K^+ and pH. Simultaneous measurement of four biologically relevant parameters in small sample volume (0.83 µL), either static or in-line with microfluidic cell culture devices clearly distinguish our device from previous systems.

The problem of integration of four different sensors was solved through adequate platform design and fabrication protocols. We found, PBS was the best buffer to store the sensors while maintaining their best performance. The four types of sensors exhibited a good behaviour towards linear response in a wide range of concentrations, with low LOD, high sensitivity, rapid response time and long lifetime. The DO sensor showed a sensitivity of 3.60 ± 0.2 nA (mg L^{-1}) in a wide range of concentrations, with a LOD and LOQ of 0.11 ± 0.02 mg L^{-1} and 0.38 ± 0.05 mg L^{-1} respectively. For the µISE, the use of PPy[3,3′-Co(1,2-$C_2B_9H_{11}$)$_2$] as an internal contact layer between the polymeric sensitive membrane and the gold substrate provided good performance allowing a good ion-transfer and long term potential stability. Na^+ and K^+ µISE exhibited sensitivities of 57 ± 1 mV decade^{-1} and 52 ± 2 mV decade^{-1} respectively, in a wide liner range, from 10^{-5} M to 10^{-4} M and low LOD, 5×10^{-6} M and 0.5×10^{-5} M for Na^+ and K^+ µISE respectively. The pH sensor, prepared by electrochemical deposition of IrOx, exhibited a sensitivity of 69 ± 1 mV decade^{-1} with a linear response between pH 2 and

11. DO sensor showed long life times providing by the sensors reactivated before use.

Concentrations of Na^+, K^+ and pH were successfully determined in AU samples. As a proof-of-concept, the usefulness of the platform was also demonstrated in RU samples, where the values were in good agreement with those obtained by flame photometry. So, the fabrication and operation of different sensors within the same platform has been demonstrated, overcoming the use of several commercial sensors at the same time in terms of cost, time, simplicity and versatility principally.

Appendix A. Supplementary data

Supplementary data associated with this article can be found, in the online version, at http://dx.doi.org/10.1016/j.snb.2017.09.104.

References

[1] Y.S. Zhang, A. Khademhosseini, Seeking the right context for evaluating nanomedicine: from tissue models in petri dishes to microfluidic organs-on-a-chip, Nanomedicine 10 (2015) 685–688, https://doi.org/10.2217/nnm.15.18.
[2] M. Baker, Tissue models: a living system on a chip, Nature 471 (2011) 661–665, https://doi.org/10.1038/471661a.
[3] D. Huh, G.A. Hamilton, D.E. Ingber, From three-dimensional cell culture to Organs-on-Chips, Trends Cell Biol. 21 (2011) 745, https://doi.org/10.1016/j.tcb.2011.09.005.
[4] A. Perestrelo, A. Águas, A. Rainer, G. Forte, Microfluidic Organ/Body-on-a-Chip devices at the convergence of biology and microengineering, Sensors 15 (2015) 31142–31170, https://doi.org/10.3390/s151229848.
[5] E.R. Shamir, A.J. Ewald, Three-dimensional organotypic culture: experimental models of mammalian biology and disease, Nat. Rev. Mol. Cell Biol. 15 (2014) 647–664, https://doi.org/10.1038/nrm3873.
[6] K.-J. Jang, A.P. Mehr, G.A. Hamilton, L.A. McPartlin, S. Chung, K.-Y. Suh, D.E. Ingber, Human kidney proximal tubule-on-a-chip for drug transport and nephrotoxicity assessment, Integr. Biol. 5 (2013) 1119, https://doi.org/10.1039/c3ib40049b.
[7] K.-J. Jang, K.-Y. Suh, A multi-layer microfluidic device for efficient culture and analysis of renal tubular cells, Lab Chip. 10 (2010) 36–42, https://doi.org/10.1039/B907515A.
[8] M.-H. Wu, S.-B. Huang, G.-B. Lee, Microfluidic cell culture systems for drug research, Lab. Chip. 10 (2010) 939, https://doi.org/10.1039/b921695b.
[9] F. Zheng, F. Fu, Y. Cheng, C. Wang, Y. Zhao, Z. Gu, Organ-on-a-Chip systems microengineering to biomimic living systems, Small 12 (2016) 2253–2282, https://doi.org/10.1002/smll.201503208.
[10] V. Marx, Tissue engineering: organs from the lab, Nature 522 (2015) 373–377, https://doi.org/10.1038/522373a.
[11] R. Toczyłowska-Mamińska, A. Lewenstam, K. Dołowy, Multielectrode bisensor system for time-resolved monitoring of ion transport across an epithelial cell layer, Anal. Chem. 86 (2014) 390–394, https://doi.org/10.1021/ac403808f.
[12] D. Bavli, S. Prill, E. Ezra, G. Levy, M. Cohen, M. Vinken, J. Vanfleteren, M. Jaeger, Y. Nahmias, Real-time monitoring of metabolic function in liver-on-chip microdevices tracks the dynamics of mitochondrial dysfunction, Proc. Natl. Acad. Sci. 113 (2016) E2231–E2240, https://doi.org/10.1073/pnas.1522556113.
[13] S.E. Eklund, D. Taylor, E. Kozlov, A. Prokop, D.E. Cliffel, A microphysiometer for simultaneous measurement of changes in extracellular glucose, lactate, oxygen,

and acidification rate, Anal. Chem. 76 (2004) 519–527, https://doi.org/10.1021/ac034641z.

[14] F. Hafner, Cytosensor Microphysiometer: technology and recent applications, Biosens. Bioelectron. 15 (2000) 149–158.

[15] J.R. McKenzie, A.M. Palubinsky, J.E. Brown, B. McLaughlin, D.E. Cliffel, Metabolic multianalyte microphysiometry reveals extracellular acidosis is an essential mediator of neuronal preconditioning, ACS Chem. Neurosci. 3 (2012) 510–518, https://doi.org/10.1021/cn300003r.

[16] M. Lehmann, W. Baumann, M. Brischwein, H.-J. Gahle, I. Freund, R. Ehret, S. Drechsler, H. Palzer, M. Kleintges, U. Sieben, B. Wolf, Simultaneous measurement of cellular respiration and acidification with a single CMOS ISFET, Biosens. Bioelectron. 16 (2001) 195–203, https://doi.org/10.1016/S0956-5663(01)00123-3.

[17] S.M. Bonk, M. Stubbe, S.M. Buehler, C. Tautorat, W. Baumann, E.-D. Klinkenberg, J. Gimsa, Design and characterization of a sensorized microfluidic cell-culture system with electro-thermal micro-pumps and sensors for cell adhesion, oxygen, and pH on a glass chip, Biosensors 5 (2015) 513–536, https://doi.org/10.3390/bios5030513.

[18] P.-A. Ruffieux, U. von Stockar, I.W. Marison, Measurement of volumetric (OUR) and determination of specific (qO2) oxygen uptake rates in animal cell cultures, J. Biotechnol. 63 (1998) 85–95, https://doi.org/10.1016/S0168-1656(98)00046-7.

[19] J.C. Owicki, J. Wallace Parce, Biosensors based on the energy metabolism of living cells: the physical chemistry and cell biology of extracellular acidification, Biosens. Bioelectron. 7 (1992) 255–272, https://doi.org/10.1016/0956-5663(92)87004-9.

[20] O.T. Guenat, S. Generelli, N.F. de Rooij, M. Koudelka-Hep, F. Berthiaume, M.L. Yarmush, Development of an array of ion-selective microelectrodes aimed for the monitoring of extracellular ionic activities, Anal. Chem. 78 (2006) 7453–7460, https://doi.org/10.1021/ac0609733.

[21] Y. Kong, H. Chen, Y. Wang, S.A. Soper, Fabrication of a gold microelectrode for amperometric detection on a polycarbonate electrophoresis chip by photodirected electroless plating, Electrophoresis 27 (2006) 2940–2950, https://doi.org/10.1002/elps.200500750.

[22] X. Illa, O. Ordeig, D. Snakenborg, A. Romano-Rodríguez, R.G. Compton, J.P. Kutter, A cyclo olefin polymer microfluidic chip with integrated gold microelectrodes for aqueous and non-aqueous electrochemistry, Lab. Chip. 10 (2010) 1254–1261, https://doi.org/10.1039/B926737A.

[23] S. Metz, R. Holzer, P. Renaud, Polyimide-based microfluidic devices, Lab. Chip. 1 (2001) 29–34, https://doi.org/10.1039/b103896f.

[24] V.V. Cosofret, M. Erdosy, T.A. Johnson, R.P. Buck, R.B. Ash, M.R. Neuman, Microfabricated sensor arrays sensitive to pH and K+ for ionic distribution measurements in the beating heart, Anal. Chem. 67 (1995) 1647–1653, https://doi.org/10.1021/ac00106a001.

[25] E. Lindner, R.P. Buck, Microfabricated potentiometric electrodes and their In vivo applications, Anal. Chem. 72 (2000) 336 A–345 A, https://doi.org/10.1021/ac002805v.

[26] F.J. del Campo, Miniaturization of electrochemical flow devices: a mini-review, Electrochem. Commun. 45 (2014) 91–94, https://doi.org/10.1016/j.elecom.2014.05.013.

[27] M.J. González-Guerrero, J.P. Esquivel, D. Sánchez-Molas, P. Godignon, F.X. Muñoz, F.J. del Campo, F. Giroud, S.D. Minteer, N. Sabaté, Membraneless glucose/O2 microfluidic enzymatic biofuel cell using pyrolyzed photoresist film electrodes, Lab. Chip 13 (2013) 2972–2979, https://doi.org/10.1039/c3lc50319d.

[28] E.M. Zahran, A. New, V. Gavalas, L.G. Bachas, Polymeric plasticizer extends the lifetime of PVC-membrane ion-selective electrodes, The Analyst 139 (2014) 757–763, https://doi.org/10.1039/C3AN01963B.

[29] U. Oesch, D. Ammann, W. Simon, Ion-selective membrane electrodes for clinical use, Clin. Chem. 32 (1986) 1448–1459.

[30] L.F. Ramos-De Valle, Principles of polymer processing, in: E. Saldívar-Guerra, E. Vivaldo-Lima (Eds.), Handb. Polym. Synth. Charact. Process, John Wiley & Sons, Inc., 2013, pp. 451–461.

[31] A. Cadogan, Z. Gao, A. Lewenstam, A. Ivaska, D. Diamond, All-solid-state sodium-selective electrode based on a calixarene ionophore in a poly(vinyl chloride) membrane with a polypyrrole solid contact, Anal. Chem. 64 (1992) 2496–2501, https://doi.org/10.1021/ac00045a007.

[32] A.M. Cruz, L. Abad, N.M. Carretero, J. Moral-Vico, J. Fraxedas, P. Lozano, G. Subías, V. Padial, M. Carballo, J.E. Collazos-Castro, N. Casañ-Pastor, Iridium oxohydroxide, a significant member in the family of iridium oxides. stoichiometry, characterization, and implications in bioelectrodes, J. Phys. Chem. C. 116 (2012) 5155–5168, https://doi.org/10.1021/jp212275q.

[33] W.-D. Huang, H. Cao, S. Deb, M. Chiao, J.C. Chiao, A flexible pH sensor based on the iridium oxide sensing film, Sens. Actuators Phys. 169 (2011) 1–11, https://doi.org/10.1016/j.sna.2011.05.016.

[34] P.E. Oomen, M.D. Skolimowski, E. Verpoorte, Implementing oxygen control in chip-based cell and tissue culture systems, Lab. Chip. 16 (2016) 3394–3414, https://doi.org/10.1039/c6lc00772d.

[35] A. Moya, X. Guimerà, F.J. del Campo, E. Prats-Alfonso, A.D. Dorado, M. Baeza, R. Villa, D. Gabriel, X. Gamisans, G. Gabriel, Profiling of oxygen in biofilms us-

ing individually addressable disk microelectrodes on a microfabricated needle, Microchim. Acta. 182 (2014) 985–993, https://doi.org/10.1007/s00604-014-1405-4.

[36] L.M. Fischer, M. Tenje, A.R. Heiskanen, N. Masuda, J. Castillo, A. Bentien, J. Émneus, M.H. Jakobsen, A. Boisen, Gold cleaning methods for electrochemical detection applications, Microelectron. Eng. 86 (2009) 1282–1285, https://doi.org/10.1016/j.mee.2008.11.045.

[37] A.J. Bard, L.R. Faulkner, Electrochemical Methods: Fundamentals and Applications, Wiley, New York, 2001.

[38] X. Jin, J. Lu, P. Liu, H. Tong, The electrochemical formation and reduction of a thick AgCl deposition layer on a silver substrate, J. Electroanal. Chem. 542 (2003) 85–96, https://doi.org/10.1016/S0022-0728(02)01474-2.

[39] T. Guinovart, G.A. Crespo, F.X. Rius, F.J. Andrade, A reference electrode based on polyvinyl butyral (PVB) polymer for decentralized chemical measurements, Anal. Chim. Acta. 821 (2014) 72–80, https://doi.org/10.1016/j.aca.2014.02.028.

[40] L.C. Clark, R. Wolf, D. Granger, Z. Taylor, Continuous recording of blood oxygen tensions by polarography, J. Appl. Physiol. 6 (1953) 189–193.

[41] L.A. Currie, Limits for qualitative detection and quantitative determination. Application to radiochemistry, Anal. Chem. 40 (1968) 586–593, https://doi.org/10.1021/ac60259a007.

[42] Z. Mousavi, K. Granholm, T. Sokalski, A. Lewenstam, All-solid-state electrochemical platform for potentiometric measurements, Sens. Actuators B Chem. 207 (2015) 895–899, https://doi.org/10.1016/j.snb.2014.06.067.

[43] N. Zine, J. Bausells, F. Teixidor, C. Viñas, C. Masalles, J. Samitier, A. Errachid, All-solid-state hydrogen sensing microelectrodes based on novel PPy[3, 3′-Co(1, 2-C2B9H11)2] as a solid internal contact, Mater. Sci. Eng. C. 26 (2006) 399–404, https://doi.org/10.1016/j.msec.2005.10.073.

[44] C. Masalles, F. Teixidor, S. Borrós, C. Viñas, Cobaltabisdicarbollide anion [Co(C2B9H11)2]- as doping agent on intelligent membranes for ion capture, J. Organomet. Chem. 657 (2002) 239–246, https://doi.org/10.1016/S0022-328X(02)01432-8.

[45] E. Bakker, P. Bühlmann, E. Pretsch, Carrier-Based ion-selective electrodes and bulk optodes. 1. General characteristics, Chem. Rev. 97 (1997) 3083–3132, https://doi.org/10.1021/cr940394a.

[46] N. Zine, J. Bausells, F. Vocanson, R. Lamartine, Z. Asfari, F. Teixidor, E. Crespo, I.A.M. de Oliveira, J. Samitier, A. Errachid, Potassium-ion selective solid contact microelectrode based on a novel 1,3-(di-4-oxabutanol)-calix[4]arene-crown-5 neutral carrier, Electrochim. Acta 51 (2006) 5075–5079, https://doi.org/10.1016/j.electacta.2006.03.060.

[47] I.A.M. de Oliveira, D. Risco, F. Vocanson, E. Crespo, F. Teixidor, N. Zine, J. Bausells, J. Samitier, A. Errachid, Sodium ion sensitive microelectrode based on a p-tert-butylcalix[4] arene ethyl ester, Sens. Actuators B-Chem. 130 (2008) 295–299, https://doi.org/10.1016/j.snb.2007.08.026.

[48] I.A. Marques de Oliveira, M. Pla-Roca, L. Escriche, J. Casabó, N. Zine, J. Bausells, F. Teixidor, E. Crespo, A. Errachid, J. Samitier, Novel all-solid-state copper(II) microelectrode based on a dithiomacrocycle as a neutral carrier, Electrochim. Acta 51 (2006) 5070–5074, https://doi.org/10.1016/j.electacta.2006.03.042.

[49] P. Debye, E. Hückel, Zur Theorie der Elektrolyte. I. Gefrierpunktserniedrigung und verwandte Erscheinungen, Phys. Z. 24 (1923) 185–206.

[50] S. Chutipongtanate, V. Thongboonkerd, Systematic comparisons of artificial urine formulas for in vitro cellular study, Anal. Biochem. 402 (2010) 110–112, https://doi.org/10.1016/j.ab.2010.03.031.

[51] Y. Lazo-Fernández, G. Baile, P. Meade, P. Torcal, L. Martínez, C. Ibañez, M.L. Bernal, B. Viollet, I. Giménez, Kidney-specific genetic deletion of both AMPK α-subunits causes salt and water wasting, Am. J. Physiol. Renal Physiol. 312 (2017) F352–F365, https://doi.org/10.1152/ajprenal.00169.2016.

[52] Z. Xu, Q. Dong, B. Otieno, Y. Liu, I. Williams, D. Cai, Y. Li, Y. Lei, B. Li, Real-time in situ sensing of multiple water quality related parameters using micro-electrode array (MEA) fabricated by inkjet-printing technology (IPT), Sens. Actuators B Chem. 237 (2016) 1108–1119, https://doi.org/10.1016/j.snb.2016.09.040.

[53] B. Zhou, C. Bian, J. Tong, S. Xia, Fabrication of a miniature multi-parameter sensor chip for water quality assessment, Sensors 17 (2017) https://doi.org/10.3390/s17010157.

[54] D.K. Roe, Analytical electrochemistry: theory and instrumentation of dynamic techniques, Anal. Chem. 50 (1978) 9–16, https://doi.org/10.1021/ac50028a002.

[55] R.G. Compton, A.C. Fisher, R.G. Wellington, P.J. Dobson, P.A. Leigh, Hydrodynamic voltammetry with microelectrodes: channel microband electrodes; theory and experiment, J. Phys. Chem. 97 (1993) 10410–10415, https://doi.org/10.1021/j100142a024.

[56] J.A. Alden, R.G. Compton, Hydrodynamic voltammetry with channel microband electrodes: axial diffusion effects, J. Electroanal. Chem. 404 (1996) 27–35, https://doi.org/10.1016/0022-0728(95)04399-3.

[57] H.-J. Kim, J.W. Hummel, S.J. Birrell, Evaluation of nitrate and potassium ion-selective membranes for soil macronutrient sensing, Trans. ASABE. 49 (2006) 597, https://doi.org/10.13031/2013.20476.

[58] S. Kim, H. Kim, K.H. Noh, S.H. Lee, S.K. Kim, J.S. Kim, Potassium ion-selec-
     tive membrane electrodes based on 1,3-alternate calix[4] crown-5-azacrown-5,
     Talanta 61 (2003) 709–716, https://doi.org/10.1016/s0039-9140(03)00329-1.
[59] E. Bakker, P. Bühlmann, E. Pretsch, Polymer membrane ion-selective elec-
     trodes-what are the limits?, Electroanalysis 11 (1999) 915–933, doi:10.1002/(
     SICI)1521-4109(199909)11:13<915::AID-ELAN915>3.0.CO;2-J..
[60] P.B. Yoshio Umezawa, Potentiometric selectivity coefficients of IonSelective
     electrodes. part I. Inorganic cations (Technical report), Pure Appl. Chem.
     72 (2000) 1851–2082, https://doi.org/10.1351/pac200072101851.
[61] Y. Umezawa, K. Umezawa, H. Sato, Selectivity coefficients for ion-selective
     electrodes: recommended methods for reporting $K_{A,B}^{pot}$ values (Technical Re-
     port), Pure Appl. Chem. 67 (1995) 507–518, https://doi.org/10.1351/
     pac199567030507.
[62] W. Olthuis, M.A.M. Robben, P. Bergveld, M. Bos, W.E. van der Linden, pH
     sensor properties of electrochemically grown iridium oxide, Sens. Actuators B
     Chem. 2 (1990) 247–256, https://doi.org/10.1016/0925-4005(90)80150-X.
[63] E. Prats-Alfonso, L. Abad, N. Casañ-Pastor, J. Gonzalo-Ruiz, E. Baldrich, Irid-
     ium oxide pH sensor for biomedical applications. Case urea-urease in real urine
     samples, Biosens. Bioelectron. 39 (2013) 163–169, https://doi.org/10.1016/j.
     bios.2012.07.022.
[64] P. Bühlmann, M. Hayakawa, T. Ohshiro, S. Amemiya, Y. Umezawa, Influence
     of natural, electrically neutral lipids on the potentiometric responses of cation-se-
     lective polymeric membrane electrodes, Anal. Chem. 73 (2001) 3199–3205,
     https://doi.org/10.1021/ac0015016.
[65] T. Guinovart, D. Hernández-Alonso, L. Adriaenssens, P. Blondeau, F.X. Rius, P.
     Ballester, F.J. Andrade, Characterization of a new ionophore-based ion-selective
     electrode for the potentiometric determination of creatinine in urine, Biosens.
     Bioelectron. 87 (2017) 587–592, https://doi.org/10.1016/j.bios.2016.08.025.
[66] D.C. Harris, Quantitative Chemical Analysis, edición: 0007, W H Freeman &
     Co, New York, 2006.

Ana Moya obtained an Engineering of Telecommunications degree
from the Universitat Autònoma de Barcelona, Spain, in 2008. She
has been working with the Biomedical Application's Group in the In-
stitut de Microelectrònica de Barcelona, Centro Nacional de Micro-
electrónica, (IMB-CNM, CSIC), Spain, from 2008 to 2012, contracted
by CIBER-BBN. Currently she is predoctoral FPI-2012 fellow at the
Biomedical Application's Group at IMB-CNM. Specialized in elec-
tronic systems, her current researches interested are focused on design
and development of electronic systems for biomedical applications,
and also on electrochemical sensors for microfluidic cell culture de-
vices.

Xavi Illa is a researcher of the CIBER-BBN enroled in the Biomedical
Application's Group of the Microelectronics Institute of Barcelona,
IMB-CNM (CSIC). He obtained the physics degree from the Univer-
sity of Barcelona in 2004, and the Ph.D. from the same institution in
2010 with a work focused on the development of a HPLC on-chip de-
vice on new polymeric substrates. Now, his research interests are the
design and fabrication of lab-on-a-chip devices for biomedical appli-
cations, based on both silicon and polymeric microtechnologies.

Ignacio Giménez obtained a Medical Doctor degree from University
of Zaragoza (Spain) in 1992 and a PhD in Physiology in 1997. He
gained postdoctoral experience at Yale University School of Medi-
cine Department of Cell and Molecular Physiology (1998–2003) prior
to his return to Spain as a Ramón y Cajal researcher (2003–2008).
Since 2008 he is associate professor of Physiolgy at University of
Zaragoza and Senior Researcher at Aragón's Health Sciences Insti-
tute. Dr. Gimenez's broad research interest is in establishing cell and
molecular physiopathological mechanisms in renal and cardiovascular
diseases. Currently his laboratory focuses in the development of bio-
mimetic in vitro models of renal tubule function and disease.

Yoskaly Lazo obtained a degree in Pharmaceutical Sciences from
University of La Habana (Cuba) in 2003 and a PhD degree in Phys-
iology in 2009 from University of Zaragoza. After a two-year post-
doctoral training at the National Health Institute (Bethesda, USA) he
moved to the Department of Medicine, Emory University School of
Medicine where he is currently studying the function of ion transport
in in vivo and ex vivo models of renal function and disease.

Rosa Villa is a permanent member of CSIC scientific staff since 1992.
Obtained a medical degree from the University of Barcelona in 1981,
and her Ph.D. from the Autonomous University of Barcelona in 1993.
Currently she leads the Biomedical Application's Group of the Micro-
electronics Institute of Barcelona, which main research interests are
the design and fabrication of Micro and Nano Systems for Biomedical
Applications.

Abdelhamid Errachid graduated in physics from the University M.
Ismail, Meknes, 1992 and received a PhD degree in electronic engi-
neering from the Universitat Autonoma de Barcelona, Spain, in 1998.
Since 2008, he had joined Laboratory of Analytical Sciences in Claude
Bernard University-Lyon 1 as a full professor. He is now involved in
several national and European projects. His current research activity
is focused on bioelectronics, biofunctionalization and nanobiotechnol-
ogy.

Gemma Gabriel obtained a chemistry degree from the Autonomous
University of Barcelona in 2000, and her PhD in Materials Science in
2005. She joined a post-doc member of CSIC in the Biomedical Ap-
plication's Group of the Microelectronics Institute of Barcelona. She
is currently researcher (permanent staff of CSIC) in the Biomedical
Applications Group. Her main research interests are development of
technologies and to craft innovative multisensing devices (impedance,
oxygen, pH) capable of providing novel solutions to different applica-
tions in the biomonitoring field. Novel materials such as carbon nan-
otubes and graphene are implemented as biocompatible materials in
biomedical applications.

Miniaturized multiparametric flexible platform for the simultaneous monitoring of ionic compounds: Application in real urine

[1]**Ana Moya[a,d,e], Xavi Illa[a,d], Ignacio Gimenez[b], Yoskaly Lazo[b], Rosa Villa[a,d], Abdelhamid Errachid[c], Gemma Gabriel[a,d,*]**

[a]*Instituto de Microelectrónica de Barcelona, IMB-CNM (CSIC), Esfera UAB, Campus Universitat Autònoma de Barcelona, 08193 Bellaterra, Barcelona, Spain*
[b]*Instituto Aragonés de Ciencias de la Salud (IACS), IIS Aragón, Universidad de Zaragoza, Spain*
[c]*Université de Lyon, Institut des Sciences Analytiques, UMR 5280, CNRS, Université Lyon 1, ENS Lyon, 5 rue de la Doua, F-69100 Villeurbanne, France.*
[d]*Biomedical Research Networking Center in Bioengineering, Biomaterials and Nanomedicine (CIBER-BBN), Spain*
[e]*PhD in Electrical and Telecomunicacion Engineering, Universitat Autònoma de Barcelona (UAB), Spain*

Supplementary data

Artificial urine preparation

Artificial urine (AU) is widely used for in vitro cellular study. However, there are a number of well-established protocols for preparing AU with different compositions for different purpose. Since, we want that the developed multi-sensor platform be used in different applications, in this work, we have used the AU components formula reported in [1] that is for multiple purpose.

Compostion	mM
Urea	200
Acid Uric	1
Creatinine	4
$Na_3C_6H_5O_7$	5
NaCl	54
KCl	30
NH_4Cl	15
$CaCl_2$	3
$MgSO_4$	2
$NaHCO_3$	2
$Na_2C_2O_4$	0,1
Na_2SO_4	9
NaH_2PO_4	3,6
Na_2HPO_4	0,4

Table S1. Artificial urine composition used for the calibration of the sensors.

Microelectrodes characterization

Characterization of the gold electrodes by cyclic vomtammetry in Ferro/Ferricyanide, after its activation

---

[*] Corresponding author. Tel.: +34 93 594 77 00; fax: +34 93 580 02 67. *E-mail address:* gemma.gabriel@imb-cnm.csic.es
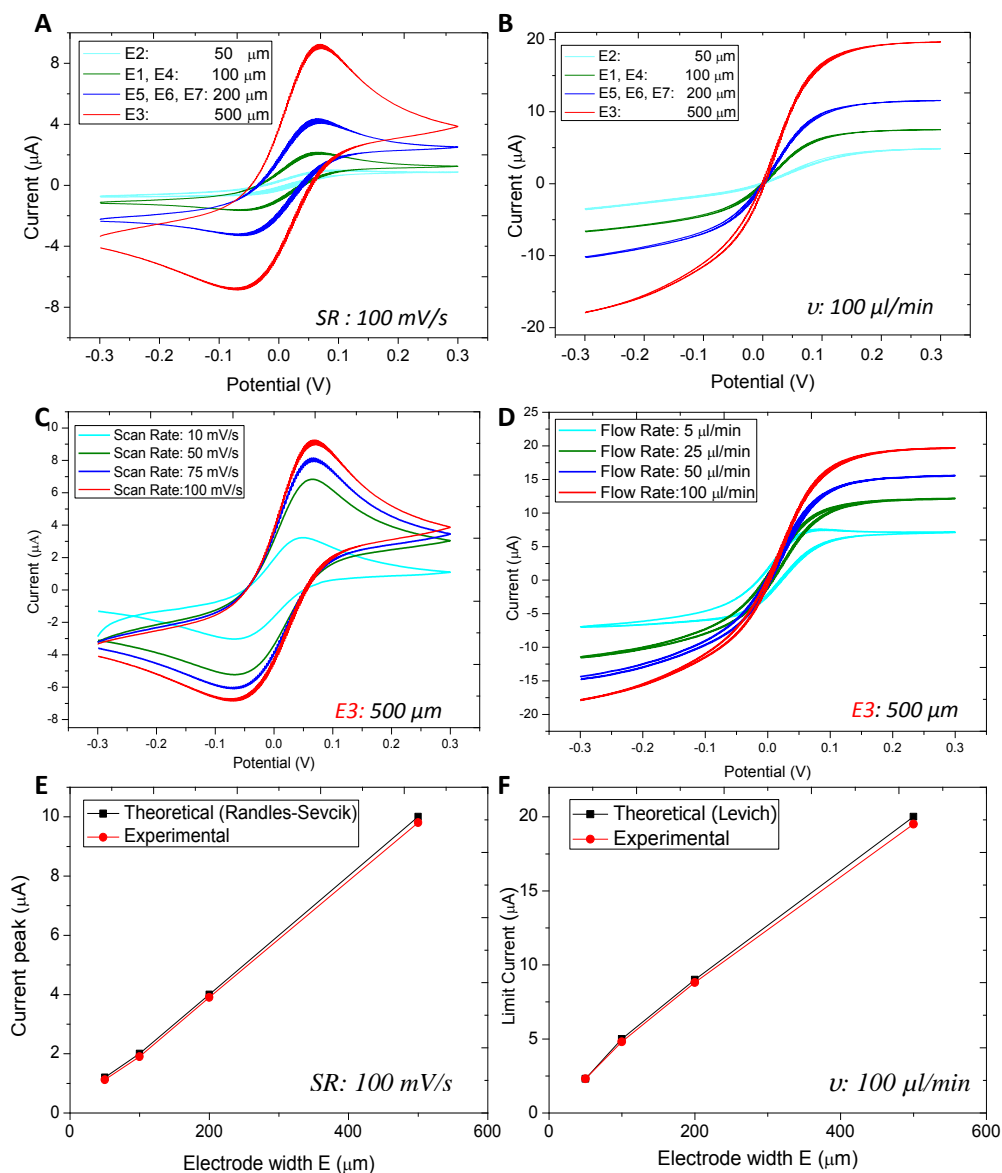
Figure S1. Cyclic voltammetry of $K_3Fe(CN)_6$/$K_4Fe(CN)_6$ redox couple in 0.1 M KNO_3 at different electrodes size, A) at a fixed Scan Rate (SR) of 100 mV/s, and B) at a fixed flow rate (υ) of 100 μl/min, and fixing de electrode width E3: 500 μm C) at a different SR and D) at a different υ. E) and F) compare the experimental currents with the theoretical equations at different electrodes width.

DO sensor calibration

Fig. S2A shows linear sweep voltammograms from 0 to − 1V at scan rate of 25 mV·s^{-1} in a 8 mg·L^{-1} oxygen solution using the commercial Ag/AgCl RE and CE, and with both integrated pRE and CE in the platform. These voltammograms allowed us to select the − 850 mV for both electrodes configuration as the optimal potential value for determination of dissolved oxygen concentration. Fig S2B shows the calibration curve in the range between 0 and 8 mg·L^{-1}. The concentration of DO in the cell was measured with commercial DO probe and correlated with the measured polarization currents in order to build the calibration curves.
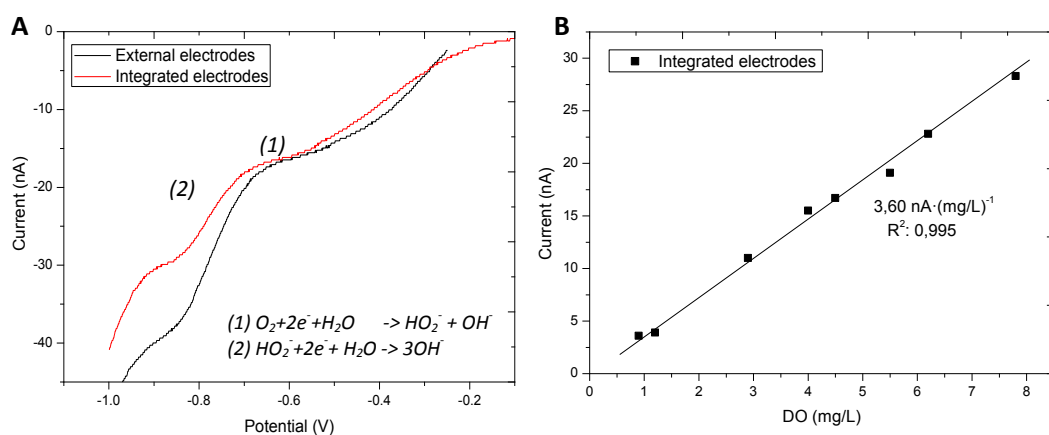
Figure S2. A) Linear sweep voltammetry results made in an oxygen satured saline solution (8 mg·L^{-1}) with external electrodes and with the integrated ones, B) DO calibration curve obtained from the reduction of oxygen at – 850 mV using the integrated electrodes.

Na$^+$ and K$^+$ µISE calibration
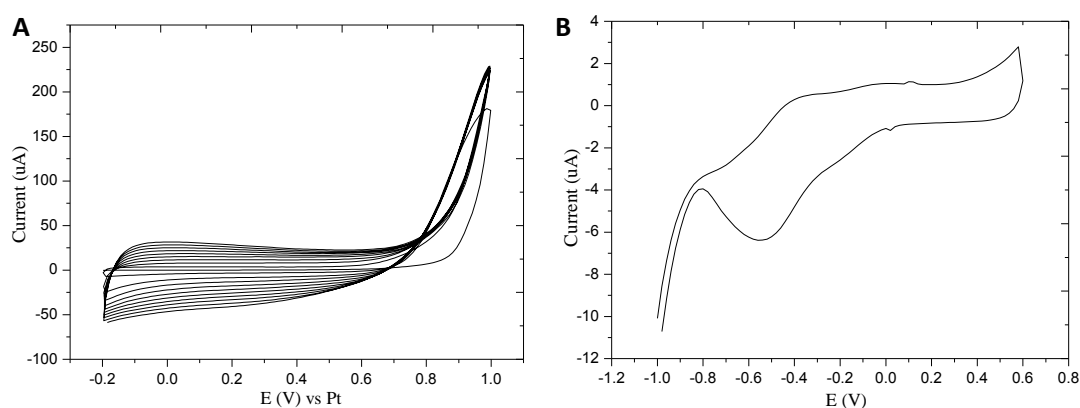
Figure S3. A) Electropolymerization of PPy layer by cyclic voltammetry at gold microelectrodes, B) Cyclic voltammetry of the PPy coated gold microelectrode in 0.1M NaCl supporting electrolyte solution at scan rate of 20 mV·s^{-1}.
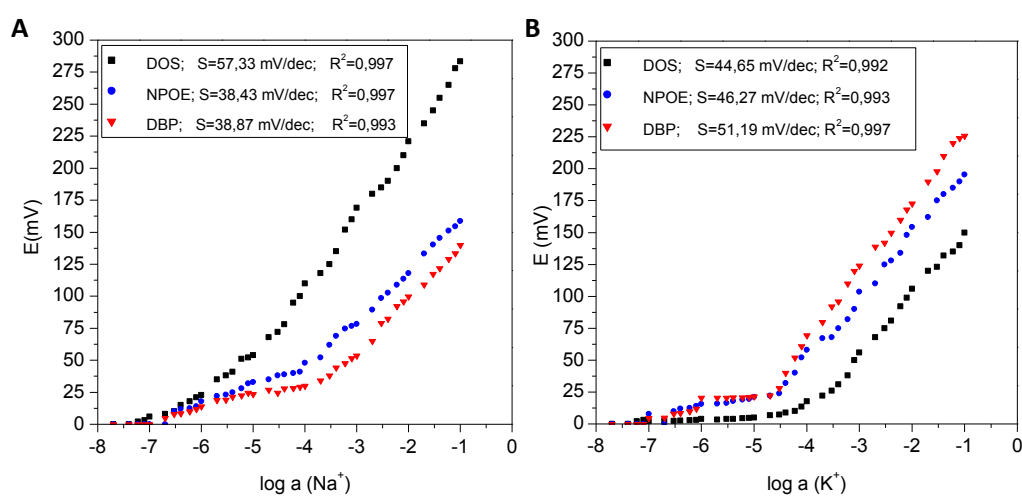
Figure S4. Potential response of each µISE PVC membrane developed with different plasticizers (DOS, o_NPOE and DBP) and using commercial ionophore for A) Na$^+$ concentration changes and B) K$^+$ concentration changes.

ISE sensor specifications compared with other works

	Ref	Linear Response (M)	Sensitivity (mV·decade^{-1})	Selectivity coefficient($log\ k_{kj}^{pot}$)	pH Range	Response Time (s)
Na$^+$ µISE	This work	1 x10^{-5} to 1x10^{-1}	57.33	MPM method -2.31 (K$^+$) -2.33 (Li$^+$) -4.41 (Mg^{2+}) -4.41 (Ca^{2+})	3-12	< 5
	[2]	3 x10^{-6} to 1x10^{-1}	58.65	MPM method -2.20 (K$^+$) -2.97 (Li$^+$) -4.60 (Mg^{2+}) -4.60 (Ca^{2+})	3-10	< 14
	[3]	1 x10^{-5} to 1x10^{-1}	57.10	SSM method -3.1 (K$^+$) -3.2 (Li$^+$) -4.4 (Mg^{2+}) -3.9 (Ca^{2+})	NM	6
	[4]	1 x10^{-4} to 1x10^{-1}	58.1	SSM method - 3.8 (K$^+$) -3.9 (Li$^+$) -4.6 (Mg^{2+}) -4.9 (Ca^{2+})	3-10	8
	[5]	1 x10^{-4} to 1x10^{-1}	58.7	SSM method -2.7 (K$^+$) -3.4 (Li$^+$)	NM	< 20
	[6]	3 x10^{-6} to 1x10^{-1}	55	FIM method -3.35 (K$^+$) -3.2 (Li$^+$)	6.5 - 9.5	< 15
	[7]	1 x10^{-5} to 1x10$^{-1.5}$	55.2	NM	5.5-7.5	< 10
	[8]	1 x10^{-3} to 1x10^{-1}	59.2	FIM method -2.25 (K$^+$) -2.25 (Li$^+$) -2.64 (Mg^{2+}) -2.71 (Ca^{2+})	NM	< 13.5
K$^+$ µIS	This work	8 x10^{-5} to 1x10^{-1}	51.19	MPM method -2.11 (Na$^+$) -2.45 (Li$^+$) -3.69 (Mg^{2+}) -3.75 (Ca^{2+})	3-12	< 5

	Ref	Range	Slope	Method	pH	Time
	[9]	1×10^{-5} to 1×10^{-1}	58.3	FIM method	4-12	
				-3.6 (Na^+)		
				-4.4 (Li^+)		
				-4.6 (Ca^{2+})		
	[10]	6×10^{-6} to 1×10^{-1}	51	MPM method	3-12	< 14
				-2 (Na^+)		
	[3]	1×10^{-6} to 1×10^{-1}	59.21	-4.6 (Na^+)	NM	5
				-4.4 (Li^+)		
				-6.5 (Mg^{2+})		
				-5.7 (Ca^{2+})		
	[11]	1×10^{-6} to 1×10^{-1}	58.6	FIM method	NM	< 7
				-4.6(Na^+)		
	[7]	1×10^{-5} to $1 \times 10^{-1.5}$	56.3	NM	5.5-7.5	< 10
	[12]	1×10^{-5} to 1×10^{-1}	60.5	FIM method	6.5-8.3	<15
				-3.43 (Na^+)		
				-3.48 (Ca^{2+})		

NM.: Not Mentioned. SSM: Separate Solution Method. MPM: Matched Potential Method. FIM: Fixed Interference Method.

Table S2. Comparison of specification of the proposed Na^+ and K^+ µISE with some reported previously.

Response time

Fig S5 shows the corresponding potential versus time trace for different concentration changes. The practical response time was recorded after step changes in the concentration of the ion in solution, and was determined by measuring the time required to achieve a steady potential when the ion concentration increases. This improvement in the response time was achieve through the PPy[3,3'-Co(1,2-$C_2B_9H_{11}$)$_2$] layer due its high ion-transfer and ion mobility and good adherence of the membrane to the gold microelectrodes.
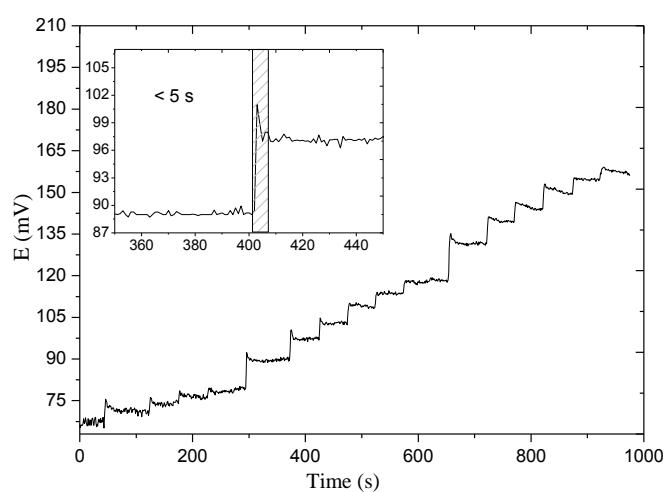
Figure S5. Dynamic response curve for one Na^+ µISE to the step changes of ion from 10^{-8} M to 10^{-1} M.

Effect of pH

The effect of the pH on the potentiometric response of the microelectrodes was examined by following the potential variation over a pH between 3 and 12 at a fixed concentration of Na^+ and K^+ ion (10^{-3} M). The pH of the solution was adjusted by addition of either nitric acid (10^{-1} M) or ammonia (10^{-1} M). It was observed that the potential response of the microelectrode was not influenced in the range between pH 3 to 11. The same behaviour was obtained with both types of µISE.
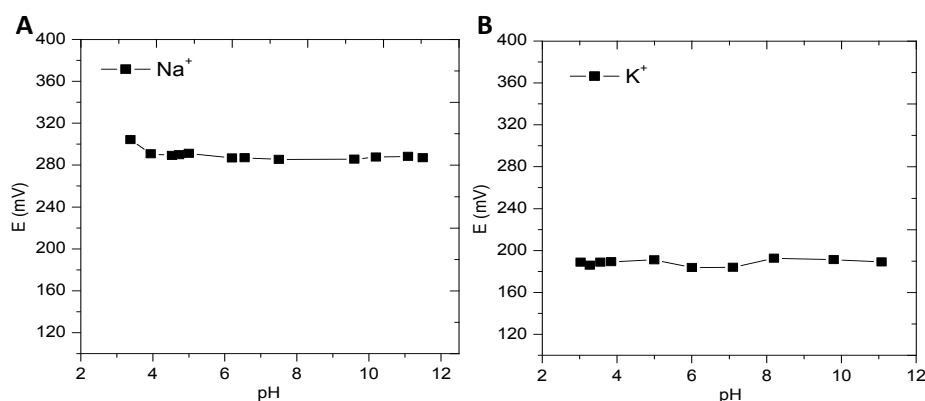
Figure S6. Influence of the pH on the potential response of (a) Na^+-µISE and (b) K^+-µISE.

Interference ion background

Fig. S7 A and B show the selectivity obtained for the Na^+ membrane log ($Na^{pot}_{ion,M}$) was approximately - 2.31 for the K^+ activity and -2.33 for the Li^+ using the Matched Potential Method (MPM). The selective over the divalent cations was highly (- 4.41 for Ca^{2+} and - 4.41 for Mg^{2+}). For the K^+ µISE, the log ($K^{pot}_{ion,M}$) was approximately - 2.11 for the Na^+ activity, - 2.45 for the Li^+, and for the divalent cations was - 3.69 for Ca^{2+} and - 3.75 for Mg^{2+}.

The corresponding selectivity coefficients log ($Na^{pot}_{ion,M}$) and log ($K^{pot}_{ion,M}$) were also studied by the Separate Solution Method (SSM) [13]. Table S3 shows the results compared with both method. Slightly smaller selectivity values were obtained with the SSM.

The response of the Na^+ membrane was also evaluated in the presence of Li^+ (0.1 M) and K^+ (0.1 M) ions (see Figure S7C). For K^+ membrane the response was examined in the presence of Li^+ (0.1 M) and Na^+ (0.1 M) ions (see figure S7D).
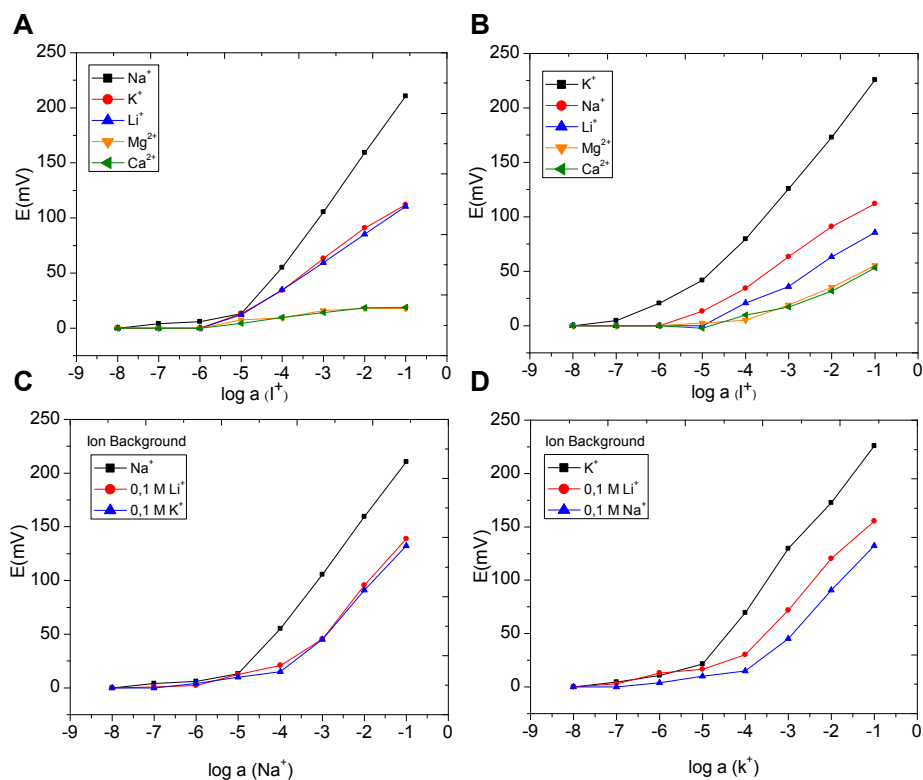
Figure S7. Potential response of the microelectrodes based on commercial ionophore for different metal ions (Na$^+$, K$^+$, Li$^+$, Mg^{2+} and Ca^{2+}), for the (a) Na$^+$ μISE and (b) K$^+$ μISE. And response curve with an interfering ion in the solution with different concentration, for the (c) Na$^+$ μISE and (d) K$^+$ μISE.

Selectivity	Na$^+$		K$^+$		Li$^+$	
Method	MPM	SSM	MPM	SSM	MPM	SSM
Log ($Na_{ion,N}^{pot}$)	-	-	-2.31	-2	-2.33	-2.12
Log ($K_{ion,N}^{pot}$)	-2.11	-1.91	-	-	-2.45	-2.34

Table S3. Comparison of the calculated selective coefficients calculated with two methods, the MPM methods and the SSM method.

Evolution of the sensitivity

The response of the sensors was evaluated periodically showing the best performance during the first two weeks after its development. The third week the sensitivity decreases slightly, remaining constant the rest of the days. The lifetime of the μISE was determined by recording its potentials and plotting the calibration curves for a period of 100 days. During this time, the microelectrodes exhibit a linear response to the changes of the ion concentrations. This shows that the lifetime of the microelectrodes is longer than 3 months.
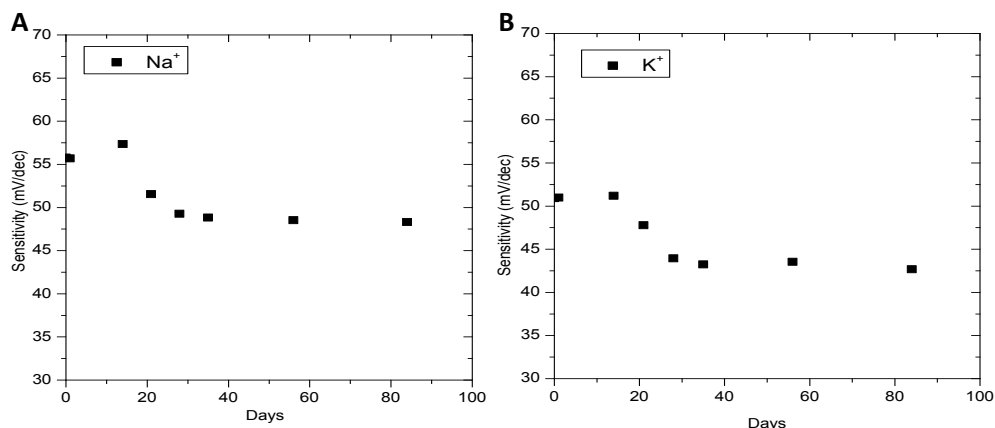
Fig. S8. Evaluation of the changes of the sensitivity response of microelectrodes during three months for the (a) Na$^+$-μISE and (b) K$^+$-μISE.

pH sensor calibration

Initial pH of the artificial urine is 6.2.
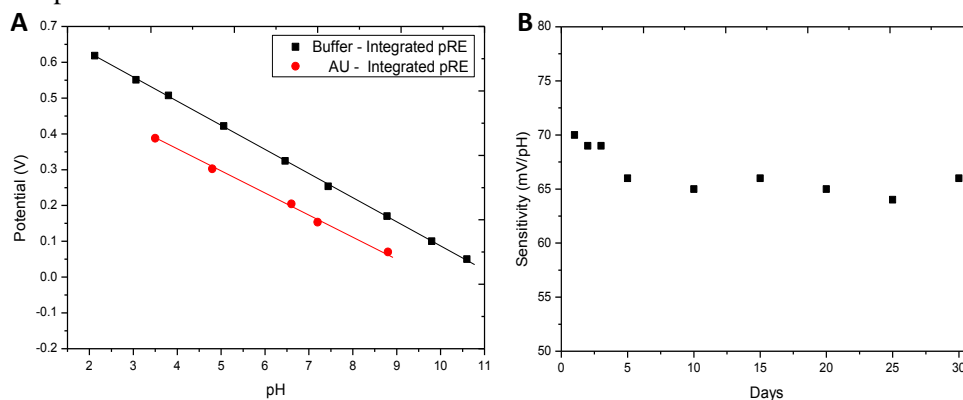
Figure S9. A) pH sensor calibration using addition of HCl or NaOH starting in a PBS Buffer and in AU, B) Evolution of the sensitivity response of the pH sensor during 30 days.

References

[1] S. Chutipongtanate, V. Thongboonkerd, Systematic comparisons of artificial urine formulas for in vitro cellular study, Anal. Biochem. 402 (2010) 110–112. doi:10.1016/j.ab.2010.03.031.

[2] I.A.M. de Oliveira, D. Risco, F. Vocanson, E. Crespo, F. Teixidor, N. Zine, J. Bausells, J. Samitier, A. Errachid, Sodium ion sensitive microelectrode based on a p-tert-butylcalix[4]arene ethyl ester, Sens. Actuators B-Chem. 130 (2008) 295–299. doi:10.1016/j.snb.2007.08.026.

[3] B. Paczosa-Bator, L. Cabaj, M. Raś, B. Baś, R. Piech, Potentiometric sensor platform based on a carbon black modified electrodes, Int. J. Electrochem. Sci. 9 (2014) 2816–2823.

[4] L.Y. Heng, E.A.. Hall, Assessing a photocured self-plasticised acrylic membrane recipe for Na+ and K+ ion selective electrodes, Anal. Chim. Acta. 443 (2001) 25–40. doi:10.1016/S0003-2670(01)01195-3.

[5] A. Cadogan, Z. Gao, A. Lewenstam, A. Ivaska, D. Diamond, All-solid-state sodium-selective electrode based on a calixarene ionophore in a poly(vinyl chloride) membrane

with a polypyrrole solid contact, Anal. Chem. 64 (1992) 2496–2501. doi:10.1021/ac00045a007.

[6] S. Chandra, H. Lang, A new sodium ion selective electrode based on a novel silacrown ether, Sens. Actuators B Chem. 114 (2006) 849–854. doi:10.1016/j.snb.2005.08.023.

[7] R. Toczyłowska-Mamińska, M. Kloch, A. Zawistowska-Deniziak, A. Bala, Design and characterization of novel all-solid-state potentiometric sensor array dedicated to physiological measurements, Talanta. 159 (2016) 7–13. doi:10.1016/j.talanta.2016.06.001.

[8] M. Parrilla, J. Ferré, T. Guinovart, F.J. Andrade, Wearable Potentiometric Sensors Based on Commercial Carbon Fibres for Monitoring Sodium in Sweat, Electroanalysis. 28 (2016) 1267–1275. doi:10.1002/elan.201600070.

[9] V.V. Cosofret, M. Erdosy, T.A. Johnson, R.P. Buck, R.B. Ash, M.R. Neuman, Microfabricated Sensor Arrays Sensitive to pH and K+ for Ionic Distribution Measurements in the Beating Heart, Anal. Chem. 67 (1995) 1647–1653. doi:10.1021/ac00106a001.

[10] N. Zine, J. Bausells, F. Vocanson, R. Lamartine, Z. Asfari, F. Teixidor, E. Crespo, I.A.M. de Oliveira, J. Samitier, A. Errachid, Potassium-ion selective solid contact microelectrode based on a novel 1,3-(di-4-oxabutanol)-calix[4]arene-crown-5 neutral carrier, Electrochimica Acta. 51 (2006) 5075–5079. doi:10.1016/j.electacta.2006.03.060.

[11] O.T. Guenat, S. Generelli, N.F. De Rooij, M. Koudelka-Hep, F. Berthiaume, M.L. Yarmush, Development of an array of ion-selective microelectrodes aimed for the monitoring of extracellular ionic activities, Anal. Chem. 78 (2006) 7453–7460. doi:10.1021/ac0609733.

[12] H. Xu, X. Yang, Y. Wang, J. Zheng, Z. Luo, G. Li, Disposable blood potassium sensors based on screen-printed thick film electrodes, Meas. Sci. Technol. 21 (2010) 055802. doi:10.1088/0957-0233/21/5/055802.

[13] Y. Umezawa, K. Umezawa, H. Sato, Selectivity coefficients for ion-selective electrodes: Recommended methods for reporting $K_{A,B}^{pot}$ values (Technical Report), Pure Appl. Chem. 67 (1995) 507–518. doi:10.1351/pac199567030507.

Inkjet-printed electrochemical sensors embedded in an Organ-On-a-Chip

In this chapter we propose a new approach to monitor oxygen levels by embedding sensors inside an Organ-On-a-Chip (OOC) system with the integration of electrochemical dissolved oxygen (DO) sensors in the cell culture membrane area. This challenge is achieved thanks to the advantages that Inkjet Printing IJP technology offers. This chapter includes a detailed explanation and description of the IJP technology, the development and characterization of DO sensors fully fabricated by IJP onto polymeric substrate and finally the integration of these sensors in the delicate porous membrane of an OOC system. Finally, the integrated system is validated with the DO monitoring of an hepatocyte cell culture.

4.1   Overview of Printed Electronics

From newspapers to food packaging, from magazines to roadside advertising, we live in a world of printed materials. Printing techniques become an essential part of graphic arts for some centuries. Over the past decades, the fast growing of the printing technology become in the emergence of the concept of Printed Electronics (PE), also known as organic electronics, plastic electronics, flexible electronics or oven is more generally named **additive manufacturing** regarding to their working principles [221, 222]. New domains in electronic technology related to new materials, new devices, new functionalities and new production techniques announcing a revolution in microelectronics industry that is currently focused in silicon and microfabrication techniques.
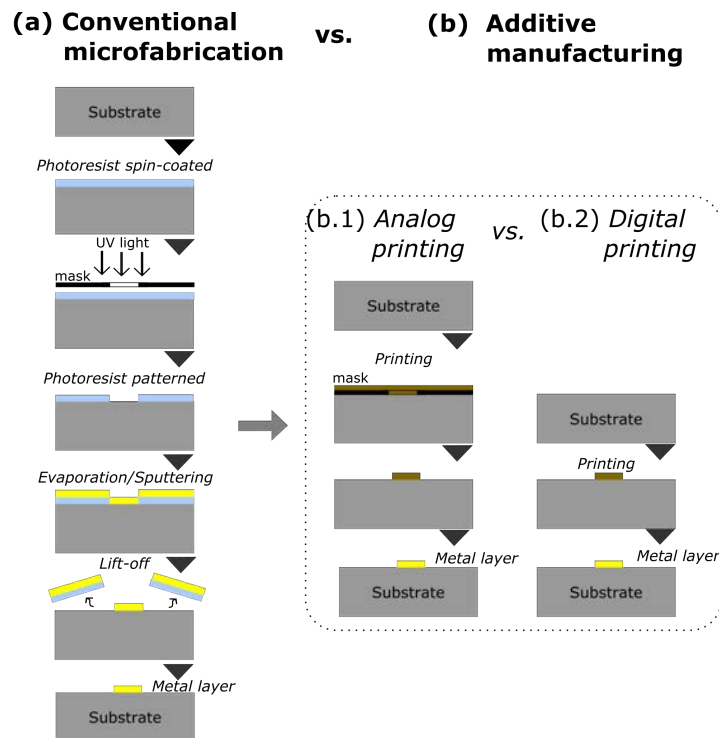
Figure 4.1 | Schematic diagram depicting the fabrication steps for deposition a metallic layer electrode with (a) microfabrication technology compared with (b) additive manufacturing technology, in both (b.1) analog and (b.2) digital printing approaches.

PE is an additive manufacturing technique where layers of functional materials are patterned and stacked on a substrate like other manufacturing techniques [223]. However, in contrast to conventional microfabrication that require multiple steps as it was described in Chapter 3, PE results in a much simpler and cost-effective way to fabricate devices. There are a set of PE methods with different basis to work but, in general, all of them required a more reduced number of steps to fabricate a device: the deposition of the functional material in a form of ink in PE, and the post-processing of the ink to make it functional, generally related to the sintering or curing of the ink. Figure 4.1 shows an example of the necessary fabrication steps to pattern a conductive material over a substrate comparing both fabrication approaches. As

the conventional microfabrication is an additive/subtractive manufacturing technique (Figure 4.1(a)), for the deposition of a metallic layer it is required more fabrications steps than the necessary to fabricate the same pattern using just an additive manufacturing technique (Figure 4.1(b)).

The PE industry has made significant progresses over the last few years, and has established itself as a competitive growth industry. It has been proven that more and more products have matured onto the global market. Organic light emitting diodes (OLED) displays, for example, have become a truly mass-produced industrial product. But this is just the tip of the iceberg. This state of-the-art technology is now being used in a variety of important industry sectors. Companies active in the areas of automotive, consumer electronics, household appliances, packaging, pharmaceutical, and healthcare have already launched products with integrated PE devices. Lightweight, robust, and economical to manufacture: these key features distinguish PE from traditional microfabrication technologies. PE is being used in more products as technology development continues to advance, and open up new areas of applications using novel approaches to manufacturing electronics.

4.1.1   Printing techniques

A wide range of large area deposition and patterning techniques can be used for PE. Each printing technique operates in different manner depending on the many interface relations concerning the designed pattern structure (thickness and resolution requirements), the physical and chemical properties of the deposited functional inks, and the selected substrate characteristics. Printing techniques can be divided in two groups depending to their printing method: printing techniques that require an exclusive mask or special framework for a contact process called **analog printing** (Figure 4.1(b.1)) and the mask-less non-contact methods called **digital printing** (Figure 4.1(b.2)).

Analog printing

Analog printing methods, including offset, flexography, gravure or screen printing, have evolved over several centuries and have now achieved remarkable levels of quality. All these processes share a common feature: the pattern to be printed is embodied in a physical form such as a mask, roll, plate, or screen (Figure 4.1(b.1)). This template is transferred during the act of printing through direct or indirect contact with the substrate. Changes in the patterns can only be achieved by changing the master pattern, which involves making physical changes to the template within the printing machine, and this is time consuming and increases the cost of the fabricated device. Offset, gravure and flexography are the most common for high-volume production and are based in roll-to-roll approach. Screen-printing can be used in sheet-based method, for the purpose of low-volume production and high precision work, and also it can be used in a roll-to-toll approach [223–225].

Digital printing

Unlike analog printing techniques, digital printing works without a physical, pre-manufactured master printing plate and prints without a significant impact force onto the substrate or sublayer [226] (Figure

4.1(b.2)). IJP is the dominant digital technique which works in sheet-based approach and also it can be work in roll-to-roll approach. The basic premise of digital printing is the accurate positioning of a liquid droplet with small volume directly correlated under digital control with the presence of information at each binary unit of the image to be reproduced. As a result, digital printing does not have the key disadvantaged of analog printing, related with the investment to generate the masters, with in-line variable data. However, digital printing has certain drawbacks especially with respect to average throughput when compared to high-end analog printing technologies. Digital printing is still substantially more expensive than analog printing in terms of the cost of their inks. However, the low amount of ink used in digital printing makes them also a low-cost technique.

4.1.1.1 Comparison between printing techniques

Special characteristics of the most common used printing techniques are summarized in Figure 4.2. In terms of resolution, each printing technique has its individual constrains, and in general a process with high resolution has smaller throughput and viceversa as shown in Figure 4.3.

Offset printing
- Printed pattern defined by differences
  in wetting of a plane surface.
- Thin layers down to 0.5 µm possible;
  high resolution (< 20 µm).
- Dynamic viscosity of ink: 40 to 100 Pa·s.

Gravure printing
- Printed pattern defined by surface relief
  (recessed) of master.
- Broad thickness range (from 1 to 8 µm)
  high resolution (< 20 µm).
- Dynamic viscosity of ink: 0.05 to 0.2 Pa·s.

Flexographic printing
- Printed pattern defined by surface relied
  (raised features) of master.
- Thin layers of about 1 µm possible;
  high resolution (< 20 µm).
- Dynamic viscosity of ink: 0.05 to 0.5 Pa·s.

Screen printing
- Printed pattern defined by opennings in
  printing master.
- Thick layers (> 10 µm) possible;
  low resolution (100 µm).
- Very broad dynamic viscosity range; from
  gravure inks to offset inks.

Inkjet printing
- Master-less; droplet size determined by
  nozzle diameter and wavform.
- Thin layers down to 100 nm possible;
  moderate resolution (10-50 µm).
- Dynamic viscosity of ink: 1 to 20 mPa·s.
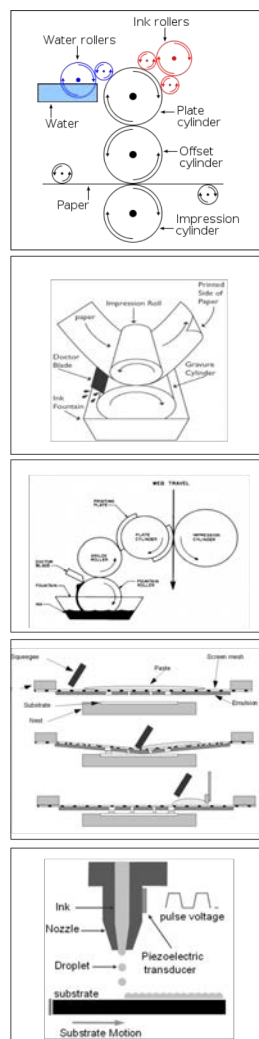
Figure 4.2 | General specifications of the most common printing techniques.

The lateral resolution of the printing techniques (smaller feature that can be printed) typical goes from 10 μm to 100 μm depending on the process, throughput, substrate and ink properties [227]. Film thickness can range from well under tens of nm up to tens of μm. Each process has its own strengthless, e.g. screen is excellent for stacking multiple thick films, while gravure combines high throughput with robust printing forms and can deliver homogeneous thin films. Offset combines high throughput with small feature size but formulating suitable functional inks has proven to be major challenge. These printing processes can have enormous throughput and low production cost, but have demanding requirements on the functional inks in terms of properties like viscosity. Progress in improving the resolution of these mass printing processes has continued growing year by year, and lines down to 20 μm are now obtainable with screen printing using new lattice materials, and even smaller features with flexography and gravure using new plate and form manufacturing methods and materials. Also useful for depositing materials is hot stamping. Nano-imprint lithography is another way to pattern materials at high resolution (under 1 μm) and recently it has been shown that the process can be implemented roll-to-roll. Microcontact printing has also seen growing interest for sub-μm patterning. Pad printing has been proven useful for printing on non-planar surfaces.

Among digital patterning processes, inkjet printing has received the most attention as a way to deposit functional materials. As a digital printing process, it enables variable printing since no printing plate is needed, and thus can correct in-line for distortion. Inkjet printing head developers have continued to improve with finer and finer printheads, which are starting to enable features of few μm. Also, throughput has been substantially improved with the development of multi-head printers. On a lab scale, new superfine inkjet printers are able to form features down to 1 μm, but these have not yet been scaled up to production. Recently, aerosol jet printing has also received a lot of attention, which is especially suitable for deposition onto three-dimensional (3D) substrates.

Inkjet printing is the selected technique used in the development of this work and it will be further explained in Section 4.2.
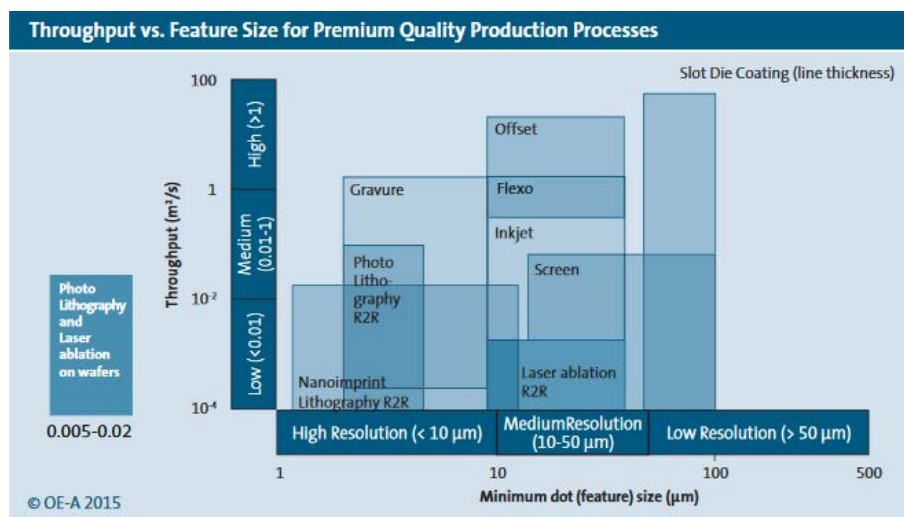
Figure 4.3 Resolution and throughput for different printing techniques. [Source: OE-A] [11]

4.1.2 Substrates and functional inks for Printed Electronics

Substrates

Most PE devices target the use of flexible and potentially low-cost substrates to enable large area and/or more rugged products enabling a higher freedom of design. Since the device manufacturing process usually starts with the substrate onto which several layers of functional materials are deposited, the compatibility of the substrates with the inks and processes used is critical to obtain a suitable product. Substrates vary widely depending on the application requirements. In general, **glass and metal** (stainless steel, aluminum or titanium foil, etc.) are still the only substrates readily available with intrinsically high and reliable barrier properties; a key requirement for many applications (OLED lighting or displays and organic photovoltaics).

Plastic substrates have received much interest in PE, being the most common ones the polyesters based materials as PEN and PET. Nevertheless, their low Tg (lower than 180 °C) and the large thermal expansion coefficient constitute their main drawback, because turn them incompatible with materials or processes where high temperatures are need. In this case, PI films are widely used, being Kapton® the most common one. Besides, PI films are employed due their chemical and physical resistance to prolonged exposure temperatures up to 300 °C. Surface modification with planarization, hard coats or other modifiers is also a common approach for plastic substrates.

Recently there has also been growing interest in **paper**. It is a disposable material made from renewable resources which has unique properties and compatibility with chemicals and biochemicals. While some simple devices can be made on standard paper, special coated papers like paper microfluidics are also available, and some standard packaging papers appear to be promising as well. Microfluidic paper-based analytical devices (PADs) devices are targeting healthcare-related diagnostics, where the impact of cost reduction and simplicity is deemed to be highest, other fields of applications, such as environmental monitoring, explosives detection, or screening for food [228].

Functional inks

The number of functional inks used in PE is very high and vary in formulation depending on its use. The first used inks in inkjet printing were the colorants (pigments or dyes) for graphic art. With the emergence of electronics devices manufactured by printing means, a wide range of conductive, semiconductive and dielectric inks has been developed for the different printed techniques [222].

- **Conductive** patterns are mostly printed using inks based on metal nanoparticles, organometallic compounds, and carbon nanostructures. They have been developed to fulfill the widespreading demand for fully PE manufacturing. Metal inks based on nanoparticles or precursors are commonly employed as conductive elements in PE due to its reliable and stable conductivity [222]. The choice of conducting material is strongly dependent on their application. Silver is most common printable metal conductor, and formulations for common printing technologies such as screen, flexo, gravure and inkjet are widely available, as well as inks that are more flexible or stretchable when sintered.

- **Semiconducting** materials represent the key element for multipurpose in PE [226]. During ink formulation of semiconducting compounds, different choice are possible taking into account the electrical

requirements and the material restrictions. In general terms, the conductivity values of semiconducting materials can range from 10^2 to 10^{-6} $\Omega^{-1}\cdot cm^{-1}$ [229]. While inorganic semiconductors show better electrical performance and stability, organic semiconductors generally ensure cheaper and easier synthesis production (low-temperature processing), and higher mechanical flexibility.

- **Dielectrics** are passive materials which are used in many types of devices. Numerous dielectrics are solution processable and can be printed. The dielectric materials can play an important role in the device performance. They have diverse useful purposes, spanning form avoiding possible short-circuits into multi-layered conductive structures, enhancing the capacitance in electronic devices such as capacitors or transistors. Printable dielectric materials can be classified in inorganic materials, polymers and organic/inorganic hybrid materials [222].

4.1.3 Applications of printed electronics

4.1.3.1 Application benefits

The aim of PE industry is effectively implementing this technology in products in order to achieve some benefit. Various cases show that PE offers specific advantages in performance, cost or form factor over conventional solutions [230]. Consensus appears to be growing that many applications will involve hybrid system integration in the short to medium term, with the computation based on silicon electronics and other parts of the system enabled by printing.

Some of the application benefits of PE to be considered are:

1. **Flexibility.** It is a ready route to flexible components. Clear examples are the flexible displays for mobile devices and smart textiles.
2. **Integration.** It allows complete system integration since printing could be capable of the assembly of devices using multiple technologies (logic, memory, battery, displays, etc.).
3. **Speed.** Printing can be much faster than traditional microelectronics fabrication. Estimations put this speed difference as 4 orders of magnitude per device [11]. This is the key to low cost production and is the facilitator of disposable electronics.
4. **Large area.** It allows printing on large surfaces not constrained by wafer size, more closer to display technologies.
5. **Environmentally friendly.** Organic materials use more efficient printing processes in terms of low power consumption and selective deposition processes improving the environmental impact of electronic industry.
6. **Bio-compatibility.** Using organic materials in biomedicine can improve acceptance of these systems in contact with human body.
7. **Investment cost.** Printing has a low capital investment cost than other fabrication techniques. It is estimated that a PE plant will cost 25 million €, just a fraction of a 2.5 billion €, of a conventional silicon fabrication plant [11].

4.1.3.2 Current applications, challenges and trends

These last years the interest in the establishment of PE it has been growing in important industrial sectors as healthcare, smart buildings, automotive, packaging and the Internet of Things (IoT). These industry sectors implement solutions from a wide range of technology applications. A combination of simple printed devices, paves the way for low-cost and large area production of more complex flexible electronics circuits. PE is based on the combination of new materials and cost-effective, large-area production processes to enable new applications not possible with conventional electronics.

Current applications

Figure 4.4 summarizes PE solutions finding their way into major industry sectors and shows the key trend in PE industry. Some of these solutions are already commercial on significant scale, while others are still proof-of-concept prototypes. Some of the most important include:

- **OLED lighting:** It is moving from an expensive design option into more mainstream architectural lighting as prices are beginning to decrease. Non-planar and bendable lighting has appeared in initial products, such as automotive taillights and bendable OLED lighting panels. Complete flexible and transparent OLEDs are intended to be commercial products in medium-term [11].

- **Organic photovoltaic (OPV):** OPV have been significant breakthroughs in efficiency and in semi-transparent modules, detailed environmental impact studies are available, and lifetimes up to 20 years have been reported. Production capacity has increased, flexible OPV modules can be bought online for a low price, and more building integration installations have been built, however their complete integration is expected to be in medium-term.

- **Flexible OLED displays:** Major display technologies used for portable electronic devices are liquid crystal display (LCD), OLED display, and electrophoretic displays (EPD). OLED is a self-emitting technology showing an advantage of higher contrast, wider viewing angle and faster response time. For the moment OLEDs represent the biggest success story in PE as rigid, glass-based displays. Flexible or conformable displays are starting to become more widespread as well. Curved OLED displays are already being used in products such as TVs, mobile phones and watches.

- **Electronics and components:** Electronic devices and components are generally divided into two main families: passive or active elements. *Passive devices* are commonly two-terminal uncomplicated structures, formed by a single functional conductive material [231]. For instance, passive components are conducting pad-stripes, resistors, capacitors, inductors which do not introduce any energy into the electronic system and do not rely on any source power. On the contrary, *active devices* are typically more complex structures than passive elements. Transistors, diodes, batteries, solar cells rely on a source of power and inject net energy into the electronics system [232]. Active PE devices are not established in the market yet, even though organic semiconductors are already compatible with inorganic materials.

- **Integrated Smart Systems (ISS):** Smart systems refer to products that integrate multiple functionalities and technologies to create added value. The hybrid system integration of PE, e.g. for

sensing, interconnects, antennas and energy harvesting/storage, with the computing power of small silicon chips is becoming recognized as an area where PE can be a true enabler. Wearable health and wellbeing applications are also emerging. In the sensing area, with the emergence of the need for POC devices, the use of PE, in particular, screen-printing and IJP techniques have become widely used [233]. In Section 4.3 an overview of printed electrochemical sensors is presented.

	Existing 2017	Short Term 2018-2010	Medium Term 2021-2023	Long Term 2024 +	
OLED Lighting	Rigid white OLED modules; rigid red OLEDs for automotive applications	Flexible OLEDs (color); flexible OLEDs (white)	Transparent OLEDs; flexible red OLED for automotive applications	3D OLEDs; dynamic OLED signage (segmented); long stripes; OLED in general lighting	
OPV	Portable OPV chargers; personal electronics power supply	Large area OPV foil; OPV objects; opaque OPV for building integration	OPV integrated in building products	OPV in packaging; energy harvesting combined with storage	
Flexible & OLED Displays	Curved OLED displays, EPD shelf-edge labels, EPD secondary displays on phones; displays for wearables	EPD wrist band; transparent displays; conformable OLCD; enhanced display integration in wearables	Curved displays for autmotive interior; integration into clothing; white goods displays	Wallpaper displays; displays in everyday objects; foldable displays	
Electronics & Components	Printed devices: memory, RFID antenna, primary battery, active backplane; sensors: glucose, touch, temperature, humidity	Printed mobile communication devices based on antennas, light sensor; stretchable conductors / resistors; 3D touch sensors	Printed lithium ion battery; printed super caps; active touch & gesture sensors	Printed complex logic; 3D & large area flexible electronics	
Integrated Smart Systems	Glucose in-body sensing; pressure sensor arrays; NFC labels; hybrid RFID; HMIs (sensors)	Smart labels (discrete); HMI (embedded electronics & displays)	Human monitoring patches (single parameter, point of care, on-skin); disposable & quantitative sensors for food safety; biomedical sensors	Fully printed RFID / NFC label; ambient intelligence (connected); sensors for security (explosives)	

Figure 4.4 PE applications, with a forecast for the marking entry for the different applications. Source: [OE-A] [11].

Current challenges and trends for Integrated Smart Systems (ISS)

The recent progress in materials and process technology have been key challenge for the advance in ISS devices. Some of these key challenges in materials and processes are related to the print quality (resolution and uniformity), printing substrates (low-cost substrates are necessary for ISS) and ink properties (to improve PE, more available inks of different materials are needed). However, currently the key challenges are more focused on production, use and cost than on basic technology, which reflects the growing market orientation of PE. Related to the ISS, concretely, the sensors field, the key challenge that sensors need to overcome in order to develop a product in the market are:

- **Cost reduction:** Sensors fabricated by using PE technologies should be cheaper due to the lower manufacturing cost and (potentially) lower material cost.

- **Encapsulation:** Not only lower cost but also stretchable encapsulation materials are needed to make them compatible, and in the biomedical field and biocompatible.

- **Scalability:** From lab to industrial production and from small to large areas while keeping performance high.

- **Inspection/yield:** Progress in both yield improvement and in-line inspection and recognition of defects is needed for competitiveness.

- **Standards and regulations:** The standard and regulations for PE are under discussion, but not yet implemented.

Figure 4.5 shows the future of PE up to 2020 inside the Print Market Industry. The key challenges described above have pushed a market valued at 4.6 billion €, in 2010 to 22.3 €, billion in 2016 (Figure 4.5(a)). This has seen its share of global functional and industrial print demand rise from 17.4 % at the beginning of the decade to 33 % by its midpoint. By its close, further investment, new material sets, and the evolution of new applications will see this climb to a 39.8 % share (Figure 4.5(b)). By 2020, it is expected by Smithers Pira company [12] that a year-on-year market value increase of 13.9 % for PE, as opposed to 9.9 % for the functional print market as a whole. Another active area of research is related to biomedical applications that is focused in the development of low-cost printed sensors. Opportunities for cheap, flexible skin-mounted sensors also exists in healthcare. This is based on the emergence of telemedicine through the expensive and time-consuming compliance procedure for medical devices will slow this deployment. It is expected that biomedical sector achieve the 4.9 % of the printed industry.
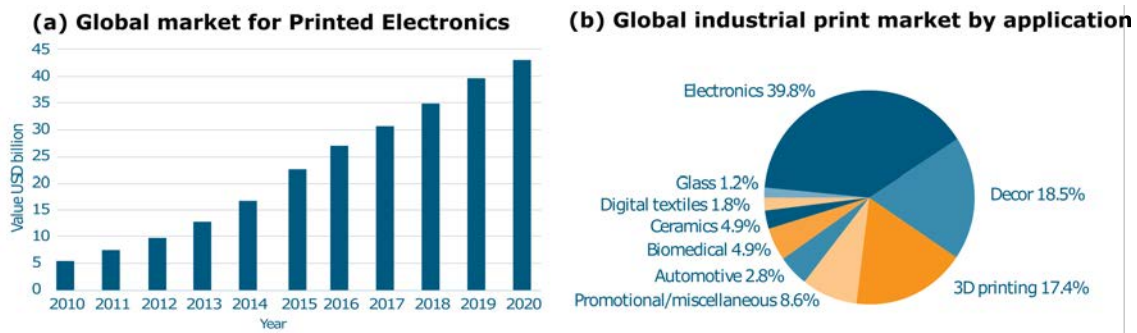
Figure 4.5 (a) Global market for printed products by 2020, and (b) global application in print market by 2020. Source: Smithers Pira [12].

4.2 Inkjet printing technology

Although the traditional and wider use of IJP technology has been centered in conventional graphic applications, the ability to accurately position picoliter drop volumes (down to 1 pL) of a large range of materials under digital control has been more recently exploited to pattern and manufacture novel functional surfaces and devices in many fields of science and technology [234].

The great advantage of IJP is that it is a digital technique based in a mask-less process, meaning that it can quickly switch from one design to another without the need for a new set of expensive masks, which enables a more flexible processing flow [234]. In addition, it is a non-contact technique where the materials are deposited onto the substrate in a drop-by-drop manner. It is a suitable technology for a wide range of production scales, with a lower initial investment than other printing techniques. The ink consumption and material wastage are minimal and it can produce patterned thin films [235]. As a drawback, the current resolution of IJP is on the order of micrometer and, therefore, cannot be compared with the resolution of microtechnology techniques which have a resolution in nanometers, but in contrast, IJP is not limited to a few rigid substrates, such as silicon or glass. Therefore, a trade-off exists between resolution and flexibility. Finally, another important drawback is the narrow properties that inks for inkjet need to feed, for this reason, IJP has more restrictions in the materials to be printed than other printing techniques and more investigation in inks development is required.

4.2.1 Inkjet printing technique

The inkjet technique is broadly classified into two categories, based on the mechanism of droplet generation classified in two groups: **continuous inkjet (CIJ)** and **drop-on-demand (DOD)** (Figure 4.6).
CIJ was the first existing inkjet technology [236]. It relies on a continuous ink ejection, where the stream is adapted into volume-controlled droplets generated by acoustic pressure waves as sketched in Figure 4.6(a). This inkjet technique is used for very low-cost system where no need of high resolution is necessary. The resulting evolution of continuous inkjet leads to the **DOD inkjet**, where a single drop is ejected by the cartridge nozzles only when required to achieve the final pattern. Applications of IJP in the commercial world have been developed rapidly, predominating the use of DOD technology.

DOD technique is in turn, classified into three types, namely thermal inkjet, piezo inkjet and electrostatic inkjet. Most current techniques are thermal (Figure 4.6(b.1)) and piezo inkjet(Figure 4.6(b.2)). Domestic inkjet printers mainly use thermal inkjet.
A ***thermal jet*** nozzle consists of an ink reservoir and a small resistive heater. A pulse of current is injected on the resistive heater to vaporize the ink around, forming a bubble and creating a pressure force to push out the ink in form of a droplet (Figure 4.6(b.1)). The heater then cools down, resulting in a vacuum thus refilling the ink reservoir for a new ejection [234]. Thermal jet has several disadvantages. Nozzles typically suffer from a short lifespan due to residue build-up on the resistive heater, and also, special ink is required to resist rapid thermal changes. For the aforementioned reasons, thermal jet technology is not suitable for functional materials, where the inks used are not compatible with heat stress, e.g. metal nanoparticle can
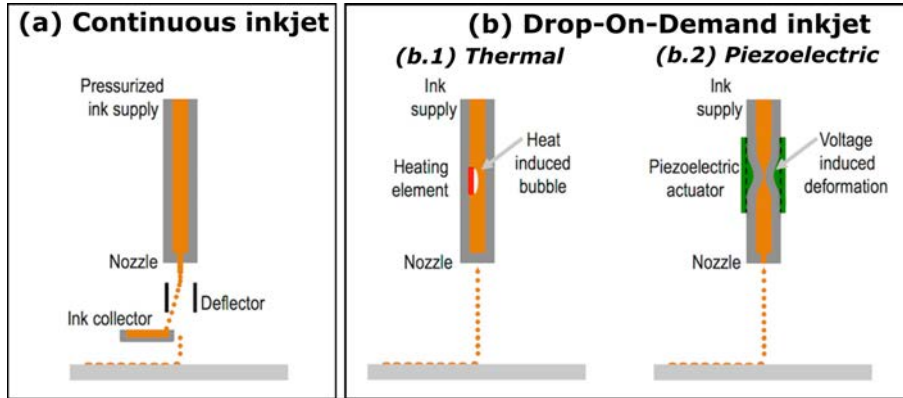
Figure 4.6 | Schematic representation of (a) continuous, and (b) drop-on-demand inkjet printing system using (b.1) thermal and (b.2) piezoelectric technology. Source: [13].

be sintered inside the chamber due to the heat, resulting in the deposition of metal layers on the resistive heater elements thus causing the malfunction of the nozzle.

Piezoelectric system is the most popular technique. A voltage pulse is applied to the piezoelectric plate to cause a deflection, creating an acoustic wave that propagates inside the chamber and ejects the droplet (Figure 4.6(b.2)). Due to the fast actuation of the piezoelectric plate (in the range of μs), the piezoelectric type can jet faster than the thermal type typically limited by the extra time required in the cooling step. The IJP resolution is basically limited by the minimum drop volume ejected by the nozzle system. Currently, inkjet printheads are delivering liquid droplets with a volume starting at 1 pL, which creates spots >15 μm in diameter on the substrate, depending on the liquid contact angle and the substrate surface conditions. Typically, the serial printing characteristic of the inkjet system limits the throughput of the deposition. To overcome this disadvantage, industrial inkjet printheads utilizes hundreds to thousands of nozzles to realize throughput enhancement via parallelization.

The printer used in this work is based on piezoelectric system. In a piezoelectric inkjet system the piezoelectric transducer is actuated by a voltage pulse, named waveform, that is the responsible for the jetting through nozzles (Figure 4.7a). As illustrated in Figure 4.7(b), the droplet formation is driven by the wave-
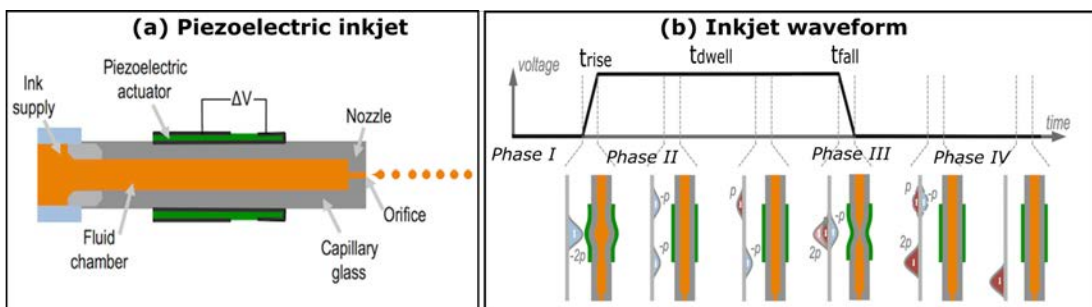
Figure 4.7 | (a) Detailed schematic structure of a piezoelectric single nozzle printhead, and (b) pressure perturbation generation, propagation and reflection upon trapezoidal voltage application

form that can be divided into different phases. Each phase has three properties: duration, level and slew rate. The applied voltage relates directly to the volume of the pumping chamber, and the slew rate how fast is that operation. It has been experimentally observed that the drop formation process and ejected drop characteristics strongly depend on the pulse characteristics [237][238][239]. Short rise and fall times, in the order of few microsenconds, are needed to have jet formation. More in detail, the start phase brings the piezoelectric to a relaxed position with the chamber at its maximum volume (Phase I). Immediately a decreased voltage is applied to retract the piezoelectric drawing fluid into the pumping chamber and followed by a settling time (Phase II). In this phase the fluid is pulled into the chamber through the inlet and two in-phase acoustic waves are created in both ends of the chamber traveling in opposite directions. The end of this phase need to be aligned with the beginning of the next one to expand the piezoelectric precisely when the two waves meet at the center of the pumping chamber to push out a droplet with its maximum energy (Phase III)[237]. During the last phase (phase IV), the piezoelectric retracts slightly breaking the droplet from the chamber and the voltage returns back to the standby state.

4.2.2 Requirements for inkjet printing

The different types of IJP technologies mentioned earlier have the same working principle and more or less have similar requirement with respect to substrates and inks. These requirements are addressed in this section. Figure 4.8 shows a general schematic of how an IJP system works. After the digital design of the patterns (Figure 4.8(a)) the printer can be equipped with the selected substrate and ink ((Figure 4.8(b)). Ink and substrate are the two materials that need to be compatible with the printer to obtain the desired printed pattern (Figure 4.8(c)).
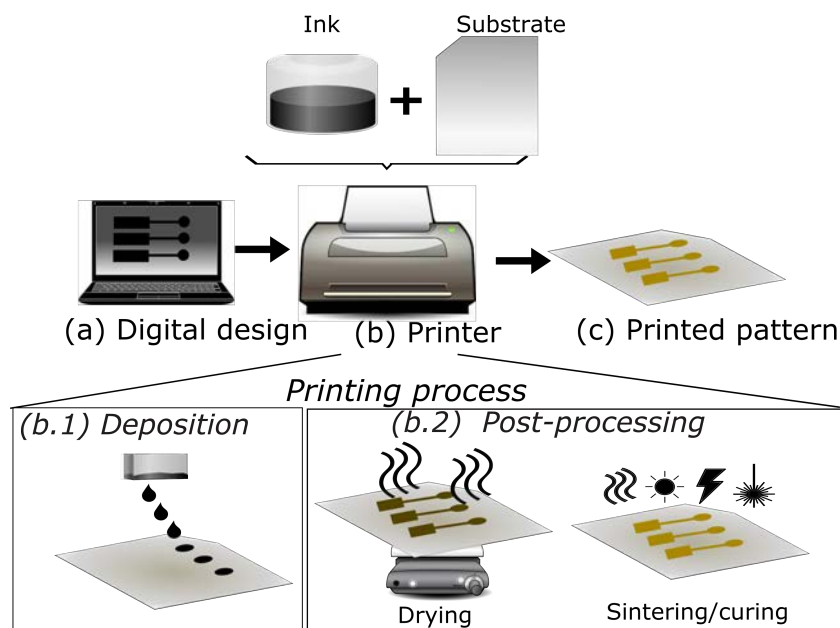
Figure 4.8 | Schematic of the basis of an inkjet-printed complete process from the (a) digital design, (b) printing process which implies the (b.1) ink deposition and (b.2) material post-processing, until (c) final fabricated device.

In general terms, the working principle of a printing process can be simplified in two steps: ink deposition and material post-processing. In the ink deposition step (Figure 4.8(b.1)), the printed material is deposited drop-by-drop using digital pixel pattern. In this step, the user need to define important printing parameters, such as the waveform applied, the working frequency or the distance between two consecutive drops, called drop spacing (DS). In the second step, the functional inks require a suitable transformation of the deposited ink layer to render its functionality (Figure 4.8(b.2)). This is achieved by removing the solvent and other additives such as surfactants, dispersants, humectants, adhesion enhancers, etc. which forms part of the ink. This process should be done in two step; the drying, which is used basically to evaporate the solvent and can be done at low temperatures (around 100 ºC), and the sintering/curing, where the dried structure enhance its functionality by applying an external energy typically a heat. UV, radiation, plasma treatment, laser, flash or microwave are different sintering techniques. As an example, in the case of metal nanoparticle inks, after the sintering process the nanoparticles are joined together and form a continuous solvent evaporation and other mechanisms that result in a dry solid film [16] as it is shown in Figure 4.9).
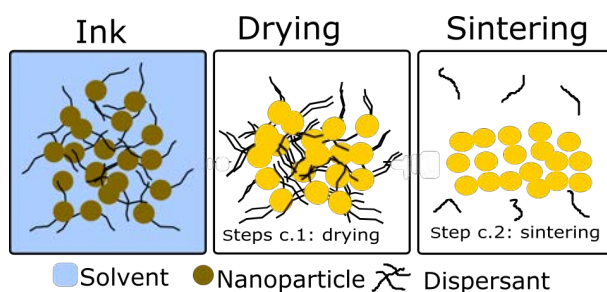
Figure 4.9 Sequence of the post-process of a metal nanoparticle-based ink with the drying and sintering steps.

4.2.2.1   Substrates, inks and printer for inkjet printing

At present, inkjet technology, in addition to graphic applications, has found numerous applications in many fields of science and technology. This is mainly thanks to the evolution of the three key points of the IJP: inks, substrates and printers (Figure 4.10). In order for the system to work each must be compatible with the other two. In this section, a general description of the substrates, inks and printer used in this work is presented.

Substrate

IJP technology is exceptionally encouraging because of its compatibility with different substrates. As it has been described before (Section 4.1.2), polymers are the best candidates used in PE, and also in IJP technology, mainly due to their low-cost and flexibility. Polymers offer a broad range of parameters as well as material and surface chemical properties. They are widely used for disposable devices in clinical applications. Thermosets polymers, such as PEN [240][241], PET [242] and Kapton® [243] are the most common ones in IJP.

Surface free energy of the substrate, together with the surface tension of the ink, are important parameters in defining the wettability and adhesion between ink and substrate. To improve this, different treatments can be applied to the substrate before its use. As an example, plasma treatment is widely used in plastic
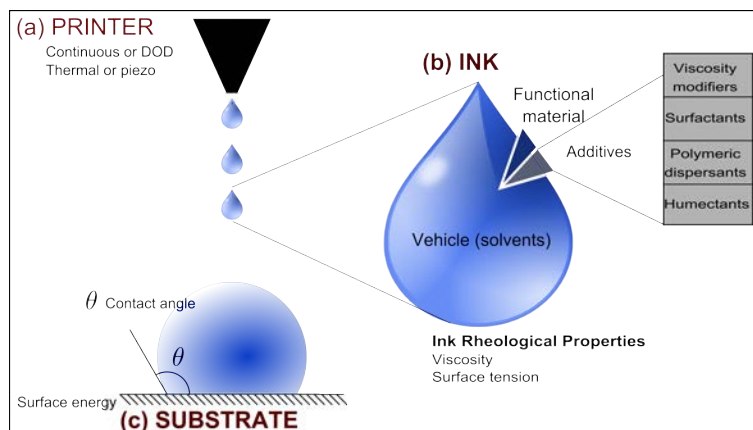
Figure 4.10 | Schematic of the combination between (a) printer, (b) ink, and (c) substrate, showing the particularity of each one.

substrates in order the improve the wettability and adhesion of the ink.

The emergence of the POC systems is demanding the use of paper as a substrate [228]. Using paper substrate has enhanced the advantages of IJP technology because paper is eco-friendly and extremely a low-cost material.

Inks

As mentioned in section 4.1.2, inks can be divided in three types: conducting, semiconducting and dielectric. As the aim of this work is the development of electrochemical devices, special attention in the selection of biocompatible conductive and dielectric inks is required.

Inkjet-printed **conductive inks** has been used in many applications, such as interconnections for a circuitry on printed circuit boards, disposable displays, radio frequency identification systems, organic thin-film transistors, electrochromic and electrochemical devices, etc. There has been progress in lowering the sintering temperature of nanoparticle inks, and this has made the inks more compatible with fast roll-to-roll processing and delicate substrates. Currently, the most used ink in inkjet is the silver [244]. However, in many applications, the use of gold material is preferable over silver because of the chemical inertness of this metal, specially for bio-applications [233, 245]. Typical organic conductive materials are polymer composites, such as poly(3,4-ethylenedioxythiophene) polystyrene sulfonate (PEDOT:PSS) [246], PPY and PANI [247], which are appealing since they are semi-transparent, flexible, light-weight, biocompatible and at the same time they ensure low-cost synthesis. Nevertheless, organic polymers reach low conductivity values ($10^{-3}/10^{-4} S * cm^{-1}$), which states a very restricting drawback in several application areas. PEDOT:PSS inks are continuing to improve in performance and are becoming viable as alternative to iridium tin oxide (ITO) especially in flexible products. Finally, other conducting organic materials, including carbon-based graphene [248] and CNTs [249] have been demonstrated as suitable conductive materials for flexible transparent printed devices.

In this work, inkjet-printed **dielectrics** are basically used to passivate conductive elements that can not be exposed to some medium or some other structure. A wide range of dielectrics are solution processable that

can be inkjet-printed. Poly(amic acid) [243] and SU-8 [250] are popular photoresist used in microfabrication technology that in some cases (depending their rheological properties) can be inkjet-printed. SU-8 is widely used in bioapplications due to their biocompatibility [251].

Dimatix Material Printer

The printer used in this work is the piezoelectric Dimatix DMP-2831 model shown in Figure 4.11(a). It is a versatile system for inkjet deposition development mainly used in research area. It is a self-contained system that allows the deposition of materials on substrates up to A4 size and utilizes disposable piezoelectric cartridges featuring 16 nozzles (Figure 4.11(b)). It incorporates two cameras; a drop watcher system and a fiducial camera for alignment. The drop watcher adds the capability to characterize and develop the jettable materials, examining the drop formation and progression from each of the printhead's nozzles. A reticule enables drop quality, trajectory and drop speed. Simultaneous and real-time control over the electronics driving signals supplied to the printhead allows to explore fluid jetting properties, understand its suitability for inkjet deposition, and establish conditions for printing. The fiducial camera allows the inspection and alignment of the printed layers. The different parts of the printer are also detailed in Figure 4.11(a). More details of the printer can be found in [14].
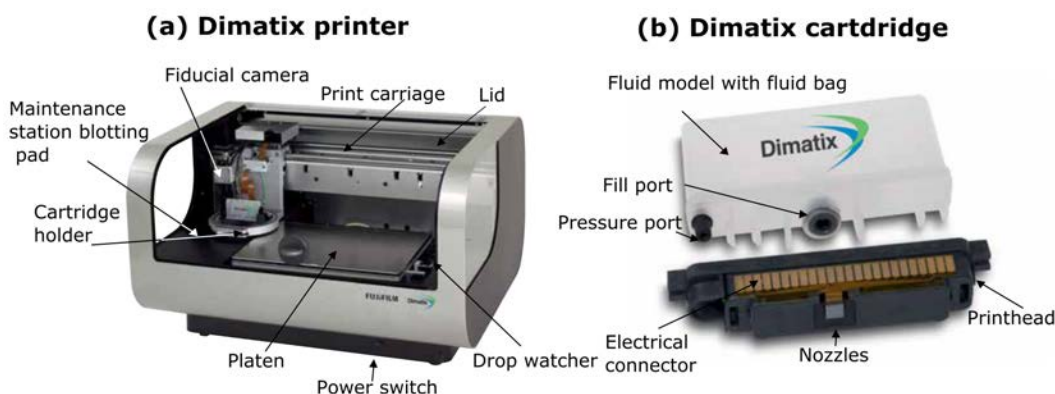
Figure 4.11 | a) Dimatix material printer and (b) Printhead and cartridge. Source: [14]

Print patterns can be created using the editor program provided or derived from images to create complex structures. The substrate platen can be heated up to 60 °C. The use of substrate heating can be used to slightly enhance the drop drying in order to improve the film formation. But the substrate heating can unintentionally raise the nozzle temperature and degrade the jetting. It is important to study carefully the optimum applied temperature to the substrate.

General purpose printheads are equipped with nozzles delivering a drop volume of 10 pL. A picture of the several parts of the printhead are detailed in Figure 4.11(b). Additionally, printheads with 1 pL nozzles are also available from Fujifilm Dimatix. These smaller printheads make difficult the printing of nanoparticle-based inks due to the high evaporation rate at the meniscus, causing frequent clogging of the nozzles.

In the Dimatix system, a drop velocity of 6-10 m·s^{-1} is desired; therefore, an ink with a viscosity below 15 cP and surface tension of 28-33 dyn·cm^{-1} is recommended to obtain stable jetting [14].

4.2.2.2 Ink requirements for inkjet

Owing to the complex nature of inkjet inks, their design and preparation is often very complex. In addition to the conventional requirements, such as long shelf-life, the ink must have physicochemical properties that are specific to the various printing devices. Besides the waveform formation, which confers energy to the leaving column of ink, fluid properties strongly influence the process of drop formation after jet ejection [235]. Two physical properties dominate the behavior of the liquid jets and drops: surface tension and viscosity [252] (Figure 4.10).

The **surface tension** of a liquid reflects the fact that atoms or molecules at a free surface have a higher energy than those in the bulk. When the liquid is in contact with the substrate, then it is necessary to consider not only the energy of its free surface (which is usually in contact with air or solvent) but also the energy of the interface between the liquid and the substrate. The **viscosity** of a liquid is a measure of its resistance to gradual deformation by shear stress. Each printhead has a specific range of surface tension and viscosity, which enable proper jetting. Piezoelectric printheads usually function at ink viscosity in the range of 8–15 cP [252], while thermal printheads require viscosities below 2 cP. Proper selection of the ink vehicle is also very important. Such selection can be affected tremendously not only by the requirements regarding the quality of the printed pattern on a specific substrate but also by the final application and the printing environment. Figure 4.10 shows a scheme of the main parameters that forms the ink and its iteration with the substrate.

In order to eject well-controlled drops of material, the jetted droplet needs to thin and break up after leaving the nozzle (Figure 4.12). This thinning, which is driven by surface tension forces, is balanced by viscous and inertial forces. For Newtonian liquids with a sufficiently high viscosity, the surface tension that induces jet squeezing is opposed by the viscous stresses within the filament. On the other hand, for liquids of low viscosity, the inertia of the accelerating fluid within the jet is the one opposing the thinning of the jet [252].
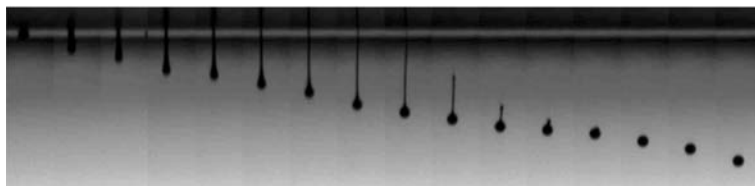
Figure 4.12 | Sequence of photographs showing the drop formation process using piezo-electric printhead. Source: [13]

Wolfgang von Ohnesorge introduced, well before the advent of IJP, a new dimensionless grouping of numbers to understand and define the different regimes found for the jet breaking after it leaves the nozzle [15] using the Weber number (We) and Reynols number (Re). The Ohnesorge number (Oh) (Equation 4.1) eliminates the speed of the drop and therefore depends only on the intrinsic physical properties of the fluid and the

dimensions of the ejecting nozzle (usually similar to the drop diameter):

$$Oh = \frac{\sqrt{We}}{Re} = \frac{\eta}{\sqrt{\gamma \rho a}} \qquad (4.1)$$

where η is the viscosity, γ is the surface tension, ρ is the density of the fluid and a the diameter of the nozzle orifice.

It is known from experimental studies that stable drop ejection typically takes place for certain range of Oh numbers, between 0.1 and 1 [15]. This set of limits for Oh, We and Re dimensionless numbers allow us to limit the properties of the printable fluids using inkjet as schematically presented in Figure 4.13.
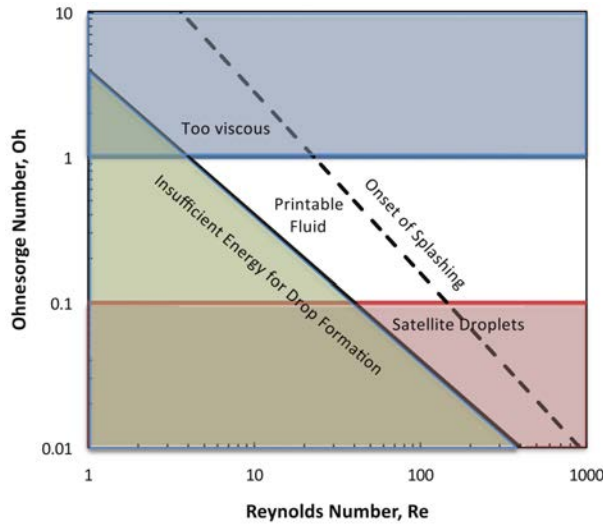
Figure 4.13 | Parameter space of inkjet printable fluids. Source: [15].

4.2.2.3 Drop deposition on the substrate and ink fixation

The science of inkjet and droplets is concerned far more with how fluids can be formed into jets and drops, which travel to and impact the substrate and then spread (or interact) and dry (or cure), than with the engineering and science needed to manufacture inkjet print heads and printing machines. As explained in previous sections, many factors can influence the final inkjet-printed pattern or structure. These factors are such as the ink rheology, the substrate properties before and after possible surface treatment, the surrounding environment (humidity), the pattern geometry, the interfaces interaction within multi-layered structures and the sintering method (laser, pulsed light, microwave, conventional oven) among others. An accurate procedure that dominates the combination of these factors is crucial.

Basically, the working principle of a printing process consists of three steps: (1) droplet formation, (2) positioning, spreading and ink coalescence on a substrate and (3) solvent evaporation and other mechanisms that result in a dry solid film [16] (Figure 4.14).

After leaving the nozzle, the droplet flies towards the target substrate. The spreading of the drop when reaches the substrate and its underlying mechanism after impact can be again understood by performing
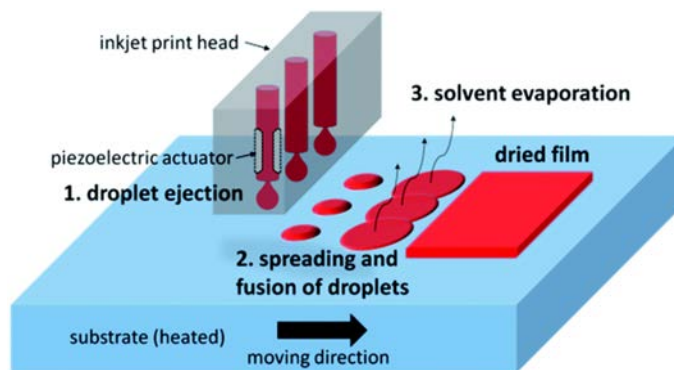
Figure 4.14 | Inkjet printing processes: (1) drop ejection, (2) spreading and fusion of droplets and (3) solvent evaporation. Source: [16].

non-dimensional analysis using We, Re and Oh numbers [15]. For common inks and conditions of IJP with droplets diameter of tens of microns impacting with speeds of few meters per second, gravitational effects can be neglected and splashing is not expected to happen. The drop initially spreads just after impact being this behaviour controlled by inertial forces (impact driven regime). The kinetic energy of the drop is transformed into surface energy by spreading over the dry substrate. After the spreading there is a surface tension driven retraction of the extended drop followed by oscillations of the droplet in which energy is dissipated by viscous forces taking more and more importance capillary forces (capillary driven regime) until the deposited drop reaches the stationary shape that is dictated by surface energy forces [17]. As a result, the size of the relaxed deposited drop, and therefore the resolution of IJP technique depends on the size of the ejected drop and the equilibrium contact angle of the ink on the substrate.

The spreading of the droplet on the substrate is followed by the drying phase, in which the liquid contained in the droplet evaporates and after a total drying a solid residual layer remains on the substrate. The timescale for drying depends on the ambient temperature and humidity, on the droplet size and on the ink solvents. The drying phase is followed by the sintering/curing process. This step is performance in order to make functional the printed patterns. In a nanoparticle based ink, the sintering process melts the metallic nanoparticle resulting in a metal thin film. The required temperature for the sintering of the nanoparticles is determined by the size of the particles and the encapsulant/dispersant. The melting point of metal nanoparticle is significantly reduced (relative to the bulk melting point) due to a high surface-to-volume ratio. The processing temperature needs to be below the Tg of the substrate materials.

Wetting of inks on surfaces: coffee ring effect

Depending on the process of ink drying, different effects can be observed in the ink fixation. The coffee ring effect was first explained by Deegan et al. [253]. A coffee ring stain can easily be obtained when the inkjetted drop completely wets the surface leading to an excess of solute at the edges, as shown in Figure 4.15a. This is due to higher evaporation at the outer edges of the deposited drop, causing an outward convective flow to replenish the lost solvent thus resulting in the accumulation of solute at the edges. The coffee ring effect can be reduced using several methods: e.g. changing the substrate temperature has been

demonstrated to eliminate the coffee ring [254]. Another method is based in the incorporation of a co-solvent system with a higher boiling point and a lower surface tension to suppress coffee ring [255]. Figure 4.15b illustrates this principle. Due to higher evaporation at the outer edges, the solvent composition at the outer edges becomes mainly the solvent with high boiling point. As a result, the solvent at the edges has a lower surface tension than in the center, resulting in a surface tension gradient, then a surface-tension driven Marangoni flow occurs to carry the solute inward to the center [256].
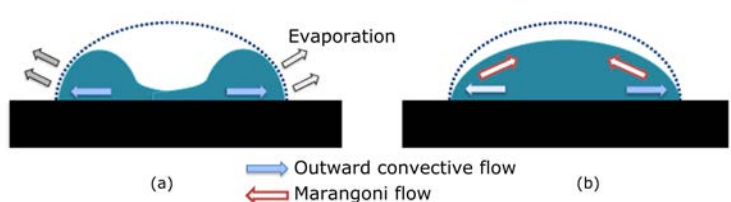
Figure 4.15 The process of drop drying after deposition with inkjet printing: (a) Coffee ring formation, (b) coffee ring suppressed by Marangoni flow [17].

Drop spacing

Beyond the printing of isolated dots, functional devices need also continuous printed tracks or areas so individual droplets have to be overlapped and the resultant features should be stable to maintain their shape and functionality. When drops of ink are deposited along a line, each overlapping with the previously deposited one, they coalesce into a single liquid bead. If the bead has a freely moving contact line it will be inherently unstable as a jet of water experiences. A rich phenomenology is observed when varying the distance between sequentially ejected drops that is common for many other sets of inks and substrates. As shown in Figure 4.16, for large distances between drops, DS, such that they do not interact on spreading, the individual printed appear as individual dots (Figure 4.16a). As the distance between printed dots becomes smaller, drop coalescence takes place, forming a line with a rounded contour, reminiscent of the individual contact lines of the original landed droplets Figure 4.16b). If DS is further decreased, the wavy contact lines disappear and a transition to parallel side edges is observed (Figure 4.16c). If spacing decreases even more, line widening can occur however eventually a bulging instability with regions that outflow the line and other where the line remains uniform might appear (Figure 4.16d).
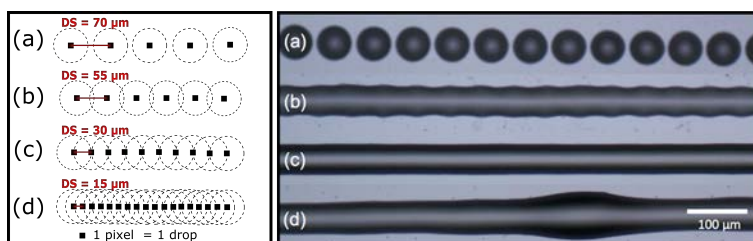
Figure 4.16 Droplets deposited along a line with decreasing distance between adjacent drops (from a to d) showing different behaviours: (a) isolated dots; (b) line with rounded contour; (c) line with straight contour and (d) line bulging. Source: [13]

4.3 Electrochemical sensors fabricated by inkjet printing

Sensing technology helps drive the digital era by allowing real-time information about our interactions with the environment to be collected in increasingly sophisticated ways. Traditionally, sensors are classified according to the transduction methodology employed, as optical, thermal, electromagnetic, mechanical, and electrochemical. Among them, the electrochemical transduction method has been showcased successfully as a robust powerful tool for obtaining real-time information. It is inherently sensitive and selective toward electroactive species, fast and accurate, compact, portable, and inexpensive. Such capabilities have already made a significant impact on the area of decentralized clinical analysis.

Using state-of-the-art printing technologies to produce these types of sensors is an exciting concept, given its unique ability to address the issue of low-cost manufacturing. Indeed, PE, of which inkjet-printed sensors are a subset of, is beginning to yield success. The manufacture of sensors using printing techniques is an emerging research and development area.

4.3.1 Paper III: Inkjet-printed electrochemical sensors

The first paper presented in this Chapter, **Paper III**, is a published review about the used of printing techniques for the development of electrochemical sensors, entitle: *Inkjet-printed electrochemical sensors.* This review takes a detailed look at the current state-of-the-art in printed electrochemical sensors in the last two years. Specifically, IJP processes and materials for electrochemical sensors and their components are discussed.

This article has been reproduced from Current Opinion in Electrochemistry with permision from Elsevier*:
A. Moya, G. Gabriel, R. Villa, F. Javier del Campo, **Inkjet-printed electrochemical sensors**, April 2017, Curr. Opin. Electrochem. doi:10.1016/j.coelec.2017.05.003.

* Note that sections, equations and references numbering in the reproduced research article follow the ones of the published version.

Available online at www.sciencedirect.com

ScienceDirect

Current Opinion in
Electrochemistry

ELSEVIER

Review Article
Inkjet-printed electrochemical sensors

Ana Moya[1,2], Gemma Gabriel[2,3], Rosa Villa[2,3] and F. Javier del
Campo[3,*]

Inkjet printing is a digital and non-contact printing technique that is beginning to be used in the manufacture of electronic devices, including electrochemical sensors. This article covers the main works featuring inkjet printing for the production of electrochemical sensors, and focuses especially on the works reported since 2015. The main factor limiting the application of inkjet printing in the manufacture of advanced devices stems mainly from the strict rheological conditions that the ink needs to meet. This is the reason why inkjet is best used in combination with other manufacturing techniques. Given their high degree of maturity and accessibility, home/office printers will likely lead a future wave in the manufacture of electronic devices, particularly at the development and prototyping stages.

Addresses
[1] PhD in Electrical and Telecomunicacion Engineering, Universitat Autònoma de Barcelona (UAB), Spain.
[2] Biomedical Research Networking Center in Bioengineering, Biomaterials, and Nanomedicine (CIBER-BBN). 08193 Bellaterra, Barcelona, Spain
[3] Instituto de Microelectrónica de Barcelona, IMB-CNM (CSIC). Esfera UAB. Campus Universitat Autònoma de Barcelona, 08193 Bellaterra, Barcelona, Spain

Corresponding author: Javier del Campo, F. (javier.delcampo@csic.es)

Introduction

Hundreds of new electrochemical sensors are reported in the scientific literature every year [1–3]. However, only a meagre fraction of these ever gets to be used outside the research laboratory where they were first developed. Manufacturability or, rather, the lack of it, is what sentences many of these new developments to remain in the library forever. This article focuses on the works, reported in the literature over the past 2 years, relying on inkjet printing for the fabrication of electrochemical sensors. Figure 1

shows the state of the field of inkjet-printed electrochemical sensors compared to screen-printed electrochemical sensors. Although screen printing and inkjet printing are extremely different technologies, they have both matured in the graphic arts sector before becoming electronic devices manufacturing techniques. As Figure 1 shows, inkjet printing is currently at the foot of its own S-curve [4], more or less at the point where screen printing was 20 years ago. This means that new applications can be expected to appear exponentially within the next few years as the technology consolidates in manufacturing. As Figure 1 shows, biomedical applications are currently drawing the most attention, followed by environmental and food safety applications. Inkjet printing, which principles may be found in excellent books and reviews [5–11], is a non-contact technique in which ink microdroplets are deposited on a substrate through a micrometric nozzle head [6] that relies on piezoelectric [12], thermal [13], or electrohydrodynamic [14] actuation for droplet ejection.

Construction of inkjet-printed sensors

Figure 2 schematizes the construction of electrochemical sensors by inkjet printing. The process is similar to that using other additive techniques, such as microfabrication or screen printing, where layers of conducting and dielectric materials are patterned and stacked on a substrate. However, in contrast to other manufacturing techniques that require photomasks, stencils, or other physical aids to facilitate patterning, inkjet printing is an entirely digital technique, which means that print designs may be changed with little cost impact. This makes inkjet not only attractive for production environments, but also highly suitable for research and prototyping purposes [15]. An additional advantage of inkjet is that it uses very little material, leading to the formation of layers less than 1 µm thin, and only where it is needed. This is in contrast to screen printing where coatings are in the range of a few microns, and large amounts of ink are required to print successfully [16].

The most common conducting materials used in (inkjet-printed) electrochemical sensors are based on silver [17,18], gold [15,19••–23••], carbon nanomaterials [19••,24–27], including graphene [28,29], and conducting polymers such as poly(3,4 ethylene dioxythiophene)-poly(styrenesulfonate) (PEDOT:PSS) [23••,30]*, polyaniline (PANI) [31•–33•]. The dielectric materials used to protect conducting tracks and to define electrode active areas are usually polymers such as poly(amic acid) [22], or SU-8 [15,34], a popular photoresist used in

2 **Sensors and Biosensors 2017**
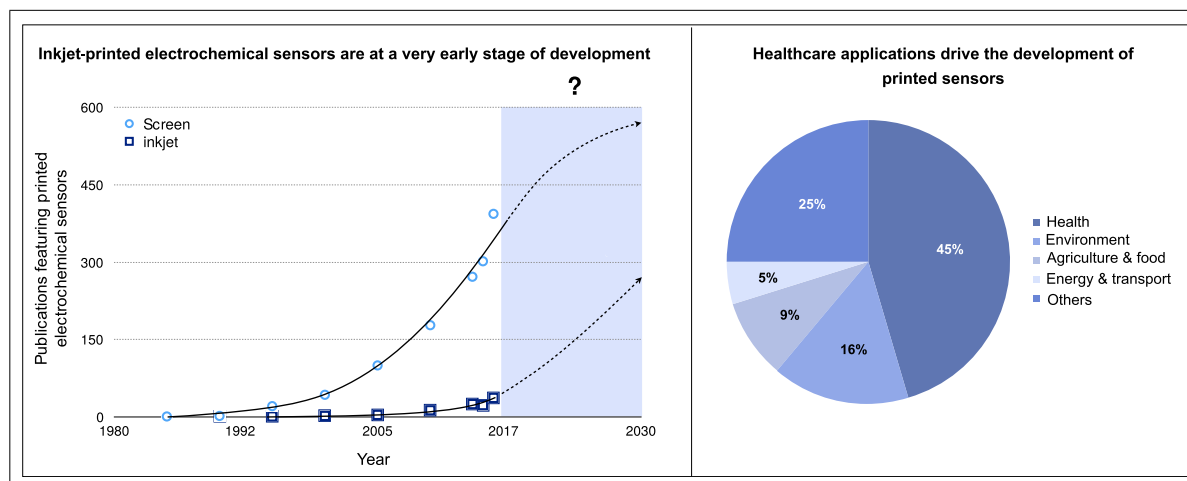
Figure 1

Inkjet-printed electrochemical sensors state of the art. Source: Scopus. Search carried out on April 12, 2017.

Figure 2
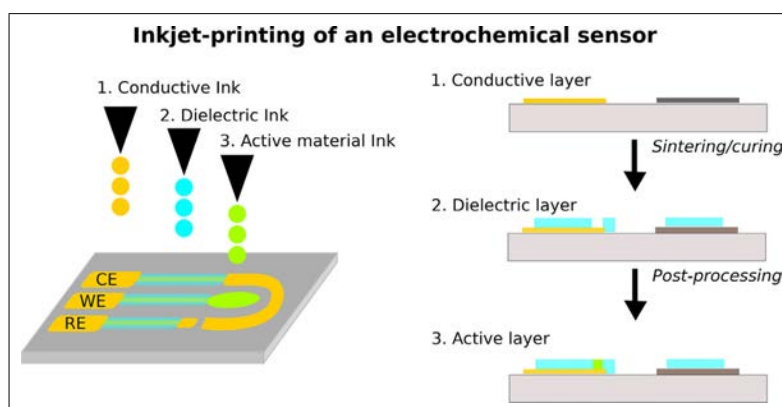
Schematic representation of the fabrication of electrochemical sensors by inkjet printing. A minimum of two inks are required to produce the transducers, and an additional ink is often needed to improve sensor performance.

MEMS [35]. Last, most selective coatings reported to date are based on conducting polymers [36•,37] and enzymes [13,38,39]. In terms of substrates, inkjet printing is most commonly used on flexible substrates such as PEN [19••], PET [25], Kapton® (a polyimide) [22], and paper [33•,40], but it can also be applied to rigid substrates such as glass [34] or silicon [18], and even 3D structures [38,41].

On the other hand, inkjet printing inks have to meet very specific rheological requirements, as viscosity and surface tension need to be within very narrow margins; 1–30 cP and 25–40 mN m^{-1}, respectively [42]. This, and the high cost of research equipment are the main factors lim-

iting technology adoption nowadays. Commercial functional inks are scarce, expensive, and have very limited shelf-life. Consequently, nearly all the works reported to date involve the in-house development of one or several inks. Table 1 summarizes the main works reporting inkjet-printed electrochemical sensors over the past 2 years, and the following sections provide an overview of the main achievements, limitations and opportunities.

Inkjet materials and processing

The success of inkjet technology in sensor manufacturing strongly depends on the availability of functional materials and suitable post-processing techniques. One of

www.sciencedirect.com

Please cite this article as: Moya *et al.*, Inkjet-printed electrochemical sensors, Current Opinion in Electrochemistry (2017), http://dx.doi.org/10.1016/j.coelec.2017.05.003

Current Opinion in Electrochemistry 2017, 000:1–11

JID: COELEC

ARTICLE IN PRESS

[mNS;June 1, 2017;20:24]

Inkjet-printed electrochemical sensors Moya *et al.*   3

Table 1

Summary of the main works reporting inkjet-printed electrochemical sensors in the period 2015-2016.

Detection method	Main analyte	Standard method	Sensor features	Printer	Ink	Substrate	REF
Potentiometry	pH	Glass electrode. Sensitivity: 59 mV•decade^{-1} (25 °C). Range: 0-14 pH. Resolution: 0.01 pH.	Inkjet + drop-casting. Sensitivity: 48.1 mV•decade^{-1} (Glass). 45.7 mV•decade^{-1} (PES). 46.1 mV•decade^{-1} (LCP). Hysteresis: 4 mV. Linear Range: 3- 11 pH. Response time: 7 seconds.	Meyer Burger (piezo).	Carbon nanotubes (commercial).	Glass, Polyether-sulfone and Liquid Cristal polymer.	[27]
	pH	See above.	Inkjet + drop-casting Sensitivity: 60.6 mV•decade^{-1} (Glass). 57 mV•decade^{-1} (Kapton).	Dimatix DMP (piezo).	Silver and dielectric (commercial) and Palladium.	Glass and Kapton[*].	[34]
	K$^+$ ion	Ion selective electrode (ISE). Range: $10^{-6} - 10^{-1}$ M. Sensitivity: 56 mV•decade^{-1}.	Inkjet + drop-casting. Range: 10^{-5} M to 10^{-1} M Sensitivity: 50.9 mV•decade^{-1}.	Dimatix DMP (piezo).	PEDOT(PSS) (commercial) and gold and dielectric.	Paper.	[23••]
Amperometry	Dissolved oxygen	Clark electrode. Range: 0-1 atm pO$_2$. Detection limit: 0.05-0.3 μM.	Fully-inkjet. Range: 0-8 mg•L^{-1}. Detection Limit: 0.11 mg•L^{-1}.	Dimatix DMP (piezo).	Gold, Silver and dielectric (commercial).	PEN.	[15]
	Dissolved oxygen and pH	*See above.*	Fully-inkjet. Sensitivity: DO: $4•10^{-7}$ A•(mg•L)$^{-1}$. pH: 67.5 mV•decade^{-1}.	Dimatix DMP (piezo).	Silver and dielectric (commercial) and Gold.	Kapton[*].	[22]
	H$_2$O$_2$	Clark-type electrode. Range: 0-200 mg•L^{-1}. Detection limit: 0.05 mg•L^{-1}.	Fully-inkjet. Sheet resistance: 0,7 kΩ•□$^{-1}$ (UV laser annealing). Sensitivity: 3,32 μA•mM^{-1}. Response time: < 5seconds.	Dimatix DMP (piezo).	Graphene.	Paper.	[28]
	Metal organic framework (MOF) nitrate sensor	Clark-type electrode. Range: 0-500 μM (in water). Detection limit: 0.1-0.5 μM.	Fully-inkjet. Sensitivity: 40.6 μA•mM^{-1} cm^{-2}. Detection limit: 0.72 μM.	MicroFab JetLab4 (piezo).	MOF-525 crystals.	ITO-glass.	[45]
	Polyphenolic antioxidant	High performance liquid chromatography (HPLC) Detection limits: (ng-μg) mL^{-1}.	SP + inkjet. Range: 0.01-10 μg•mL^{-1}. Detection limit: 1.38 ng•L^{-1}.	Dimatix DMP (piezo).	Graphene-polyaniline.	PET.	[31•]

Table 1 (*continued*)

Detection method	Main analyte	Standard method	Sensor features	Printer	Ink	Substrate	REF
	Iron ion (Fe^{2+}) and dopamine (DA)	DA: High performance liquid chromatography (HPLC).	Fully-inkjet. Range: 10 μM-200 μM (Fe^{2+}). 10 μM - 100 μM (DA).	HP Deskjet (thermal).	Dielectric (commercial) and carbon nanotubes.	Paper.	[24]
	Thyroid stimulating hormone (TSH) and atrazine (ATR)	Enzyme linked immunosorbent assay (ELISA).	Fully-inkjet Detection limit: ATR: 0.01 μg$\bullet$L^{-1}. TSH: 0.5 μIU$\bullet$L^{-1}.	X-series CeraPrinter (piezo).	Carbon nanotubes, silver and dielectric (commercial).	PET.	[25]
	Glucose	Photometric enzymatic method (hexokinase). Range: 0-500 mg$\bullet$dL^{-1}.	Inkjet on printed circuit board. Range: 0-40 mg$\bullet$dL^{-1}. Detection Limit: 0.3 mg$\bullet$dL^{-1}.	Home-made printer (piezo).	Graphene (commercial).	Polyimide.	[29]
	Cholesterol	Photometric enzymatic test. Range 0-1000 mgdL^{-1}.	Screen printing +inkjet. Range: 0-15 mM. Sensitivity: 2.1 μA$\bullet$mM^{-1} cm^{-2}. Detection limit: 0.02 mM.	Dimatix DMP (piezo).	Prussian blue nanoparticles .	Polyester.	[54]
	Salmonella	Plate counting (most probable number methods). Detection limit: 1cfu mL^{-1}. Analysis time: 16-18 h.	Nanoimprint+inkjet. Microelectrodes integrated in lab-on-chip. Range: 0-10^6 CFU$\bullet$mL^{-1}.	Dimatix DMP (piezo).	Silver and gold (commercial).	PET.	[53]
Redox cycling	Ferrocene dimethanol		Fully-inkjet. Sensitivity: 3.1×10^3 A$\bullet$(m$^2\bullet$M)$^{-1}$.	OmniJet (piezo).	silver and dielectric (commercial) and Carbon, gold and polystyrene.	PEN.	[19••]
	Glucose	*See above.*	Fully-inkjet. Electrodes resistance: 16.6 Ω.	Dimatix DMP (piezo).	Silver (commercial).	PDMS.	[55]
chemresistive	pH, H_2O_2	*See above.*	Fully-inkjet Minimum printable resolution: 200 μm Polyaniline layer sheet resistance: 5k$\Omega\bullet\square^{-1}$.	HP DeskJet (thermal).	Carbon nanotubes (commercial) and Polyaniline nanowires.	Transparency film.	[56]
chemresistive	Glucose	*See above.*	Inkjet + drop-casting. Range 0-10 mM. Detection Limit: 2 mM.	HP Deskjet (Thermal).	Carbon nanotube and polyaniline.	PET.	[57]

(*continued on next page*)

Table 1 (*continued*)

Detection method	Main analyte	Standard method	Sensor features	Printer	Ink	Substrate	REF
Cyclic voltammetry	Free Chlorine	Photometric (DPD) assay. Range: 0.1-3.5 mg mL^{-1}.	Fully-inkjet Range: 1-100 mg•L^{-1}. Detection limit: 2 mg•L^{-1}.	Dimatix DMP (piezo).	Silver and dielectric (commercial).	Kapton*.	[17]
	Antioxidants	Antioxidant capacity methods are based on fluorescence detection of radicals.	Fully-inkjet. Parallel acrylamide printing and UV photopolymerization.	Dimatix DMP (piezo).	Silver, dielectric and carbon nanotubes (commercial) and acrylamide.	Kapton*.	[26•]
	Antioxidants (ascorbic acid (AA))	Redox titration. μM range detection limit.	Fully-inkjet Antioxidant Power: 128 nW (0.5 mM AA) Antioxidant Power: 253 nW (1 mM AA)	Dimatix DMP (piezo).	Silver, dielectric and carbon nanotubes (commercial).	Kapton*.	[47•]
	Human papillomavirus	Polymerase chain reaction (PCR). Detection limit: 2 ng. Linear Range: $100 - 2000$ (ng•mL^{-1}).	Wax printing + Screen printing + inkjet. Detection limit: 2.3 nM. Linear range: 10-200 nM.	Dimatix DMP (piezo)	Graphene-Polyaniline.	Paper.	[33•]
	Unspecified		Physical Vapor Desposition + inkjet. Resistivity $< 3•10^{-6}$ Ohms•cm.	Home-made printer (piezo).	PEDOT:PSS (commercial).•	Paper.	[30]
Impedance spectroscopy	Ammonia	Ion selective electrode (ISE). Range: $5 \times 10^{-7} - 1$ M.	Screen printing + inkjet. Range: 25-200 μM. Detection limit: 12 μM.	Dimatix DMP (piezo).	Polyaniline.	PET.	[36•]
	Ammonia	*See above.*	Screen printing + inkjet. Range: 0-200 μM. Detection Limit: 25 μM.	Dimatix DMP (piezo).	Polyaniline.	PET.	[32]
	Ammonia	*See above.*	Inkjet + drop-casting. Range: 0-100 mg•L^{-1}. Detection limit: < 25 mg•L^{-1}.	Dimatix DMP (piezo).	Silver (commercial).	Si/SiO$_2$.	[18]

(*continued on next page*)

Table 1 (continued)

Detection method	Main analyte	Standard method	Sensor features	Printer	Ink	Substrate	REF
	DNA oligomers	Polymerase chain reaction (PCR).	Physical Vapor Desposition +-inkjet. Conductivity range.	Dimatix DMP (piezo).	tetraethylene-glycol polythiophene (TEGPT) and biotinfunction-alised TEGPT (b-TEGPT).	Paper.	[51]
	Antioxidant Pyrogallol	*See above.*	Inkjet + Gravure. Conductivity: $5 \cdot 10^6$ $S \cdot m^{-1}$. Fingers: 100 μm. Li Detection: 200 μM. Sensitivity: 5.68 $Ohms \cdot \mu m^{-1}$.	Dimatix DMP (piezo).	Gold and silver (commercial)	PEN, PET, PQA1.	[21]
	Unspecified		Lesker e-beam evaporator + -inkjet Low double layer impedance	Brother MFC (thermal).	Silver (commercial).	Paper.	[58]
	Bioelectronic interface	Electrocardiograph.	Inkjet + spin-coated. Conductivity: $5 \cdot 10^6$ $S \cdot m^{-1}$.	Dimatix DMP (piezo).	Gold (commercial).	PEN.	[20]
	Neuromuscular recording	See above.	Inkjet + drop-casting. Signal-to-noise ratio: 24.8 dB.	Dimatix DMP (piezo).	Silver and dielectric (commercial).	Kapton®.	[44]

the main challenges is the development of low sintering temperature metallic inks. Inkjet printing is particularly well suited for handling flexible substrates, but the materials that are more interesting from a cost standpoint (such as PET) are incompatible with sintering temperatures above 130 °C, which are required by most metal-based inks nowadays [43]. This has been overcome by conducting polymer inks which, in addition to displaying low curing temperatures, are also water-based [44]. But regardless of ink type, the main component is solvent which, together with other additives, needs to be removed after printing through post-processing steps to transform the ink into functional films. Post-processing may simply involve the evaporation of the solvent and additives or more complex processes such as sintering and polymerization.

Sometimes it is important to be able to cure a material immediately after printing. Lesch *et al.* demonstrated the simultaneous inkjet printing and UV photopolymerization of aqueous acrylamine/bis ink formulations, resulting in a compact and mechanically stable nonporous polyacrylamide (PA) coating over carbon nanotube electrodes [26•]. They demonstrated that the PA hydrogel coating provides an enhanced response. For the simultaneous inkjet and polymerization processes, a desktop piezoelectric printer was custom-made modified allowing the mounting of a liquid light guide connected to a UV lamp. Another interesting strategy has been reported by Su *et al.* [45], who developed porphyrinic metal-organic framework (MOF) thin films for electrocatalysis. They avoid additional curing or post-processing step, preparing a well-dispersed suspension of the as-synthesized MOF crystals and utilizing it as the ink for inkjet printing. He studied various thicknesses ranging from 3.8 µm to 25.2 µm by increasing the number of printed layers, and Das *et al.* [28] demonstrated how pulsed UV laser irradiation can improve the electrical conductivity of graphene coatings.

Desktop printers require external instrumentation to develop the post-processing steps, while more advanced machines incorporate them inline. Recently, Jović *et al.* demonstrated a large-scale fabrication of microtiter plates fully by inkjet printing in an automated process that combines printing and sintering steps [25].

How feasible are fully inkjet-printed electrochemical sensors?

Fully inkjet-printed electrochemical sensors [14,25,46] are rather uncommon (see Table 1) due to difficulties to inkjet print all of the components required. Whilst the deposition of conducting tracks and transducers in different materials [15,24,26•] is well established, very often the sensing material cannot be inkjet-printed, and other techniques such as drop casting [23••], or gravure printing [21] have been used to complete the fabrication. Lesch *et al.* [26•,47•] have worked on fully

inkjet sensor for the detection of antioxidants (such as ascorbic acid). In this case, both, the electrodes structure and the sensing layer (carbon nanotubes) were deposited by inkjet printing. Figure 3 shows the excellent electrochemical response and reproducibility achievable by inkjet printing of different materials, such as carbon-nanotubes, gold, and graphene.

In the simplest sensors, the transducer material also acts as sensing material. This is the case of the works reported by Lesch [26•], Jović [17], and Moya *et al.* [15], who reported, respectively, –ascorbic acid sensors using a carbon-nanotube-based transducer, a chlorine sensor for the control of swimming pool waters using silver electrodes, and a gold microelectrode-based oxygen sensor printed on flexible substrates. Another interesting recent example of transducer fabrication was recently reported by Adly *et al.* [19••], who demonstrated the ability to print a multilayer stack of four different material inks onto a plastic substrate. A commercially available nano-silver ink was used to form the feed lines for electrical connections, followed by printing of electrodes using tailor-made gold and carbon inks, and a dielectric polyamide ink was used to define the electrode areas. The most original part in this work is perhaps the printing of a polystyrene nanosphere ink that can be modified for biosensing applications. This layer is reported to improve the mechanical stability of the layers deposited on top of it, in this case a carbon electrode.

Combination with other techniques

The fabrication of more complex electrochemical sensors using inkjet seems to be limited to a few cases, and the main trend is to combine inkjet printing with other manufacturing techniques to improve the manufacturability of devices. Because of its simplicity and suitability for mass production, screen printing remains the major technology used for the fabrication of planar electrodes, which form the basis for a variety of electrochemical sensors [48]. However, most screen-printed sensors are functionalized manually by drop-casting [49,50].

Several workers have substituted the pipette with an inkjet printer seeking to automate the process while minimizing waste, improving reproducibility, and avoiding the risk of contamination [51]. Brannelly and Killard's recent work [32,36•] is a noteworthy example of this approach, pioneered by Kimura [52•] and Turner [39]. The ammonia sensor reported was designed as a two-electrode device using screen-printed interdigitated electrodes modified with polyaniline ink by inkjet printing. The printed sensors were assembled into a device that incorporates a gas permeable membrane and create a sample chamber with a capacity of 52 µl. Polyaniline was also used as a sensing element by Bardpho *et al.* [31•] In this case, a homemade graphene-polyaniline (G-PANI) ink was used for the modification of screen-printed

Figure 3
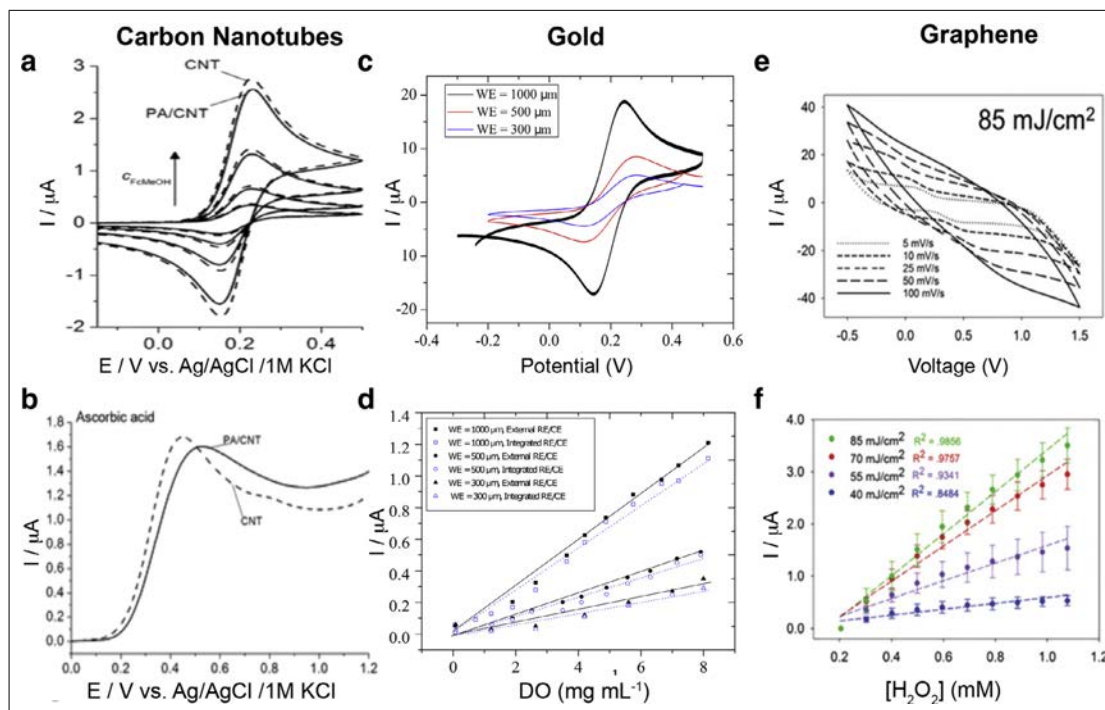
(a) Ferrocenemethanol cyclic voltammetry of inkjet-printed CNT and PA/CNT electrodes at different solution concentrations and (b) Linear sweep voltammetry in 2 mM ascorbic acid and 0.1 M acetate buffer. *Adapted from Ref. [26•]*. (c) Ferro/Ferricyanide cyclic voltammetry of inkjet-printed gold electrodes with different working electrode diameter and d) Dissolved oxygen calibration curve of three inkjet-printed sensors. *Adapted from Ref. [15]*. (e) Ferricyanide cyclic voltammetry of inkjet-printed graphene electrode at different scan rates and (f) Hydrogen peroxide calibration curves from electrodes cured at different laser power densities. *Adapted from Ref. [28]*.

electrodes to develop an electrochemical sensor for chromatographic determination of ascorbic acid. Graphene is a highly useful material for electroanalysis due to its very large two-dimensional electrical conductivity and excellent electron transfer. To prevent the agglomeration of graphene platelets and to improve graphene distribution on the electrode surface, polyaniline was added to the ink. The same G-PANI ink developed by Bardpho *et al.* has been used by Teengam *et al.* for the fabrication of an electrochemical sensor based on an anthraquinone-labeled pyrrolidinyl peptide nucleic acid (acpcPNA) probe for human papillomavirus detection [33•]. This work combines three different printing techniques; wax printing to create hydrophobic barriers into the paper substrate, screen printing for the three-electrode system fabrication, and inkjet printing for the modification of the working electrode with the G-PANI ink. However, the PNA was immobilized onto the G-PANI by drop-casting.

Chen *et al.* [53] combined nano-imprint with inkjet technologies to develop flexible microfluidic devices for elec-

trochemical detection. They used UV nanoimprint lithography to define microchannels structure on PET films and the electrodes were inkjet-printed and photonically sintered on another PET film. This film was bonded directly to the channel-containing layer to form sealed fluidic device.

Other workers have aimed at replacing microfabrication with inkjet processes. This is the case of works describing devices based on smooth, thin layers that are out of reach for conventional screen printing processes. Sjöberg *et al.* [23••] presented a potentiometric ion sensor platform fabricated quasi-fully by inkjet printing. Both the sensing electrodes and the solid contact layer (PEDOT:PSS) were inkjet-printed. However, due to the high viscosity of ionophore membrane solutions, the PVC-K^+ selective membrane and the protective non-selective reference membrane had to be drop-cast. Despite the authors' claim that they will further study the printability of PVC-based membrane, this is a significant challenge given the rheology of most PVC-membrane formulations. Similar techniques were reported by Le *et al.* [18], who

printed interdigitated electrodes onto a SiO_2/Si substrate for ammonia sensing. The electrodes were printed from a nano-silver ink, although the sensing element, polyaniline, was drop-cast. They studied different dimensions of interdigitated electrodes since the resistance of the polyaniline depends strongly on the dimensions of the silver electrodes. The range of widths and the gap between the interdigitates came from 100 to 400 µm. The smaller resistance (about 13.7 kΩ) was achieved with the smaller possible printed dimensions. To prevent short-circuits between microbands, minimum gaps of 112 µm were left between electrodes.

Another device for measuring pH has been reported by Qin *et al.* [34]. In this case, the pH sensor is based on inkjet-printed palladium material. The palladium ink was converted to metallic palladium using a two-step thermolysis after printing. Next, an SU-8 ink was inkjet-printed as an interfacial layer between Ag (to be print in the next step) and the substrate. The reference electrode consisted of a silver printed layer that was chlorinated with NaClO pippeted onto the Ag surface, resulting in an Ag/AgCl electrode. In addition, they prepared a printable ink for the solid electrolyte by dissolving poly(vynil chloride) in KCl and AgCl to protect the reference electrodes, but due to the limited jetting capabilities of inkjet, this membrane was finally pipette on the Ag/AgCl electrode.

Pavinatto *et al.* [21] also combined printing techniques to fabricate a complete biosensor for Pyrogallol detection. In this case, inkjet printing was used to fabricate the interdigitated structure and gravure printing was the selected technique to deposit a Tyrosinase ink on top.

Conclusions

Inkjet printing may be an ideal fabrication technique in cases when thin (100–500 nm) layers of material are needed, when contact with the substrate needs to be avoided, or when the material to be deposited is scarce, expensive, or highly toxic. This is why the mass production of electrochemical sensors may benefit from inkjet printing combined with other printing processes, such as screen, flexo, and gravure. The main bottleneck today is imposed by the strict rheological conditions that inks need to meet, particularly in terms of viscosity and surface tension, but new jettable materials can be expected to appear in the coming years. Nanomaterials are excellent candidates for their inclusion in functional inks, which means that collaboration between materials scientists, inkjet printing specialists, and electrochemists can fast-track progress in this area. Inkjet printing will gain importance both within research and production environments, driven by applications such as disposable sensors in healthcare, environment, and food safety.

A likely breakthrough in the field will likely come from the use of desktop photographic printers. These often mount the same heads as industrial plotters, but cost a fraction of the price. Although still in clear minority, in the coming years we will see an increasing number of workers using home/office thermal and piezoelectric printers. Here is a clear opportunity for software developers. Raster image processor software is routinely used in the graphic arts for the right application of color. Similar software can be developed for the handling of functional inks and the application of different materials. This will make the prototyping, development and production of electronic devices, including electrochemical sensors, hugely available in low-tech, low-cost settings.

References and recommended reading

Papers of particular interest, published within the period of review, have been highlighted as:

- • Paper of special interest
- •• Paper of outstanding interest.

1. Jadon N, Jain R, Sharma S, Singh K: **Recent trends in electrochemical sensors for multianalyte detection – a review**. *Talanta* 2016, **161**:894–916.

2. Labib M, Sargent EH, Kelley SO: **Electrochemical methods for the analysis of clinically relevant biomolecules**. *Chem Rev* 2016, **116**:9001–9090.

3. Bakker E: **Electrochemical sensors**. *Anal Chem* 2004, **76**:3285–3298.

4. Foster RN: *Innovation: The Attacker's Advantage*. New York: Summit Books; 1986.

5. Wu L, Dong Z, Li F, Zhou H, Song Y: **Emerging progress of inkjet technology in printing optical materials**. *Adv Opt Mat* 2016, **4**:1915–1932.

6. Hoath SD: *Fundamentals of Inkjet Printing*. Edited by Hoath SD. Weinheim, Germany,: Wiley-VCH Verlag GmbH & Co. KGaA; 2015.

7. Komuro N, Takaki S, Suzuki K, Citterio D: **Inkjet printed (bio)chemical sensing devices**. *Anal Bioanal Chem* 2013, **405**:5785–5805.

8. Li J, Rossignol F, Macdonald J: **Inkjet printing for biosensor fabrication: combining chemistry and technology for advanced manufacturing**. *Lab Chip* 2015, **15**:2538–2558.

9. Cummins G, Desmulliez MPY: **Inkjet printing of conductive materials: a review**. *Circuit World* 2012, **38**:193–213.

10. Khan S, Lorenzelli L, Dahiya RS: **Technologies for printing sensors and electronics over large flexible substrates: a review**. *IEEE Sensors J* 2015, **15**:3164–3185.

11. Singh M, Haverinen HM, Dhagat P, Jabbour GE: **Inkjet printing-process and its applications**. *Adv Mater* 2010, **22**:673–685.

12. Wijshoff H: **The dynamics of the Piezo inkjet printhead operation☆**. *Phys Rep* 2010, **491**:77–177.

13. Setti L, Fraleoni-Morgera A, Ballarin B, Filippini A, Frascaro D, Piana C: **An amperometric glucose biosensor prototype fabricated by thermal inkjet printing**. *Biosens Bioelectron* 2005, **20**:2019–2026.

10   Sensors and Biosensors 2017

14. Ali S, Hassan A, Hassan G, Bae J, Lee CH: **All-printed humidity sensor based on graphene/methyl-red composite with high sensitivity**. *Carbon* 2016, **105**:23–32.

15. Moya A, Sowade E, del Campo FJ, Mitra KY, Ramon E, Villa R, Baumann RR, Gabriel G: **All-inkjet-printed dissolved oxygen sensors on flexible plastic substrates**. *Organ Electron* 2016, **39**:168–176.

16. Banks CE, Foster CW, Kadara RO: *Screen-Printing Electrochemical Architectures*. Cham Springer International Publishing; 2016.

17. Jović M, Cortés-Salazar F, Lesch A, Amstutz V, Bi H, Girault HH: **Electrochemical detection of free chlorine at inkjet printed silver electrodes**. *J Electroanal Chem* 2015, **756**:171–178.

18. Le DD, Nguyen TNN, Doan DCT, Dang TMD, Dang MC: **Fabrication of interdigitated electrodes by inkjet printing technology for apllication in ammonia sensing**. *Adv Nat Sci Nanosci Nanotechnol*, vol 7 2016 025002.

19. Adly NY, Bachmann B, Krause KJ, Offenhäusser A, Wolfrum B, ●● Yakushenko A: **Three-dimensional inkjet-printed redox cycling sensor**. *RSC Adv* 2017, **7**:5473–5479.
This paper reports a multi-layer 3D interdigitated structure with a porous nanogap that allows highly efficient redox cycling.

20. Khan Y, Pavinatto FJ, Lin MC, Liao A, Swisher SL, Mann K, Subramanian V, Maharbiz MM, Arias AC: **Inkjet-Printed Flexible Gold Electrode Arrays for Bioelectronic Interfaces**. *Adv Funct Mater* 2016, **26**:1004–1013.

21. Pavinatto FJ, Paschoal CW, Arias AC: **Printed and flexible biosensor for antioxidants using interdigitated ink-jetted electrodes and gravure-deposited active layer**. *Biosens Bioelectron* 2015, **67**:553–559.

22. Xu Z, Dong Q, Otieno B, Liu Y, Williams I, Cai D, Li Y, Lei Y, Li B: **Real-time in situ sensing of multiple water quality related parameters using micro-electrode array (MEA) fabricated by inkjet-printing technology (IPT)**. *Sens Actuators, B* 2016, **237**:1108–1119.

23. Sjöberg P, Määttänen A, Vanamo U, Novell M, Ihalainen P, ●● Andrade FJ, Bobacka J, Peltonen J: **Paper-based potentiometric ion sensors constructed on ink-jet printed gold electrodes**. *Sens Actuators B: Chem* 2016, **224**:325–332.
This paper reports the fabrication of potentiometric K+ sensors on paper. Gold transducers and PEDOT:PSS solid contacts are inkjet-printed, although the valynomicin membrane is drop cast on top of the PEDOT:PSS layer.

24. da Costa TH, Song E, Tortorich RP, Choi J-W: **A paper-based electrochemical sensor using inkjet-printed carbon nanotube electrodes**. *ECS J Solid State Sci Technol* 2015, **4**:S3044–S3047.

25. Jović M, Zhu Y, Lesch A, Bondarenko A, Cortés-Salazar F, Gumy F, Girault HH: **Inkjet-printed microtiter plates for portable electrochemical immunoassays**. *J Electroanal Chem* 2017, **786**:69–76.

26. Lesch A, Cortes-Salazar F, Amstutz V, Tacchini P, Girault HH: ● **Inkjet printed nanohydrogel coated carbon nanotubes electrodes for matrix independent sensing**. *Anal Chem* 2015, **87**:1026–1033.
This paper reports an fully inkjet printed sensor for antioxidant detection in fruit juice and wine. Electrode passivation is prevented by a printable polyacrylamide membrane that is UV cured during the printing process.

27. Qin Y, Kwon H-J, Subrahmanyam A, Howlader MMR, Selvaganapathy PR, Adronov A, Deen MJ: **Inkjet-printed bifunctional carbon nanotubes for pH sensing**. *Mater Lett* 2016, **176**:68–70.

28. Das SR, Nian Q, Cargill AA, Hondred JA, Ding S, Saei M, Cheng GJ, Claussen JC: **3D nanostructured inkjet printed graphene via UV-pulsed laser irradiation enables paper-based electronics and electrochemical devices**. *Nanoscale* 2016, **8**:15870–15879.

29. Pu Z, Wang R, Wu J, Yu H, Xu K, Li D: **A flexible electrochemical glucose sensor with composite nanostructured surface of the working electrode**. *Sens Actuators, B* 2016, **230**:801–809.

30. Ihalainen P, Määttänen A, Pesonen M, Sjöberg P, Sarfraz J, Österbacka R, Peltonen J: **Paper-supported nanostructured ultrathin gold film electrodes – Characterization and functionalization**. *Appl Surf Sci* 2015, **329**:321–329.

31. Bardpho C, Rattanarat P, Siangproh W, Chailapakul O: **Ultra-high** ● **performance liquid chromatographic determination of antioxidants in teas using inkjet-printed graphene-polyaniline electrode**. *Talanta* 2016, **148**:673–679.
This paper reports the fabrication of an HPLC detector for the detection of polyphenols in tea. The detector consists of an inkjet-printed graphene-PANI on a screen-printed graphite electrode.

32. Brannelly NT, Killard AJ: **A printed and microfabricated sensor device for the sensitive low volume measurement of aqueous ammonia**. *Electroanalysis* 2017, **29**:162–171.

33. Teengam P, Siangproh W, Tuantranont A, Henry CS, Vilaivan T, ● Chailapakul O: **Electrochemical paper-based peptide nucleic acid biosensor for detecting human papillomavirus**. *Anal Chim Acta* 2017, **952**:32–40.
This paper reports the fabrication of an electrochemical sensor for human papillomavirus detection using inkjet printing graphene-PANI on a screen-printing carbon electrodes.

34. Qin Y, Alam AU, Howlader MMR, Hu N-X, Deen MJ: **Inkjet printing of a highly loaded palladium ink for integrated, low-Cost pH sensors**. *Adv Funct Mater* 2016, **26**:4923–4933.

35. Liu C: **Recent developments in polymer MEMS**. *Adv Mater* 2007, **19**:3783–3790.

36. Brannelly NT, Killard AJ: **An electrochemical sensor device for** ● **measuring blood ammonia at the point of care**. *Talanta* 2017, **167**:296–301.
This paper describes the fabrication of a sensor for ammonia in blood. The sensor combines screen-printed transducers and an inkjet-printed active layer composed of polyaniline nanoparticles.

37. Weng B, Shepherd RL, Crowley K, Killard AJ, Wallace GG: **Printing conducting polymers**. *Analyst* 2010, **135**:2779–2789.

38. Khan MS, Fon D, Li X, Tian J, Forsythe J, Garnier G, Shen W: **Biosurface engineering through ink jet printing**. *Colloids Surf B* 2010, **75**:441–447.

39. Newman JD, Turner APF, Marrazza G: **Ink-jet printing for the fabrication of amperometric glucose biosensors**. *Anal Chim Acta* 1992, **262**:13–17.

40. Hu C, Bai X, Wang Y, Jin W, Zhang X, Hu S: **Inkjet printing of nanoporous gold electrode arrays on cellulose membranes for high-sensitive paper-like electrochemical oxygen sensors using ionic liquid electrolytes**. *Anal Chem* 2012, **84**:3745–3750.

41. Haque RI, Ogam E, Loussert C, Benaben P, Boddaert X: **Fabrication of capacitive acoustic resonators combining 3D printing and 2D inkjet printing techniques**. *Sensors* 2015, **15**:26018–26038.

42. Madgdassi S: *The Chemistry of Inkjet Inks*. Ed. London: World Scientific; 2010.

43. Rajan K, Roppolo I, Chiappone A, Bocchini S, Perrone D, Chiolerio A: **Silver nanoparticle ink technology: state of the art**. *Nanotechnol Sci Appl*, vol 9 2016.

44. Roberts T, De Graaf JB, Nicol C, Herve T, Fiocchi M, Sanaur S: **Flexible inkjet-printed multielectrode arrays for neuromuscular cartography**. *Adv Healthc Mater* 2016, **5**:1462–1470.

45. Su C-H, Kung C-W, Chang T-H, Lu H-C, Ho K-C, Liao Y-C: **Inkjet-printed porphyrinic metal–organic framework thin films for electrocatalysis**. *J Mater Chem A* 2016, **4**:11094–11102.

46. Tseng C-C, Chou Y-H, Hsieh T-W, Wang M-W, Shu Y-Y, Ger M-D: **Interdigitated electrode fabricated by integration of ink-jet printing with electroless plating and its application in gas sensor**. *Colloids Surf A: Physicochem Eng Aspects* 2012, **402**:45–52.

47. Lesch A, Cortés-Salazar F, Prudent M, Delobel J, Rastgar S, ● Lion N, Tissot J-D, Tacchini P, Girault HH: **Large scale inkjet-printing of carbon nanotubes electrodes for antioxidant assays in blood bags**. *J Electroanal Chem* 2014:61–68 717–718.

This article reports one of the first fully printed electrochemical sensors, which show better performance than screen-printed graphite. A straightforward method is presented for the electrochemical determination of antioxidant capacity of samples, using ascorbic acid as model system.

48. Metters JP, Kadara RO, Banks CE: **New directions in screen printed electroanalytical sensors: an overview of recent developments**. *Analyst* 2011, **136**:1067–1076.

49. Hughes G, Westmacott K, Honeychurch KC, Crew A, Pemberton RM, Hart JP: **Recent advances in the fabrication and application of screen-printed electrochemical (Bio)sensors based on carbon materials for biomedical, Agri-food and environmental analyses**. *Biosensors*, vol 6 2016.

50. Jensen GC, Krause CE, Sotzing GA, Rusling JF: **Inkjet-printed gold nanoparticle electrochemical arrays on plastic. Application to immunodetection of a cancer biomarker protein**. *Phys Chem Chem Phys* 2011, **13**:4888–4894.

51. Ihalainen P, Pesonen M, Sund P, Viitala T, Määttänen A, Sarfraz J, Wilén C-E, Österbacka R, Peltonen J: **Printed biotin-functionalised polythiophene films as biorecognition layers in the development of paper-based biosensors**. *Appl Surf Sci* 2016, **364**:477–483.

52. Kimura J, Kawana Y, Kuriyama T: **An immobilized enzyme mebrane fabrication method using an ink jet nozzle**. *Biosensors* 1988, **4**:41–52 .

This is the first ever article reporting the use of inkjet printing for the fabrication of electrochemical sensors. The enzymes glucose oxidase and urease were deposited by inkjet on ISFET gates.

53. Chen J, Zhou Y, Wang D, He F, Rotello VM, Carter KR, Watkins JJ, Nugen SR: **UV-nanoimprint lithography as a tool to develop flexible microfluidic devices for electrochemical detection**. *Lab Chip* 2015, **15**:3086–3094.

54. Cinti S, Arduini F, Moscone D, Palleschi G, Gonzalez-Macia L, Killard AJ: **Cholesterol biosensor based on inkjet-printed Prussian blue nanoparticle-modified screen-printed electrodes**. *Sens Actuators B: Chem* 2015, **221**:187–190.

55. Wu J, Wang R, Yu H, Li G, Xu K, Tien NC, Roberts RC, Li D: **Inkjet-printed microelectrodes on PDMS as biosensors for functionalized microfluidic systems**. *Lab Chip* 2015, **15**:690–695.

56. Song E, Tortorich RP, da Costa TH, Choi J-W: **Inkjet printing of conductive polymer nanowire network on flexible substrates and its application in chemical sensing**. *Microelectron Eng* 2015, **145**:143–148.

57. Song E, da Costa TH, Choi J-W: **A chemiresistive glucose sensor fabricated by inkjet printing**. *Microsyst Technol* 2016, **85**:1–7.

58. Ma H, Su Y, Jiang C, Nathan A: **Inkjet-printed Ag electrodes on paper for high sensitivity impedance measurements**. *RSC Adv* 2016, **6**:84547–84552.

4.4 Application of inkjet-printed sensors for Organ-On-a-Chip monitoring

In this section is shown the development of the monitoring tools using IJP technology, addressed to monitor levels of DO inside the OOC systems. This section is divided in two subsections, where each one corresponds to a published work in first-quartile journals.

4.4.1 Paper IV: All-inkjet-printed dissolved oxygen sensors on flexible plastic substrates

The second paper presented in this Chapter, **Paper IV**, is a published article about the development of DO sensors, fabricated fully by IJP in a plastic substrate. The article is focused in the complete characterization of the functional inks that can be processed and sintered at low temperature (120 ºC) to be compatible with polymeric substrates. Different dimensions of inkjet-printed DO sensors are fabricated and their electrochemical response and validation is presented.

This article has been reproduced from Organic Electronics journal, with permission from Elsevier*:

A. Moya, E. Sowade, F.J. del Campo, K.Y. Mitra, E. Ramon, R. Villa, R.R. Baumann, G. Gabriel, **All-inkjet-printed dissolved oxygen sensors on flexible plastic substrates.** 39 (2016) 168–176. doi:10.1016/j.orgel.2016.10.002.

This work has been also presented in different conferences with their corresponding Proceedings:

- Conference **LOPEC2016**: A. Moya, E. Sowade, F.J. del Campo, K.Y. Mitra, E. Ramon, R. Villa, R.R. Baumann, G. Gabriel, All-inkjet-printed dissolved oxygen sensors on flexible plastic substrates. Oral presentation.

- Conference **BIOSENSORS2016**: A. Moya, E. Sowade, F.J. del Campo, K.Y. Mitra, E. Ramon, R. Villa, R.R. Baumann, G. Gabriel, All-inkjet-printed dissolved oxygen sensors on flexible plastic substrates. Poster presentation.

- Conference **SPIE2017**: A.Moya, M. Zea, E. Sowade, R. Villa, E. Ramon, R.R. Baumann, G. Gabriel. Inkjet-Printed Dissolved Oxygen and pH Sensors on Flexible Plastic Substrates. Oral presentation. Proceedings Volume 10246, Smart Sensors, Actuators, and MEMS VIII; 102460F (2017); doi: 10.1117/12.2264912.

The development of this work has led to the development of other types of sensors on plastic substrates fabricated by IJP (glucose and sulfur). The following works have been submitted for publication:

- Romeo Agostino; Moya Ana; Leung Tammy; Gabriel Gemma; Villa Rosa; Sanchez Samuel. *Inkjet Printed Flexible Non-Enzymatic Glucose Sensor for Tear Fluid Analysis*. This article has been SUBMITTED to ACS Sensors Journal.

- Pol Roberto; Moya Ana; Gabriel Gemma; Gabriel David; Cespedes Francisco; Baeza Mireia. *Inkjet-printed sulfide-selective electrode*. This article has been SUBMITTED to Analytical Chemistry.

Note that sections, equations and references numbering in the reproduced research article follow the ones of the published version.

CrossMark

All-inkjet-printed dissolved oxygen sensors on flexible plastic substrates

Ana Moya [a, d], Enrico Sowade [b], Francisco J. del Campo [a], Kalyan Y. Mitra [b], Eloi Ramon [a], Rosa Villa [a, d], Reinhard R. Baumann [b, c], Gemma Gabriel [a, d, *]

[a] Instituto de Microelectrónica de Barcelona, IMB-CNM (CSIC), Esfera UAB, Campus Universitat Autònoma de Barcelona, 08193, Bellaterra, Barcelona, Spain
[b] Technische Universität Chemnitz, Digital Printing and Imaging Technology, 09126, Chemnitz, Germany
[c] Fraunhofer Institute for Electronic Nano Systems (ENAS), Printed Functionalities, 09126, Chemnitz, Germany
[d] Research Networking Center in Bioengineering, Biomaterials and Nanomedicine (CIBER-BBN), 08193, Barcelona, Spain

ARTICLE INFO

ABSTRACT

Inkjet printing is a promising alternative manufacturing method to conventional standard micro-fabrication techniques for the development of flexible and low-cost devices. Although the use of inkjet printing for the deposition of selected materials for the development of sensor devices has been reported many times in literature, it is still a challenge and a potential route towards commercialization to completely manufacture sensor devices with inkjet technology. In this work is demonstrated the fabrication of a functional low-cost dissolved oxygen (DO) amperometric sensor with feature sizes in the micrometer range using inkjet printing. All the required technological steps for the fabrication of a complete electrochemical three electrodes system are discussed in detail. The working and counter electrodes have been printed using a gold nanoparticle ink, whereas a silver nanoparticle ink was used to print a pseudo-reference electrode. Both inks are commercially available and can be sintered at low temperatures, starting already at 120 °C, which allows the use of plastic substrates. In addition, a printable SU8 ink formulation cured by UV is applied as passivation layer in the sensor device. Finally, as the performance of analytical methods strongly depends on the working electrode material, is demonstrated the electrochemical feasibility of this printed DO sensor, which shows a linear response in the range between 0 and 8 mg L^{-1} of DO, and affords a detection limit of 0.11 mg L^{-1}, and a sensitivity of 0.03 μA L mg^{-1}. The use of flexible plastic substrates and biocompatible inks, and the rapid prototyping and low-cost of the fabricated sensors, makes that the proposed manufacturing approach opens new opportunities in the field of biological and medical sensor applications.

1. Introduction

Inkjet printing is attracting increasing interest in the area of micro-sensors technology, e.g. for the determination of biological or chemical parameters with a high spatial resolution [1,2,3]. The inkjet printing method is considered a promising alternative to traditional sensor manufacturing techniques, as it is an additive and non-contact approach that allows the mask-less deposition of different functional materials on rigid and flexible substrates. Even though screen-printing still remains the most used printing technique employed for the production of low-cost and disposable sensors [4,5], the emerging inkjet printing technology has many advantages over it, such as easily changeable layouts without the need of physical stencils or screens, the reduction of the generated waste material and the non-contact deposition. The latter feature helps prevent substrate contamination, and it allows the technique to be used on delicate substrates that may be damaged by the force applied in the screen-printing process. Moreover, the direct writing approach without any need for screens drastically reduces the overall fabrication time and costs of an entire device, and also facilities iterative design changes during development. Therefore, inkjet printing can be ideal in prototyping as well as in applications requiring heterogeneous integration of different components and materials [6]. Several attempts have been made until now using inkjet printing for the fabrication of printed chemical sensors.

---

* Corresponding author. Instituto de Microelectrónica de Barcelona, IMB-CNM (CSIC), Esfera UAB, Campus Universitat Autònoma de Barcelona, 08193, Bellaterra, Barcelona, Spain.
E-mail address: gemma.gabriel@imb-cnm.csic.es (G. Gabriel).

However, the number of reports about biosensors in flexible devices is still limited. Some of the first inkjet-printed biosensors were reported back in 1992 by Newman et al. [7] demonstrating the usefulness of the inkjet technology by printing a glucose sensor. More recently, other works have been presented, such as those by Jensen et al. [2], providing the viability of detecting a cancer biomarker in serum by printing an array of gold electrodes functionalized with 3-mercaptopropionic acid, or by Khan et al. [8] reporting a flexible gold electrode array to be used as bioelectronic interface. Furthermore, many other publications can be found on electrochemical biosensors [9,10], pH sensors [11,12], ion sensors [13], gas and vapor sensors [1,14–16] and photosensors [17] electromyography biosensors [18]. However, most of the printed sensors reported in the literature have only some of their elements printed while others are still manufactured by traditional lithography-based or related methods.

We recently demonstrated the fabrication of an electrochemical micro-sensor for the measurement of dissolved oxygen (DO) using standard microfabrication techniques [19]. Microfabrication yields highly reproducible and reliable microelectrodes with a sensing response comparable to commercially available dissolved oxygen sensors [20]. However, these standard microfabrication techniques require multiple complex and time consuming processing steps including the application of photoresist, UV-light exposure through chromium masks, etching and deposition of adhesion and electrode materials. The nature and high number of process steps increases the cost per micro-sensor, thus limiting their application as disposable devices.

The aim of this work is to demonstrate the potential of inkjet printing technology as an alternative to standard microfabrication techniques in the area of micro-sensors fabricating on a flexible plastic substrate. Polymeric substrates such as PEN are promising candidates for disposable low-cost sensors. They are flexible, inexpensive, and available in large quantities, facilitating roll-to-roll processing [21]. However, usually they are sensitive towards high temperatures due to their comparable low glass transition temperature. Therefore, all required manufacturing processes have to be performed at low temperatures, preferable much below 200 °C. Although gold is one of the most important electrical conductive materials for a wide range of applications, the processing of the inkjet printing inks is still a challenge due to the high sintering temperatures reported until now. Different strategies have been developed for the drying and sintering process to limit the temperature effect on polymer substrates such as the usage of intense pulsed light [22], laser [23] or infrared technology [24,25]. Since there are rarely Au ink formulations on the market that can be sintered at low temperatures compatible with low Tg polymer substrates, several authors overcome these problems synthesizing their low-curing inks [2,26,27]. However the stability and reproducibility of these custom-made inks is still limited [28,29]. Furthermore, the synthesis of these inks is difficult, and not always in the field of expertise of research groups that are focused on the final application. Nowadays, ink materials are the most important drawback that limits inkjet printing technology to be widely used. This especially affects to novel materials such as gold and platinum. However, silver nanoparticle inks are state-of-the-art. There is currently a large variety of silver nanoparticle inks for different applications commercially available [30].

We aim to develop an all-inkjet-printed sensor using stable and commercially available inks that can be processed and sintered at low temperature (120 °C). These inks allow the usage of flexible Polyethylene Naphthalate (PEN) substrate and are commercial and reliable in terms of stability. The inks are used to develop a fully inkjet-printed oxygen amperometric sensor using different metal nanoparticle inks and a dielectric ink formulation (gold for the counter (CE) and working electrode (WE); silver for the pseudoreference electrode (pRE), and the dielectric SU8 as passivation). Our proposed manufacturing strategy is very attractive due to its simplicity and rapidity, and the good performance of the microelectrodes through their lifetime. Taking advantage of the low-cost provided by inkjet printing, these electrochemical platforms presented here potentially enable novel devices in a broad range of applications such as analytical sensors, biosensing and medical applications.

2. Material and methods

2.1. Materials and chemicals

For the development of the DO sensor we used three commercially available inks. A low-curing gold nanoparticle ink (Au-LT-20 from Fraunhofer IKTS, Germany) was employed for the WE and CE development. A silver nanoparticle ink (DGP-40LT-15C from ANP, Korea) was used for the development of the pRE electrode. The passivation of the electrodes was done using the SU8 ink (2002 from MicroChem, USA). The inks show drop-on-demand (DoD) inkjet compatible specifications presented in Table S1 (Supplementary Information). Teonex Polyethylene Naphthalate PEN films (Q65HA DuPont Teijin Films) with a thickness of 125 μm and a surface pre-treatment for improved adhesion was selected as substrate.

Ethanol (LC/MS grade), sodium nitrate (KNO_3), potassium hexacyanoferrate(III) ($K_3[Fe(CN)_6]$) and Potassium hexacyanoferrate(II) trihydrate ($K_4[Fe(CN)_6]$) (all from Sigma Aldrich, Spain) were used for surface cleaning, activation and characterization of the printed sensor. Hydrochloric acid (0.1 M) was electrochemically applied for the chlorination of the printed silver layers, and potassium chloride (KCl) for testing the open circuit potential of the pRE (both from Sigma Aldrich, Spain).

2.2. Instrumentation

A piezoelectric Dimatix Material Printer (DMP 2831 from FUJIFILM-Dimatix, Inc., USA) was employed for the inkjet printing of the three inks on the PEN substrate. The printer was equipped with user fillable 10 pL nominal drop volume printheads having 16 nozzles each with a diameter of 21.5 μm. Printing patterns were made using Electronic Design Automation (EDA) layout software and imported with the Dimatix Bitmap editor software. The substrate vacuum plate is temperature controllable. The printing processes were carried out in a standard laboratory environment in ambient condition, without non-particulate filtered enclosure systems and without control of temperature or humidity to determine the extent to which the sensor devices could be manufactured on an industrial-scale printing system.

Scanning Electron Microscopy (SEM, Auriga-40 from Carl Zeiss) was used to study the morphology of each printed layer. An Atomic Force Microscope (AFM, Nanoscope IV controller and Dimension 3100 head from Veeco) was employed to analyze the topography of the printed layers and a profilometer Dektak 150 (Veeco) was used for the thickness measurement of the layers. The sheet resistance of each conductive layer was determined with a Hewlett Packard HP4155 Semiconductor Parameter Analyzer connected to a manual probe station PM5 (Süss Microtec Gmbh). The contact angle measurement system MobileDrop GH11 (Krüss Gmbh) was used to investigate the surface energy of the substrate.

The electrochemical characterization and calibration of the sensors was performed with an 8-channel potentiostat 1030A Electrochemical Analyzer (CH Instruments, USA). Control experiments were performed using a commercial Ag/AgCl (3 M KCl)

electrode as RE and a platinum ring electrode as CE, both from (Metrohm, Germany). Printed sensors were calibrated in a controlled dissolved oxygen solution against an OXI 325 (WTW, Germany) oxygen probe.

2.3. Inkjet-printing process

The DO sensors were inkjet-printed on PEN substrates. The PEN film was placed on the stage of the DMP 2831 printer and heated up to a temperature of 40 °C. Three individual ink cartridges were filled with about 1 ml of the different ink formulations (gold, silver and SU8). The drop ejection behaviour of the inkjet nozzle was visually checked using the integrated drop-watcher camera to ensure reliable process conditions. The relative distribution of deposited material across the printer geometry was controlled by adjusting parameters such as the printhead nozzle temperature, the jetting frequency, the jetting waveform and the maximum voltage applied to the printhead nozzles. These parameters have been optimized for each ink. Images of the drop ejection of each ink and the corresponding waveforms are given in Fig. S1 and Table S2 (Supplementary Information). The three elements of the sensor were printed using; the gold ink for the development of the WE and CE and the silver ink for the RE. Post-processing of the deposited conductive inks was done in a hot-plate. After the printing of the metallic materials, the cartridge filled with SU8 polymeric ink was insert in the printer and used passivate the tracks. The curing of the SU8 was done by UV treatment for 15 s. After all the printing steps, the printed silver electrode was chlorinated by cyclic voltammetry in 0.1 M HCl, scanning the potential from 0 V to 0.2 V versus Ag/AgCl commercial reference electrode at 20 mV s^{-1} to obtain a stable Ag/AgCl pseudo-reference electrode (pRE) [31].

2.4. Characterization and calibration of DO sensor

The gold WE of the DO sensors require activation before use. For that, several gold-cleaning methods were investigated [32]. Among them, we chose the application of a suitable potential waveform to clean the inkjet-printed electrodes. In particular, five pulses alternating between - 2 V and 0 V for 10 s in a KNO$_3$ electrolyte solution were performed. Subsequently, in order to verify the optimal activation response, cyclic voltammetry measurements in ferro/ferricyanide (10 mM) at different scan rates were carried out. Finally, sensors were calibrated in the oxygen concentration range between 0 and 8 mg L^{-1} DO range according to Wolff and Mottola [33]. The sensor was polarized at −800 mV vs. Ag/AgCl (3 M KCl). The DO concentration was adjusted bubbling different nitrogen (O$_2$ free) - air (21% O$_2$) mixtures through a 0.1 M KNO$_3$ solution, and a magnetic stirrer was used to ensure better mixing of the solution. The concentration of DO in the cell was measured with a commercial (OXI-325) DO probe and correlated with the measured polarization.

3. Results and discussion

3.1. All-inkjet-printed sensor fabrication

The surface energy of the PEN substrate was measured to evaluate its suitability for the different ink formulations. The surface energy was determined to be about 38 mN m^{-1} with a high disperse part of about 34 mN m^{-1} and a polar part of only about 4 mN m^{-1} using the Owens, Wendt, Rabel, and Kaelble method. This indicates difficult wetting of water-based ink formulations on the substrate [34]. Further information about the measurement is found in Fig. S2 (Supplementary Information). The procedure for the manufacturing of the DO sensor is illustrated in Fig. 1. The first step is the printing of the gold nanoparticle ink for the

development of the WE and the CE (Fig. 1a). The gold ink was printed using a drop spacing (DS) of 15 μm representing a print resolution of 1693 dpi (dots per inch). The DS represents the center-to-center distance between the printed droplets and 15 μm was found to be the optimum compromise between low line width (small feature size of the sensor device) and stable, continuous line formation without interruptions resulting in open electrical contacts. The selection of the DS for each ink is discussed in Section 3.2.1. After the deposition process, the gold ink cartridge was replaced by another cartridge containing the silver nanoparticle ink to print the pRE (Fig. 1b). The DS for the printing of the silver ink was changed to 40 μm (635 dpi). Then, both printed inks were thermally dried and sintered. The temperature processing of the inks can be understood as two consecutive steps: First, drying of the layer is initiated expelling all solvent and decomposing polymeric stabilizing agents of the nanoparticles and second, a sintering process takes place fusing the nanoparticles. The printed structures were dried for 5 min at 100 °C in order to evaporate the solvent of the ink (Fig. 1c.1), followed by sintering at 150 °C for 30 min. This ensured the electrical conductivity of the layer (Fig. 1c.2). This two-step procedure is particularly critical in the case of the gold ink. If the wet gold ink is cured directly at 150 °C, intense crack formation appears along the layer, reducing significantly its conductivity. These cracks can be avoided with the described two-step curing methodology. Fig. 2 shows some SEM images as examples of samples with two steps curing and with just one. The problem of crack formation did not occur for the silver ink that could be cured directly at 150 °C. In order to precisely define the desired active electrode and pad connections area, a passivation layer is formed by printing the dielectric SU8 (Fig. 1d). The photoresist SU8 has been already previously used as a passivation due to the high chemical resistance, the excellent thermal stability, the low Young's modulus, the low temperature cure and is also optical transparency [35]. SU8 was printed on top of the metallic printed patterns aiming to precisely passivate the tracks. The DS used to print SU8 ink was 15 μm (1693 dpi). The curing of the SU8 was done in two steps, first heated at 100 °C for 5 min for solvent evaporation and afterwards by UV treatment for 15 s to polymerize the layer by cross-linking (Fig. 1e). Then, the printed RE was chlorinated by cyclic voltammetry as shown in Fig. 1f. Potential stability of the pRE was studied against a commercial Ag/AgCl RE for 24 h in a 3 M KCl solution, exhibiting a good stability with a drift rate less than 0.13 mV h^{-1}. The chlorinated process and the stability measured are shown in Fig. S3 in the Supplementary Information. Fig. 1g shows a picture of three finished platforms with the three all-inkjet-printed microelectrodes (WE, CE and pRE) that conform the final DO sensor platform. In Fig. S4a (Supplementary Information) is presented the pattern layout of the platform where it can be observed that each one incorporate three DO sensors with different diameters of the WE (300 μm, 500 μm and 1000 μm).

Inkjet printing is cost-efficient and environmentally friendly, and enables rapid prototyping due to its additive nature. The connector used in this case is reusable Zero Insertion Force (ZIF) (see Fig. S4b in the Supplementary Information), avoiding other expensive methods such as wire-bonding. Moreover, the costs of the ink materials of the manufactured inkjet-printed sensors are presented in detail in Table S3 in the Supplementary Information.

3.2. Morphology and electrical characterization of inkjet-printed layers

3.2.1. Drop spacing selection
A dedicated test print pattern was developed that allows the deposition of lines with different DS but with a fixed width of 1 px (pixel). Fig. S5 (Supplementary Information) shows the print
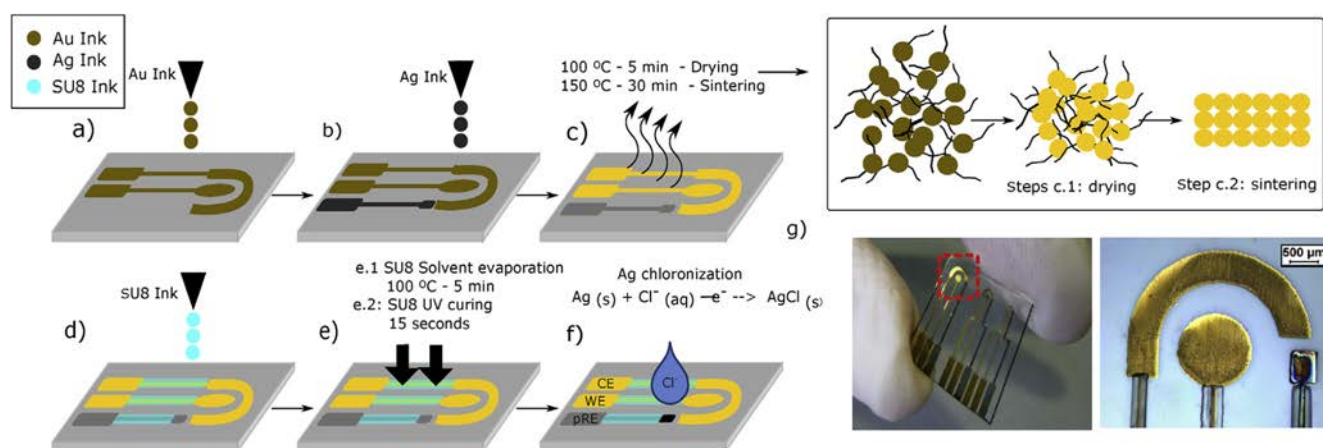
Fig. 1. (a) Inkjet printing of gold CE and WE, (b) inkjet printing of silver pRE, (c) thermal sintering of Au and Ag layers, (d) inkjet printing of passivation layer SU8, (e) curing of SU8 at 100 °C for 5 min and UV cross-linking for 15 s, (f) Chlorinated pRE, (g) resulted printed platform with 3 DO sensors with different WE diameters (300 μm, 500 μm and 1000 μm) and microscope image of the biggest printed electrodes.
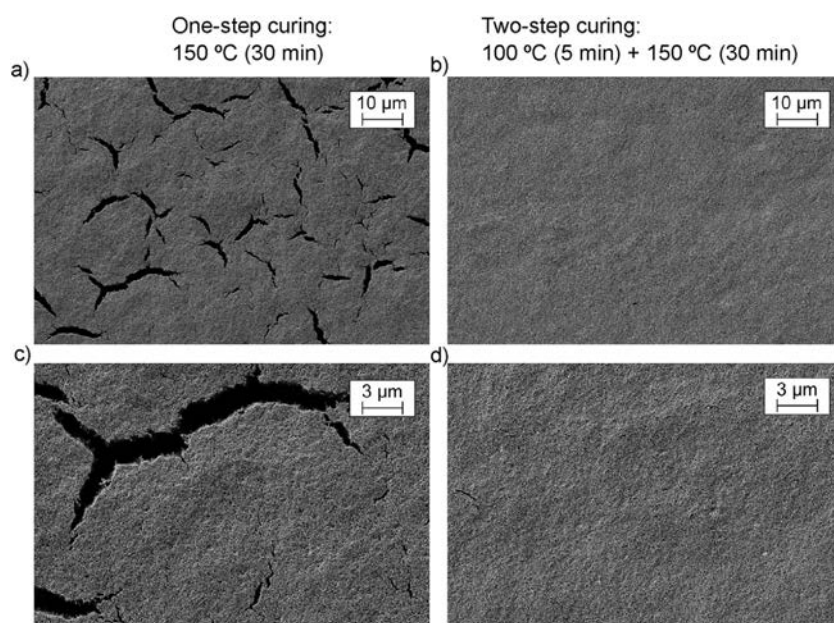

Fig. 2. SEM images of printed gold layer with, a) a curing done in one step at 150 °C, causing intense crack formation, and b) curing done in two steps, avoiding the crack formation, c) and d) are magnified images of a) and b).

pattern as well as the resulting line pattern for each used inks. These print patterns were deposited with a printer platen temperature of 40 °C. Fig. 3a shows the resulting width of each printed continuous line formation and its deviation for the three used inks. The DS was selected taking into account the width and the thickness that we aimed to obtain for our sensor design with a continuous line formation. The line morphology strongly depends on the diameter of a single printed drop. The surface tension of the ink and the wettability of the surface play a key role in determining the final diameter of the deposited droplet. All the tests were done with the same printing setup (10 pL printhead and PEN substrate heated up 40 °C) allowing to compare the deposits of the different inks. For the gold ink, the single drop diameter was determined to about 40 ± 2 μm. A DS of 15 μm was selected for the line pattern which results in a line width of about 78.5 ± 7.9 μm and a thickness of approximately 238 ± 20 nm. In comparison, the single drop

diameter of the silver ink was about 55 ± 1 μm and the line width and line height at a DS of 40 μm were determined to 53.1 ± 7.8 μm and 233 ± 35 nm, respectively. For the SU8 ink, the obtained single drop diameter was 46 ± 2 μm. At a DS of 15 μm, a line width of 69.0 ± 10 μm was obtained. The thickness of the line for the selected DS is about 1.8 ± 0.05 μm. Thus, the SU8 layer is about nine times higher than the electrode layers due to the low amount of solvent in the ink formulation.

3.2.2. Plastic compatible low-temperature sintering

Our efforts have focused on determining the optimal printing and post-processing conditions to form a highly conductive layer with low sintering temperature and in a short time. Electrical characterization of the printed patterns for different sintering conditions was done using various van der Pauw [36] patterns. Each van der Pauw pattern was sintered at different temperatures and
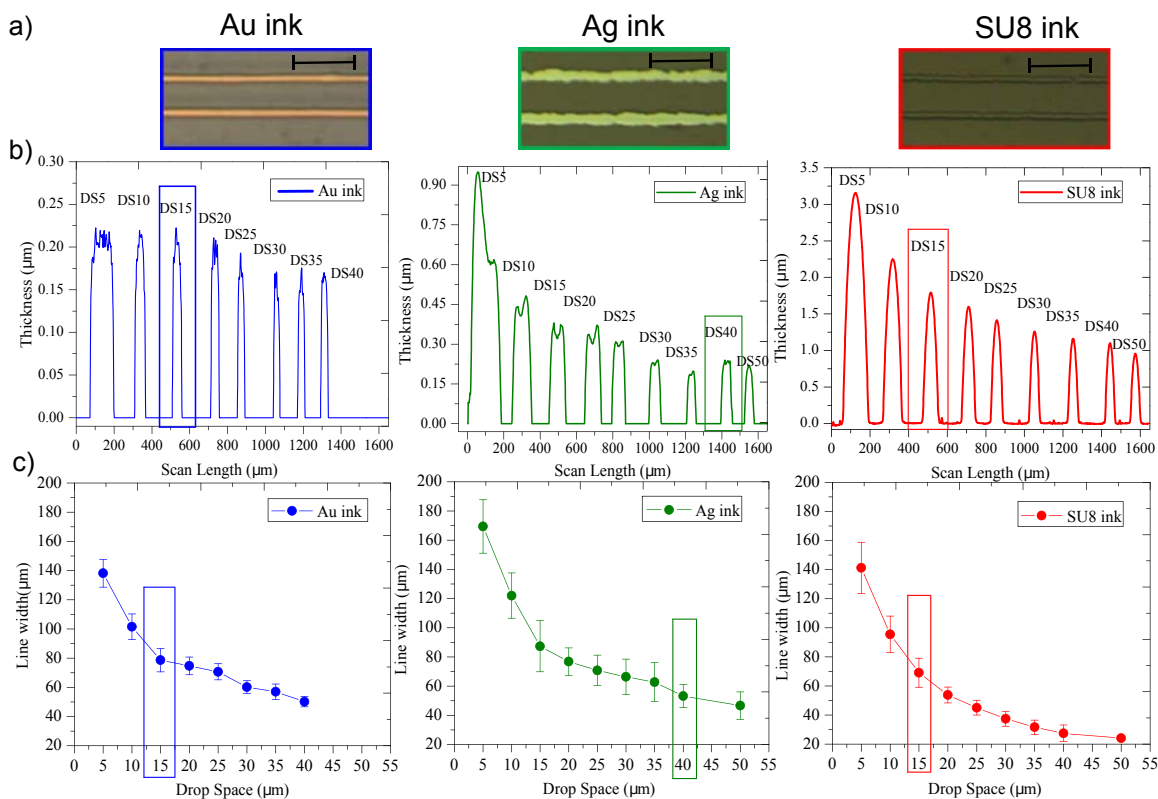
Fig. 3. a) Printed lines one PEN substrate at different drop spacing for gold, silver and SU8 inks (scale 500 µm), b) thickness printed lines at different DS, and c) line width at different drop spacing for the gold, silver and SU8 ink.

times. Fig. 4 shows the measured sheet resistance versus the curing temperatures for the gold and silver inks used in this work. The conductivity of the layers was calculated measuring their thickness by a profilometer. Starting at 120 °C both inks show already reasonable good conductivities. Finally, a sintering temperature of 150 °C for 30 min was selected for the conductive layers of the DO sensor since we obtained similar conductivities compared with higher temperature and long times of sintering. The resulting sheet resistances were about $0.55 \pm 0.11\ \Omega/\square$ for gold and $0.31 \pm 0.05\ \Omega/\square$ for silver ink. The PEN substrate supported this temperatures and times without any deformation [8]. Taking into account the measured thickness of each layer, the conductivity was calculated to about $7.64 \cdot 10^6\ \mathrm{S\ m}^{-1}$ for the gold ink and $1.38 \cdot 10^7\ \mathrm{S}^{-1}\ \mathrm{m}^{-1}$ for the silver ink. These values correspond to approximately 18% and

22% conductivity of the conductivity of bulk gold and bulk silver.

3.2.3. Morphology and topography

The morphology and topography of the printed layers were also studied. Fig. 5 left shows the SEM images of the inkjet-printed gold and silver ink before and after the sintering process onto the PEN substrate. The removal of surfactants from the surface of the nanoparticles plays a significant role in enhancing conductivity of the printed films [37]. These images demonstrate that after the curing process, the particles are agglomerated and a continuous conductive network is formed. For the gold ink, changes in particle morphology before and after the sintering process are hard to notice. This is because the gold particles, having a size of about 40 nm, neither melt nor deform at our working temperature of
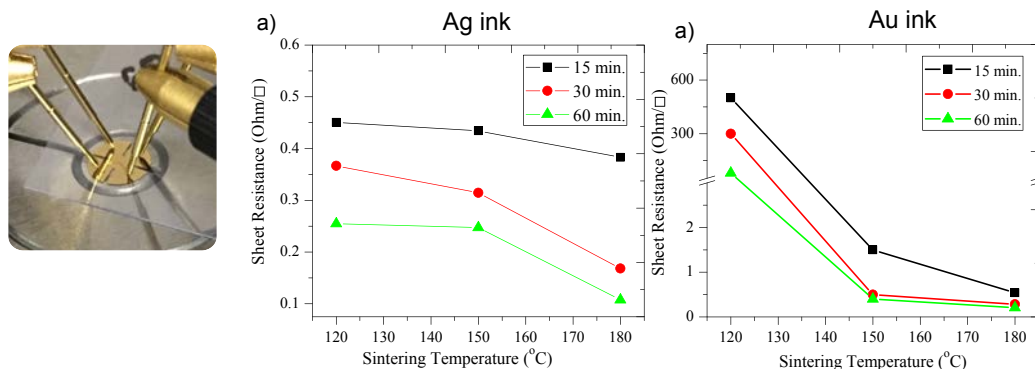
Fig. 4. Sheet resistance measurement for different sintering temperatures and times, a) for the gold ink, and b) for the silver ink.
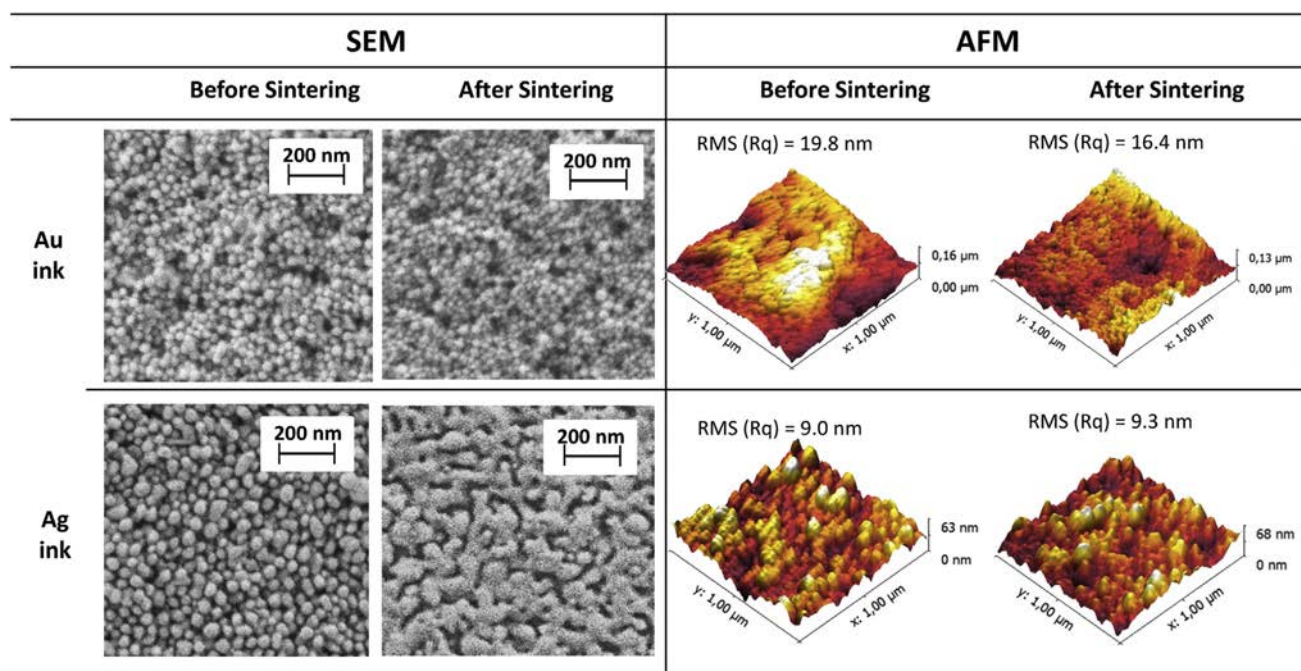
Fig. 5. Morphology of the printed and sintered layers. Left: SEM images of gold and silver ink before and after sintering process (150 °C for 30 min). Right: AFM images of gold and silver ink before and after sintering process.

150 °C [29]. For the silver ink, there was a clearly agglomeration of the nanoparticles at 150 °C forming larger structures. In addition, AFM topographical images indicate that the roughness of the gold layer is slightly higher than the silver layer (Fig. 5 right). The root-mean-square (RMS) roughness of the gold electrode surface was about 16 nm and of the silver layer about 9 nm. Before the sintering the images show how the particles are not well resolved due to the presence of surfactant and stabilizers of the ink formulation.

### 3.3. Electrochemical response of gold inkjet printing DO sensor

Cyclic voltammetry (CV) is a commonly used technique for comparing and studying the behaviour of the electrodes. The electrochemical reversible ferri(III)/ferro(II)-cyanide redox couple $[Fe(CN)_6]^{3-} + e^- \leftrightarrow [Fe(CN)_6]^{4-}$ was chosen as a model analyte for the CV experiments carried out. Fig. 6a shows the CV of the redox couple obtained by measuring the current at the WE before and after its activation. As can be seen in Fig. 6a, the optimized electrochemical activation is very important to ensure a good performance of the electrodes. The characterization and calibration of the sensor was done using the set-up described in Fig. S6 (Supplementary Information). In a first step, an external configuration of commercial CE and RE was used in order to compare the behaviour of the printed gold WE employing external electrodes and, in a second step, it was repeated using the printed CE and pRE. The CVs shown in Fig. 6b demonstrate the good performance of the sensor using the three printed electrodes. There were no differences between using the commercial CE or the printed CE. The small shift of the potential observed with the use of the integrated pRE is attributed to the difference of chloride concentration in contact with the surface of the electrode (pRE, 0.1 M versus 3 M KCl in the internal solution of the commercial reference). In the same way, the behaviour of the different dimensions of WE were tested. Fig. 6c shows the CV in ferro(II)/ferri(III)-cyanide obtained for three different dimension of WE. The anodic/cathodic peak current values (I_p) are directly proportional to the WE area as shown in the

theoretically Randles-Sĕvčik equation. To determine if the electrodes are working properly we compared the obtained I_p with the theory, using Randles-Sĕvčik's equation [38].

$$I_p = 0.4463 \cdot \left(\frac{F^3}{RT} \right)^{1/2} \cdot n^{3/2} \cdot A \cdot D^{1/2} \cdot R_0 \cdot v^{1/2} \tag{1}$$

where n is the number of electrons participating in the redox process, F is the Faraday Constant [C·mol^{-1}], A is the electrochemically active electrode area [m^2], R_0 is the initial concentration of analyte [mol·m^{-3}], D is the diffusion coefficient [m^2·s^{-1}], v is the scan rate [V·s^{-1}], R is the gas constant [J·K^{-1}·mol^{-1}] and T is the temperature [K].

The printed electrodes have heterogeneous behaviour onto the plastic substrate causing different electrochemical properties of the electrodes. Other parameter of interest for the characterization of the electrodes is the peak-to-peak separation (ΔE_p) over a range of scan-rates. The reduction of ferri(III) to ferro(II)cyanide is a one electron process for which, under fast electrode kinetics, a ΔE_p of 59 mV at room temperature is anticipated [39]. Our printed electrodes display a ΔE_p around 100 mV up to scan rates of 100 mV s^{-1}. There is a number of possible reasons that may increase the peak separation larger than the theoretical 59 mV, most probably small holes, cracks, wettability of the electrodes and organic contamination still remaining after the drying and sintering process [40]. Fig. 6d shows that the peak current increases linearly as a function of the square root of the scan rate (until 100 mV s^{-1}) as is typical for a diffusion-controlled process. For scan rates higher than 100 mV s^{-1} (Fig. 6e) the peak separation increases. This is due to quasi-reversible kinetics of the electron transfer at the printed electrode. The value of the electron transfer rate constant was calculated using the approach described by Matsuda and Ayabe [41], using the following relation to describe heterogeneous charge transfer:
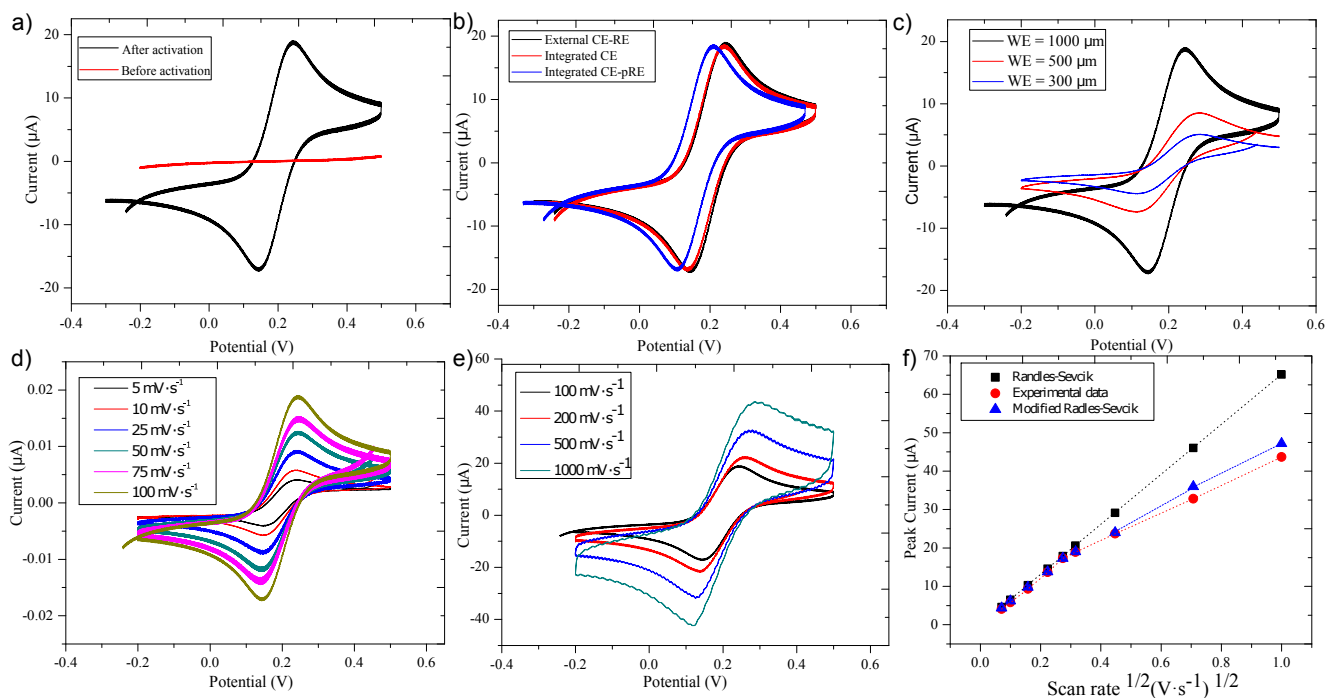
Fig. 6. Cyclic voltammetry of $K_3Fe(CN)_6$/$K_4Fe(CN)_6$ redox couple in 0.1 M KNO_3, a) before and after the activation of the electrodes, b) using external commercial RE and CE configuration versus integrated printed electrodes, c) with different diameters of WE, d) varying scan rate until 100 mV s^{-1}, e) varying scan rate from 100 mV s^{-1} to 1 V s^{-1} f) correlation of the theoretical versus experimental current peak in function of square root of the scan rate using the Standard Randles- Sěvčik equation and compared with the modified Randles- Sěvčik equation.

$$\wedge = k_s \cdot (n \cdot F \cdot v \cdot D / R \cdot T)^{-1/2} \qquad (2)$$

at $\wedge = 1$, which occurs at the scan rate at which $\varDelta E_p$ begins to depart from ideality. In equation (2), k_s is the electron transfer rate constant (m·s^{-1}), and the rest of parameters are the same involved in equation (1). Fig. S7 in the Supplementary Information shows the determination of k_s. In our sensor this occurs at scan rate of 100 mV s^{-1} where it can be calculated the $k_s = 6.4 \cdot 10^{-5}$ m s^{-1}. For $k_s > 2 \cdot 10^{-4}$ m s^{-1} the system can be considered electrochemically reversible, for k_s between $2 \cdot 10^{-4}$ and $5 \cdot 10^{-5}$ m s^{-1} the system can be considered quasi-reversible and for $k_s < 5 \cdot 10^{-5}$ m s^{-1} the system will be irreversible. Our system may be considered quasi-reversible up to a scan rate of 200 mV s^{-1} allowing to perform the analytical measurements of the sensors. Table S4 in the Supplementary Information presents the calculation of $\wedge$, k_s and I_p for scan rates from 5 mV s^{-1} until 1 V s^{-1}. In this case, a modified Randles-Sěvčik equation [42] was applied to correlate the experimental I_p with theoretical equations as shown in Fig. 6f. Finally, the sensors were calibrated. The oxygen reduction amperometric signal is affected by medium composition and also by the electrocatalytic properties of the printed electrodes, which can be improved thorough the activation procedures. The sensor was polarized at −800 mV as the optimal potential value for the determination of the DO concentration (Fig. S8 in Supplementary Information). The linearity and sensitivity of the electrochemical response of the inkjet-printed DO sensors were verified in the calibration medium (0.1 M KNO_3) by bubbling a series nitrogen/air gas mixtures. In a first stage, the response of the sensor was measured using external RE and CE. Following this, the measurements were repeated using the inkjet-printed CE and the pRE. Fig. 7 summarizes the reduction currents measured at the WE under different DO concentrations with both configuration of electrodes and the three dimensions of WE
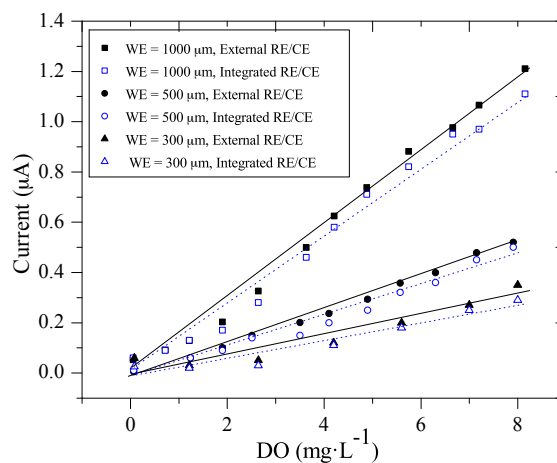
Fig. 7. Calibration curve of the printed DO sensor for three dimensions of WE, using external configuration of electrodes versus the integrated printed electrodes.

(1000 μm, 500 μm and 300 μm). The sensors display excellent linearity between 0 and 8 mg L^{-1} range, with correlation factors greater than 0.99 using the external of CE and RE and greater than 0.97 using the internal configuration, demonstrating that the DO sensor is suitable for the determination of DO. A total of twelve platforms (four for each WE diameter design) were calibrated. The sensors with a WE diameter of 1000 μm have a sensitivity of 0.14 ± 0.01 μA L mg^{-1} using the external commercial electrodes and 0.12 ± 0.01 μA L mg^{-1} using the integrated printed electrodes, demonstrating a satisfying response. The limits of determination and quantification for these sensors were 0.23 and 0.72 mg L^{-1}, respectively. For the sensors with a WE diameter of 500 μm, the

obtained sensitivity was 0.066 ± 0.005 µA L mg^{-1} and 0.048 ± 0.008 µA L mg^{-1} using external and integrated electrodes configuration, respectively, showing a suitable performance. Its limits of determination and quantification were 0.17 and 0.58 mg L^{-1}, respectively. For the smaller WE diameter (300 µm) the obtained sensitivity were 0.031 ± 0.009 µA L mg^{-1} and 0.029 ± 0.011 µA L mg^{-1} for the external and the integrated electrodes configuration respectively, with limits of determination and quantification of 0.11 and 0.34 mg L^{-1} respectively. The response time of the sensors was around 30 s for the bigger dimensions electrodes, and approximately 20 s for the other two smaller dimensions. The platform was characterized and calibrate over a period of 6 months, maintaining their performance and functionality always after the activation of the gold and the re-chlorinated of the silver.

4. Conclusions

We demonstrated the manufacturing of a flexible DO sensor based on inkjet printing in ambient conditions without the need for clean room environment. The sensor consists of three different materials that were patterned on a flexible polymer substrate: Gold, silver and SU8. The careful selection of commercial low-curing ink formulations and the optimization of the inkjet printing as well as drying and sintering process allowed the manufacturing of the sensor at low temperature and in short time. Both the low processing temperature and the short processing time are promising parameters towards a novel industrial manufacturing route for low-costs sensors as alternative to traditional lithography-based manufacturing. All this makes the presented manufacturing approach interesting for a wide range of sensor applications. Our proposed manufacturing strategy for DO sensors is very attractive due to its simplicity and rapidity, and the good performance of the microelectrodes through their lifetime. The sensors exhibited an excellent linear response in the range between 0 and 8 mg L^{-1} of DO, obtaining low limits of detection, in detail 0.11 mg L^{-1} and a sensitivity of 0.03 µA L mg^{-1} for the 300 µm WE diameter, which is comparable to sensors manufactured with traditional technologies.

Appendix A. Supplementary data

Supplementary data related to this article can be found at http://dx.doi.org/10.1016/j.orgel.2016.10.002.

References

[1] C. Hu, X. Bai, Y. Wang, W. Jin, X. Zhang, S. Hu, Inkjet printing of nanoporous gold electrode arrays on cellulose membranes for high-sensitive paper-like electrochemical oxygen sensors using ionic liquid electrolytes, Anal. Chem. 84 (2012) 3745–3750, http://dx.doi.org/10.1021/ac3003243.

[2] G.C. Jensen, C.E. Krause, G.A. Sotzing, J.F. Rusling, Inkjet-printed gold nano-particle electrochemical arrays on plastic. Application to immunodetection of a cancer biomarker protein, Phys. Chem. Chem. Phys. PCCP 13 (2011) 4888–4894, http://dx.doi.org/10.1039/c0cp01755h.

[3] N. Komuro, S. Takaki, K. Suzuki, D. Citterio, Inkjet printed (bio)chemical sensing devices, Anal. Bioanal. Chem. 405 (2013) 5785–5805, http://dx.doi.org/10.1007/s00216-013-7013-z.

[4] D.K. Kampouris, R.O. Kadara, N. Jenkinson, C.E. Banks, Screen printed electrochemical platforms for pH sensing, Anal. Methods 1 (2009) 25–28, http://dx.doi.org/10.1039/B9AY00025A.

[5] S. Laschi, I. Palchetti, M. Mascini, Gold-based screen-printed sensor for detection of trace lead, Sens. Actuators B Chem. 114 (2006) 460–465, http://dx.doi.org/10.1016/j.snb.2005.05.028.

[6] S. Khan, L. Lorenzelli, R.S. Dahiya, Technologies for printing sensors and electronics over large flexible substrates: a review, IEEE Sens. J. 15 (2015) 3164–3185, http://dx.doi.org/10.1109/JSEN.2014.2375203.

[7] J.D. Newman, A.P.F. Turner, G. Marrazza, Ink-jet printing for the fabrication of amperometric glucose biosensors, Anal. Chim. Acta 262 (1992) 13–17, http://dx.doi.org/10.1016/0003-2670(92)80002-O.

[8] Y. Khan, F.J. Pavinatto, M.C. Lin, A. Liao, S.L. Swisher, K. Mann, V. Subramanian, M.M. Maharbiz, A.C. Arias, Inkjet-printed flexible gold electrode arrays for bioelectronic interfaces, Adv. Funct. Mater. (2015), http://dx.doi.org/10.1002/adfm.201503316.

[9] A. Lesch, F. Cortés-Salazar, V. Amstutz, P. Tacchini, H.H. Girault, Inkjet printed nanohydrogel coated carbon nanotubes electrodes for matrix independent sensing, Anal. Chem. 87 (2015) 1026–1033, http://dx.doi.org/10.1021/ac503748g.

[10] P. Ihalainen, F. Pettersson, M. Pesonen, T. Viitala, A. Määttänen, Ronald Österbacka, J. Peltonen, An impedimetric study of DNA hybridization on paper-supported inkjet-printed gold electrodes, Nanotechnology 25 (2014) 94009, http://dx.doi.org/10.1088/0957-4484/25/9/094009.

[11] A. Määttänen, U. Vanamo, P. Ihalainen, P. Pulkkinen, H. Tenhu, J. Bobacka, J. Peltonen, A low-cost paper-based inkjet-printed platform for electrochemical analyses, Sens. Actuators B Chem. 177 (2013) 153–162, http://dx.doi.org/10.1016/j.snb.2012.10.113.

[12] E. Song, R.P. Tortorich, T.H. da Costa, J.-W. Choi, Inkjet printing of conductive polymer nanowire network on flexible substrates and its application in chemical sensing, Microelectron. Eng. 145 (2015) 143–148, http://dx.doi.org/10.1016/j.mee.2015.04.004.

[13] K. Crowley, E. O'Malley, A. Morrin, M.R. Smyth, A.J. Killard, An aqueous ammonia sensor based on an inkjet-printed polyaniline nanoparticle-modified electrode, Analyst 133 (2008) 391–399, http://dx.doi.org/10.1039/B716154A.

[14] T. Hibbard, K. Crowley, F. Kelly, F. Ward, J. Holian, A. Watson, A.J. Killard, Point of care monitoring of hemodialysis patients with a breath ammonia measurement device based on printed polyaniline nanoparticle sensors, Anal. Chem. 85 (2013) 12158–12165, http://dx.doi.org/10.1021/ac403472d.

[15] E. Danesh, F. Molina-Lopez, M. Camara, A. Bontempi, A.V. Quintero, D. Teyssieux, L. Thiery, D. Briand, N.F. de Rooij, K.C. Persaud, Development of a new generation of ammonia sensors on printed polymeric hotplates, Anal. Chem. 86 (2014) 8951–8958, http://dx.doi.org/10.1021/ac501908c.

[16] P. Lorwongtragool, E. Sowade, N. Watthanawisuth, R.R. Baumann, T. Kerdcharoen, A novel wearable electronic nose for healthcare based on flexible printed chemical sensor array, Sensors 14 (2014) 19700–19712, http://dx.doi.org/10.3390/s141019700.

[17] L.L. Lavery, G.L. Whiting, A.C. Arias, All ink-jet printed polyfluorene photosensor for high illuminance detection, Org. Electron 12 (2011) 682–685, http://dx.doi.org/10.1016/j.orgel.2011.01.023.

[18] R.G. Scalisi, M. Paleari, A. Favetto, M. Stoppa, P. Ariano, P. Pandolfi, A. Chiolerio, Inkjet printed flexible electrodes for surface electromyography, Org. Electron 18 (2015) 89–94, http://dx.doi.org/10.1016/j.orgel.2014.12.017.

[19] A. Moya, X. Guimerà, F.J. del Campo, E. Prats-Alfonso, A.D. Dorado, M. Baeza, R. Villa, D. Gabriel, X. Gamisans, G. Gabriel, Profiling of oxygen in biofilms using individually addressable disk microelectrodes on a microfabricated needle, Microchim. Acta 182 (2014) 985–993, http://dx.doi.org/10.1007/s00604-014-1405-4.

[20] L.C. Clark, R. Wolf, D. Granger, Z. Taylor, Continuous recording of blood oxygen tensions by polarography, J. Appl. Physiol. 6 (1953) 189–193.

[21] E. Sowade, K.Y. Mitra, E. Ramon, C. Martinez-Domingo, F. Villani, F. Loffredo, H.L. Gomes, R.R. Baumann, Up-scaling of the manufacturing of all-inkjet-printed organic thin-film transistors: device performance and manufacturing yield of transistor arrays, Org. Electron 30 (2016) 237–246, http://dx.doi.org/10.1016/j.orgel.2015.12.018.

[22] H. Kang, E. Sowade, R.R. Baumann, Direct intense pulsed light sintering of inkjet-printed copper oxide layers within six milliseconds, ACS Appl. Mater. Interfaces 6 (2014) 1682–1687, http://dx.doi.org/10.1021/am404581b.

[23] J. Niittynen, E. Sowade, H. Kang, R.R. Baumann, M. Mäntysalo, Comparison of laser and intense pulsed light sintering (IPL) for inkjet-printed copper

nanoparticle layers, Sci. Rep. 5 (2015) 8832, http://dx.doi.org/10.1038/srep08832.

[24] E. Sowade, H. Kang, K.Y. Mitra, O.J. Weiß, J. Weber, R.R. Baumann, Roll-to-roll infrared (IR) drying and sintering of an inkjet-printed silver nanoparticle ink within 1 second, J. Mater. Chem. C 3 (2015) 11815—11826, http://dx.doi.org/10.1039/C5TC02291F.

[25] A. Määttänen, P. Ihalainen, P. Pulkkinen, S. Wang, H. Tenhu, J. Peltonen, Inkjet-printed gold electrodes on paper: characterization and functionalization, ACS Appl. Mater. Interfaces 4 (2012) 955—964, http://dx.doi.org/10.1021/am201609w.

[26] T. Bakhishev, V. Subramanian, Investigation of gold nanoparticle inks for low-temperature lead-free packaging technology, J. Electron. Mater. 38 (2009) 2720, http://dx.doi.org/10.1007/s11664-009-0918-9.

[27] D. Huang, F. Liao, S. Molesa, D. Redinger, V. Subramanian, Plastic-compatible low resistance printable gold nanoparticle conductors for flexible electronics, J. Electrochem. Soc. 150 (2003) G412, http://dx.doi.org/10.1149/1.1582466.

[28] S.-P. Chen, H.-L. Chiu, P.-H. Wang, Y.-C. Liao, Inkjet printed conductive tracks for printed electronics, ECS J. Solid State Sci. Technol. 4 (2015) P3026—P3033, http://dx.doi.org/10.1149/2.0061504jss.

[29] A. Kamyshny, Metal-based inkjet inks for printed electronics, Open Appl. Phys. J. 4 (2011) 19—36, http://dx.doi.org/10.2174/1874183501104010019.

[30] A. Chiolerio, K. Rajan, I. Roppolo, A. Chiappone, S. Bocchini, D. Perrone, Silver nanoparticle ink technology: state of the art, Nanotechnol. Sci. Appl. (2016) 1, http://dx.doi.org/10.2147/NSA.S68080.

[31] X. Jin, J. Lu, P. Liu, H. Tong, The electrochemical formation and reduction of a thick AgCl deposition layer on a silver substrate, J. Electroanal. Chem. 542 (2003) 85—96, http://dx.doi.org/10.1016/S0022-0728(02)01474-2.

[32] L.M. Fischer, M. Tenje, A.R. Heiskanen, N. Masuda, J. Castillo, A. Bentien, J. Émneus, M.H. Jakobsen, A. Boisen, Gold cleaning methods for electrochemical detection applications, Microelectron. Eng. 86 (2009) 1282—1285, http://dx.doi.org/10.1016/j.mee.2008.11.045.

[33] C.M. Wolff, H.A. Mottola, Enzymic substrate determination in closed flow-through systems by sample injection and amperometric monitoring of dissolved oxygen levels, Anal. Chem. 50 (1978) 94—98, http://dx.doi.org/10.1021/ac50023a026.

[34] P.Q.M. Nguyen, L.-P. Yeo, B.-K. Lok, Y.-C. Lam, Patterned surface with controllable wettability for inkjet printing of flexible printed electronics, ACS Appl. Mater. Interfaces 6 (2014) 4011—4016, http://dx.doi.org/10.1021/am4054546.

[35] F.J. del Campo, L. Abad, X. Illa, E. Prats-Alfonso, X. Borrisé, J.M. Cirera, H.-Y. Bai, Y.-C. Tsai, Determination of heterogeneous electron transfer rate constants at interdigitated nanoband electrodes fabricated by an optical mix-and-match process, Sens. Actuators B Chem. 194 (2014) 86—95, http://dx.doi.org/10.1016/j.snb.2013.12.016.

[36] L.J. van der Pauw, A method of measuring specific resistivity and hall effect of discs of arbitrary shape, Philips Res. Rep. 13 (1958) 1—9.

[37] G. Cummins, M.P.Y. Desmulliez, Inkjet printing of conductive materials: a review, Circuit World 38 (2012) 193—213, http://dx.doi.org/10.1108/03056121211280413.

[38] A.J. Bard, L.R. Faulkner, Electrochemical Methods: Fundamentals and Applications, Wiley, New York, 2001.

[39] P.T. Kissinger, W.R. Heineman, Cyclic voltammetry, J. Chem. Educ. 60 (1983) 702, http://dx.doi.org/10.1021/ed060p702.

[40] R.O. Kadara, N. Jenkinson, C.E. Banks, Characterisation of commercially available electrochemical sensing platforms, Sens. Actuators B Chem. 138 (2009) 556—562, http://dx.doi.org/10.1016/j.snb.2009.01.044.

[41] H. Matsuda, Y. Ayabe, Theoretical analysis of polarographic waves. I. Reduction of simple metal ions, Bull. Chem. Soc. Jpn. 28 (1955) 422—428, http://dx.doi.org/10.1246/bcsj.28.422.

[42] F.J. Del Campo, A. Neudeck, R.G. Compton, F. Marken, Low-temperature sonoelectrochemical processes: Part 1. Mass transport and cavitation effects of 20 kHz ultrasound in liquid ammonia, J. Electroanal. Chem. 477 (1999) 71—78, http://dx.doi.org/10.1016/S0022-0728(99)00391-5.

Appendix A. Supplementary data

Ink properties

Table S1. Detailed composition of Au, Ag and SU8 inks according to the manufacturer.

	Au (IKTS)	Ag (ANP)	SU8 (MicroChem)
Viscosity (mPas)	8	10-18	7,5
Surface tension (mN/m)	30 – 35	35-40	30,1
Solid content (wt. %)	20	30-35	29
Particle Size (nm)	30	< 50	-
Vehicle	Water + Ethyleneglycol	Triethylene glycol monomethyl ether	Cyclopentanone
Density (g/cm^3)	1,25	1,45	1,12
Sintering/curing process	> 120ºC	> 120 ºC	UV curing
Shelf life (months)	6	6	12

Parameters of the fabrication process

Different waveforms were developed to fine-tune the drop ejection of the inkjet printheads. Finally, three reliable waveforms were obtained as shown below enabling reliable printing with multiple nozzles and the deposition on defined positions due to a droplet trajectory perpendicular to the nozzle plate (high jet straightness). If multiple nozzles were activated for the printing process, the speed of all the droplets was set similar by variation of the maximum jetting voltage. The Au ink was jetted in form of a spherical regular droplet indicating a comparable high surface tension and low viscosity of the ink. In contrast, the Ag ink as well as the SU8 ink show drops with long fluid tails. However, the tails did not rapture leading to satellite drops. Instead, the tails catch up during the flight and merge with the leading droplet prior to the impact on the substrate. This will ensure high print quality.
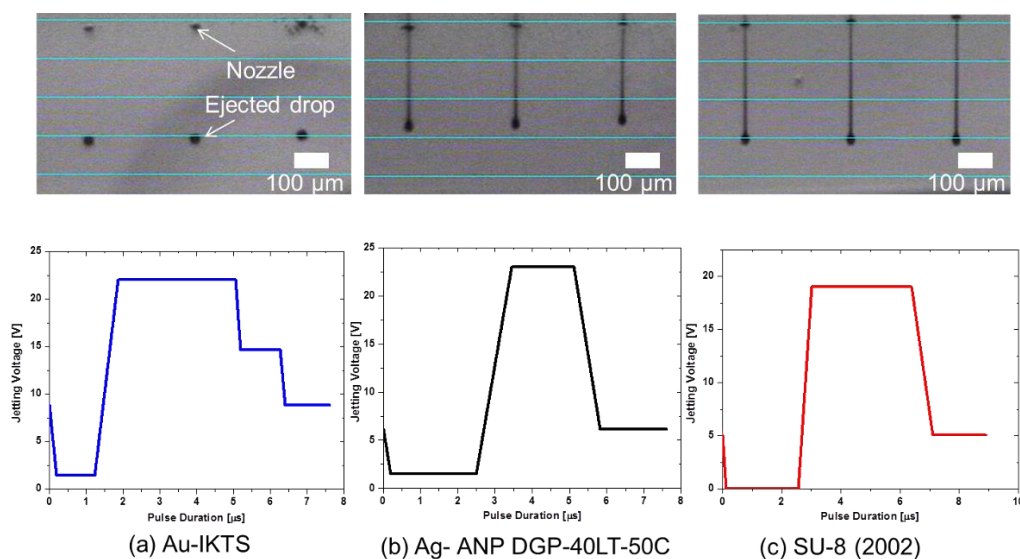
Fig. S1. Dropwatcher images of ejected droplets from the inkjet printhead (upper row) and corresponding waveforms (lower row) applied to the piezoelectric transducer of the printhead for the gold, silver and SU8 ink formulation.
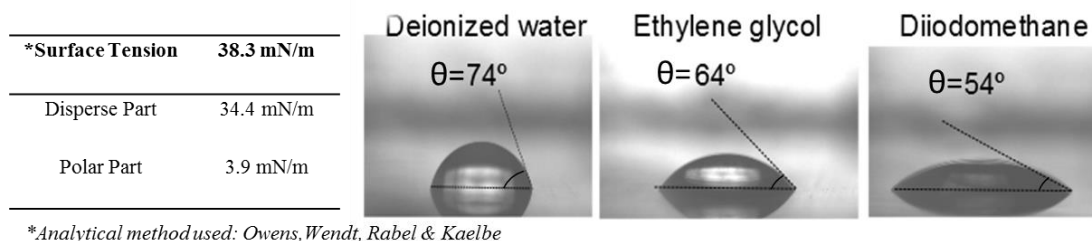
Table S2. Fabrication process parameters for printing gold, silver and SU8 inks for the development of the DO sensor.

Ink	Number of Layers	Print Resolution/ Drop Space	Maximum Jetting Frequency	Maximum Jetting Voltage	Maximum Number of Nozzles	Post treatment
Au-LT-20	1	1693 dpi/ 15 µm	5 kHz	20-22 V	5	100ºC for 5 min + 150 °C for 30 min
Ag ANP-DGP-40LT-50C	1	635 dpi/ 40 µm	5 kHz	20-23 V	16	100ºC for 5 min + 150 °C for 30 min
SU8-2002	1	1693 dpi/ 15 µm	5 kHz	19-20 V	16	100 ºC for 5 min + UV curing for 15 sec

**Surface energy of the PEN substrate**

The spreading of the inks on the substrates depends to a high degree on the surface energy of PEN. Therefore, the surface energy of the PEN substrate was measured with the MobileDrop GH11 system. The liquids tested were deionized water, ethylene glycol and diiodomethane. Ten droplets of each liquid with 2 µL in volume were deposited on the PEN surface. The contact

angle θ of each droplet was measured and the surface energy determined based on the method of Owens, Wendt, Rabel, and Kaelble. The small polar part indicates low affinity to polar solvent such as water. As a consequence, the contact angle of polar solvents will be comparable high as shown below in the case of water.

*Surface Tension	38.3 mN/m
Disperse Part	34.4 mN/m
Polar Part	3.9 mN/m

Analytical method used: Owens, Wendt, Rabel & Kaelbe

Fig. S2. Contact angle measurement and determination of the surface energy of PEN substrates. The volume of the shown droplets is about 2 μL.

Pseudo-reference electrode
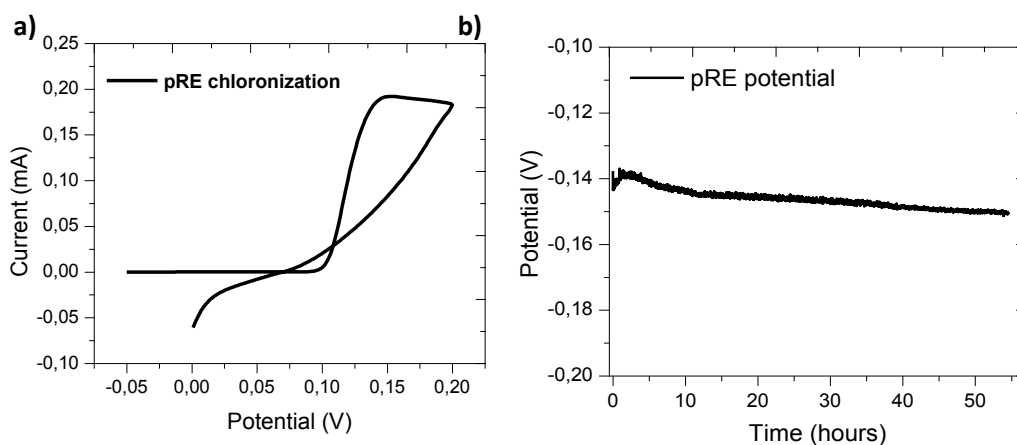
Fig. S3. a) Cyclic voltammetry applied for the chlorinated process of the printed silver, b) Potential stability of the developed pRE over time.
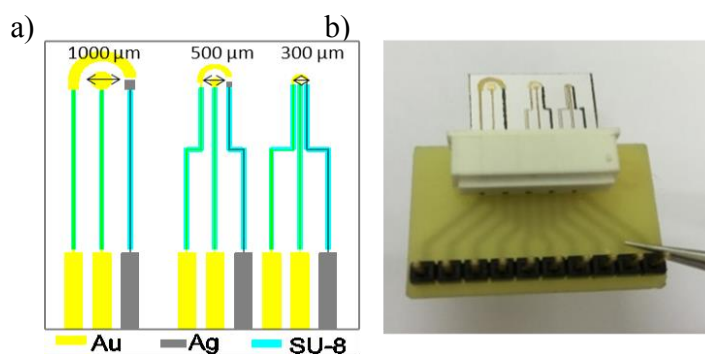
Fig. S4. a) Pattern layout of the designed platform with three sizes of DO sensors, b) printed platform connected with a ZIF connector.

Inkjet-Printed DO sensor: material costs

The materials costs for the inks per sensor size were calculated. The number of deposited droplets was determined and the ink volume approximated assuming a nominal droplet volume of 10 pL. The costs of the inks are according to the standard catalog price without discount. Since we ordered only small quantities, the price per mL is still comparable high. The ordering of higher quantities will result in a reduction of the price per mL. The costs were calculated without taking into account the contact pads. This part can be reduced with the use of another type of connector. Furthermore, other materials could be used such as carbon.

Table S3. Calculation of the material costs per sensor

Ø = 1000 μm	Droplet [#]	Ink Quantity [pL]	Ink Price [€/mL]	Cost [€ cent]
Au	14790	147900	125	1.848
Ag	322	3220	20.01	0.006
SU8	8820	88200	1.38	0.012
			Total Cost	**1.866 € cent**

Ø = 500 μm	Droplets [#]	Ink Quantity [pL]	Ink Price [€/mL]	Cost [€ cent]
Au	5421	54210	125	0.677
Ag	202	2020	20.01	0.004
SU8	9156	91560	1.38	0.012
			Total Cost	**0.693 € cent**

Ø = 300 μm	Droplets [#]	Ink Quantity [pL]	Ink Price [€/mL]	Cost [€ cent]

Au	3841	38410	125	0.480
Ag	124	1240	20.01	0.002
SU8	9156	91560	1.38	0.012
			Total Cost	**0.494 € cent**

Line Pattern test
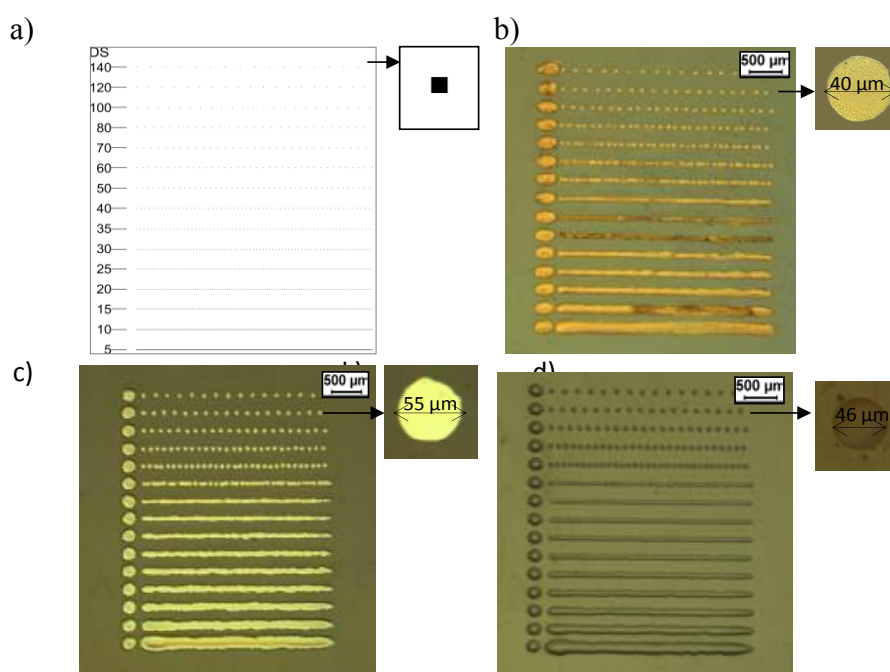
Fig. S5. a) Line formation regimes depending on the drop spacing selected for b) gold ink, c) silver ink and d) SU-8 ink.

Detailed schematic of the calibration set-up

The inkjet-printed sensor was calibrated in the 3-electrode calibration cell, with a commercial RE and CE and the printed platform. A potentiostat was used to apply the voltages and to measure the currents during sensor calibration. The DO concentration inside the calibration cell was adjusted by bubbling a gas mixture O2/N2 and measured by a commercial DO sensor.
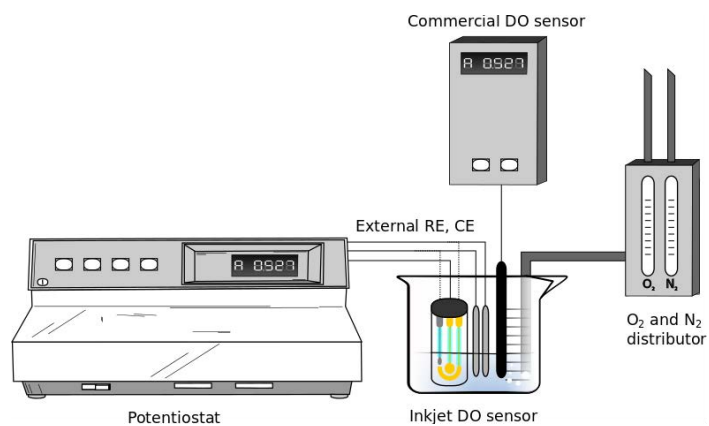
Fig. S6. Schematic of the set-up for the characterization and calibration of the DO sensor

Electrochemical response of the printed gold electrodes
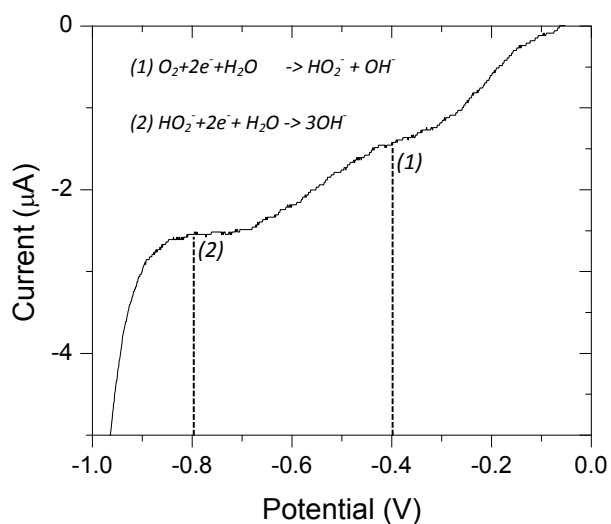
Figure S7. First (1) and second (2) reduction peaks observed in linear sweep voltammograms made in an oxygen saturated saline solution (8 mg·L^{-1}).

Fig. S8. Peak to peak separtion of the Cyclic voltammetry $K_3Fe(CN)_6$/$K_4Fe(CN)_6$ redox couple in 0.1 M KNO_3, versus the logarithmic of the scan rate, that shows when the heterogeneous charge transfer Λ=1.

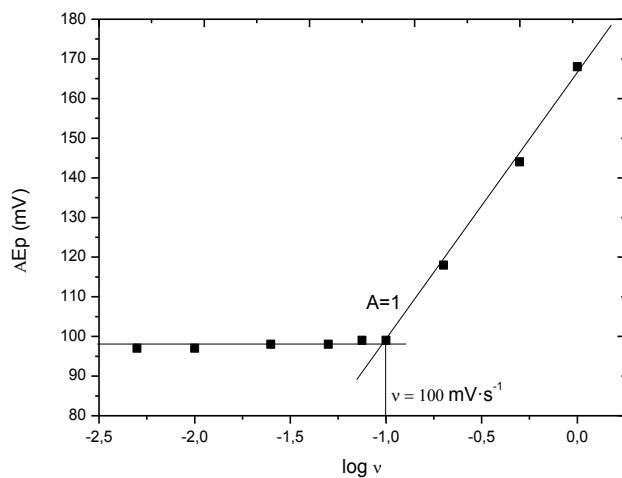**Table S4.** Current peak, heterogeneous charge transfer and electron transfer rate constant calculation form ΔEp for different scan rates.

Scan rate [$V \cdot s^{-1}$]	ΔEp [V]	Ip[A]	Λ	Ks [$m \cdot s^{-1}$]
0.005	0.097	$4,4 \cdot 10^{-6}$	1.17	$7.5 \cdot 10^{-5}$
0.010	0.097	$6.2 \cdot 10^{-6}$	1.17	$7.5 \cdot 10^{-5}$
0.025	0.098	$9,8 \cdot 10^{-6}$	1.14	$7.3 \cdot 10^{-5}$
0.050	0.100	$1.4 \cdot 10^{-5}$	1.08	$6.9 \cdot 10^{-5}$
0.075	0.101	$1.7 \cdot 10^{-5}$	1.05	$6.7 \cdot 10^{-5}$
0.100	**0.103**	**$1.9 \cdot 10^{-5}$**	**1.00**	**$6.4 \cdot 10^{-5}$**
0.200	0.118	$2.7 \cdot 10^{-5}$	0.73	$4.7 \cdot 10^{-5}$
0.500	0.144	$3.6 \cdot 10^{-5}$	0.47	$3.0 \cdot 10^{-5}$
1.000	0.168	$4.7 \cdot 10^{-5}$	0.34	$2.2 \cdot 10^{-5}$

4.4.2 Paper V: Real-time oxygen monitoring inside an organ-on-chip device using integrated inkjet-printed sensors

The fifth paper presented in this Chapter, **Paper V**, is a published article about the integration of DO sensors, fabricated fully by IJP in a cell culture membrane of an OOC. For the first time, the integration of oxygen sensors inside an OOC system to achieve *in-situ* and real-time monitoring of oxygen zonation along the cell culture microfluidic chamber. Inkjet-printed technology is selected for the fabrication of the sensors in order to allow the integration of the sensors in a delicate porous membrane and to achieve a cost effective sensing platform.

This article has been send to Lab-on-Chip journal and currently is under review*:
A. Moya, M. Ortega-Ribera, E. Sowade, M. Zea, X. Illa, E. Ramon, R. Villa, R. R. Baumann, J. Gracia-Sancho, G. Gabriel. **Real-time oxygen monitoring inside an organ-on-chip device using integrated inkjet-printed sensor.**

The development of this work has given rise to other publications:

- Martí Ortega-Ribera; Anabel Fernández-Iglesias; Xavi Illa; Ana Moya; Victor Molina; Constantino Fondevila; Carmen Peralta; Rosa Villa; Jordi Gracia-Sancho. *Maintenance of hepatocyte-differentiated phenotype requires paracrine support from functional sinusoidal endothelial cells.* This article has been SUBMITTED to Hepatology Journal.

Note that sections, equations and references numbering in the reproduced research article follow the ones of the published version.

Lab on a Chip

PAPER

ROYAL SOCIETY
OF CHEMISTRY

Real-time oxygen monitoring inside an organ-on-a-chip device using integrated inkjet-printed sensors

A. Moya,[a,e] M. Ortega-Ribera,[b] E. Sowade,[c] M. Zea,[a,e] X. Illa,[a,e] E. Ramon,[a] R. Villa,[a,e] R. R. Baumann,[c,d] J. Gracia-Sancho,[b,f] G. Gabriel[a,e]

The demand for real-time monitoring of cell functions and cell conditions, e.g. their response to drugs or other stimulation, has dramatically increased with the emergence of Organ-on-a-Chip (OOC) systems allowing the simulation of *in-vivo* conditions for cell cultures. In this work, we present a novel approach to integrate sensors in OOC systems based on the digital material deposition technology inkjet printing (IJP). Electrochemical dissolved oxygen (DO) sensors were inkjet-printed on a porous and flexible cell culture membrane in order to monitor in real-time the oxygen consumption of cells. The cell culture membrane was applied as a printing substrate. Conductive and dielectric materials were deposited by IJP in a non-contact manner on the delicate membrane aiming to build up the sensor device. The manufacturing process does not require any masks and is carried out at low temperatures. In order to allow the deposition of uniform gold and silver layers on the membrane, a primer layer using the dielectric material SU-8 was used to seal the porosity of the membrane at defined areas. Three DO sensors have been printed and integrated on the cell culture membrane to monitor the oxygen zonation along the microfluidic channel. The printed sensors have a linear response in the range of about 0 mg·L^{-1} to 9 mg·L^{-1} of DO and a limit of detection of 0.11 mg·L^{-1} was obtained. As a proof-of-concept, experiments with cell cultures of human and rat hepatocytes were performed in a previously described bioreactor. The oxygen consumption was stimulated with carbonyl-cyanide-4-(trifluoromethoxy)phenylhydrazone (FCCP) from about 7 mg·L^{-1} to 2 mg·L^{-1}. The experimental results show that the proposed manufacturing approach based on IJP has tremendous potential in the field of OOC systems with real-time monitoring capabilities.

Introduction

The field of cell biology is complex and represents a challenge in itself. Over the past two decades, multidisciplinary efforts in cell biology and bioengineering have led to highly functional *in-vitro* culture platforms enabling the depiction of micro-environmental signals.[1] The purpose of the *in-vitro* culture platforms is the reproduction of the reality with the highest possible attention to detail in order to mimic human (or any other animal species) pathophysiology. Therefore, cell biology systems are moving from the conventional *in-vitro* models[2] to more complex systems aiming to capture the critical features of the cellular microenvironments and thus solving the discrepancies to the reality.[3] Based on this context, the concept of 'Organ-on-a-Chip' (OOC) emerged.[4,5] Micro-engineering strategies such as microfabrication and microfluidic technologies provides a number of unique advantages and benefits in studying organ biology.[6] An OOC system consists of a microfluidic cell culture device that contains continuously perfused chambers inhabited by living cells arranged to simulate tissue- and organ-level physiology.[7,8]

These miniaturized organ models have several advantages over conventional models, such as more accurate prediction of human responses, since they are able to capture the structural, mechanical, chemical, and communicative complexities on *in-vivo* systems.[3] For this reason, OOC systems try to replace animal tests since the process of testing drugs with animals often fails to predict human pathophysiology.[9,10]

Besides the development of micro-physiological environments of human tissue or organ recapitulating *in-vivo* structure and function, the capability to monitor its condition and to analyse its response to drugs or other stimulation in real-time is of utmost importance. On one hand, the precise control over physical cell culture parameters such as temperature, pH-value and levels of oxygen and humidity are required.[9] One the other hand, the application of these *in-vitro*

a. Instituto de Microelectrónica de Barcelona, IMB-CNM (CSIC), Esfera UAB, Campus Universitat Autònoma de Barcelona, 08193 Bellaterra, Barcelona, Spain.
b. Liver Vascular Biology Research Group, Barcelona Hepatic Hemodynamic Laboratory, IDIBAPS Biomedical Research Institute, Barcelona, Spain.
c. Technische Universität Chemnitz, Digital Printing and Imaging Technology, 09126, Chemnitz, Germany.
d. Fraunhofer Institute for Electronic Nano Systems (ENAS), Printed Functionalities, 09126, Chemnitz, Germany.
e. Biomedical Research Networking Center in Bioengineering, Biomaterials and Nanomedicine (CIBER-BBN), Spain.
f. CIBERehd, Madrid, Spain

models for drugs tests requires the evaluation of outcomes in a quantitative and real-time manner.[11] For these reasons, the incorporation of real-time monitoring tools in OOC systems is essential to allow the continuous improvement of the models.

Currently, the analysis of OOC cell cultures mainly relies on optical measurement techniques using time-lapse bright field and fluorescence microscopy[11] in combination with various staining techniques as well as collection of supernatants and tissues samples for analysis with conventional analytical tools.[12] This traditional analysis approach is very time-consuming, requires manual sample collection from microfluidic system, large working volumes, and frequent system disturbance, and thus is not suitable for miniaturized cell culture systems. As a consequence, tremendous progress has been initiated towards the development of sensors for cell biology applications over the past few decades. Great efforts have been made up to now for the development of miniaturized sensors, improving their sensitivities and limits of detection.[13] A broad variety of online measurement tools have been already integrated to measure crucial parameters such as oxygen[14–16] and pH,[17] glucose and lactate.[18] However, most of these systems are not compatible with microfluidic OOC models. The principal reason of this incompatibility are complex fabrication processes of the sensors along with more cost-intensive and bulky experimental setups,[19,20] which increase the overall probability of failure. In particular, current manufacturing processes of the sensors do not allow their direct integration in the OOC systems, e.g. due to high temperatures or material incompatibility.[21]

Recently published review articles about cell monitoring and OOC systems claim for the necessity of integrating functional and real-time monitoring tools.[22–26] Hence, there is a strong demand for the integration of online sensor capabilities. However, only few research works describing the integration of sensors in OOC systems can be found. Zhang et al.[20] presented a fully integrated multi-sensing platform to achieve automated in-situ monitoring of biophysical and biochemical parameters. These sensors were manufactured in clean room environments using a complex, multi-step lithography process and the sensing elements were placed outside the OOC chambers. Weise et al.[19] integrated optical oxygen sensors in a bioreactor to monitor the differences of oxygen consumption between a monolayer cell structure and a three-dimensional cell culture in static and dynamic manner. More recently, Curto et al.[25] presented for the first time the coupling of organic electrochemical transistors with microfluidics to achieve multi-parametric monitoring of live cells. Their sensing elements were placed at the glass bottom cover of the system using conventional microtechnology techniques. Lind et al.[27] presented a new approach to integrate sensors inside a cell incubator environment fully based on three-dimensional printing techniques for continuous electronic readout of contractile stress of cardiac micro-tissues.

Inkjet printing (IJP) technology has recently been applied for the integration of electrodes in microfluidic systems[28] or

even for the development of parts of the microfluidic channels.[29] In IJP, droplets of liquids are ejected from a small nozzle. There is no direct contact between the printhead and the substrate. In addition, no mask is required for the process since the droplets are transferred directly to the substrate. This direct writing approach without any need of masks drastically reduces the overall fabrication time and cost of the sensors, thus facilitating iterative design changes during the sensor development and sensor customization for future applications.

Among all the necessary parameters to be monitored inside an OOC system, the amount of oxygen is one of the most important parameters. Oxygen is an important regulatory parameter, influencing cell differentiation and tissue zonation.[23] In addition, cellular function and behaviour are affected by partial pressure of oxygen or oxygen tension in the micro-enviroments.[24] For this reason changes in oxygen tension, from above physiological oxygen tension (hyperoxia) to below physiological levels (hypoxia) or even complete absence of oxygen (anoxia), trigger potent biological responses and need to be controlled precisely.

In this research study, we present for the first time, to the best of our knowledge, the integration of oxygen sensors in an OOC system to achieve in-situ and real-time monitoring of oxygen zonation along the cell culture microfluidic chamber. The used OOC system is a liver-on-chip device that is a recently developed fluidic bioreactor, named as Exoliver, described by Illa et al.[30]. It is a modular bioreactor consisting of two plates and a commercial porous membrane suitable for in vitro analysis of the liver sinusoid. The challenge was to integrate cost-effectively the sensors in the membrane without damaging it. For this purpose, IJP was selected as alternative to the conventional microelectronic technologies for the fabrication of the electrochemical dissolved oxygen (DO) sensors integrated in the OOC systems.[31] The main reason of using IJP is that it allows the direct integration of an array of sensors on the delicate porous membrane, without any direct contact. This will avoid the damage and contamination of the membrane. In addition, the membrane can not withstand temperatures higher than 130 °C. The IJP process does not require high temperatures and can meet this requirement. The principle fabrication approach based on IJP and the morphological and functional characterization of the DO sensors has been already demonstrated in our previous work.[32] Here, an array of DO sensors was placed on the porous cell membrane investigating the concept of a printed primer layer to partially seal the membrane porosity.

Biological validation of these sensors was performed using primary human or rat hepatocytes cultured in the Exoliver bioreactor. DO changes in culture media were induced with Carbonyl-cyanide-4-(trifluoromethoxy)phenylhydrazone (FCCP), a mitochondrial oxidative phosphorylation uncoupler that disrupts ATP synthesis by transporting protons across cell membranes.[33] Because FCCP depolarizes mitochondrial membrane potential, it promotes an increase in hepatocytes respiration and hence in oxygen consumption. In addition, our

system also permits the monitoring of the zonation effect since three sensors were inkjet-printed along the microfluidic channel.

Experimental

Materials and equipment

Three commercially available ink formulations were used for the printing of the DO sensors. A low-curing gold nanoparticle ink formulation (Au-LT-20 from Fraunhofer IKTS, Germany) was employed for the working electrode (WE) and counter electrode (CE). A silver nanoparticle ink (DGP-40LT-15C from ANP, Korea) was used for the development of the pseudo-reference electrode (pRE). The dielectric photoresist SU-8 (SU-8 2002 from MicroChem, USA) was used as the ink to be applied for the passivation layer for the electrodes and the development of a primer layer on the cell culture membrane. Ethanol (LC/MS grade), sodium nitrate (KNO_3), potassium hexacyanoferrate(III) ($K3[Fe(CN)_6]$) and potassium hexacyanoferrate(II) trihydrate ($K_4[Fe(CN)_6]$) (all from Sigma Aldrich, Spain) were used for surface cleaning, activation and characterization of the printed sensor. Hydrochloric acid (0.1 M) was applied for the chlorination of the printed silver electrodes. Microporous polytetrafluoroethylene (PTFE) membrane filters (JGWP04700 from Milipore, USA) were employed as substrates.

All the ink formulations were printed with the drop-on-demand Dimatix Materials Printer (DMP 2831 from Fujifilm Dimatix, USA). The printer operates with piezoelectric inkjet printheads. The printheads have 16 individually addressable nozzles with nominal droplet volumes of 10 pL. Printing patterns were generated using the Electronic Design Automation (EDA) layout software. The printing was carried out in a standard laboratory environment in ambient conditions, without non-particulate filtered enclosure systems and without precise control of temperature or humidity. Different treatment processes were performed to change the properties of the printed layers. The dielectric SU-8 was cured with a Dymax BlueWave 75 UV spot lamp. A standard laboratory hotplate was employed for the drying and sintering of the conductive inks. An oxygen plasma treatment was carried out to adjust the surface energy of the printed layers (SmartPlasma, Plasma technology Gmbh). The MobileDrop (GH11, Krüss Gmbh) contact angle analysis system was employed to determine the surface energy of the layers.

Scanning Electron Microscopy (SEM, Auriga-40 from Carl Zeiss) was performed to analyse the surface structure of the porous PTFE membrane and to study the morphology of each printed layer.

The electrochemical characterization of the sensors and the experimental procedure were performed with an 8-channel potentiostat 1030B Electrochemical Analyzer (CH Instruments, USA). A Clark-type commercial microelectrode (OX-NP, Unisense, Denmark) with a top diameter of 25 μm was used to correlate the DO printed sensors measurements with a 4-channel amplifier microsensor multimeter (Unisense, Denmark). The control of oxygen in the calibration buffers was done using the commercial oxygen probe OXI 325 (WTW, Germany).

Hepatocytes were isolated using Collagenase A (103586, Roche), $CaCl_2$ (C3306, Sigma) and Hepes (H3375, Sigma) all dissolved in Hanks Balanced Solution salt (HBSS; H8264, Sigma). Dulbecco's Modified Eagle's Medium (DMEMF12; 11320074, Gibco) was the selected culture media for primary hepatocyte supplemented with 2% Fetal Bovine Serum (FBS; 04-001-1A, Reactiva), 1% penicillin plus 1% streptomycin (03-331-1C, Reactiva), 2 mM L-glutamine (25030-024, Gibco), 1% amphotericin B (03-029-1C, Reactiva), 1 μM dexamethasone (D4902, Sigma), Dextran (31392, Sigma) and 1 μM insulin (103755, HCB). Hepatocytes were cultured on Poly methyl methacrylate (PMMA) plates previously treated with plasma (BD-10AV, Electro-technic products) and coated with 0.1 mg·mL^{-1} collagen type 1 rat tail (A10483-01, GIBCO).

For the experimental procedure, the cells were washed with Dulbecco's phosphate-buffered saline (DPBS; 02-023-1A, Reactiva). Indirect dynamic stimulation of the cell culture was performed through the perfusion system of the device connected to a peristaltic pump (HV707000-HARVARD peristaltic pump P70). FCCP (370-86-5, Cayman Chemical) was used to increase the oxygen consumption of the hepatocytes.

Porous membrane requirements

The bioreactor is a modular system comprising two plates separated by a commercial porous membrane with the aim to facilitate the study of the liver sinusoid.[30]

The function of the membrane is to separate the inner compartment of the bioreactor in two parallel micro-channels in order to enable analysis of tissue barrier functions and transcellular transport, absorption and secretion. Cells in tissues adhered to the flexible membrane can be exposed simultaneously to cyclic mechanical deformation and fluid shear stresses, similar to what most cells experience in living organs during processes such as breathing, peristalsis and cardiovascular cycling.[8]

The used membrane is a commercially available PTFE filter and it has specific properties that we need to take into account for the integration of the sensors. The cell culture area of the system where sensors need to be placed has a total dimension of 34 x 28.5 mm². The membrane is 65 μm thick, has a 0.2 μm pore size with 80% of porosity and a special chemical treatment to convert the hydrophobic PTFE into hydrophilic. In order to maintain the hydrophilicity of the membrane, its maximum working temperature is 130 °C.

Fig. 1 shows a SEM image where the high pore density of the membrane can be observed.

Inkjet-printed sensor layers

A primer layer was printed on the membrane in order to selectively seal the porosity where the sensors are placed. The strategy to print a primer layer with IJP has been already

demonstrated for paper-based substrates.[34,35] The SU-8 ink was selected for printing the primer and the passivation tracks layers due to its properties and biocompatibility with cell culture systems. Biocompatibility tests were done for the used inks by culturing hepatocytes onto a membrane with printed patterns of the three different inks. Fig. S1 (ESI†) shows that the cells achieve their morphological properties by maintaining their viability as it is also the case for membranes without sensors.

The description and characterization of the amperometric sensor layers printed with the different ink formulations in terms of printability, conductivity and morphology are explained in our previous research work.[32] However, the IJP process parameters were slightly optimized in order to allow a proper layer formation on thin PTFE substrate. In addition, a special aluminium holder was designed to fix the PTFE substrate during the printing process in a plane, without any wrinkling.

The first printing step was the primer layer using SU-8 ink. Two SU-8 layers were printed in wet-on-wet way using a spacing between drops (DS) of 15 µm representing a print resolution of 1693 dpi (dots per inch). This DS provides overlap as each drop spread. The SU-8 was cured by UV during 15 s to polymerize the layer by cross-linking. After this, gold elements (WE and CE) were printed using also a DS of 15 µm between each pixel. Platen temperature was set up to 40 °C in order to evaporate the solvent during the printing process and to improve the layer homogeneity The next step was printing the silver elements using a DS of 30 µm (846 dpi). Then, both printed inks were thermally dried and sintered on a hotplate. With the drying step at 100 °C during 5 min, it was initiated spelling all solvent and decomposing polymeric stabilizing agents of the nanoparticles. The drying was followed by the sintering process, in this case, at 130 °C during 40 min. The sintering temperature was selected as it is the maximum temperature that the PTFE membrane can withstand without destroying its hydrophilic treatment. The conditions were selected in order to obtain the desirable conductivity of the printed patterns, lower than $1 \ \Omega \cdot \square^{-1}$. Afterwards, in order to precisely define the active area of the electrodes and the pad connections, dielectric SU-8 was printed over the sintered layers and after a plasma treatment. The DS of 15 µm (1693 dpi) was selected to print the dielectric and cured using an UV lamp for 15 s.

Finally, two electrochemical steps were required to achieve functional sensors. The chlorination of the silver in order to obtain a stable Ag/AgCl pRE and the activation of the WE.

Cell culture procedure

For the biological validation of the sensors within the OOC device, primary hepatocytes were isolated from male Wistar Han rats (Charles River Laboratories Barcelona, Spain) weighting 300-350 g kept at the University of Barcelona (UB) facilities or from remnant peritumoral tissue obtained after partial hepatectomy in humans.

All experiments were approved by the Laboratory Animal Care and Use Committee of the University of Barcelona and were conducted in accordance with the European Community guidelines for the protection of animals used for experimental and other scientific purposes (European Economic Community (EEC) Directive 86/609). Regarding human tissue, Ethics Committee of the Hospital Clínic de Barcelona approved the experimental protocol (HCB/2015/0624) and in all cases patients received and agreed informed consent.

Hepatocytes were isolated as previously described in[36]. Briefly, liver tissue was rinsed and digested with 0.015% collagenase A in Hank's containing 12 mM hepes (pH 7.4) and 4 mM $CaCl_2$ for 10 min at 37 °C. Disaggregated tissue was filtered using 100 µm nylon strainer, collected in cold Krebs' buffer and centrifuged at 50 g for 5 min. Pellet containing hepatocytes was rinsed three times with HBSS. Hepatocytes above 80% viability (evaluated by trypan blue exclusion), were cultured in PMMA platforms (previously treated with oxygen plasma and collagen type 1 coating) with enriched culture media and maintained O/N at 37 °C in a humidified atmosphere of 5% CO_2.

16h after the isolation, hepatocytes were rinsed twice with DPBS and media was changed to DMEMF12 supplemented with 2.97% dextran (to simulate blood viscosity) also containing the previously mentioned additives

Experimental procedure

Before the incorporation of the membrane with the inkjet-printed sensors in the Exoliver, the calibration of the sensor platform was performed. The calibration solution was used with the same temperature and salinity of the sample of interest. For this reason, two point calibration measurements were done with a cell culture medium buffer at atmospheric and at Zero oxygen reading. Zero oxygen buffer was achieved by the addition of sodium sulphite to the medium. The DO value of both calibrated buffers was controlled with a commercial oxygen probe. Moreover, a commercial Clark-type oxygen sensor was also incorporated inside the Exoliver as a validation of our sensors and it was calibrated following the same procedure. In this work, cells were plated in the lower plate of the system, for this reason, the sensors were printed in the bottom part of the porous membrane.

The inkjet-printed membrane was assembled in the Exoliver as it is described in[30] and the perfusion of the dynamic culture started. Dynamic stimulation of the culture started with $0.1 \ dyn \cdot cm^{-2}$ and the flow rate was gradually increased until reaching $1.15 \ dyn \cdot cm^{-2}$, with a total amount of 43 mL unidirectional recirculating culture media. Exoliver, reservoir, filters and most of the tubing were placed inside an incubator in order to maintain physiological conditions (37 °C, 5 % CO_2).

Fig. S2 (ESI†) shows the setup of the experimental procedure. In the current set-up, the peristaltic pump and all the instrumentation to measure the sensor properties were placed outside the incubator. DO was recorded in real-time and simultaneously every 15 min in the three points of cell

culture area where the inkjet-printed sensors were placed. Clark was set to measure continuously every second.

After 3 h of culture stabilization, the increase in oxygen consumption from hepatocytes was induced adding FCCP to the culture reservoir. Real time oxygen assessment was performed for up to 5h after drug administration to the cell culture. Control experiments without cells were also performed.

Results and discussion

Strategy of blocking the porous membrane with SU-8

To electrically isolate the sensors from the microfluidic medium in order to avoid short circuits and to strictly control the electrode area the porosity of the membrane was sealed using a primer layer. The general concept of this blocking strategy is shown in Fig. 1A. With this strategy, a smooth and non-porous surface is obtained. SU-8 was selected because it is a biocompatible dielectric material that can be easily polymerized by UV radiation. Since it is a UV curable ink formulation, it will form quite thick layers compared to standard solvent-based ink formulations allowing to efficiently seal the porous membrane.

Different numbers of SU-8 layers were printed with a drop space of 15 µm (non-primer (0L), one (1L), two (2L), three (3L) and four layers (4L)) were tested. Fig. 1B1 shows the sealing of a 10 µL volume water drop on top of different number of primer layers. Additionally, Fig. 1B2 shows the cross section of the membrane showing the SU-8 penetration for the different number of layers applied. For the case of 1L, the water droplet is completely absorbed by the porous membrane and does not form a sessile droplet on top. In this case it is very difficult to observe the SU-8 in the membrane. Comparing 0L and 1L, there seems to be nearly no difference. For the case of 2L, the porosity of the membrane is already blocked. The SU-8 has a penetration depth of about 21 ± 4 µm as shown in Fig. 1B2. Fig. S3 (ESI†) shows an image magnification of the cross-section of the membrane before and after the printing of the SU-8. For the case of 3L and 4L it can be considered that the polymer is completely blocking the membrane. The SU-8 forms already a thin layer on top of the membrane. In the case of 3L, the ink penetrates depth in the membrane was about 30 ± 9 µm and the layer thickness on top of the membrane about 5 ± 1 µm. For the 4L the penetration depth of SU-8 was about 31 ± 4 µm and the SU-8 formed smooth layer on top of the membrane of about 16 ± 0.5 µm.

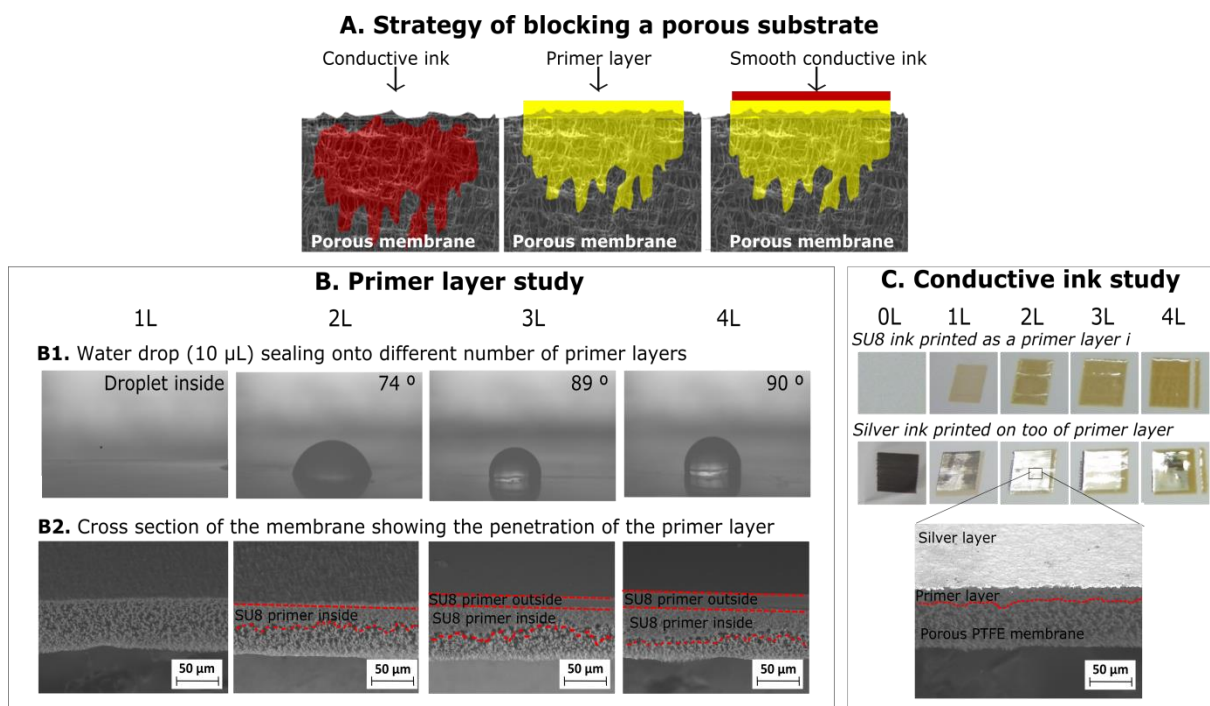### Printing of the conductive inks onto the primer layer

Fig. 1 A) Schematic of the strategy to block a porous substrate using a primer layer, B) Study of the primer layer for the case of use one (1L), two (2L), three (3L) and four layers (4L), in B1). is presented the sealing of a water drop on top of different numer of layers, in B2) the cross section of the membrane with the SU-8 penetrated on it. C) Silver ink printed onto different number of primer layers.
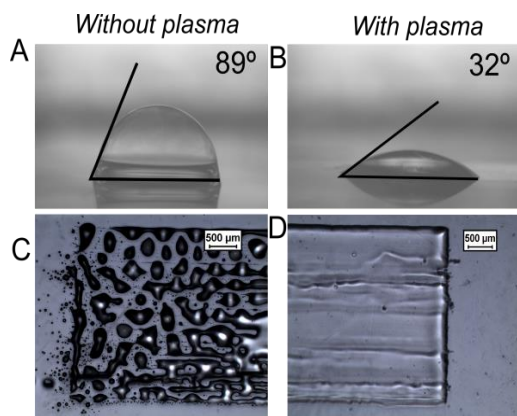
Fig. 2. Contact angle of deionized water on a SU-8 layer measured A) before and B) after the treatment of the substrate with oxygen plasma. A pattern of SU-8 printed over cured SU-8 C) before and D) after the treatment of the surface with plasma.

The printing behaviour of gold and silver inks on top of the primer deposited on the porous membrane was studied. One layer of the conductive inks was printed in patterns of 4 x 4 mm² over a SU-8 pattern of 5 x 5 mm². Fig. 1C shows the top and bottom sides of the membrane after printing conductive inks on the top face. With 1 layer (1L) of primer, the silver ink penetrated completely inside the membrane and no conductivity was achieved. Also we can observe some parts of the ink crossing to the bottom part of the membrane. In the other cases; 2L, 3L and 4L of silver, a well-defined square could be obtained with sheet resistance values below 1 $\Omega\cdot\square^{-1}$ after the sintering process of 130 °C for 40 min.

In the case of gold, similar results were obtained and 2 printed layers (2L) of primer ink were enough to form a smooth printed layer with a sheet resistance of $< 2\ \Omega\cdot\square^{-1}$ after a sintering process of 130 °C for 40 min as shown in Figure S5 (ESI†). Unlike silver, for the case of the gold ink, 2L was the only working option since for the 3L and 4L, a continuous layer was not obtained and the printed gold layer was splitting up in individual, isolated droplets on top of SU-8 due to its high hydrophobicity. However, since the wettability was enough for the printed of both conductive inks onto the 2L of primer layer, this was the final selection.

Passivation strategy

The surface energy of the SU-8 printed layers was determined to be about 30.1 mN·m^{-1} with a high disperse part of about 25.4 mN·m^{-1} and a polar part of only 4.7 mN·m^{-1} using the Owens, Wendt, Rabel, and Kaelble method.[37] This small polar part lead to a difficult wetting of water-based ink formulations on the substrate.[38] As it has been explained in the previous section, this surface energy has enough wettability for printing the gold and silver inks onto 2L of SU-8 primer. However, this hydrophobic surface makes difficult the printability of the SU-8 insulator on top of the SU-8 primer layer, obtaining splitting droplets as it is shown in Fig. 2C. To improve the wettability of the SU-8 ink, an oxygen plasma treatment can be done[39] to increase the amount of oxygen and carboxyl groups at the surface and, thus, in an increased surface energy.[40] The very gentle plasma conditions to change the affinity of the primer and the passivation layers were found as 24 W during 30 s with an oxygen gas pressure of 0.5 bar. With this plasma conditions,
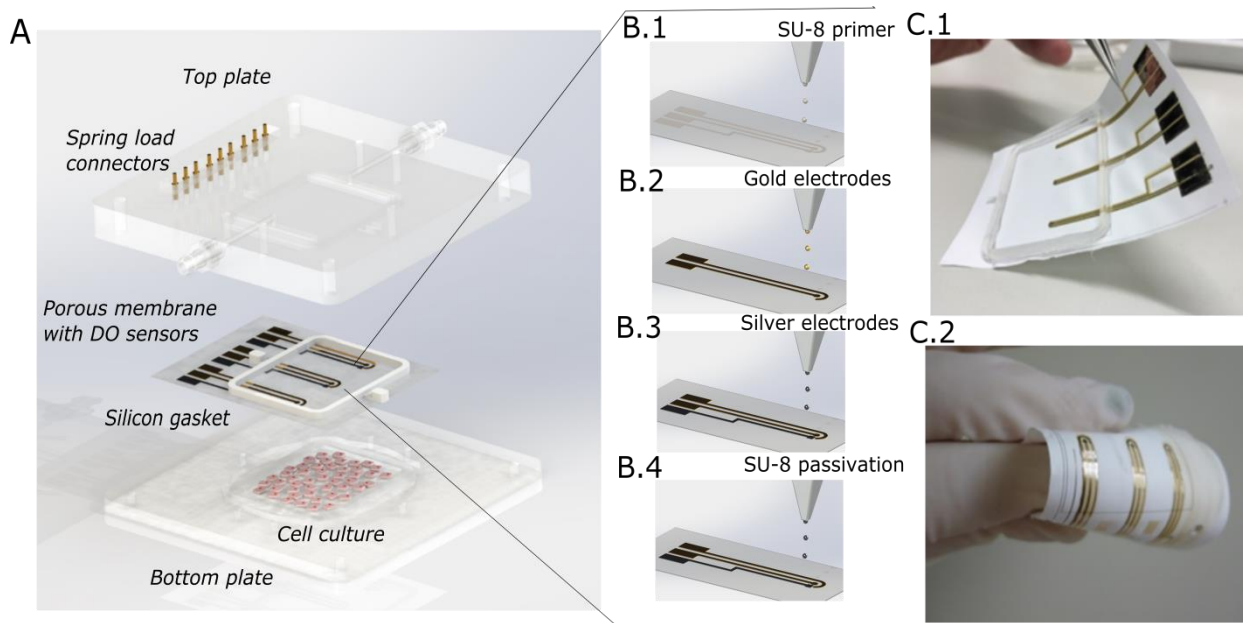

Fig. 3: A) Schematic of the OOC system, B) Fabrication process of the DO sensor based on IJP; B.1) Printing of the primer layer, B.2) Printing of the gold elements, B.3) Printing of the silver elements, B.4) Printing of the passivation layer, C.1) and C.2) photographs of the final DO sensors with the attached silicon o-ring on the porous membrane

a change in the water contact angle from 89° to only 32° was achieved (Fig. 2A and B) which in turn improves remarkably the layer formation as it is observed in Fig. 2D. The plasma treatment increases the wettability of the material, achieving surface energy values of about 37.3 mN·m^{-1} with a reduction of the disperse part about 21.8 mN·m^{-1} and high increase in the polar part from 4.7 mN·m^{-1} to 15.5 mN·m^{-1}.

Inkjet-printed sensors integration in the OOC system

The same electrochemical three electrodes structure described in our previous work[32] was used for the development of the DO sensors. In particular, sensors with a smaller WE diameter (500 μm and 300 μm) were fabricated and tested in this work.

From the point of view of the application, there were two requirements: i) to simultaneously monitor the oxygen at three points of the cell culture area, at the inflow (periportal-like), at the middle and at the outflow (perivenous-like); ii) to minimally modify and easily adapt the membrane to the liver-on-chip bioreactor.

Fig. 3 shows a schematic of the OOC system used in this work. A more detailed description of the sensors fabrication in the membrane is shown in Fig. S4 (ESI†). To facilitate the alignment of the o-ring elastomer used to define the cell culture area and to seal the bioreactor, alignment marks were deposited using the silver ink before the printing of the sensor electrodes. After this step, the silver and gold elements that conforms the three electrodes structure of the DO sensors were printed. Once all the printing steps were done, an o-ring silicone based elastomeric gasket was attached on it as it is described in [30], encompassing a cell culture area of 969 mm^2 (34 mm x 28.5 mm).

The detailed fabrication of the used bioreactor is described in[30]. Minimal changes were done to allow the connection of the sensors, the integration of an external Ag/AgCl RE and the Clark-type oxygen sensor, as shown in Fig. 4A. These two external elements were incorporated at the top plate of the system to support the functionality and response of our developed sensors. In particular, for the connection of the printed sensors to an external potentiostat, individual spring load connectors were incorporated in the top plate of the bioreactor as shown in Fig. 4A. Fig. 4B shows the membrane with the printed sensors assembled with the gasket. The complete system is shown in Fig. 4C detailing the inflow and outflow of the system.

Sensors characterization and validation

To finish the preparation of the printed sensors, the pRE was chlorinated by cyclic voltammetry to achieve a stable Ag/AgCl pRE, and the WE was activated. The electrochemical activation for cleaning the gold WE surface was required to enhance its the electron transfer kinetics.[41] The best activation conditions found were 2 pulses alternating between - 2 V and 0 V for 5 s in PBS electrolyte solution. The membrane with the printed sensors can be reused in different experiments after

rechlorination and reactivation of the electrodes which in our case, was always done just at the beginning of each experiment to ensure that the sensors were working properly.

The sensors were electrochemically characterized in a similar way as is described in our previous work.[32] After the activation, the electrodes behaviour was studied by cyclic voltammetry in ferro/ferricyanide (10 mM) solution as shown in Fig. S6A (ESI†). The anodic/cathodic peak current (I_p) values are directly proportional to the WE area as described the Randles-Sěvčik equation.[42] With our printed sensors we obtained I_p= 5.2 ± 0.5 μA for a WE diameter of 500 μm and I_p= 1.2 ± 0.2 μA for a WE diameter of 300 μm. These I_p values are in good agreement with the values calculated with the Randles-Sěvčik equation. In addition, the sensors can be sterilized with ethanol and UV light without any loss of sensor function and response.

The measurement of oxygen is based on an oxygen reduction reaction at the WE which results in a detectable current. During this process, the oxygen is consumed at the WE. The oxygen concentration was measured with the three inkjet-printed sensors simultaneously every 15 min. As the detection reaction implies oxygen consumption, the final interval time for measurement is a compromise between obtaining a real time monitoring and do not altering the cell culture medium. Each amperometric DO measurement takes about 60 s. The printed sensors with a diameter of 300 μm have an oxygen consumption of about $2.94 \cdot 10^{-8}$ mgDO·s^{-1} per sensor in each measurement. This consumption is sufficiently low compared to the DO consumption caused by the hepatocyte. According to literature [43], the DO consumption for 10^6 hepatocytes ranges from about 0.96 to $2.88 \cdot 10^{-5}$ mgDO·s^{-1}
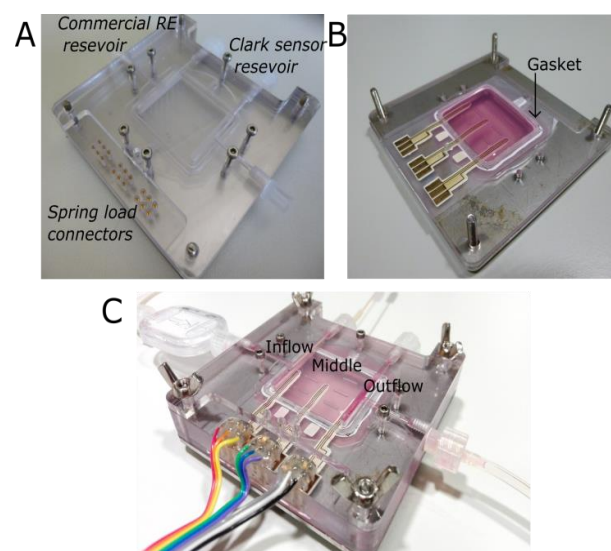

Fig. 4. A) Bioreactor modification to incorporate the control external elements and the spring load for the connectors on the top plate. B) Sensors assembled with the gasket in the middle part of the system. C) Bottom plate, middle part with DO sensors and top plate make up the OOC system with all the fluidic and electrical connections.

Therefore, it can be considered that the viability of the cell culture remains unaltered. The Clark-type sensor was set to measure continuously each second because it is located on the top cover where the medium is freshly maintained by the microfluidics. The DO consumption caused by the Clark-type sensor is very low with about $4.1 \cdot 10^{-11}$ mgDO·s^{-1} due to the small tip dimensions.

The sensor calibration was done by polarization at - 650 mV. This value was found as the optimal potential value for the determination of the DO concentration without interfering with the electro-active compound of the medium. The linearity and sensibility of the sensors were verified in the calibrated medium (PBS) by bubbling a series of nitrogen/air gas mixtures. Fig. S6B (ESI†) shows the calibration curves for the two electrodes dimensions used in this work (WE = 500 μm and WE = 300 μm). In total, 28 platforms each with three fully-printed DO sensors were fabricated and calibrated. The sensors show excellent linearity in the range of 0 to 9 mg·L^{-1}, with a sensitivity of 63 ± 2 nA·L·mg^{-1} (WE = 500 μm) and 28 ± 1 nA·L·mg^{-1} (WE = 300 μm) with correlation factors > 0.99. The limits of detection were 0.17 mg·L^{-1} and 0.11 mg·L^{-1} for WE = 500 μm and WE = 300 μm respectively.

DO monitoring inside the Exoliver

To assess the functionality of the printed sensors, two types of experiments were carried out using the Exoliver. On the one hand, the Exoliver system was assembled without primary cells (acellular Exoliver) allowing to monitor the supply of oxygen to the culture media as a control of the system. On the other hand, the printed DO sensors were assembled in the Exoliver after properly culturing the bottom plate with primary hepatocytes freshly isolated from rats and human livers. Fig. 5A shows the culture area of the system with the three printed sensors along the microfluidic channel and with the external RE and the Clark-type oxygen sensor. Fig. 5B and C show the measured results without cells and with rat hepatocytes respectively, detailing the DO concentrations in the three zones of the bioreactor. In addition, the oxygen was continuously measured with the commercial Clark-type sensor which was placed in the upper channel at the perivenous zone, due to the difficulty of physical integration in other side without interfering with the cells. This physical limitation demonstrates the high potential of inkjet-printed sensors, as they can be easily configured in size and shape to be integrated in the membrane that is usually used in many OOC systems.

In all experiments (n=3), the first three hours were set as the stabilization time required for the microfluidic system. During this period, the oxygen consumption was stable with approximately 7 mg·L^{-1}. Continuous flux of nutrients supplied by the fluidic system ensured long-term viability and functionality of the culture. After the stabilization period, 0.5 μM of FCCP was added to the culture media reservoir and DO concentrations were registered in real-time during the following 5 hours. This drug was employed to boost hepatocytes respiration, provoking the increase of the oxygen

consumption and therefore a decrease in the DO concentration of the medium. As expected for the control experiments, the oxygen in the medium was maintained in the optimal values without observing any change, thus demonstrating that FCCP has no effect on the behaviour of the sensors. For the experiment with cells, the response of the hepatocytes was slightly different between experimental replicates but all replicates followed the same biological tendency.

Deviations between the three experiments per parameter set are represented as a shaded error bar in Fig. 5B.1 and C.1. The maximum deviation between experiments in the stabilization time was ± 0.4 mg·L^{-1} (6%) in the acellular Exoliver and ± 0.6 mg·L^{-1} (9%) in the experiments with rat hepatocytes. These small deviations might be caused by the oxygen conditions of the cell culture medium, its oxygenation inside the incubator or the intra-animal variability. These results show that the cell media has enough proteins to keep an adequate DO level and to maintain the viability of the cell culture inside the Exoliver in both upper and lower plate areas.

Deviation between experiments after the first FCCP addition had a maximum of ± 0.8 mg·L^{-1}, which might be caused by the usage of primary cells, which were isolated from different animals, and therefore their metabolic response may differ. In order to increase the respiratory activity of cells and to measure a higher consumption of oxygen, FCCP was applied in cumulative doses. Finally, a DO concentration of about 2.4 ± 0.4 mg·L^{-1} was determined in the medium.

Interestingly, the DO concentration measured at the outflow is smaller than the DO concentration at the inflow for the case of the Exoliver cultured with rat hepatocytes (Fig. 5C.2). This effect can be explained by the consumption of the cells along the microfluidic channel of the bioreactor resulting in lower DO values at the lower plate and outflow area of the system. In general, the commercial sensor data is in good agreement with the measurement of our printed sensors, thus validating the experiment.

The same experimental approach was performed in an Exoliver cultured with primary human hepatocytes. The results, which confirm the data from rat hepatocytes, are shown in Fig. S7 (ESI†). In this case, higher variations were observed between experiments due to the difference in human liver donors.

A different oxygen concentration was measured along the periportal zone (inflow) and the perivenous zone (outflow). Fig. 5B.2 and C.2 shows how the consumption of DO differs between inflow, middle and outflow zones in the lower plate. The commercial Clark sensors did not measure these variations since it can only measure at one position in the sensor at the outflow of the upper channel. Changes up to 17.5 % were measured between the inflow to the outflow. Because zonation directly affects macronutrient metabolism, morphology and xenobiotic transformation in hepatocytes, oxygen gradient found in our device could indeed contribute to better reproduce the sinusoidal milieu and therefore to the maintenance of hepatocytes.[44]
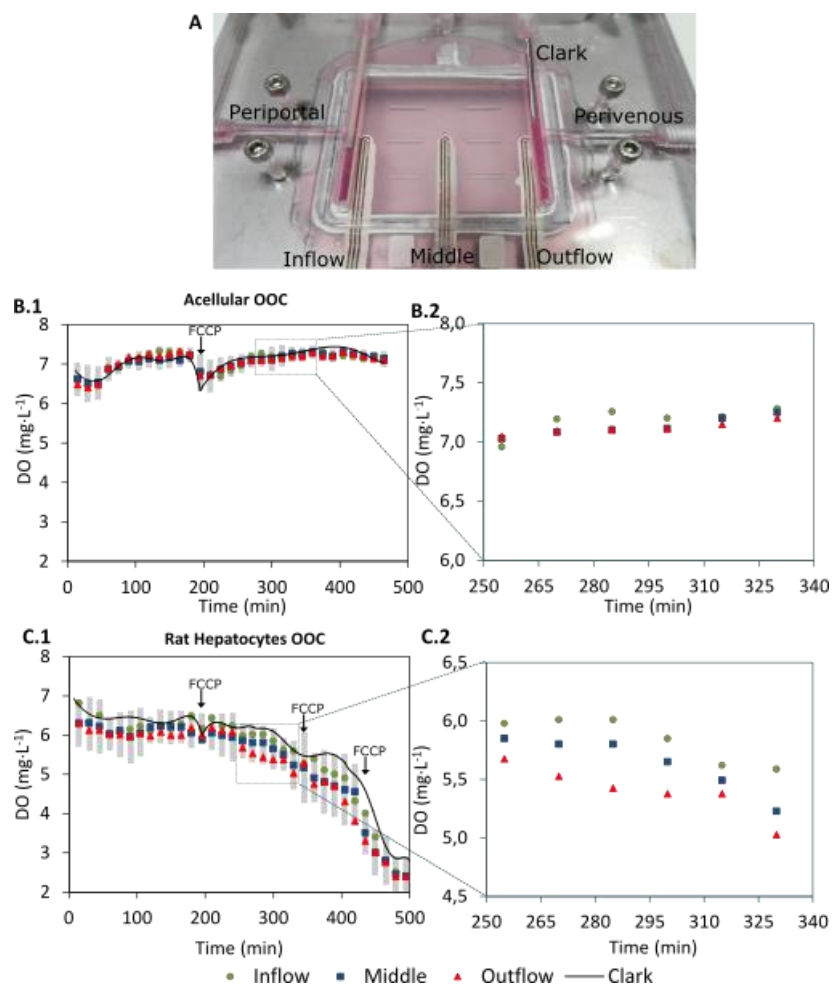
Fig. 5 A) Image of the cell culture area of the Exoliver system with the three printed sensors along the microfluidic channel and the external RE and Clark-type oxygen elements. DO monitored during 8 hours (green for the inflow, blue in the middle, red in the outflow and black for the commercial Clark-type sensor) for B.1) control without primary cells (acellular OOC) and C.1) with rat hepatocytes cell culture. Sections of the of the graphs are plotted in B.2) for the acellular OOC and C.2) for the hepatocytes cell culture for better

At the end of each experiment, hepatocyte viability was evaluated by trypan blue exclusion demonstrating the maintenance of the cell culture. These results obtained with the Exoliver showing that the sensors response is reliable for monitoring DO changes in real-time and at different areas in order to evaluate the zonation of the system, paves the way for using this approach in any other OOC system.

Conclusions

We presented a novel approach for integrating sensors in an OOC system using IJP technology to allow in-situ measurements in real-time. We have demonstrated the potential that IJP has as an alternative to standard microelectronics technology for the fabrication of electrochemical sensors. Particularly advantageous was the possibility to integrate the DO sensors directly on the thin, flexible, delicate and porous cell culture membrane, which was used as a printing substrate.

The strategy of locally sealing the porosity of the membrane using a biocompatible dielectric ink was studied, detailed and successfully applied on the membrane. In fact, the full process to fabricate inkjet-printed sensors on a porous membrane was developed for the first time, to the best of our knowledge. In particular a sensor array with three electrochemical DO sensors was fabricated on a thin cell culture membrane in order to monitor in real time the the oxygen concentration in different locations of an OOC system. The printed DO sensors were integrated in the Exoliver, a previously described liver-on-a-chip system and exhibited a good performance, with a linear response in a wide range of oxygen and with low limit of detection. Its response was verified with a standard, commercially available Clark-type DO sensor. Currently, the functionality of the developed sensors was successfully demonstrated with rat and human hepatocyte cell cultures in the Exoliver.

Inkjet-printed DO sensors have a small footprint, they can be arranged in arrays and due to the low thickness and the customizable size and shape, they allow a flexible, simple and

seamless integration in different OOC systems. In the future, other sensor types such as pH or temperature sensors could be also integrated allowing a more accurate in-situ control of the OOC system, and opening the opportunity to understood biological processes in real-time redefining the way to use these systems for drug testing.

Acknowledgements

References

1 G. H. Underhill, G. Peter, C. S. Chen and S. N. Bhatia, *Annu. Rev. Cell Dev. Biol.*, 2012, **28**, 385–410.

2 M. Mehling and S. Tay, *Curr. Opin. Biotechnol.*, 2014, **25**, 95–102.

3 E. W. Esch, A. Bahinski and D. Huh, *Nat. Rev. Drug Discov.*, 2015, **14**, 248–260.

4 H. Kimura, T. Yamamoto, H. Sakai, Y. Sakai and T. Fujii, *Lab. Chip*, 2008, **8**, 741–746.

5 H. J. Kim, D. Huh, G. Hamilton and D. E. Ingber, *Lab. Chip*, 2012, **12**, 2165–2174.

6 D. Huh, G. A. Hamilton and D. E. Ingber, *Trends Cell Biol.*, 2011, **21**, 745.

7 L. Kim, Y.-C. Toh, J. Voldman and H. Yu, *Lab. Chip*, 2007, **7**, 681–694.

8 S. N. Bhatia and D. E. Ingber, *Nat. Biotechnol.*, 2014, **32**, 760–772.

9 U. Marx, T. B. Andersson, A. Bahinski, M. Beilmann, S. Beken, F. R. Cassee, M. Cirit, M. Daneshian, S. Fitzpatrick, O. Frey, C. Gaertner, C. Giese, L. Griffith, T. Hartung, M. B. Heringa, J. Hoeng, W. H. de Jong, H. Kojima, J. Kuehnl, A. Luch, I. Maschmeyer, D. Sakharov, A. J. A. M. Sips, T. Steger-Hartmann, D. A. Tagle, A. Tonevitsky, T. Tralau, S. Tsyb, A. van de Stolpe, R. Vandebriel, P. Vulto, J. Wang, J. Wiest, M. Rodenburg and A. Roth, *ALTEX*, 2016, **33**, 272–321.

10 S. J. Morgan, C. S. Elangbam, S. Berens, E. Janovitz, A. Vitsky, T. Zabka and L. Conour, *Toxicol. Pathol.*, 2013, **41**, 508–518.

11 M. Vinci, S. Gowan, F. Boxall, L. Patterson, M. Zimmermann, W. Court, C. Lomas, M. Mendiola, D. Hardisson and S. A. Eccles, *BMC Biol.*, 2012, **10**, 29.

12 L.-T. Cheah, Y.-H. Dou, A.-M. L. Seymour, C. E. Dyer, S. J. Haswell, J. D. Wadhawan and J. Greenman, *Lab. Chip*, 2010, **10**, 2720–2726.

13 A. Escarpa and M. A. López, in *Environmental Analysis by Electrochemical Sensors and Biosensors*, eds. L. M. Moretto and K. Kalcher, Springer New York, 2014, pp. 615–650.

14 C.-C. Wu, T. Yasukawa, H. Shiku and T. Matsue, *Sens. Actuators B Chem.*, 2005, **110**, 342–349.

15 C.-C. Wu, H.-N. Luk, Y.-T. T. Lin and C.-Y. Yuan, *Talanta*, 2010, **81**, 228–234.

16 N.-C. Yip, F. J. Rawson, C. W. Tsang and P. M. Mendes, *Biosens. Bioelectron.*, 2014, **57**, 303–309.

17 S. A. Mousavi Shaegh, F. De Ferrari, Y. S. Zhang, M. Nabavinia, N. Binth Mohammad, J. Ryan, A. Pourmand, E. Laukaitis, R. Banan Sadeghian, A. Nadhman, S. R. Shin, A. S. Nezhad, A. Khademhosseini and M. R. Dokmeci, *Biomicrofluidics*, 2016, **10**, 044111.

18 A. Weltin, K. Slotwinski, J. Kieninger, I. Moser, G. Jobst, M. Wego, R. Ehret and G. A. Urban, *Lab. Chip*, 2013, **14**, 138–146.

19 F. Weise, U. Fernekorn, J. Hampl, M. Klett and A. Schober, *Biotechnol. Bioeng.*, 2013, **110**, 2504–2512.

20 Y. S. Zhang, J. Aleman, S. R. Shin, T. Kilic, D. Kim, S. A. Mousavi Shaegh, S. Massa, R. Riahi, S. Chae, N. Hu, H. Avci, W. Zhang, A. Silvestri, A. Sanati Nezhad, A. Manbohi, F. De Ferrari, A. Polini, G. Calzone, N. Shaikh, P. Alerasool, E. Budina, J. Kang, N. Bhise, J. Ribas, A. Pourmand, A. Skardal, T. Shupe, C. E. Bishop, M. R. Dokmeci, A. Atala and A. Khademhosseini, *Proc. Natl. Acad. Sci. U. S. A.*, 2017, **114**, E2293–E2302.

21 K. Domansky, W. Inman, J. Serdy, A. Dash, M. H. M. Lim and L. G. Griffith, *Lab. Chip*, 2010, **10**, 51–58.

22 J. Rogal, C. Probst and P. Loskill, *Future Sci. OA*, 2017, **3**, Art. FSO180, 12.

23 P. E. Oomen, M. D. Skolimowski and E. Verpoorte, *Lab. Chip*, 2016, **16**, 3394–3414.

24 M. D. Brennan, M. L. Rexius-Hall, L. J. Elgass and D. T. Eddington, *Lab. Chip*, 2014, **14**, 4305–4318.

25 V. F. Curto, B. Marchiori, A. Hama, A.-M. Pappa, M. P. Ferro, M. Braendlein, J. Rivnay, M. Fiocchi, G. G. Malliaras, M. Ramuz and R. M. Owens, *Microsyst. Nanoeng.*, 2017, **3**, 17028.

26 A. Polini, L. Prodanov, N. S. Bhise, V. Manoharan, M. R. Dokmeci and A. Khademhosseini, *Expert Opin. Drug Discov.*, 2014, **9**, 335–352.

27 J. U. Lind, T. A. Busbee, A. D. Valentine, F. S. Pasqualini, H. Yuan, M. Yadid, S.-J. Park, A. Kotikian, A. P. Nesmith, P. H. Campbell, J. J. Vlassak, J. A. Lewis and K. K. Parker, *Nat. Mater.*, 2017, **16**, 303–308.

28 J. Wu, R. Wang, H. Yu, G. Li, K. Xu, N. C. Tien, R. C. Roberts and D. Li, *Lab. Chip*, 2015, **15**, 690–695.

29 G. Jenkins, Y. Wang, Y. L. Xie, Q. Wu, W. Huang, L. Wang and X. Yang, *Microfluid. Nanofluidics*, 2015, **19**, 251–261.

30 X. Illa, S. Vila, J. Yeste, C. Peralta, J. Gracia-Sancho and R. Villa, *PLOS ONE*, 2014, **9**, e111864.

31 J. Li, F. Rossignol and J. Macdonald, *Lab. Chip*, 2015, **15**, 2538–2558.

32 A. Moya, E. Sowade, F. J. del Campo, K. Y. Mitra, E. Ramon, R. Villa, R. R. Baumann and G. Gabriel, *Org. Electron.*, 2016, **39**, 168–176.

33 M.-S. To, E. C. Aromataris, J. Castro, M. L. Roberts, G. J. Barritt and G. Y. Rychkov, *Arch. Biochem. Biophys.*, 2010, **495**, 152–158.

34 E. Sowade, F. Göthel, R. Zichner and R. R. Baumann, *Appl. Surf. Sci.*, 2015, **332**, 500–506.

35 A. Denneulin, J. Bras, A. Blayo and C. Neuman, *Appl. Surf. Sci.*, 2011, **257**, 3645–3651.

36 P. Godoy, N. J. Hewitt, U. Albrecht, M. E. Andersen, N. Ansari, S. Bhattacharya, J. G. Bode, J. Bolleyn, C. Borner, J. Böttger, A. Braeuning, R. A. Budinsky, B. Burkhardt, N. R. Cameron, G. Camussi, C.-S. Cho, Y.-J. Choi, J. Craig Rowlands, U. Dahmen, G. Damm, O. Dirsch, M. T. Donato, J. Dong, S. Dooley, D. Drasdo, R. Eakins, K. S. Ferreira, V. Fonsato, J. Fraczek, R. Gebhardt, A.

Gibson, M. Glanemann, C. E. P. Goldring, M. J. Gómez-Lechón, G. M. M. Groothuis, L. Gustavsson, C. Guyot, D. Hallifax, S. Hammad, A. Hayward, D. Häussinger, C. Hellerbrand, P. Hewitt, S. Hoehme, H.-G. Holzhütter, J. B. Houston, J. Hrach, K. Ito, H. Jaeschke, V. Keitel, J. M. Kelm, B. Kevin Park, C. Kordes, G. A. Kullak-Ublick, E. L. LeCluyse, P. Lu, J. Luebke-Wheeler, A. Lutz, D. J. Maltman, M. Matz-Soja, P. McMullen, I. Merfort, S. Messner, C. Meyer, J. Mwinyi, D. J. Naisbitt, A. K. Nussler, P. Olinga, F. Pampaloni, J. Pi, L. Pluta, S. A. Przyborski, A. Ramachandran, V. Rogiers, C. Rowe, C. Schelcher, K. Schmich, M. Schwarz, B. Singh, E. H. K. Stelzer, B. Stieger, R. Stöber, Y. Sugiyama, C. Tetta, W. E. Thasler, T. Vanhaecke, M. Vinken, T. S. Weiss, A. Widera, C. G. Woods, J. J. Xu, K. M. Yarborough and J. G. Hengstler, *Arch. Toxicol.*, 2013, **87**, 1315–1530.

37 D. K. Owens and R. C. Wendt, *J. Appl. Polym. Sci.*, 1969, **13**, 1741–1747.

38 P. Q. M. Nguyen, L.-P. Yeo, B.-K. Lok and Y.-C. Lam, *ACS Appl. Mater. Interfaces*, 2014, **6**, 4011–4016.

39 H. Y. Park, B. J. Kang, D. Lee and J. H. Oh, *Thin Solid Films*, 2013, **546**, 162–166.

40 F. Walther, T. Drobek, A. M. Gigler, M. Hennemeyer, M. Kaiser, H. Herberg, T. Shimitsu, G. E. Morfill and R. W. Stark, *Surf. Interface Anal.*, 2010, **42**, 1735–1744.

41 L. M. Fischer, M. Tenje, A. R. Heiskanen, N. Masuda, J. Castillo, A. Bentien, J. Émneus, M. H. Jakobsen and A. Boisen, *Microelectron. Eng.*, 2009, **86**, 1282–1285.

42 A. J. Bard and L. R. Faulkner, *Electrochemical methods: fundamentals and applications*, Wiley, New York, 2001.

43 M. Shulman and Y. Nahmias, *Methods Mol. Biol. Clifton NJ*, 2013, **945**, 287–302.

44 T. Kietzmann, *Redox Biol.*, 2017, **11**, 622–630.

Real-time oxygen monitoring inside an organ-on-chip device using integrated inkjet-printed sensors

A. Moya,[a,e] M. Ortega-Ribera,[b] E. Sowade,[c] M. Zea,[a,e] X. Illa,[a,e] E. Ramon,[a] R. Villa,[a,e] R. R. Baumann[c,d] J. Gracia-Sancho,[b,f] G.Gabriel[a,e]

Electronic Supplementary Information (ESI)
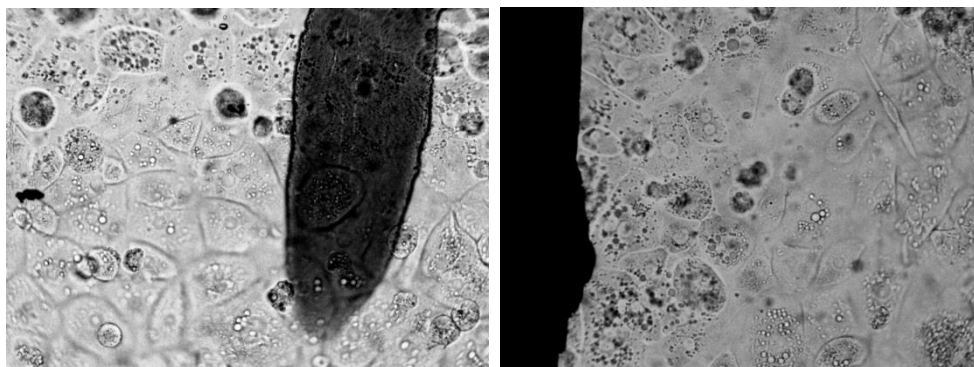
Biocompatibility test

Fig. S1. Primary human hepatocytes cultured along over a printed Au, Ag and SU8 printed patterns. Representative images of the cells above the printed materials were taken using a bright field microscope (Olympus BX51) at 20X magnification.
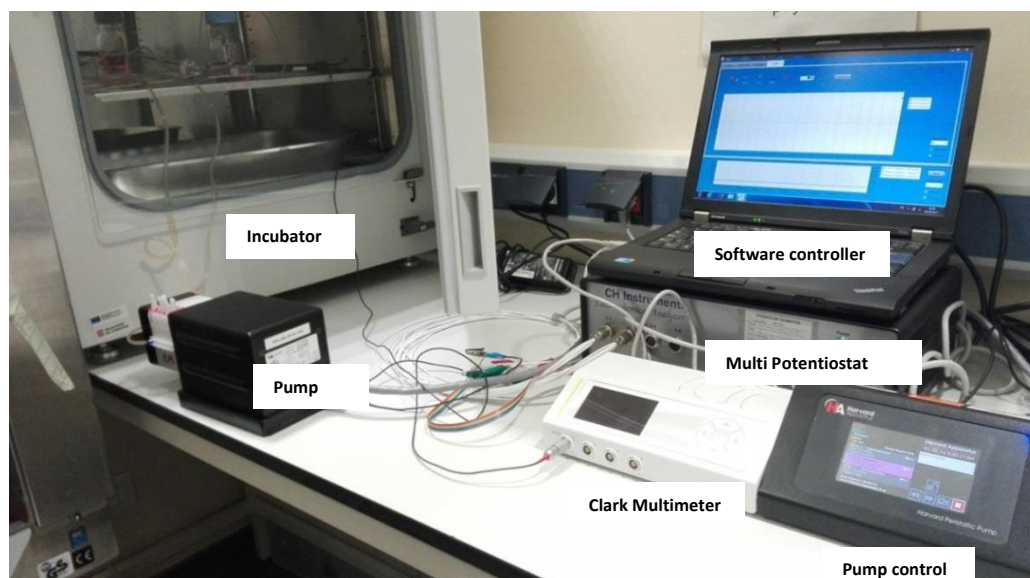
Experimental Set up

Fig. S2. Experimental set-up to monitor the DO sensor inside an OOC system.
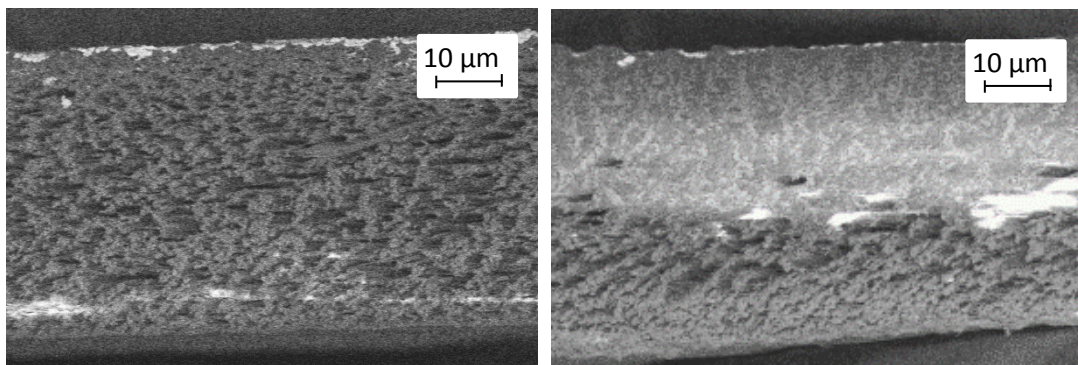
Porous membrane substrate
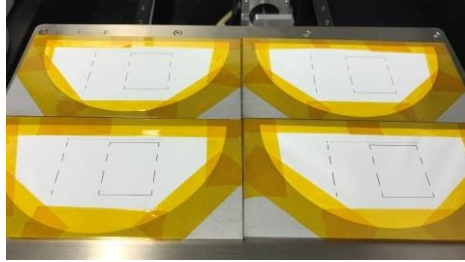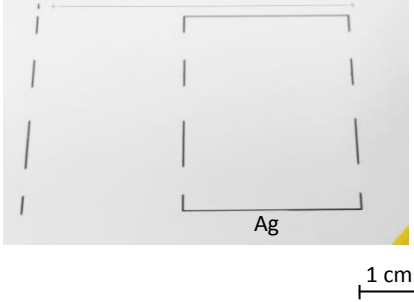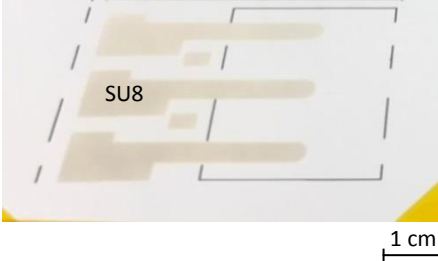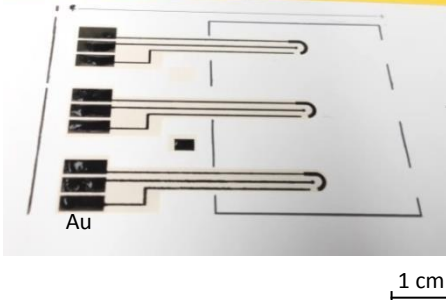
Fig. S3. SEM image of the cross-section of the porous membrane, A) before the printing of the SU8 layer, B) after the printing of the primer layer

IJP Fabrication procedure

DS: Drop Space

Printing of the alignment patterns of the membrane Ink: Silver DS: 30 µm $T_{substrate}$: 40ºC Layers: 1		
Printing of the primer layer. Cured with UV radiation 15 seconds. Ink: SU8 Ds:15 µm $T_{substrate}$: 40ºC Layers: 2		
Printing of the gold electrodes Ink: Au Ds:15 µm $T_{substrate}$: 40ºC Layers: 1		
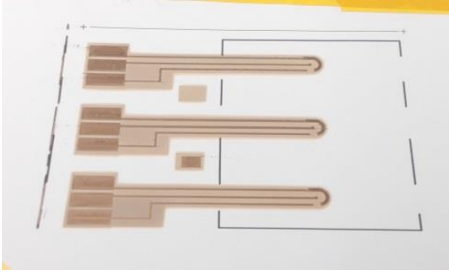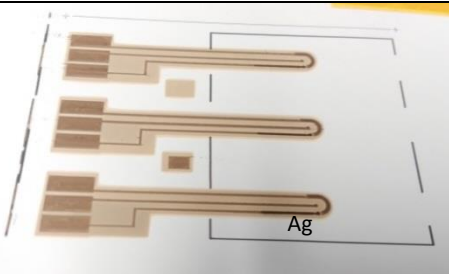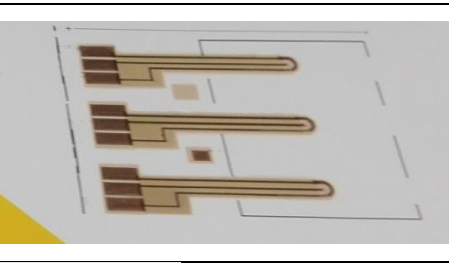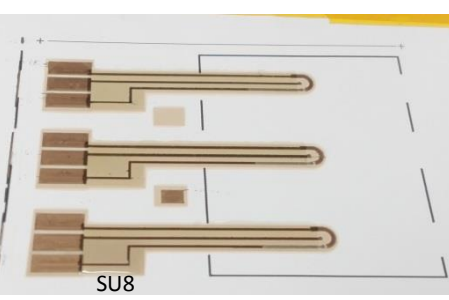
Drying of the gold pattern at 100 °C for 10 minutes.		
Printing of the silver electrodes Ink: Ag Ds: 30 µm $T_{substrate}$: 40 °C Layers: 1		 Ag
Sintering of both conductive inks at 130 °C during 40 minutes		
Plasma treatment to allow the printing of the SU8 passivation layer. Conditions: 24 W, 30 s. and 0.5 bar O_2.	 http://www.plasma-treating.com/	
Passivation layer to isolate the tracks. Ink: SU8 Ds: 15 µm $T_{substrate}$: 40 °C Layers: 1		 SU8

| Attachment of the silicon gasket to define the cell culture area | | |

Fig. S4. Step-by-step fabrication procedure of the IJP oxygen sensors.

Sheet resistance measurement
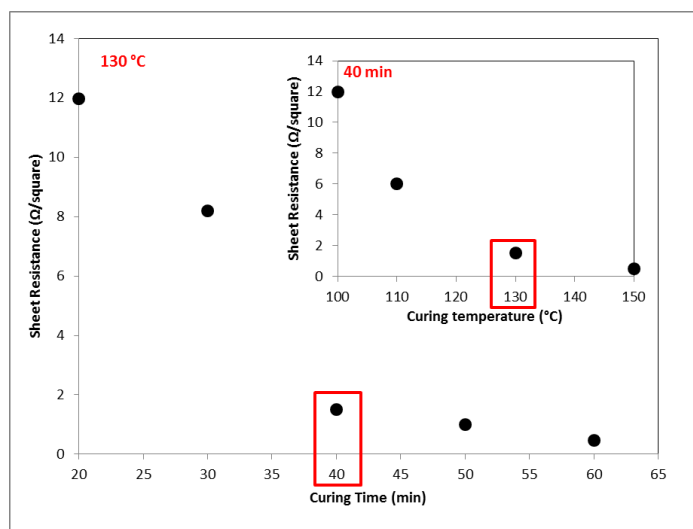
Fig. S5. Sheet resistance of the gold ink at different sintering time and temperature

Electrochemical characterization
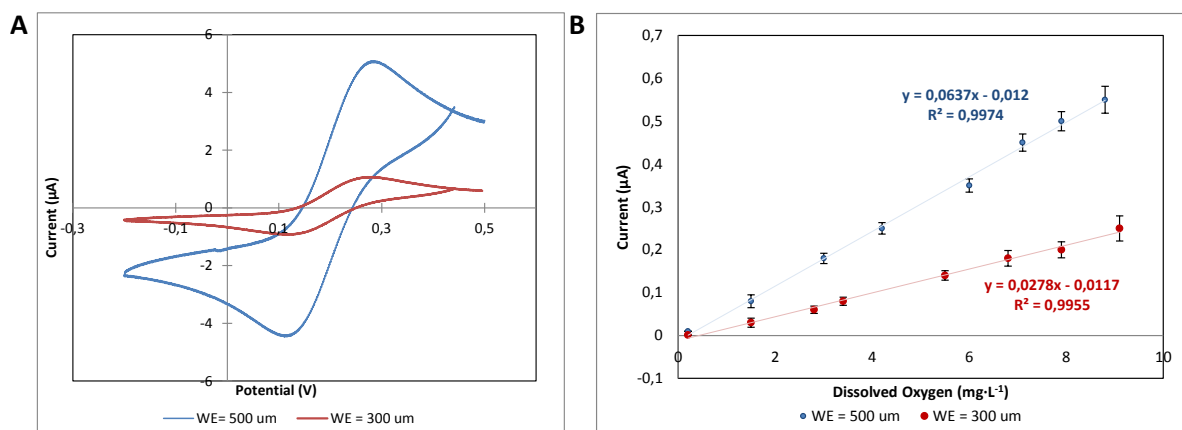
Fig. S6. A) Cyclic voltammetry of gold WE in ferro/ferricyanide (10 mM) and B) calibration curves at different concentrations of oxygen in the range from 0-to 9 mg·L^{-1} for the two electrodes dimensions used in this work (WE = 500 μm and WE = 300 μm).

DO monitoring inside an OOC system
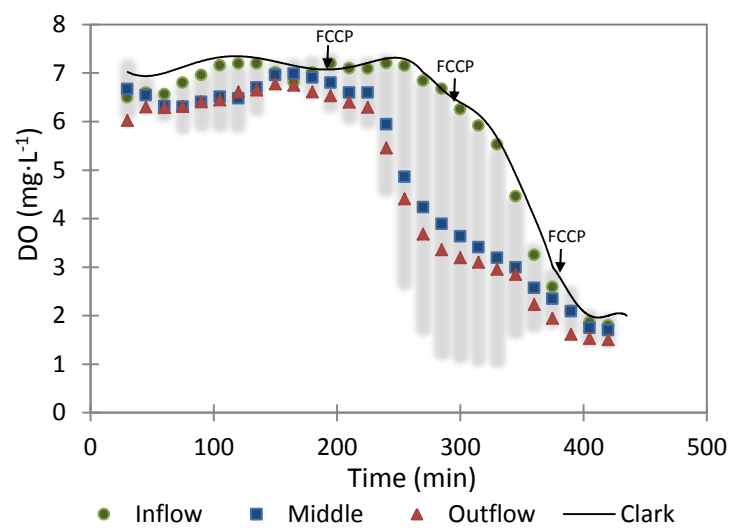
Fig. S7. DO monitoring inside an OOC system with primary human hepatocytes with the addition of the FCCP drug after the 3 hours of stabilization.

Graphical Abstract
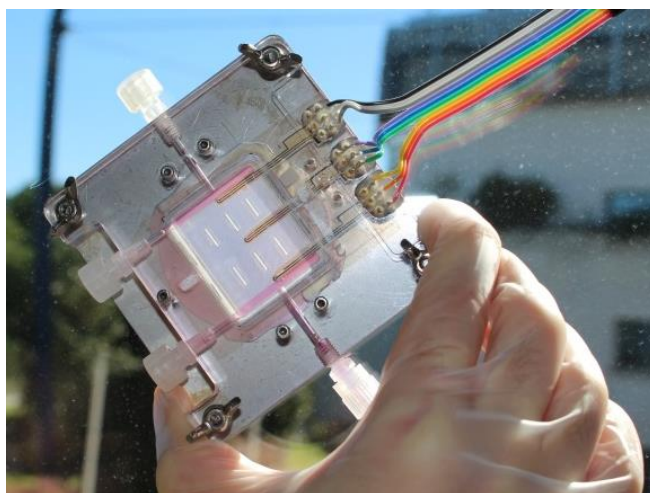
Conclusions

This Chapter describes the most relevant goals achieved during the development of the present thesis work to cover the necessities to develop monitoring tools compatible with Organ-On-a-Chip (OOC) systems.

5.1 Concluding remarks

As the analysis of the Organ-On-a-Chip (OOC) systems are mainly based on conventional analytical methods, the aim og this thesis work has been the development of functional sensing tools compatible with them.

The main goal has been to provide valuable tools for a better understanding of the complex biological processes that occur in the OOC system. Specifically, the developed devices have had the common objective to be compatible with microfluidic OOC systems, overcoming the drawbacks of current analysis methods which in most cases imply the death of cell culture, the disturbance of the microfluidic system for sample collection, the impossibility to observe real-time events, or even the increase of the cost and the complexity of the whole systems.

As each OOC system developed require from different monitoring requirements, in this thesis work, two approximations for physicochemical sensing parameters have been proposed. The final fabricated devices can be seen in Figure 5.1.

(a) External sensing platform   **(b) Embedded sensor in OOC**
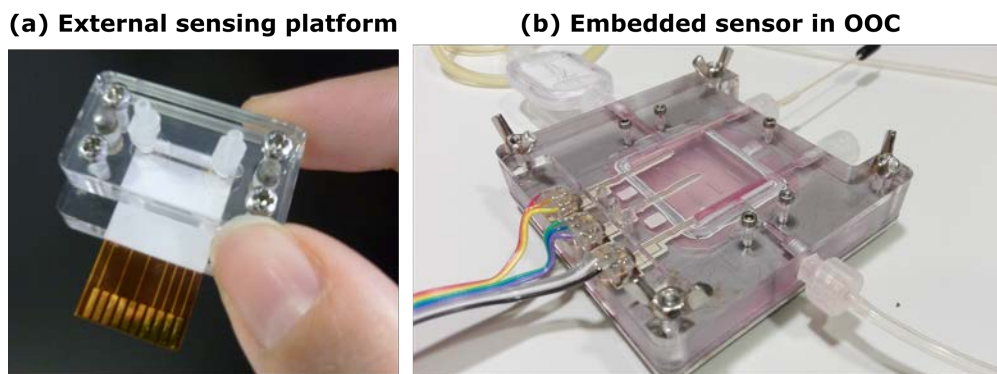
Figure 5.1 | Two strategies developed in this thesis for the monitoring of physicochemical parameters in an OOC system using, (a) a multi-sensing platform connected externally to an OOC platform, and (b) embedded sensors in the cell culture membrane of an OOC system.

The first approach (Figure 5.1(a)) is a modular platform that can be connected to the inlet or outlet ports of any microfluidic system for measuring physicochemical parameters. Specifically, four electrochemical sensors have been integrated in the platform for the simultaneous monitoring of dissolved oxygen (DO), pH, Na^+ and K^+, with the purpose to be used in the measurement of a Kidney-On-a-Chip system. The second approximation dealt with the monitoring inside the own OOC system. To do this, the sensors have been embedded on the cell culture membrane of the OOC platform. To achieve this goal, the sensor manufacturing processes changed from the conventional microfabrication techniques to inkjet printing (IJP) techniques. IJP has enabled to embed some DO sensors, previously developed in Pyrex® and polyimide substrate, in a porous and ultra-thin membrane.

The key results of the work are presented schematically in Figure 5.2. As can be seen, the evolution of the work has been always looking for a simpler, cheaper and friendly devices while adapting these approaches

to the requirements of each system.

Following, specific conclusions of each developed monitoring tools are presented.
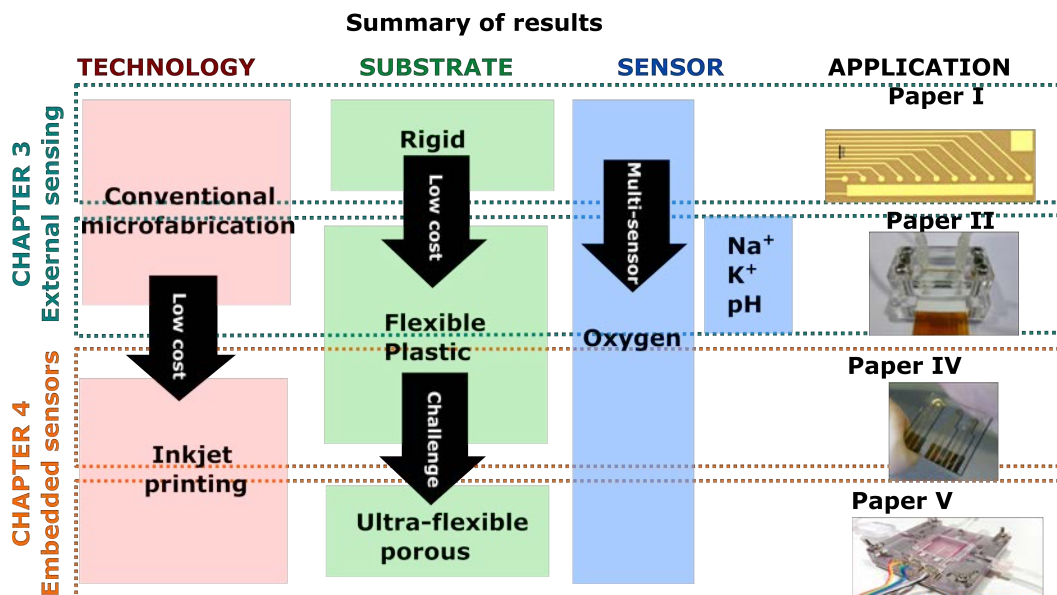
Figure 5.2 | Summarized of the evolution of the work showing the key advances to solve different monitoring necessities.

External monitoring tools

The devices to measure externally to a microfluidic system have been developed using conventional microfabrication techniques. This technology provided the possibility to build small electrodes with different materials (platinum, gold, etc.) in different substrates (rigid or flexible). Electrochemical techniques has been selected as a sensing mechanism, due to their simple, fast and high sensitive characteristics to measure physicochemical parameters of a cell culture.

The first monitoring tool has been addressed with the development of a multi-electrode array for measuring DO. The results of the work can be summarized as:

- An array of microelectrodes on a Pyrex® needle has been fabricated for simultaneous DO measurements. The standard microfabrication techniques allowed the miniaturization of electrochemical structures with electrodes having dimensions between 10 and 50 μm.

- The developed microelectrode array for measuring DO has been completely characterized, showing a good performance in different conditions and mediums, and providing reliable simultaneous multi-point measurements. The DO sensor exhibited an excellent linear response in the range 0-8 mg·L^{-1} affording low Limit of detection (LOD) and Limit of quantification (LOQ).

- The sensors have been validated obtaining the DO profile within a biofilm grown in a flat-plate bioreactor. These measurements helped to enable advances in biofilm characterization.

The second monitoring tool has been addressed with the development of a multi-sensing analytical tool that integrates DO, Na$^+$, K$^+$ and pH sensors in a single solution. As is shown in Figure 5.2, the evolution

has gone from Pyrex$^{\circledR}$ to polymeric substrate and from a single to an integrated multisensing device. The results of the work can be summarized as:

- It has been developed a platform that integrates DO, Na$^+$, K$^+$ and pH sensors on the PI Kapton$^{\circledR}$ substrate. The measurements can be done simultaneously and with very low samples volumes (0.83 μL).

- The platform has been fabricated using rapid-prototyping techniques in order to reduce the development costs of the system.

- The versatility and modularity of the platform have allowed their connection in the inlet and outlet ports of a microfluidic systems without disturbing the performance of the cell culture system. Furthermore, the platform could be used individually, without their connection to a microfluidic system, in order to analyze physiological samples.

- The electrochemical DO sensor has shown a sensitivity of 3.60 nA$\cdot$(mg$\cdot$L^{-1}) in a wide range of concentrations, with a LOD and LOQ of 0.11 mg$\cdot$L^{-1} and 0.38 mg$\cdot$L^{-1} respectively. Na$^+$ and K$^+$ have been developed as an ISE using an internal contact layer between the polymeric sensitive membrane and the gold substrate allowing a good ion-transfer and long term potential stability of the sensors. Na$^+$ and K$^+$ ISE exhibited sensitivities of 57 mV$\cdot$decade^{-1} and 52 mV$\cdot$decade^{-1} respectively, in a wide liner range, from 10^{-5} M to 10^{-4} M and low LOD $5\cdot10^{-6}$ M and $0.5\cdot10^{-5}$ M for Na$^+$ and K$^+$ μ respectively. The pH sensor, prepared by electrochemical deposition of IrOx, exhibited a sensitivity of 69 mV$\cdot$decade^{-1} with a linear response ranging from pH 2 and 11.

- Concentrations of Na$^+$, K$^+$ and pH has been successfully determined in artificial urine samples. As a proof-of-concept, the usefulness of the platform has been also demonstrated in real urine, where several mice were feed with different diets rich in sodium or potassium. The obtained values using the multi-sensing platform were in good agreement with those obtained by flame photometry.

Sensors embedded in OOC

As the complexity of the biological systems has increased, the complexity of integrating monitoring tools has also increased. Some parameters occurs in very short time, and other, must be monitored in the same cell culture area. It is in this context that the second part of this thesis work has been focused in the development of tools with the aim of monitoring physicochemical parameters inside the cell culture area of an OOC system. IJP technology has been selected in order to address this complex goal, due to their advantages since it is a non-contact technique, which permit to be applied in a wide range of substrates, including delicate substrates, as it is the case of a cell culture membrane.

The third monitoring tool has been addressed with the development of a DO sensor by IJP technology. The evolution in this case is related with the change of the used manufacturing technology as shown in Figure 5.2. The results of the work are summarized as:

- The used materials for the development of the electrochemical sensors (silver, gold and SU-8) have been characterized in terms of printability, morphology and conductivity. The metallic inks have the

particularity that can been sintered at low-temperature, and this is required in order to work with the majority of polymeric substrates.

- Different dimensions of electrochemical DO sensors (from 300 μm to 1000 μm of diameter) have been fabricated on PET substrate in a cost-effective, simple and fast way. The printed DO sensors exhibited a linear response in the range between 0 - 8 mg·L^{-1} obtaining low LOD.

The fourth monitoring tool, that is the biggest challenge faced in this work, has been addressed with the development of DO sensors inside the OOC platform by IJP technology. The sensors have been embedded in the cell culture membrane, which has the particularity to be extremely thin, flexible, delicate and highly porous. The results of the work are summarized as:

- Three DO sensors have been embedded directly on a cell culture membrane using IJP technology along the microfluidic channel in order to monitor in real-time the oxygen concentration in different locations of an OOC system.

- The strategy of locally sealing the porosity of the membrane using a biocompatible dielectric ink has been studied, detailed and successfully applied on the porous membrane.

- Inkjet-printed DO sensors exhibited a good performance, with a linear response in a wide range of oxygen and with low LOD. Its response has been verified with a standard commercial Clark-type DO sensor.

- Biological validation of these sensors have been performed using primary human or rat hepatocytes cultured in an Liver-On-a-Chip system. DO changes in culture media have been induced with Carbonyl-cyanide-4-(trifluoromethoxy)phenylhydrazone (FCCP) and the consumption of the DO along the cell culture chamber has been monitored.

- Inkjet-printed DO sensors having a small footprint, can be arranged in arrays and due to the low thickness and the customizable size and shape, they allow a flexible, simple and seamless integration in different OOC systems.

References

[1] E. W. K. Young and D. J. Beebe. *Fundamentals of microfluidic cell culture in controlled microenvironments.* Chemical Society reviews, 39(3):1036–1048, 2010. doi:10.1039/b909900j.

[2] D. Huh, B. D. Matthews, A. Mammoto, M. Montoya-Zavala, H. Y. Hsin and D. E. Ingber. *Reconstituting organ-level lung functions on a chip.* Science, 328(5986):1662–1668, 2010. doi:10.1126/science.1188302.

[3] H. J. Kim, D. Huh, G. Hamilton and D. E. Ingber. *Human gut-on-a-chip inhabited by microbial flora that experiences intestinal peristalsis-like motions and flow.* Lab Chip, 12(12):2165–2174, 2012. doi:10.1039/c2lc40074j.

[4] N. S. Bhise, V. Manoharan, S. Massa, A. Tamayol, M. Ghaderi, M. Miscuglio, Q. Lang, Y. Shrike Zhang, S. R. Shin, G. Calzone, N. Annabi, T. D. Shupe, C. E. Bishop, A. Atala, M. R. Dokmeci and A. Khademhosseini. *A liver-on-a-chip platform with bioprinted hepatic spheroids.* Biofabrication, 8(1):014101. doi:10.1088/1758-5090/8/1/014101.

[5] K.-J. Jang, H. S. Cho, D. H. Kang, W. G. Bae, T.-H. Kwon and K.-Y. Suh. *Fluid-shear-stress-induced translocation of aquaporin-2 and reorganization of actin cytoskeleton in renal tubular epithelial cells.* Integr Biol (Camb), 3(2):134–141, 2011. doi:10.1039/c0ib00018c.

[6] Y. S. Zhang, J. Aleman, S. R. Shin, T. Kilic, D. Kim, S. A. Mousavi Shaegh, S. Massa, R. Riahi, S. Chae, N. Hu, H. Avci, W. Zhang, A. Silvestri, A. Sanati Nezhad, A. Manbohi, F. De Ferrari, A. Polini, G. Calzone, N. Shaikh, P. Alerasool, E. Budina, J. Kang, N. Bhise, J. Ribas, A. Pourmand, A. Skardal, T. Shupe, C. E. Bishop, M. R. Dokmeci, A. Atala and A. Khademhosseini. *Multisensor-integrated organs-on-chips platform for automated and continual in situ monitoring of organoid behaviors.* Proc. Natl. Acad. Sci. U.S.A., 114(12):E2293–E2302, 2017. doi:10.1073/pnas.1612906114.

[7] O. Y. F. Henry, R. Villenave, M. J. Cronce, W. D. Leineweber, M. A. Benz and D. E. Ingber. *Organs-on-chips with integrated electrodes for trans-epithelial electrical resistance (TEER) measurements of human epithelial barrier function.* Lab Chip, 17(13):2264–2271, 2017. doi:10.1039/c7lc00155j.

[8] J. U. Lind, T. A. Busbee, A. D. Valentine, F. S. Pasqualini, H. Yuan, M. Yadid, S.-J. Park, A. Kotikian, A. P. Nesmith, P. H. Campbell, J. J. Vlassak, J. A. Lewis and K. K. Parker. *Instrumented cardiac microphysiological devices via multimaterial three-dimensional printing.* Nat Mater, 16(3):303–308, 2017. doi:10.1038/nmat4782.

[9] V. F. Curto, B. Marchiori, A. Hama, A.-M. Pappa, M. P. Ferro, M. Braendlein, J. Rivnay, M. Fiocchi, G. G. Malliaras, M. Ramuz and R. M. Owens. *Organic transistor platform with integrated microfluidics for in-line multi-parametric in vitro cell monitoring.* 3:micronano201728, 2017. doi:10.1038/micronano.2017.28.

[10] U. Guth, W. Vonau and J. Zosel. *Recent developments in electrochemical sensor application and technology—a review.* Meas. Sci. Technol., 20(4):042002, 2009. doi:10.1088/0957-0233/20/4/042002.

[11] *Organic Electronics Association, "Roadmap for Organic and Printed Electronics".* URL `http://www.oe-a.org/roadmap`.

[12] URL `www.smitherspira.com`.

[13] J. Alamán, R. Alicante, J. Peña and C. Sánchez-Somolinos. *Inkjet printing of functional materials for optical and photonic applications.* Materials, 9:910, 2016. doi:10.3390/ma9110910.

[14] *Dimatix materials printer dmp-2800 series user manual.* Santa Clara, CA, 2008.

[15] G. H. McKinley and M. Renardy. *Wolfgang von ohnesorge.* Physics of Fluids, 23(12):127101. doi:10.1063/1.3663616.

[16] I. Burgués-Ceballos, M. Stella, P. Lacharmoise and E. Martínez-Ferrero. *Towards industrialization of polymer solar cells: material processing for upscaling.* 2(42):17711–17722, 2014. doi:10.1039/C4TA03780D.

[17] J. A. Lim, W. H. Lee, H. S. Lee, J. H. Lee, Y. D. Park and K. Cho. *Self-organization of inkjet-printed triisopropylsilylethynyl pentacene via evaporation-induced flows in a drying droplet.* Adv. Funct. Mater., 18(2):229–234, 2008. doi:10.1002/adfm.200700859.

[18] R. G. Harrison, M. J. Greenman, F. P. Mall and C. M. Jackson. *Observations of the living developing nerve fiber.* Anat. Rec., 1(5):116–128, 1907. doi:10.1002/ar.1090010503.

[19] G. H. Underhill, P. Galie, C. S. Chen and S. N. Bhatia. *Bioengineering methods for analysis of cells in vitro.* Annu. Rev. Cell Dev. Biol., 28:385–410, 2012. doi:10.1146/annurev-cellbio-101011-155709.

[20] M. Mehling and S. Tay. *Microfluidic cell culture.* Current Opinion in Biotechnology, 25:95–102, 2014. doi:10.1016/j.copbio.2013.10.005.

[21] E. W. Esch, A. Bahinski and D. Huh. *Organs-on-chips at the frontiers of drug discovery.* Nat Rev Drug Discov, 14(4):248–260, 2015. doi:10.1038/nrd4539.

[22] H. Kimura, T. Yamamoto, H. Sakai, Y. Sakai and T. Fujii. *An integrated microfluidic system for long-term perfusion culture and on-line monitoring of intestinal tissue models.* Lab Chip, 8(5):741–746, 2008. doi:10.1039/b717091b.

[23] D. Huh, G. A. Hamilton and D. E. Ingber. *From 3d cell culture to organs-on-chips.* Trends Cell Biol., 21(12):745–754, 2011. doi:10.1016/j.tcb.2011.09.005.

[24] X. J. Li, A. V. Valadez, P. Zuo and Z. Nie. *Microfluidic 3d cell culture: potential application for tissue-based bioassays.* Bioanalysis, 4(12):1509–1525, 2012. doi:10.4155/bio.12.133.

[25] L. Kim, Y.-C. Toh, J. Voldman and H. Yu. *A practical guide to microfluidic perfusion culture of adherent mammalian cells.* Lab Chip, 7(6):681–694, 2007. doi:10.1039/b704602b.

[26] S. N. Bhatia and D. E. Ingber. *Microfluidic organs-on-chips.* Nat Biotech, 32(8):760–772, 2014. doi:10.1038/nbt.2989.

[27] U. Marx, T. B. Andersson, A. Bahinski, M. Beilmann, S. Beken, F. R. Cassee, M. Cirit, M. Daneshian, S. Fitzpatrick, O. Frey, C. Gaertner, C. Giese, L. Griffith, T. Hartung, M. B. Heringa, J. Hoeng, W. H. de Jong, H. Kojima, J. Kuehnl, M. Leist, A. Luch, I. Maschmeyer, D. Sakharov, A. J. A. M. Sips, T. Steger-Hartmann, D. A. Tagle, A. Tonevitsky, T. Tralau, S. Tsyb, A. van de Stolpe, R. Vandebriel, P. Vulto, J. Wang, J. Wiest, M. Rodenburg and A. Roth. *Biology-inspired microphysiological system approaches to solve the prediction dilemma of substance testing.* ALTEX, 33(3):272–321, 2016. doi:10.14573/altex.1603161.

[28] S. J. Morgan, C. S. Elangbam, S. Berens, E. Janovitz, A. Vitsky, T. Zabka and L. Conour. *Use of animal models of human disease for nonclinical safety assessment of novel pharmaceuticals.* Toxicol Pathol, 41(3):508–518, 2013. doi:10.1177/0192623312457273.

[29] M. Vinci, S. Gowan, F. Boxall, L. Patterson, M. Zimmermann, W. Court, C. Lomas, M. Mendiola, D. Hardisson and S. A. Eccles. *Advances in establishment and analysis of three-dimensional tumor spheroid-based functional assays for target validation and drug evaluation.* BMC Biol., 10:29, 2012. doi:10.1186/1741-7007-10-29.

[30] M.-H. Wu, S.-B. Huang and G.-B. Lee. *Microfluidic cell culture systems for drug research.* Lab Chip, 10(8):939–956, 2010. doi:10.1039/b921695b.

[31] N.-C. Yip, F. J. Rawson, C. W. Tsang and P. M. Mendes. *Real-time electrocatalytic sensing of cellular respiration.* Biosensors and Bioelectronics, 57:303–309, 2014. doi:10.1016/j.bios.2014.01.059.

[32] S. A. Mousavi Shaegh, F. De Ferrari, Y. S. Zhang, M. Nabavinia, N. Binth Mohammad, J. Ryan, A. Pourmand, E. Laukaitis, R. Banan Sadeghian, A. Nadhman, S. R. Shin, A. S. Nezhad, A. Khademhosseini and M. R. Dokmeci. *A microfluidic optical platform for real-time monitoring of pH and oxygen in microfluidic bioreactors and organ-on-chip devices.* Biomicrofluidics, 10(4):044111. doi:10.1063/1.4955155.

[33] A. Weltin, K. Slotwinski, J. Kieninger, I. Moser, G. Jobst, M. Wego, R. Ehret and G. A. Urban. *Cell culture monitoring for drug screening and cancer research: a transparent, microfluidic, multi-sensor microsystem.* Lab Chip, 14(1):138–146, 2014. doi:10.1039/c3lc50759a.

[34] J. Rogal, C. Probst and P. Loskill. *Integration concepts for multi-organ chips: how to maintain flexibility?!* Future Sci OA, 3(2), 2017. doi:10.4155/fsoa-2016-0092.

[35] P. E. Oomen, M. D. Skolimowski and E. Verpoorte. *Implementing oxygen control in chip-based cell and tissue culture systems.* Lab Chip, 16(18):3394–3414, 2016. doi:10.1039/c6lc00772d.

[36] M. D. Brennan, M. L. Rexius-Hall, L. J. Elgass and D. T. Eddington. *Oxygen control with microfluidics.* Lab Chip, 14(22):4305–4318, 2014. doi:10.1039/c4lc00853g.

[37] A. Polini, L. Prodanov, N. S. Bhise, V. Manoharan, M. R. Dokmeci and A. Khademhosseini. *Organs-on-a-chip: a new tool for drug discovery.* Expert Opin Drug Discov, 9(4):335–352, 2014. doi:10.1517/17460441.2014.886562.

[38] W. C. DeWolf. *Sydney ringer (1835-1910).* Invest Urol, 14(6):500–501, 1977.

[39] D. J. Miller. *Sydney ringer; physiological saline, calcium and the contraction of the heart.* J Physiol, 555:585–587, 2004. doi:10.1113/jphysiol.2004.060731.

[40] H. Kurz, K. Sandau and B. Christ. *On the bifurcation of blood vessels–wilhelm roux's doctoral thesis (jena 1878)–a seminal work for biophysical modelling in developmental biology.* Ann. Anat., 179(1):33–36, 1997. doi:10.1016/S0940-9602(97)80132-X.

[41] M. Abercrombie. *Ross granville harrison, 1870-1959.* 7:110–126, 1961. doi:10.1098/rsbm.1961.0009.

[42] *Centralblatt für Bakteriologie und Parasitenkunde.*, volume v.1 (1887). G. Fischer,, 1887.

[43] H. Naderi, M. M. Matin and A. R. Bahrami. *Review paper: critical issues in tissue engineering: biomaterials, cell sources, angiogenesis, and drug delivery systems.* J Biomater Appl, 26(4):383–417, 2011. doi:10.1177/0885328211408946.

[44] T. Lazic and V. Falanga. *Bioengineered skin constructs and their use in wound healing.* Plast. Reconstr. Surg., 127 Suppl 1:75S–90S, 2011. doi:10.1097/PRS.0b013e3182009d9f.

[45] P. A. Janmey and C. A. McCulloch. *Cell mechanics: integrating cell responses to mechanical stimuli.* Annu Rev Biomed Eng, 9:1–34, 2007. doi:10.1146/annurev.bioeng.9.060906.151927.

[46] R. Edmondson, J. J. Broglie, A. F. Adcock and L. Yang. *Three-dimensional cell culture systems and their applications in drug discovery and cell-based biosensors.* Assay Drug Dev Technol, 12(4):207–218, 2014. doi:10.1089/adt.2014.573.

[47] R. L. Ehrmann and G. O. Gey. *The growth of cells on a transparent gel of reconstituted rat-tail collagen.* J. Natl. Cancer Inst., 16(6):1375–1403, 1956.

[48] M. W. Tibbitt and K. S. Anseth. *Hydrogels as extracellular matrix mimics for 3d cell culture.* Biotechnol Bioeng, 103(4):655–663, 2009. doi:10.1002/bit.22361.

[49] M. J. Bissell, H. G. Hall and G. Parry. *How does the extracellular matrix direct gene expression?* J. Theor. Biol., 99(1):31–68, 1982.

[50] F. Pampaloni, E. G. Reynaud and E. H. K. Stelzer. *The third dimension bridges the gap between cell culture and live tissue.* Nat. Rev. Mol. Cell Biol., 8(10):839–845, 2007. doi:10.1038/nrm2236.

[51] L. G. Griffith and M. A. Swartz. *Capturing complex 3d tissue physiology in vitro.* Nat. Rev. Mol. Cell Biol., 7(3):211–224, 2006. doi:10.1038/nrm1858.

[52] Y. Kim and P. Rajagopalan. *3d hepatic cultures simultaneously maintain primary hepatocyte and liver sinusoidal endothelial cell phenotypes.* PLOS ONE, 5(11):e15456, 2010. doi:10.1371/journal.pone.0015456.

[53] S. C. Owen and M. S. Shoichet. *Design of three-dimensional biomimetic scaffolds.* J Biomed Mater Res A, 94(4):1321–1331, 2010. doi:10.1002/jbm.a.32834.

[54] M. Lee, J. C. Y. Dunn and B. M. Wu. *Scaffold fabrication by indirect three-dimensional printing.* Biomaterials, 26(20):4281–4289, 2005. doi:10.1016/j.biomaterials.2004.10.040.

[55] D. Li, J. Zhou, F. Chowdhury, J. Cheng, N. Wang and F. Wang. *Role of mechanical factors in fate decisions of stem cells.* Regen Med, 6(2):229–240, 2011. doi:10.2217/rme.11.2.

[56] N. J. Walters and E. Gentleman. *Evolving insights in cell–matrix interactions: Elucidating how non-soluble properties of the extracellular niche direct stem cell fate.* Acta Biomaterialia, 11:3–16, 2015. doi:10.1016/j.actbio.2014.09.038.

[57] G. M. Whitesides. *The origins and the future of microfluidics.* Nature, 442(7101):368–373, 2006. doi:10.1038/nature05058.

[58] I. Meyvantsson and D. J. Beebe. *Cell culture models in microfluidic systems.* Annu Rev Anal Chem (Palo Alto Calif), 1:423–449, 2008. doi:10.1146/annurev.anchem.1.031207.113042.

[59] D. J. Beebe, G. A. Mensing and G. M. Walker. *Physics and applications of microfluidics in biology.* Annu Rev Biomed Eng, 4:261–286, 2002. doi:10.1146/annurev.bioeng.4.112601.125916.

[60] Y. Xiao, B. Zhang, A. Hsieh, N. Thavandiran, C. Martin and M. Radisic. *Chapter 12 - microfluidic cell culture techniques.* In *Microfluidic Cell Culture Systems*, Micro and Nano Technologies, pages 303–321. William Andrew Publishing, 2017. ISBN 978-1-4377-3459-1. doi: 10.1016/B978-1-4377-3459-1.00012-0.

[61] U. Demirci and R. Langer. *Microfluidic Technologies for Human Health.* World Scientific, 2012. ISBN 978-981-4405-52-2.

[62] G. M. Walker, H. C. Zeringue and D. J. Beebe. *Microenvironment design considerations for cellular scale studies.* Lab Chip, 4(2):91–97, 2004. doi:10.1039/b311214d.

[63] R. Gebhardt, J. G. Hengstler, D. Müller, R. Glöckner, P. Buenning, B. Laube, E. Schmelzer, M. Ullrich, D. Utesch, N. Hewitt, M. Ringel, B. R. Hilz, A. Bader, A. Langsch, T. Koose, H.-J. Burger, J. Maas and F. Oesch. *New hepatocyte in vitro systems for drug metabolism: metabolic capacity and recommendations for application in basic research and drug development, standard operation procedures.* Drug Metab. Rev., 35(2):145–213, 2003. doi:10.1081/DMR-120023684.

[64] J. W. Allen, S. R. Khetani and S. N. Bhatia. *In vitro zonation and toxicity in a hepatocyte bioreactor.* Toxicol. Sci., 84(1):110–119, 2005. doi:10.1093/toxsci/kfi052.

[65] A. W. Tilles, H. Baskaran, P. Roy, M. L. Yarmush and M. Toner. *Effects of oxygenation and flow on the viability and function of rat hepatocytes cocultured in a microchannel flat-plate bioreactor.* Biotechnol. Bioeng., 73(5):379–389, 2001. doi:10.1002/bit.1071.

[66] A. L. Paguirigan and D. J. Beebe. *Microfluidics meet cell biology: bridging the gap by validation and application of microscale techniques for cell biological assays.* BioEssays: News and Reviews in Molecular, Cellular and Developmental Biology, 30(9):811–821, 2008. doi:10.1002/bies.20804.

[67] J. L. Olson, A. Atala and J. J. Yoo. *Tissue engineering: Current strategies and future directions.* Chonnam Med J, 47(1):1–13, 2011. ISSN 2233-7385. doi:10.4068/cmj.2011.47.1.1.

[68] M. Lynch and C. Fischbach. *Biomechanical forces in the skeleton and their relevance to bone metastasis: biology and engineering considerations.* Adv Drug Deliv Rev, 0:119–134, 2014. doi: 10.1016/j.addr.2014.08.009.

[69] H. E. Abaci and M. L. Shuler. *Human-on-a-chip design strategies and principles for physiologically based pharmacokinetics/pharmacodynamics modeling.* Integr Biol (Camb), 7(4):383–391, 2015. doi: 10.1039/c4ib00292j.

[70] C. Zhang, Z. Zhao, N. A. Abdul Rahim, D. van Noort and H. Yu. *Towards a human-on-chip: culturing multiple cell types on a chip with compartmentalized microenvironments.* Lab Chip, 9(22):3185–3192, 2009. doi:10.1039/b915147h.

[71] J. P. Wikswo, F. E. Block, D. E. Cliffel, C. R. Goodwin, C. C. Marasco, D. A. Markov, D. L. McLean, J. A. McLean, J. R. McKenzie, R. S. Reiserer, P. C. Samson, D. K. Schaffer, K. T. Seale and S. D. Sherrod. *Engineering challenges for instrumenting and controlling integrated organ-on-chip systems.* IEEE Trans Biomed Eng, 60(3):682–690, 2013. doi:10.1109/TBME.2013.2244891.

[72] J. P. Wikswo, E. L. Curtis, Z. E. Eagleton, B. C. Evans, A. Kole, L. H. Hofmeister and W. J. Matloff. *Scaling and systems biology for integrating multiple organs-on-a-chip.* Lab Chip, 13(18):3496–3511, 2013. doi:10.1039/c3lc50243k.

[73] K. Viravaidya, A. Sin and M. L. Shuler. *Development of a microscale cell culture analog to probe naphthalene toxicity.* Biotechnol. Prog., 20(1):316–323, 2004. doi:10.1021/bp0341996.

[74] S. K. Doke and S. C. Dhawale. *Alternatives to animal testing: A review.* Saudi Pharmaceutical Journal, 23(3):223–229, 2015. doi:10.1016/j.jsps.2013.11.002.

[75] National Research Council (US) and Institute of Medicine (US) Committee on the Use of Laboratory Animals in Biomedical and Behavioral Research. *Use of Laboratory Animals in Biomedical and Behavioral Research.* National Academies Press (US), 1988.

[76] Q. Ramadan and M. A. M. Gijs. *In vitro micro-physiological models for translational immunology.* Lab Chip, 15(3):614–636, 2015. doi:10.1039/C4LC01271B.

[77] J. Seok, H. S. Warren, A. G. Cuenca, M. N. Mindrinos, H. V. Baker, W. Xu, D. R. Richards, G. P. McDonald-Smith, H. Gao, L. Hennessy, C. C. Finnerty, C. M. López, S. Honari, E. E. Moore, J. P. Minei, J. Cuschieri, P. E. Bankey, J. L. Johnson, J. Sperry, A. B. Nathens, T. R. Billiar, M. A. West, M. G. Jeschke, M. B. Klein, R. L. Gamelli, N. S. Gibran, B. H. Brownstein, C. Miller-Graziano, S. E. Calvano, P. H. Mason, J. P. Cobb, L. G. Rahme, S. F. Lowry, R. V. Maier, L. L. Moldawer, D. N. Herndon, R. W. Davis, W. Xiao, R. G. Tompkins and Inflammation and Host Response to Injury, Large Scale Collaborative Research Program. *Genomic responses in mouse models poorly mimic human inflammatory diseases.* Proc. Natl. Acad. Sci. U.S.A., 110(9):3507–3512, 2013. doi: 10.1073/pnas.1222878110.

[78] P. Artursson and R. T. Borchardt. *Intestinal drug absorption and metabolism in cell cultures: Caco-2 and beyond.* Pharm. Res., 14(12):1655–1658, 1997.

[79] M. B. Esch, T. L. King and M. L. Shuler. *The role of body-on-a-chip devices in drug and toxicity studies.* Annu Rev Biomed Eng, 13:55–72, 2011. doi:10.1146/annurev-bioeng-071910-124629.

[80] A. D. van der Meer and A. van den Berg. *Organs-on-chips: breaking the in vitro impasse.* Integr Biol (Camb), 4(5):461–470, 2012. doi:10.1039/c2ib00176d.

[81] D. D. Nalayanda, C. Puleo, W. B. Fulton, L. M. Sharpe, T.-H. Wang and F. Abdullah. *An open-access microfluidic model for lung-specific functional studies at an air-liquid interface.* Biomed Microdevices, 11(5):1081–1089, 2009. doi:10.1007/s10544-009-9325-5.

[82] D. Huh, D. C. Leslie, B. D. Matthews, J. P. Fraser, S. Jurek, G. A. Hamilton, K. S. Thorneloe, M. A. McAlexander and D. E. Ingber. *A human disease model of drug toxicity-induced pulmonary edema in a lung-on-a-chip microdevice.* Sci Transl Med, 4(159):159ra147, 2012. doi:10.1126/scitranslmed. 3004249.

[83] R. F. Service. *Bioengineering. lung-on-a-chip breathes new life into drug discovery.* Science, 338(6108):731, 2012. doi:10.1126/science.338.6108.731.

[84] P. M. v. Midwoud, M. T. Merema, E. Verpoorte and G. M. M. Groothuis. *A microfluidic approach for in vitro assessment of interorgan interactions in drug metabolism using intestinal and liver slices.* Lab Chip, 10(20):2778–2786, 2010. doi:10.1039/C0LC00043D.

[85] S. R. Khetani and S. N. Bhatia. *Microscale culture of human liver cells for drug development.* Nat Biotech, 26(1):120–126, 2008. doi:10.1038/nbt1361.

[86] B. J. Kane, M. J. Zinner, M. L. Yarmush and M. Toner. *Liver-specific functional studies in a microfluidic array of primary mammalian hepatocytes.* Anal. Chem., 78(13):4291–4298, 2006. doi: 10.1021/ac051856v.

[87] P. J. Lee, P. J. Hung and L. P. Lee. *An artificial liver sinusoid with a microfluidic endothelial-like barrier for primary hepatocyte culture.* Biotechnol. Bioeng., 97(5):1340–1346, 2007. doi:10.1002/bit. 21360.

[88] P. M. van Midwoud, E. Verpoorte and G. M. M. Groothuis. *Microfluidic devices for in vitro studies on liver drug metabolism and toxicity.* Integr Biol (Camb), 3(5):509–521, 2011. doi:10.1039/c0ib00119h.

[89] K.-J. Jang and K.-Y. Suh. *A multi-layer microfluidic device for efficient culture and analysis of renal tubular cells.* Lab Chip, 10(1):36–42, 2010. doi:10.1039/b907515a.

[90] T. T. G. Nieskens and M. J. Wilmer. *Kidney-on-a-chip technology for renal proximal tubule tissue reconstruction.* European Journal of Pharmacology, 790:46–56, 2016. doi:10.1016/j.ejphar.2016.07. 018.

[91] G. J. Mahler, M. B. Esch, R. P. Glahn and M. L. Shuler. *Characterization of a gastrointestinal tract microscale cell culture analog used to predict drug toxicity.* Biotechnol. Bioeng., 104(1):193–205, 2009. doi:10.1002/bit.22366.

[92] Y. Imura, Y. Asano, K. Sato and E. Yoshimura. *A microfluidic system to evaluate intestinal absorption.* Anal Sci, 25(12):1403–1407, 2009.

[93] D. W. Hutmacher, R. E. Horch, D. Loessner, S. Rizzi, S. Sieh, J. C. Reichert, J. A. Clements, J. P. Beier, A. Arkudas, O. Bleiziffer and U. Kneser. *Translating tissue engineering technology platforms into cancer research.* J. Cell. Mol. Med., 13(8):1417–1427, 2009. doi:10.1111/j.1582-4934.2009.00853.x.

[94] P. C. d. Sampaio, D. Auslaender, D. Krubasik, A. V. Failla, J. N. Skepper, G. Murphy and W. R. English. *A heterogeneous in vitro three dimensional model of tumour-stroma interactions regulating sprouting angiogenesis.* PLOS ONE, 7(2):e30753, 2012. doi:10.1371/journal.pone.0030753.

[95] E. Jedrych, M. Chudy, A. Dybko and Z. Brzozka. *The microfluidic system for studies of carcinoma and normal cells interactions after photodynamic therapy (PDT) procedures.* Biomicrofluidics, 5(4):041101–041101–6, 2011. doi:10.1063/1.3658842.

[96] E. A. Phelps and A. J. García. *Engineering more than a cell: vascularization strategies in tissue engineering.* Curr. Opin. Biotechnol., 21(5):704–709, 2010. doi:10.1016/j.copbio.2010.06.005.

[97] A. Günther, S. Yasotharan, A. Vagaon, C. Lochovsky, S. Pinto, J. Yang, C. Lau, J. Voigtlaender-Bolz and S.-S. Bolz. *A microfluidic platform for probing small artery structure and function.* Lab Chip, 10(18):2341–2349, 2010. doi:10.1039/c004675b.

[98] M. Baker. *Tissue models: a living system on a chip.* Nature, 471(7340):661–665, 2011. doi:10.1038/ 471661a.

[99] P. Borel. *Petri Borelli, ... Historiarum et observationum medico-physicarum centuria prima (- secunda).* Apud A. Colomerium, 1653. OCLC: 457101780.

[100] A. v. Leeuwenhoek, A. d. Blois, J. Verkolje and H. v. Kroonevelt. *Arcana naturae detecta.* Delphis Batavorum [Delft] : Apud Henricum a Krooneveld, 1695.

[101] Z. Göröcs and A. Ozcan. *On-chip biomedical imaging.* IEEE Rev Biomed Eng, 6:29–46, 2013. doi: 10.1109/RBME.2012.2215847.

[102] J. R. Swedlow. *Innovation in biological microscopy: Current status and future directions.* Bioessays, 34(5):333–340, 2012. doi:10.1002/bies.201100168.

[103] D. Gerlich and J. Ellenberg. *4d imaging to assay complex dynamics in live specimens.* Nat. Cell Biol., Suppl:S14–19, 2003.

[104] B. N. G. Giepmans, S. R. Adams, M. H. Ellisman and R. Y. Tsien. *The fluorescent toolbox for assessing protein location and function.* Science, 312(5771):217–224, 2006. doi:10.1126/science.1124618.

[105] M. Cremer. *Über die Ursache der elektromotorischen Eigenschaften der Gewebe, zugleich ein Beitrag zur Lehre von den polyphasischen Elektrolytketten.* Oldenbourg, 1906. Google-Books-ID: J2j8tgAACAAJ.

[106] M. Dole. *The early history of the development of the glass electrode for pH measurements.* J. Chem. Educ., 57(2):134, 1980. doi:10.1021/ed057p134.

[107] P. T. Kerridge. *The use of the glass electrode in biochemistry.* Biochem J, 19(4):611–617.

[108] G. Eisenman, D. O. Rudin and J. U. Casby. *Glass electrode for measuring sodium ion.* 126(3278):831– 834. doi:10.1126/science.126.3278.831.

[109] M. S. Frant and J. W. Ross. *Potassium ion specific electrode with high selectivity for potassium over sodium.* Science, 167(3920):987–988, 1970.

[110] H. F. Bunn and R. O. Poyton. *Oxygen sensing and molecular adaptation to hypoxia.* Physiol. Rev., 76(3):839–885, 1996.

[111] L. C. Clark. *Monitor and control of blood and tissue oxygen tensions*, 1956.

[112] L. C. Clark and C. Lyons. *Electrode systems for continuous monitoring in cardiovascular surgery.* 102(1):29–45, 1962. ISSN 1749-6632. doi:10.1111/j.1749-6632.1962.tb13623.x.

[113] W. L. Clarke, D. Cox, L. A. Gonder-Frederick, W. Carter and S. L. Pohl. *Evaluating clinical accuracy of systems for self-monitoring of blood glucose.* Diabetes Care, 10(5):622–628, 19871.

[114] J. J. Pancrazio, J. P. Whelan, D. A. Borkholder, W. Ma and D. A. Stenger. *Development and application of cell-based biosensors.* Annals of Biomedical Engineering, 27(6):697–711, 1999. doi: 10.1114/1.225.

[115] G. A. Rechnitz, R. K. Kobos, S. J. Riechel and C. R. Gebauer. *A bio-selective membrane electrode prepared with living bacterial cells.* Anal. Chim. Acta, 94(2):357–365, 1977. doi:10.1016/S0003-2670(01) 84537-2.

[116] M. Quaranta, S. M. Borisov and I. Klimant. *Indicators for optical oxygen sensors.* Bioanal Rev, 4(2):115–157, 2012. doi:10.1007/s12566-012-0032-y.

[117] I. Bergman. *Rapid-response atmospheric oxygen monitor based on fluorescence quenching.* Nature, 218(5139):396–396, 1968. doi:10.1038/218396a0.

[118] D. W. Lübbers and N. Opitz. *Die pCO2-/pO2-optode: Eine neue p CO2- bzw. pO2-meßsonde zur messung des pCO2 oder pO2 von gasen und flüssigkeiten / the pCO2-/pO2-optode: A new probe for measurement of pCO2 or pO2 in fluids and gases.* 30(7):532–533, 2014. doi:10.1515/znc-1975-7-819.

[119] E.-H. Yoo and S.-Y. Lee. *Glucose biosensors: An overview of use in clinical practice.* Sensors (Basel), 10(5):4558–4576, 2010. doi:10.3390/s100504558.

[120] C. McDonagh, C. S. Burke and B. D. MacCraith. *Optical chemical sensors.* Chem. Rev., 108(2):400–422, 2008. doi:10.1021/cr068102g.

[121] J. Pine. *A history of MEA development.* In *Advances in Network Electrophysiology*, pages 3–23. Springer, Boston, MA, 2006. Doi: 10.1007/0-387-25858-2_1.

[122] C. Thomasjr, P. Springer, G. Loeb, Y. Berwaldnetter and L. Okun. *A miniature microelectrode array to monitor the bioelectric activity of cultured cells.* 74:61–66, 1972. ISSN 0014-4827.

[123] M. E. J. Obien, K. Deligkaris, T. Bullmann, D. J. Bakkum and U. Frey. *Revealing neuronal function through microelectrode array recordings.* Front Neurosci, 8, 2015. doi:10.3389/fnins.2014.00423.

[124] S. Gelfan. *The electrical conductivity of protoplasm and a new method of its determination,.* University of California press, 1927.

[125] S. Gelfan and R. W. Gerard. *STUDIES OF SINGLE MUSCLE FIBRES: II. a further analysis of the grading mechanism.* 95(2):412–416, 1930.

[126] P. Linderholm, L. Marescot, M. H. Loke and P. Renaud. *Cell culture imaging using microimpedance tomography.* 55(1):138–146, 2008. doi:10.1109/TBME.2007.910649.

[127] A. M. Leferink, C. A. van Blitterswijk and L. Moroni. *Methods of monitoring cell fate and tissue growth in three-dimensional scaffold-based strategies for in vitro tissue engineering.* Tissue Eng Part B Rev, 22(4):265–283, 2016. doi:10.1089/ten.TEB.2015.0340.

[128] R. M. Lequin. *Enzyme immunoassay (EIA)/enzyme-linked immunosorbent assay (ELISA).* 51(12):2415–2418, 2005. doi:10.1373/clinchem.2005.051532.

[129] E. Engvall and P. Perlmann. *Enzyme-linked immunosorbent assay (ELISA). quantitative assay of immunoglobulin g.* Immunochemistry, 8(9):871–874, 1971.

[130] P. M. Misun, J. Rothe, Y. R. F. Schmid, A. Hierlemann and O. Frey. *Multi-analyte biosensor interface for real-time monitoring of 3d microtissue spheroids in hanging-drop networks.* 2:micronano201622, 2016. doi:10.1038/micronano.2016.22.

[131] A. Manz, N. Graber and H. M. Widmer. *Miniaturized total chemical analysis systems: A novel concept for chemical sensing.* Sensors and Actuators B: Chemical, 1(1):244–248, 1990. doi:10.1016/0925-4005(90)80209-I.

[132] S. C. Terry, J. H. Jerman and J. B. Angell. *A gas chromatographic air analyzer fabricated on a silicon wafer.* 26(12):1880–1886, 1979. doi:10.1109/T-ED.1979.19791.

[133] I. Barbulovic-Nad, S. H. Au and A. R. Wheeler. *A microfluidic platform for complete mammalian cell culture.* Lab Chip, 10(12):1536–1542, 2010. doi:10.1039/c002147d.

[134] D. R. Gossett, W. M. Weaver, A. J. Mach, S. C. Hur, H. T. K. Tse, W. Lee, H. Amini and D. Di Carlo. *Label-free cell separation and sorting in microfluidic systems.* Anal Bioanal Chem, 397(8):3249–3267, 2010. doi:10.1007/s00216-010-3721-9.

[135] T. F. Didar and M. Tabrizian. *Adhesion based detection, sorting and enrichment of cells in microfluidic lab-on-chip devices.* Lab Chip, 10(22):3043–3053, 2010. doi:10.1039/c0lc00130a.

[136] J. T. Nevill, R. Cooper, M. Dueck, D. N. Breslauer and L. P. Lee. *Integrated microfluidic cell culture and lysis on a chip.* Lab Chip, 7(12):1689–1695, 2007. doi:10.1039/b711874k.

[137] S. E. McCalla and A. Tripathi. *Microfluidic reactors for diagnostics applications.* 13(1):321–343, 2011. doi:10.1146/annurev-bioeng-070909-105312.

[138] M.-I. Mohammed and M. P. Y. Desmulliez. *Lab-on-a-chip based immunosensor principles and technologies for the detection of cardiac biomarkers: a review.* Lab Chip, 11(4):569–595, 2011. doi:10.1039/c0lc00204f.

[139] M. B. Miller and Y.-W. Tang. *Basic concepts of microarrays and potential applications in clinical microbiology.* Clin. Microbiol. Rev., 22(4):611–633, 2009. doi:10.1128/CMR.00019-09.

[140] B. Kuswandi, Nuriman, J. Huskens and W. Verboom. *Optical sensing systems for microfluidic devices: A review.* Analytica Chimica Acta, 601(2):141–155, 2007. doi:10.1016/j.aca.2007.08.046.

[141] J. El-Ali, P. K. Sorger and K. F. Jensen. *Cells on chips.* Nature, 442(7101):403–411, 2006. doi:10.1038/nature05063.

[142] P. Lee, T. Gaige and P. Hung. *Microfluidic systems for live cell imaging.* Methods in Cell Biology, 102:77–103, 2011. doi:10.1016/B978-0-12-374912-3.00004-3.

[143] T. Chen, B. Gomez-Escoda, J. Munoz-Garcia, J. Babic, L. Griscom, P.-Y. J. Wu and D. Coudreuse. *A drug-compatible and temperature-controlled microfluidic device for live-cell imaging.* Open Biol, 6(8), 2016. doi:10.1098/rsob.160156.

[144] K. Seshan. *Handbook of Thin Film Deposition.* William Andrew, 2001. ISBN 978-0-8155-1778-8.

[145] V. R. Mamilla and K. S. Chakradhar. *Micro machining for micro electro mechanical systems (MEMS).* Procedia Materials Science, 6:1170–1177, 2014. doi:10.1016/j.mspro.2014.07.190.

[146] M. J. Madou. *Fundamentals of Microfabrication: The Science of Miniaturization, Second Edition.* CRC Press, 2002. ISBN 978-0-8493-0826-0. Google-Books-ID: 9bk3gJeQKBYC.

[147] A. Guimerà, E. Prats-Alfonso, R. Villa and F. J. d. Campo. *Chapter 2:development of microelectrode-based biosensors for biomedical analysis.* In *Electrochemical Strategies in Detection Science*, pages 19–84. 2015. doi: 10.1039/9781782622529-00019.

[148] I. Montenegro, M. A. Queirós and J. L. Daschbach. *Microelectrodes: Theory and Applications.* Springer Science & Business Media, 2012. ISBN 978-94-011-3210-7.

[149] G. Voskerician, M. S. Shive, R. S. Shawgo, H. von Recum, J. M. Anderson, M. J. Cima and R. Langer. *Biocompatibility and biofouling of MEMS drug delivery devices.* Biomaterials, 24(11):1959–1967, 2003.

[150] K. E. Petersen. *Silicon as a mechanical material.* 70(5):420–457, 1982. ISSN 0018-9219. doi: 10.1109/PROC.1982.12331.

[151] X. Illa, O. Ordeig, D. Snakenborg, A. Romano-Rodríguez, R. G. Compton and J. P. Kutter. *A cyclo olefin polymer microfluidic chip with integrated gold microelectrodes for aqueous and non-aqueous electrochemistry.* Lab Chip, 10(10):1254–1261. doi:10.1039/B926737A.

[152] H. Becker and L. E. Locascio. *Polymer microfluidic devices.* Talanta, 56(2):267–287, 2002.

[153] H. Becker and C. Gärtner. *Polymer microfabrication technologies for microfluidic systems.* Anal Bioanal Chem, 390(1):89–111, 2008. doi:10.1007/s00216-007-1692-2.

[154] D. C. Duffy, J. C. McDonald, O. J. A. Schueller and G. M. Whitesides. *Rapid prototyping of microfluidic systems in poly(dimethylsiloxane).* Anal. Chem., 70(23):4974–4984, 1998. doi:10.1021/ac980656z.

[155] F. J. del Campo. *Miniaturization of electrochemical flow devices.* Electrochemistry Communications, 45:91–94, 2014. doi:10.1016/j.elecom.2014.05.013.

[156] H. Matsuda and J. Yamada. *Limiting diffusion currents in hydrodynamic voltammetry.* Journal of Electroanalytical Chemistry and Interfacial Electrochemistry, 30(2):261–270, 1971. doi:10.1016/0368-1874(71)85063-3.

[157] C. R. Friedrich and M. J. Vasile. *The micromilling process for high aspect ratio microstructures.* Microsystem Technologies, 2(3):144–148, 1996. doi:10.1007/s005420050032.

[158] M. J. González-Guerrero, J. P. Esquivel, D. Sánchez-Molas, P. Godignon, F. X. Muñoz, F. J. del Campo, F. Giroud, S. D. Minteer and N. Sabaté. *Membraneless glucose/o2 microfluidic enzymatic biofuel cell using pyrolyzed photoresist film electrodes.* Lab Chip, 13(15):2972–2979, 2013. doi:10.1039/c3lc50319d.

[159] H. Klank, J. P. Kutter and O. Geschke. *CO(2)-laser micromachining and back-end processing for rapid production of PMMA-based microfluidic systems.* Lab Chip, 2(4):242–246, 2002. doi:10.1039/b206409j.

[160] D. Snakenborg, H. Klank and J. P. Kutter. *Microstructure fabrication with a CO 2 laser system.* J. Micromech. Microeng., 14(2):182, 2004. doi:10.1088/0960-1317/14/2/003.

[161] A. Hulanicki, S. Glab and F. Ingman. *Chemical sensors: definitions and classification.* Pure Appl. Chem., PAC, 63(9):1247–1250, 1991. ISSN 0033-4545, 1365-3075. doi:10.1351/pac199163091247.

[162] L. Nyholm. *Electrochemical techniques for lab-on-a-chip applications.* Analyst, 130(5):599–605, 2005.

[163] *Sensors: A comprehensive survey, vol. 1, fundamentals and general aspects*, 1989.

[164] D. R. Thevenot, K. Tóth, R. A. Durst and G. S. Wilson. *Electrochemical biosensors: Recommended definitions and classification.* Pure Appl. Chem., PAC, 71(12):2333–2348, 1999. doi:10.1351/pac199971122333.

[165] D. Glick. *Methods of Biochemical Analysis.* John Wiley & Sons, 2009. ISBN 978-0-470-11090-4.

[166] A. J. Bard and L. R. Faulkner. *Electrochemical Methods: Fundamentals and Applications.* Wiley.

[167] S. Alegret, M. d. Valle and A. Merkoçi. *Sensores electroquímicos: introducción a los quimiosensores y biosensores : curso teórico-práctico.* Univ. Autònoma de Barcelona, 2004. ISBN 978-84-490-2361-3.

[168] B. R. Eggins. *Chemical sensors and biosensors*, West Sussex: 2002.

[169] J. Wang. *Glucose biosensors: 40 years of advances and challenges.* Electroanalysis, 13(12):983–988, 2001. doi:10.1002/1521-4109(200108)13:12<983::AID-ELAN983>3.0.CO;2-#.

[170] L. C. Clark. *Electrochemical device for chemical analysis*, 1959. US Patent No. 2 913 386.

[171] H. Danncel. *Über den durch diffundierende gase hervorgerufenen reststrom.* Zeitschrift für Elektrochemie, 4(9):227–232, 1897. doi:10.1002/bbpc.18970040903.

[172] R. J. J. W. *Method and apparatus for electrolytically determining a species in a fluid*, 1966. US Patent No. 3 260 656 A.

[173] Y. Wang, H. Xu, J. Zhang and G. Li. *Electrochemical sensors for clinic analysis.* Sensors (Basel), 8(4):2043–2081, 2008.

[174] Y.-H. Lee and C.-C. Hu. *Electrochemical sensors for water pollution and quality monitoring.* pages 624–634, 2014. doi:10.1007/978-1-4419-6996-5_75.

[175] F. Ribet, G. Stemme and N. Roxhed. *Ultra-miniaturization of a planar amperometric sensor targeting continuous intradermal glucose monitoring.* Biosensors and Bioelectronics, 90:577–583, 2017. doi: 10.1016/j.bios.2016.10.007.

[176] M. Koudelka. *Performance characteristics of a planar 'clark-type' oxygen sensor.* Sensors and Actuators, 9(3):249–258, 1986. doi:10.1016/0250-6874(86)80025-7.

[177] H. Suzuki, E. Tamiya and I. Karube. *Fabrication of an oxygen electrode using semiconductor technology.* Anal. Chem., 60(10):1078–1080, 1988. doi:10.1021/ac00161a026.

[178] H. Suzuki, A. Sugama and N. Kojima. *Miniature clark-type oxygen electrode with a three-electrode configuration.* Sensors and Actuators B: Chemical, 2(4):297–303, 1990. doi:10.1016/0925-4005(90)80157-U.

[179] H. Suzuki, N. Kojima, A. Sugama and F. Takei. *Development of a miniature clark-type oxygen electrode using semiconductor techniques and its improvement for practical applications.* Sensors and Actuators B: Chemical, 2(3):185–191, 1990. doi:10.1016/0925-4005(90)85003-H.

[180] J. Wang. *Decentralized electrochemical monitoring of trace metals: from disposable strips to remote electrodes. plenary lecture.* Analyst, 119(5):763–766, 1994. doi:10.1039/AN9941900763.

[181] O. D. Renedo, M. A. Alonso-Lomillo and M. J. A. Martínez. *Recent developments in the field of screen-printed electrodes and their related applications.* Talanta, 73(2):202–219, 2007. doi:10.1016/j.talanta.2007.03.050.

[182] S. Kuwata, N. Miura and N. Yamazoe. *A solid-state amperometric oxygen sensor using NAFION membrane operative at room temperature.* 17(7):1197–1200, 1988. doi:10.1246/cl.1988.1197.

[183] N. Godino, D. Dávila, N. Vigués, O. Ordeig, F. J. del Campo, J. Mas and F. X. Muñoz. *Measuring acute toxicity using a solid-state microrespirometer.* Sensors and Actuators B: Chemical, 135(1):13–20, 2008. doi:10.1016/j.snb.2008.06.056.

[184] S. J. Ridge. *Oxygen reduction in a proton exchange membrane test cell.* 136(7):1902, 1989. doi: 10.1149/1.2097078.

[185] L. Liu, W. Chen and Y. Li. *An overview of the proton conductivity of nafion membranes through a statistical analysis.* Journal of Membrane Science, 504:1–9, 2016. doi:10.1016/j.memsci.2015.12.065.

[186] M. A. Modestino, A. Kusoglu, A. Hexemer, A. Z. Weber and R. A. Segalman. *Controlling nafion structure and properties via wetting interactions.* Macromolecules, 45(11):4681–4688, 2012. doi: 10.1021/ma300212f.

[187] D. S. Silvester and L. Aldous. *Chapter 10:electrochemical detection using ionic liquids.* In *Electrochemical Strategies in Detection Science*, pages 341–386. 2015.

[188] M. Nádherná, F. Opekar, J. Reiter and K. Štulík. *A planar, solid-state amperometric sensor for nitrogen dioxide, employing an ionic liquid electrolyte contained in a polymeric matrix.* Sensors and Actuators B: Chemical, 161(1):811–817, 2012. doi:10.1016/j.snb.2011.11.037.

[189] G. Jobst, G. Urban, A. Jachimowicz, F. Kohl, O. Tilado, I. Lettenbichler and G. Nauer. *Thin-film clark-type oxygen sensor based on novel polymer membrane systems for in vivo and biosensor applications.* Biosensors and Bioelectronics, 8(3):123–128, 1993. doi:10.1016/0956-5663(93)85024-I.

[190] A. Weltin, J. Kieninger, B. Enderle, A.-K. Gellner, B. Fritsch and G. A. Urban. *Polymer-based, flexible glutamate and lactate microsensors for in vivo applications.* Biosens Bioelectron, 61:192–199, 2014. doi:10.1016/j.bios.2014.05.014.

[191] H. Yang, S. K. Kang, C. A. Choi, H. Kim, D.-H. Shin, Y. S. Kim and Y. T. Kim. *An iridium oxide reference electrode for use in microfabricated biosensors and biochips.* Lab Chip, 4(1):42–46. doi:10.1039/b309899k.

[192] T. Guinovart, G. A. Crespo, F. X. Rius and F. J. Andrade. *A reference electrode based on polyvinyl butyral (PVB) polymer for decentralized chemical measurements.* Analytica Chimica Acta, 821:72–80, 2014.

[193] H. Suzuki, A. Hiratsuka, S. Sasaki and I. Karube. *Problems associated with the thin-film ag/AgCl reference electrode and a novel structure with improved durability.* Sensors and Actuators B: Chemical, 46(2):104–113. doi:10.1016/S0925-4005(98)00043-4.

[194] U. Guth, F. Gerlach, M. Decker, W. Oelßner and W. Vonau. *Solid-state reference electrodes for potentiometric sensors.* J Solid State Electrochem, 13(1):27–39, 2009. doi:10.1007/s10008-008-0574-7.

[195] J. W. Ross. *Calcium-selective electrode with liquid ion exchanger.* 156(3780):1378–1379, 1967. doi:10.1126/science.156.3780.1378.

[196] L. A. R. Pioda, V. Stankova and W. Simon. *Highly selective potassium ion responsive liquid-membrane electrode.* 2(12):665–674, 1969. doi:10.1080/00032716908051343.

[197] R. Bloch, A. Shatkay and H. A. Saroff. *Fabrication and evaluation of membranes as specific electrodes for calcium ions.* Biophys J, 7(6):865–877, 1967.

[198] E. Bakker, P. Bühlmann and E. Pretsch. *Carrier-based ion-selective electrodes and bulk optodes. 1. general characteristics.* Chem. Rev., 97(8):3083–3132, 1997.

[199] P. Bühlmann, E. Pretsch and E. Bakker. *Carrier-based ion-selective electrodes and bulk optodes. 2. ionophores for potentiometric and optical sensors.* Chem. Rev., 98(4):1593–1688, 1998. ISSN 1520-6890.

[200] R. J. Forster and T. E. Keyes. *Ion-selective electrodes in environmental analysis.* In *Encyclopedia of Analytical Chemistry.* John Wiley & Sons, Ltd, 2006. ISBN 978-0-470-02731-8.

[201] A. Radomska, S. Singhal, H. Ye, M. Lim, A. Mantalaris, X. Yue, E. M. Drakakis, C. Toumazou and A. E. G. Cass. *Biocompatible ion selective electrode for monitoring metabolic activity during the growth and cultivation of human cells.* Biosens Bioelectron, 24(3):435–441, 2008. doi:10.1016/j.bios.2008.04.026.

[202] R. W. Cattrall and H. Freiser. *Coated wire ion-selective electrodes.* Anal. Chem., 43(13):1905–1906, 1971. ISSN 0003-2700. doi:10.1021/ac60307a032.

[203] R. Mamińska and W. Wróblewski. *Solid-state microelectrodes for flow-cell analysis based on planar back-side contact transducers.* Electroanalysis, 18(13):1347–1353, 2006. doi:10.1002/elan.200603538.

[204] R. Toczyłowska-Mamińska, A. Lewenstam and K. Dołowy. *Multielectrode bisensor system for time-resolved monitoring of ion transport across an epithelial cell layer.* Anal. Chem., 86(1):390–394, 2014. doi:10.1021/ac403808f.

[205] G. N. Doku and V. P. Gadzekpo. *Simultaneous determination of lithium, sodium and potassium in blood serum by flame photometric flow-injection analysis.* Talanta, 43(5):735–739, 1996. doi:10.1016/0039-9140(95)01808-5.

[206] C. C. Young. *Evolution of blood chemistry analyzers based on ion selective electrodes.* J. Chem. Educ., 74(2):177, 1997. doi:10.1021/ed074p177.

[207] M.-R. HUANG, G.-L. GU, Y.-B. DING, X.-T. FU and R.-G. LI. *Advanced solid-contact ion selective electrode based on electrically conducting polymers.* Chinese Journal of Analytical Chemistry, 40(9):1454–1460, 2012. doi:10.1016/S1872-2040(11)60572-0.

[208] U. Mattinen, S. Rabiej, A. Lewenstam and J. Bobacka. *Impedance study of the ion-to-electron transduction process for carbon cloth as solid-contact material in potentiometric ion sensors.* Electrochimica Acta, 56(28):10683–10687, 2011. doi:10.1016/j.electacta.2011.07.082.

[209] F. X. Rius-Ruiz, G. A. Crespo, D. Bejarano-Nosas, P. Blondeau, J. Riu and F. X. Rius. *Potentiometric strip cell based on carbon nanotubes as transducer layer: Toward low-cost decentralized measurements.* Anal. Chem., 83(22):8810–8815, 2011. doi:10.1021/ac202070r.

[210] M. Pesavento, G. D'Agostino, R. Biesuz, G. Alberti and A. Profumo. *Ion selective electrode for dopamine based on a molecularly imprinted polymer.* Electroanalysis, 24(4):813–824, 2012. doi:10.1002/elan.201100509.

[211] J. Ping, Y. Wang, J. Wu and Y. Ying. *Development of an all-solid-state potassium ion-selective electrode using graphene as the solid-contact transducer.* Electrochemistry Communications, 13(12):1529–1532, 2011. doi:10.1016/j.elecom.2011.10.018.

[212] J. Hu, A. Stein and P. Bühlmann. *Rational design of all-solid-state ion-selective electrodes and reference electrodes.* TrAC Trends in Analytical Chemistry, 76:102–114, 2016. doi:10.1016/j.trac. 2015.11.004.

[213] J. T. Stock. *Einar biilmann (1873-1946): pH determination made easy.* J. Chem. Educ., 66(11):910, 1989. doi:10.1021/ed066p910.

[214] A. M. Cruz, L. Abad, N. M. Carretero, J. Moral-Vico, J. Fraxedas, P. Lozano, G. Subías, V. Padial, M. Carballo, J. E. Collazos-Castro and N. Casañ-Pastor. *Iridium oxohydroxide, a significant member in the family of iridium oxides. stoichiometry, characterization, and implications in bioelectrodes.* J. Phys. Chem. C, 116(8):5155–5168, 2012. doi:10.1021/jp212275q.

[215] Y. Qin, H.-J. Kwon, M. M. R. Howlader and M. J. Deen. *Microfabricated electrochemical pH and free chlorine sensors for water quality monitoring: recent advances and research challenges.* RSC Adv., 5(85):69086–69109, 2015. doi:10.1039/C5RA11291E.

[216] E. Gill, A. Arshak, K. Arshak and O. Korostynska. *pH sensitivity of novel PANI/PVB/PS3 composite films.* Sensors (Basel), 7(12):3329–3346, 2007.

[217] B. Lakard, O. Segut, S. Lakard, G. Herlem and T. Gharbi. *Potentiometric miniaturized pH sensors based on polypyrrole films.* Sensors and Actuators B: Chemical, 122(1):101–108, 2007. doi:10.1016/j. snb.2006.04.112.

[218] I. H. Khawaji, O. O. Awadelkarim and A. Lakhtakia. *Studies of parylene c microfibrous thin films electrical properties.* Meet. Abstr., MA2016-02(27):1840–1840, 2016.

[219] M. M. R. Howlader, T. E. Doyle, S. Mohtashami and J. R. Kish. *Charge transfer and stability of implantable electrodes on flexible substrate.* Sensors and Actuators B: Chemical, 178:132–139, 2013. doi:10.1016/j.snb.2012.12.051.

[220] C. A. Li, K. N. Han, X.-H. Pham and G. H. Seong. *A single-walled carbon nanotube thin film-based pH-sensing microfluidic chip.* Analyst, 139(8):2011–2015, 2014. doi:10.1039/C3AN02195E.

[221] K. Suganuma. *Introduction to Printed Electronics.* Springer, 2014 edition edition, 2014. ISBN 978-1-4614-9624-3.

[222] Z. Cui, C. Zhou, S. Qiu, Z. Chen, J. Lin, J. Zhao, C. Ma and W. Su. *Printed Electronics: Materials, Technologies and Applications.* Wiley, 1 edition edition, 2016. ISBN 978-1-118-92092-3.

[223] H. Kipphan. *Handbook of Print Media: Technologies and Production Methods.* Springer Science & Business Media, 2001. ISBN 978-3-540-67326-2.

[224] A. de la Fuente Vornbrock, D. Sung, H. Kang, R. Kitsomboonloha and V. Subramanian. *Fully gravure and ink-jet printed high speed pBTTT organic thin film transistors.* Organic Electronics, 11(12):2037–2044, 2010. doi:10.1016/j.orgel.2010.09.003.

[225] K. F. Hird. *Offset Lithographic Technology.* Goodheart-Willcox, 1995. ISBN 978-1-56637-191-9.

[226] I. Gibson, D. Rosen and B. Stucker. *Additive Manufacturing Technologies: 3D Printing, Rapid Prototyping, and Direct Digital Manufacturing.* Springer, 2nd ed. 2015 edition edition, 2014. ISBN 978-1-4939-2112-6.

[227] Y. Kusaka and H. Ushijima. *High resolution printing processes with high throughput, enhanced step coverage, and high design flexibility.* In *2016 International Conference on Electronics Packaging (ICEP)*, pages 120–123. 2016. doi:10.1109/ICEP.2016.7486794.

[228] K. Yamada, T. G. Henares, K. Suzuki and D. Citterio. *Paper-based inkjet-printed microfluidic analytical devices.* Angew. Chem. Int. Ed. Engl., 54(18):5294–5310, 2015. doi:10.1002/anie.201411508.

[229] D. K. Schroder. *Semiconductor Material and Device Characterization.* Wiley-IEEE Press, 3 edition edition, 2015. ISBN 978-0-471-73906-7.

[230] *Organic and printed electronics: Fundamentals and applications*, 2016.

[231] A. E. Ostfeld, I. Deckman, A. M. Gaikwad, C. M. Lochner and A. C. Arias. *Screen printed passive components for flexible power electronics.* 5:srep15959, 2015. ISSN 2045-2322. doi:10.1038/srep15959.

[232] G. H. Gelinck, H. E. A. Huitema, E. van Veenendaal, E. Cantatore, L. Schrijnemakers, J. B. P. H. van der Putten, T. C. T. Geuns, M. Beenhakkers, J. B. Giesbers, B.-H. Huisman, E. J. Meijer, E. M. Benito, F. J. Touwslager, A. W. Marsman, B. J. E. van Rens and D. M. de Leeuw. *Flexible active-matrix displays and shift registers based on solution-processed organic transistors.* Nat Mater, 3(2):106–110, 2004. doi:10.1038/nmat1061.

[233] N. Komuro, S. Takaki, K. Suzuki and D. Citterio. *Inkjet printed (bio)chemical sensing devices.* Anal Bioanal Chem, 405(17):5785–5805, 2013. doi:10.1007/s00216-013-7013-z.

[234] *Wiley: Fundamentals of inkjet printing: The science of inkjet and droplets - stephen d. hoath.* URL http://www.wiley.com/WileyCDA/WileyTitle/productCd-3527337857.html.

[235] I. M. Hutchings and G. D. Martin. *Inkjet technology for digital fabrication.* John Wiley, 2013.

[236] G. D. Martin and I. M. Hutchings. *Fundamentals of inkjet technology.* In I. M. Hutchings and G. D.rtin, editors, *Inkjet Technology for Digital Fabrication*, pages 21–44. John Wiley & Sons, Ltd, 2012. DOI: 10.1002/9781118452943.ch2.

[237] D. B. Bogy and F. E. Talke. *Experimental and theoretical study of wave propagation phenomena in drop-on-demand ink jet devices.* IBM J. Res. Dev., 28(3):314–321, 1984. doi:10.1147/rd.283.0314.

[238] K.-S. Kwon. *Experimental analysis of waveform effects on satellite and ligament behavior via in situ measurement of the drop-on-demand drop formation curve and the instantaneous jetting speed curve.* J. Micromech. Microeng., 20(11):115005. doi:10.1088/0960-1317/20/11/115005.

[239] H.-C. Wu, T.-R. Shan, W.-S. Hwang and H.-J. Lin. *Study of micro-droplet behavior for a piezoelectric inkjet printing device using a single pulse voltage pattern.* Materials Transactions, 45(5):1794–1801, 2004. doi:10.2320/matertrans.45.1794.

[240] M. Medina-Sánchez, C. Martínez-Domingo, E. Ramon and A. Merkoçi. *An inkjet-printed field-effect transistor for label-free biosensing.* Adv. Funct. Mater., 24(40):6291–6302, 2014. doi:10.1002/adfm. 201401180.

[241] N. Y. Adly, B. Bachmann, K. J. Krause, A. Offenhäusser, B. Wolfrum and A. Yakushenko. *Three-dimensional inkjet-printed redox cycling sensor.* RSC Adv., 7(9):5473–5479, 2017. doi: 10.1039/C6RA27170G.

[242] M. Jović, Y. Zhu, A. Lesch, A. Bondarenko, F. Cortés-Salazar, F. Gumy and H. H. Girault. *Inkjet-printed microtiter plates for portable electrochemical immunoassays.* Journal of Electroanalytical Chemistry, 786:69–76, 2017. doi:10.1016/j.jelechem.2016.12.051.

[243] Z. Xu, Q. Dong, B. Otieno, Y. Liu, I. Williams, D. Cai, Y. Li, Y. Lei and B. Li. *Real-time in situ sensing of multiple water quality related parameters using micro-electrode array (MEA) fabricated by inkjet-printing technology (IPT).* Sensors and Actuators B: Chemical, 237:1108–1119, 2016. doi: 10.1016/j.snb.2016.09.040.

[244] K. Rajan, I. Roppolo, A. Chiappone, S. Bocchini, D. Perrone and A. Chiolerio. *Silver nanoparticle ink technology: state of the art.* Nanotechnol Sci Appl, 9:1–13, 2016. doi:10.2147/NSA.S68080.

[245] A. Määttänen, P. Ihalainen, P. Pulkkinen, S. Wang, H. Tenhu and J. Peltonen. *Inkjet-printed gold electrodes on paper: Characterization and functionalization.* ACS Appl. Mater. Interfaces, 4(2):955–964, 2012. doi:10.1021/am201609w.

[246] P. Sjöberg, A. Määttänen, U. Vanamo, M. Novell, P. Ihalainen, F. J. Andrade, J. Bobacka and J. Peltonen. *Paper-based potentiometric ion sensors constructed on ink-jet printed gold electrodes.* Sensors and Actuators B: Chemical, 224:325–332, 2016. doi:10.1016/j.snb.2015.10.051.

[247] C. Bardpho, P. Rattanarat, W. Siangproh and O. Chailapakul. *Ultra-high performance liquid chromatographic determination of antioxidants in teas using inkjet-printed graphene–polyaniline electrode.* Talanta, 148:673–679, 2016. doi:10.1016/j.talanta.2015.05.020.

[248] S. R. Das, Q. Nian, A. A. Cargill, J. A. Hondred, S. Ding, M. Saei, G. J. Cheng and J. C. Claussen. *3d nanostructured inkjet printed graphene via UV-pulsed laser irradiation enables paper-based electronics and electrochemical devices.* Nanoscale, 8(35):15870–15879, 2016. doi:10.1039/C6NR04310K.

[249] A. Lesch, F. Cortés-Salazar, V. Amstutz, P. Tacchini and H. H. Girault. *Inkjet printed nanohydrogel coated carbon nanotubes electrodes for matrix independent sensing.* Anal. Chem., 87(2):1026–1033, 2015. doi:10.1021/ac503748g.

[250] Y. Qin, A. U. Alam, M. M. R. Howlader, N.-X. Hu and M. J. Deen. *Inkjet printing of a highly loaded palladium ink for integrated, low-cost pH sensors.* Adv. Funct. Mater., 26(27):4923–4933, 2016. doi:10.1002/adfm.201600657.

[251] F. J. del Campo, L. Abad, X. Illa, E. Prats-Alfonso, X. Borrisé, J. M. Cirera, H.-Y. Bai and Y.-C. Tsai. *Determination of heterogeneous electron transfer rate constants at interdigitated nanoband electrodes fabricated by an optical mix-and-match process.* Sensors and Actuators B: Chemical, 194:86–95, 2014. doi:10.1016/j.snb.2013.12.016.

[252] B. Derby. *Inkjet printing of functional and structural materials: Fluid property requirements, feature stability, and resolution.* 40(1):395–414, 2010. doi:10.1146/annurev-matsci-070909-104502.

[253] R. D. Deegan, O. Bakajin, T. F. Dupont, G. Huber, S. R. Nagel and T. A. Witten. *Capillary flow as the cause of ring stains from dried liquid drops.* Nature, 389(6653):827–829, 1997. doi:10.1038/39827.

[254] D. Soltman and V. Subramanian. *Inkjet-printed line morphologies and temperature control of the coffee ring effect.* Langmuir, 24(5):2224–2231, 2008. doi:10.1021/la7026847.

[255] D. Kim, S. Jeong, B. K. Park and J. Moon. *Direct writing of silver conductive patterns: Improvement of film morphology and conductance by controlling solvent compositions.* Appl. Phys. Lett., 89(26):264101, 2006. doi:10.1063/1.2424671.

[256] H. Hu and R. G. Larson. *Marangoni effect reverses coffee-ring depositions.* J. Phys. Chem. B, 110(14):7090–7094, 2006. doi:10.1021/jp0609232.